HUMAN SPACEFLIGHT COUNTERMEASURES:

CEREBRAL HEMODYNAMICS DURING SHORT-ARM HUMAN CENTRIFUGATION AND THE ROLE OF PERIPHERAL FLUID SHIFTS AND JUGULAR VENOUS CONGESTION

Charles Laing

A THESIS SUBMITTED FOR THE DEGREE
OF DOCTOR OF PHILOSOPHY TO
KING'S COLLEGE LONDON

~ 2017 ~

King's College London
Centre of Human & Aerospace
Physiological Sciences (CHAPS)
3.8 Shepherds House
Guy's Campus
London, SE1 1UL

KING'S College LONDON

for my parents

"Logic, like science, must be the servant

and not the master of man."

Sir Winston Leonard Spencer-Churchill (1874-1965)

AKNOWLEDGEMENTS

I would like to acknowledge my supervisors who have taught me so much over the last few years; Prof. Jörn Rittweger for putting his faith in me and giving me the opportunity to work in his lab; Dr. David Green for creating the position at King's for affiliation and good humour with never-ending support; and Dr. Edwin Mulder for being the go to guy when the light at the end of the tunnel seemed so far away. Special thanks to Prof. Nandu Goswami for believing in me when times got hard and giving me the confidence to carry on. I still see that trip to Austria as a real turning point - so genuinely thank you.

I am very grateful to Dr. Krassimira Ivanova whose useful insight kept me on track during the most challenging of times. She started out as a colleague, became my mentor, and ended up a good friend.

Also, I would like to thank the Helmholtz Space Life Sciences Research School (SpaceLife) and the former director of the Institute of Aerospace Medicine Prof. Rupert Gerzer for accepting me on the SpaceLife program, and allowing me to pursue my intellectual curiosities, in an area that continues to interest and fascinate me in equal measure. SpaceLife was funded in equal parts by the Helmholtz Association and the German Aerospace Centre (DLR), with contributions from the Faculty of Life Sciences and Medicine at King's College London.

To all my colleagues at the Institute for Aerospace Medicine at DLR in Cologne and in particular Bernd, Karina, Joke, Kathrin, Andy and Dajana. Thank you for helping me settle in Germany, teaching me about the German way of life, including Karnival, and of course sampling German cuisine on 'fat Fridays'.

To my wife Ayge for her continual support, encouragement, and love. I wouldn't have made it to the end of this doctorate without you. I feel so grateful that our paths crossed and we met during this journey. Finally, I would like to thank my parents Ross and Joyce to whom this thesis is dedicated. For their love and support and allowing me to get the best education possible. I appreciate their sacrifices and I wouldn't have been able to get to this stage without them. Thank you for always being there no matter what and for your belief in me and that one day your son would finish and 'get a proper job'.

SUMMARY

Spaceflight induces physiological deconditioning, despite extensive exercise countermeasures. Furthermore, post-flight orthostatic intolerance (OI) and visual impairment and intracranial pressure (VIIP) syndrome; possibly related to venous congestion (VC) suggest more holistic countermeasures, such as artificial gravity (AG) short-arm human centrifugation (SAHC) are warranted. SAHC may reduce OI and VIIP incidence through headward fluid shift/pressure reversal; and thus beneficial effects on cerebral hemodynamics. Therefore, this thesis examined how peripheral fluid shifts, induced by various orthostatic challenges, affect central, peripheral, and cerebral hemodynamics, including indices of VC, in healthy participants.

Study one induced 5 min bilateral lower-limb venous cuff occlusion (VCO) up to 120mmHg in nine participants. VCO produced significant increments in leg volume (41-158mL;$p<0.05$); however, HR and cerebral tissue oxygenation (cTSI) were unchanged, suggesting an inadequate orthostatic challenge. Study two involved twenty participants experiencing 10 min SAHC to 2.4+Gz foot-level with increased g-gradients; specifically, moving rotational axis position (RAP), independent of g-level, towards the body. Increasing SAHC g-gradients reduced the HR response and increased g-tolerance ($\chi^2(1, n=20)=8.57;p=0.003$), similar to decreasing g-level. Heart-level-RAP did not improve cTSI as hypothesised, possibly due to VC. Thus, study three used 5 min head-down tilt (HDT) to -24° and -40mmHg lower body negative pressure (LBNP) on sixteen participants to evaluate VC during headward fluid shifts.

HDT induced significant VC below -12° ($p<0.05$), abolished with -40mmHg LBNP (107±11 vs. 51±5mm^2;$p<0.05$), and increased cerebral blood flow when LBNP-peripheral and HDT-headward fluid shifts balanced (-0.71±0.56 *vs.* 4.12±1.36$cm.s^{-1}$;$p=0.013$).

This thesis suggests that VCO is a poor model of gravitational fluid shifting but large g-gradient SAHC, via heart-level-RAP, is effective; and crucially, more tolerable at higher g-levels. VC may play an important role in microgravity fluid shift related OI and VIIP, which -6° bed rest studies fail to induce. Thus, AG with optimal RAP and VC amelioration, may be a tolerable and effective spaceflight countermeasure.

TABLE OF CONTENTS

AKNOWLEDGEMENTS ..... **IV**

SUMMARY ..... **V**

TABLE OF CONTENTS ..... **VII**

TABLE OF FIGURES ..... **XII**

LIST OF TABLES ..... **XX**

LIST OF EQUATIONS ..... **XXI**

LIST OF ABBREVIATIONS ..... **XXII**

1 GENERAL INTRODUCTION **24**

1.1 Spaceflight deconditioning 25
1.1.1 Cardiovascular deconditioning 28
1.1.2 Spaceflight fluid shifts 32
1.1.3 Jugular venous congestion 34
1.2 Spaceflight analogues 35
1.2.1 Head-down bed rest (HDBR) 36
1.3 Spaceflight countermeasures 38
1.4 Artificial gravity (AG) 40
1.4.1 Short-arm human centrifugation (SAHC) 41
1.5 Orthostatic challenge 45
1.5.1 Hydrostatic gradients 46
1.5.2 Cerebral hemodynamics 47
1.6 Aims and hypothesis 52

2 MATERIAL AND METHODS **54**

2.1 Experimental methods 55
2.1.1 Bilateral lower-limb venous cuff occlusion (VCO) 55
2.1.2 Short-arm human centrifugation (SAHC) 56
2.1.3 Electronic head-down/up tilt-table (HDT and HUT) 61

2.1.4 Lower-body negative pressure (LBNP) chamber 62
2.1.5 Orthostatic challenge termination criteria 64
2.2 Cerebral measurements 66
2.2.1 Transcranial Doppler (TCD) 66
2.2.2 Cerebral near-infrared spectroscopy (cNIRS) 67
2.2.3 Internal jugular vein (IJV) cross-sectional area (CSA) ultrasonography 70
2.3 Peripheral measurements 72
2.3.1 Strain gauge plethysmography (SGP) 72
2.3.2 Muscle near-infrared spectroscopy (mNIRS) 75
2.4 Systemic measurements 76
2.4.1 Heart rate and continuous blood pressure 76
2.4.2 Additional measurements 77
2.5 Discomfort and presyncopal symptoms (PSS) 77
2.5.1 Discomfort definition 77
2.5.2 PSS definition 78
2.6 Participant selection & medical monitoring 78
2.6.1 Participant selection 78
2.6.2 Medical monitoring 81
2.7 Data handling 81
2.7.1 General study design 81
2.7.2 Statistical approaches 82

3 BILATERAL LOWER-LIMB VENOUS CUFF OCCLUSION AS A SIMULATED ORTHOSTATIC CHALLENGE AND ITS EFFECT ON CENTRAL HYPOVOLEMIA AND CEREBRAL TISSUE OXYGENATION 85

3.1 Introduction 86
3.1.1 Orthostatic challenge 88
3.1.2 Peripheral fluid displacement 89
3.1.3 Cerebral hemodynamics 91
3.1.4 Aims 92
3.1.5 Hypothesis 92
3.2 Methods 93
3.2.1 Study design and participants 93
3.2.2 Experimental protocol 94

3.2.3 Statistical analysis 99
3.3 Results 100
3.3.1 Occlusion pressure effect on cardiovascular response 101
3.3.2 Peripheral fluid displacement 104
3.3.3 Cerebral tissue oxygenation 108
3.3.4 Pain related responses 108
3.3.5 Insufficient simulated orthostatic challenge and duration 110
3.3.6 Test-retest reproducibility of 60 mmHg VCO 114
3.3.7 Invalid simulated orthostatic challenge 117
3.4 Discussion 119
3.4.1 Bilateral lower-limb venous cuff occlusion pressures 119
3.4.2 Peripheral fluid displacement 121
3.4.3 Cerebral hemodynamics 123
3.4.4 Reproducability 125
3.4.5 Insufficient simulated orthostatic challenge 126
3.4.6 Conclusion 128

4 EFFECT OF NOVEL SHORT-ARM HUMAN CENTRIFUGATION INDUCED GRAVITATIONAL GRADIENTS UPON CARDIOVASCULAR RESPONSE, CEREBRAL TISSUE OXYGENATION AND OVERALL ORTHOSTATIC TOLERANCE 130

4.1 Introduction 131
4.1.1 Spaceflight countermeasures 132
4.1.2 Hydrostatic gradient 133
4.1.3 Gender effects 135
4.1.4 Hemodynamic measurements 135
4.1.5 Aims 136
4.1.6 Hypothesis 137
4.2 Methods 138
4.2.1 Study design and participants 138
4.2.2 Experimental protocol 139
4.2.3 Statistical analysis 144
4.3 Results 147
4.3.1 G-level / g-gradient effect on cardiovascular response 148
4.3.2 G-level / g-gradient effect on lower-limb peripheral fluid displacement 153
4.3.3 G-level / g-gradient effect on cerebral perfusion 155

4.3.4 Attenuated cardiovascular response and duration 158
4.3.5 Reduced peripheral fluid displacement and duration 161
4.3.6 Ameliorated cerebral perfusion and time-course 163
4.3.7 Individual responses to altered g-gradients 164
4.3.8 Gender variances in hemodynamic response 167
4.3.9 Increased overall g-tolerance 173
4.3.10 Unsupported cerebral perfusion 174
4.4 Discussion 176
4.4.1 G-level response 177
4.4.2 Attenuated fluid displacement 177
4.4.3 Unsupported cerebral tissue oxygenation 178
4.4.4 Gravitational tolerance 180
4.4.5 Future application 183
4.4.6 Conclusion 184

5 LOWER-BODY NEGATIVE PRESSURE EFFECTS ON PERIPHERAL AND CEREBRAL HEMODYMANICS DURING HEAD-DOWN TILT INDUCED JUGULAR VENOUS CONGESTION 186

5.1 Introduction 187
5.1.1 Spaceflight analogues 189
5.1.2 Fluid displacement 191
5.1.3 Venous congestion 193
5.1.4 Aims 195
5.1.5 Hypothesis 195
5.2 Methods 196
5.2.1 Study design and participants 196
5.2.2 Experimental protocol 197
5.2.3 Statistical analysis 204
5.3 Results 205
5.3.1 Cardiovascular response 205
5.3.2 Lower-limb response 208
5.3.3 Emergence and removal of venous congestion 210
5.3.4 Cerebral hemodynamics 213
5.3.5 Time effect at 12° head-down tilt 220
5.3.6 Individual responses and correlations 223
5.4 Discussion 228

5.4.1 Emergence of venous congestion 228
5.4.2 Beneficial fluid displacement 230
5.4.3 Cerebral hemodynamics 231
5.4.4 Future direction 234
5.4.5 Conclusions 235

6 GENERAL DISCUSSION 237

6.1 Summary 238
6.2 Further studies 243

7 RESEARCH OUTPUTS 246

7.1 Published articles 246
7.2 Published abstracts 246
7.3 Congresses 247
7.4 Awards 248

8 REFERENCE LIST 249

TABLE OF FIGURES

Figure 1.1 Spaceflight adaptations, on multiple organ systems, over the course of a 6-month mission. Adapted from Davis *et al.* (2008) 26

Figure 1.2 Microgravity deconditioning, on multiple organ systems. 27

Figure 1.3 Schematic representation of blood volume fluid shift on Earth and in space. Adapted from Clément (2011). 33

Figure 1.4 Ultrasound of right internal jugular vein (IJV) cross-sectional area (CSA) pre- and during spaceflight. Adapted from Grigoriev *et al.* (2011). 35

Figure 1.5 Different methodologies of simulated and actual weightlessness exposure. Adapted from Watenpaugh (2016). 36

Figure 1.6 Current spaceflight countermeasures on-board the International Space Station (ISS). Adapted from NASA (2013). 39

Figure 1.7 Artist's impression inside the Stanford Torus with a diameter of 1.8 km. Adapted from NASA (1976). 41

Figure 1.8 Gravitational gradient as a function of rotational axis position (RAP). 42

Figure 1.9 Proposed Artificial Gravity with Ergometric Exercise (AGREE) project in the permanent multipurpose module (PMM). Adapted from ESA (2011). 44

Figure 1.10 Venous and arterial pressures across the body when standing and supine. Adapted from Gradwell and Rainford (2016). 46

Figure 1.11 Cerebral autoregulation curve. Adapted from Lassen (1959) 48

Figure 1.12 Schematic overview of cerebral autoregulation cascade. 51

Figure 2.1 Example bilateral lower-limb venous cuff occlusion (VCO) applied to the proximal end of the thigh. Credit: occlusioncuff.com. 56

Figure 2.2 Short-arm human centrifuge (SAHC) at the German Aerospace Center (DLR) :envihab in Cologne. 57

Figure 2.3 Short-arm human centrifuge (SAHC) control room with operator stations for scientists, doctors, and engineers. 60

Figure 2.4 Electronic tilt table installed at :envihab German Aerospace Center (DLR) in Cologne. Credit: DLR, 2014. 61

Figure 2.5 Lower-body negative pressure (LBNP) transparent Perspex chamber. 63

Figure 2.6 Transcranial Doppler (TCD) device focused on the middle cerebral artery (MCA) to determine cerebral blood flow velocity (cBFV). Credit: Cedars-Sinai Medical Center. 66

Figure 2.7 Schematic of transmission and absorption, of near-infrared light wavelengths (700-1300 nm), in a scattering medium. Adapted from Artinis Medical Systems. 68

Figure 2.8 Prefrontal cortex cerebral near-infrared spectroscopy (NIRS) consisting of emitter and receiver attached to the participant forehead. Credit: Artinis Medical Systems. 69

Figure 2.9 Internal jugular vein (IJV) cross-sectional area (CSA) determination using ultrasonography. 71

Figure 2.10 Strain gauge plethysmography (SGP) attached to calf mid-point. Credit: Hokanson Inc. 73

Figure 2.11 Custom-built strain gauge plethysmography (SGP) calibration device for absolute circumference determination. 74

Figure 2.12 Vascular unloading technique used by the Finometer device to measure continuous beat-by-beat blood pressure and heart rate. Credit: ProfBondi CC-BY-SA 3.0. 77

Figure 3.1 The Burette-plethysmograph apparatus used by Litter and Wood (1954) to explore the effects of graded external pressure on volume and distribution of blood in the leg. 87

Figure 3.2 Experimental overview. 95

Figure 3.3 Protocol duration with constituent occlusion, baseline and recovery phases. 96

Figure 3.4 Experimental setup. 98

Figure 3.5 Mean (±SEM) changes from baseline (BL) for cardiovascular measures in the final minute (min 5) of bilateral lower-limb venous cuff occlusion (VCO, 0 to 120 mmHg). 103

Figure 3.6 Mean (±SEM) changes from baseline (BL) for calf circumference (ΔCC) and mean calf muscle tissue saturation index (ΔmTSI) in the final minute (min 5) of bilateral lower-limb venous cuff occlusion (VCO, 0 to 120 mmHg). 104

Figure 3.7 Linear relationship between changes from baseline (BL) in mean calf muscle tissue saturation index (ΔmTSI) and mean calf circumference (ΔCC) in the final minute (min 5) of bilateral lower-limb venous cuff occlusion (VCO) pressures up to 120 mmHg. 106

Figure 3.8 Mean (±SEM) changes from baseline (BL) for prefrontal cortex cerebral tissue saturation index (ΔcTSI) in the final minute (min 5) of bilateral lower-limb venous cuff occlusion (VCO, 0 to 120 mmHg)..... 108

Figure 3.9 Comparison of mean (±SEM) changes from baseline (BL) for cardiovascular measures in the final minute (min 5) of bilateral lower-limb venous cuff occlusion (VCO, 0 to 120 mmHg) in participants verbally reporting pain and not (PAIN+ *vs.* PAIN-)..... 109

Figure 3.10 Mean (±SEM) changes from baseline (BL) for heart rate (ΔHR) and averaged mean arterial pressure (ΔMAP) during five minutes bilateral lower-limb venous cuff occlusion (VCO: min 0-5, 100 mmHg) and recovery (RR: min 5-10, 0 mmHg)..... 111

Figure 3.11 Mean (±SEM) changes from baseline (BL) for calf circumference (ΔCC) and calf muscle tissue saturation index (ΔmTSI) during five minutes bilateral lower-limb venous cuff occlusion (VCO: min 0-5, 100 mmHg) and recovery (RR: min 5-10, 0 mmHg). 112

Figure 3.12 Mean (±SEM) changes from baseline (BL) for near-infrared spectroscopy (NIRS) pre-frontal cortex cerebral tissue saturation index (ΔcTSI) during five minutes bilateral lower-limb venous cuff occlusion (VCO: min 0-5, 100 mmHg) and recovery (RR: min 5-10, 0 mmHg). 113

Figure 3.13 **A**, Relationship between changes from baseline (BL) in heart rate (ΔHR) during first and second 60 mmHg bilateral lower-limb venous cuff occlusion (VCO) in the final minute (min 5); and **B**, Bland-Altman plot of paired differences in ΔHR against a mean of both, in all participants (n=9). 115

Figure 3.14 **A**, Relationship between changes from baseline (BL) in mean arterial pressure (ΔMAP) during first and second 60 mmHg bilateral lower-limb venous cuff occlusion (VCO) in the final minute (min 5); and **B**, Bland-Altman plot of paired differences inΔMAP against a mean of both, in all participants (n=9). 115

Figure 3.15 **A**, Relationship between changes from baseline (BL) in calf circumference (ΔCC) during first and second 60 mmHg bilateral lower-limb venous cuff occlusion (VCO) in the final minute (min 5); and **B**, Bland-Altman plot of paired differences in ΔCC against a mean of both, in all participants (n=9). 116

Figure 3.16 **A**, Relationship between changes from baseline (BL) in prefrontal cortex cerebral tissue saturation index (ΔcTSI) during first and second 60 mmHg bilateral lower-limb venous cuff occlusion (VCO) in the final minute (min 5); and **B**, Bland-Altman plot of paired differences in ΔcTSI against a mean of both, in all participants (n=9). 116

Figure 3.17 Non-existent relationship between changes from baseline (BL) in mean heart rate (ΔHR) and mean prefrontal cortex cerebral tissue saturation index (ΔcTSI), and mean delta calf circumference (ΔCC) in the final minute (min 5) of bilateral lower-limb venous cuff occlusion (VCO) pressures up to 100 mmHg. 117

Figure 4.1 **A**, astronaut Timothy Peake before his space mission on Earth; and **B**, during 6 month mission to the International Space Station showing fluid shift seen here by facial edema. Adapted from European Space Agency (ESA)..... 131

Figure 4.2 Hydrostatic pressure gradient from head to foot on Earth when **A**, standing and; **B**, supine. Adapted from (Clément, 2011). 134

Figure 4.3 Protocol overview..... 141

Figure 4.4 Protocol duration with constituent centrifuge profile phases 142

Figure 4.5 Experimental setup. 143

Figure 4.6 Mean changes from baseline (BL) for cardiovascular measures in the final minute (min 10) of short-arm human centrifugation (SAHC, 1.0 to 2.4 +Gz) at position 1 (*P1*, above the head), position 2 (*P2*, apex of head), and position 3 (*P3*, heart-level)..... 152

Figure 4.7 Mean changes from baseline (BL) for calf circumference (ΔCC) in the final minute (min 10) of short-arm human centrifugation (SAHC, 1.0 to 2.4 +Gz) at position 1 (*P1*, above the head), position 2 (*P2*, apex of head), and position 3 (*P3*, heart-level)..... 155

Figure 4.8 Mean changes from baseline (BL) for near-infrared spectroscopy (NIRS) measured prefrontal cortex cerebral tissue saturation index (ΔcTSI) in the final minute (min 10) of short-arm human centrifugation (SAHC, 1.0 to 2.4 +Gz) at position 1 (*P1*, above the head), position 2 (*P2*, apex of head), and position 3 (*P3*, heart-level). 158

Figure 4.9 Mean changes from baseline (BL) for cardiovascular measures during ten minutes short-arm human centrifugation (SAHC, 2.4 +Gz) with two minutes ramp-up and –down; and recovery (RR, 10 min)..... 160

Figure 4.10 Mean changes from baseline (BL) for calf circumference (ΔCC) during ten minutes short-arm human centrifugation (SAHC, 2.4 +Gz) with two minutes ramp-up and -down; and recovery (RR, 10 min)..... 162

Figure 4.11 Mean changes from baseline (BL) for near-infrared spectroscopy (NIRS) measured prefrontal cortex cerebral tissue saturation index (ΔcTSI) during ten minutes short-arm human centrifugation (SAHC, 2.4 +Gz) with two minutes ramp-up and -down; and recovery (RR, 10 min). 164

Figure 4.12 Individual participant changes from baseline (BL) for heart rate (ΔHR) during ten minutes short-arm human centrifugation (SAHC, 2.4 +Gz) with two minutes ramp-up and –down; and recovery (RR, 10 min). 165

Figure 4.13 Individual participant changes from baseline (BL) for calf circumference (ΔCC) during ten minutes short-arm human centrifugation (SAHC, 2.4 +Gz) with two minutes ramp-up and –down; and recovery (RR, 10 min). 166

Figure 4.14 Individual participant changes from baseline (BL) for near-infrared spectroscopy (NIRS) measured prefrontal cortex cerebral tissue saturation index (ΔcTSI) during ten minutes short-arm human centrifugation (SAHC, 2.4 +Gz) with two minutes ramp-up and –down; and recovery (RR, 10 min). 167

Figure 4.15 Mean changes from baseline (BL) for cardiovascular measures in the final minute (min 10) of 2.4 +Gz short-arm human centrifugation (SAHC) at rotational axis position (RAP) 1 (*P1*, above the head), position 2 (*P2*, apex of head), and position 3 (*P3*, heart-level) between males and females. 170

Figure 4.16 Mean changes from baseline (BL) in calf circumference (ΔCC) in the final minute (min 10) of short-arm human centrifugation (SAHC, 1.0 to 2.4 +Gz) at rotational axis position (RAP) 1 (*P1*, above the head), position 2 (*P2*, apex of head), and position 3 (*P3*, heart-level) between males and females. 171

Figure 4.17 Mean changes from baseline (BL) for near-infrared spectroscopy (NIRS) measured prefrontal cortex cerebral tissue saturation index (ΔcTSI) in the final minute (min 10) of short-arm human centrifugation (SAHC, 1.0 to 2.4 +Gz) at rotational axis position (RAP) 1 (*P1*, above the head), position 2 (*P2*, apex of head), and position 3 (*P3*, heart-level) between males and females. 172

Figure 4.18 G-tolerance in each rotational axis position (RAP, *P1-3*) across all short-arm human centrifugation (SAHC) foot g-levels (1.0, 1.7 and 2.4 +Gz) in males and females. 173

Figure 4.19 G-tolerance in each rotational axis position (RAP, *P1-3*) across all short-arm human centrifugation (SAHC) foot g-levels (1.0, 1.7 and 2.4 +Gz) in all participants. 174

Figure 4.20 Relationship between mean changes from baseline (BL) in heart rate (Δ HR) and prefrontal cortex cerebral tissue saturation index (ΔcTSI) vs. calf circumference (Δ CC) during centrifugation at all g-levels (1.0-2.4 +Gz) and positions (*P1-3*)..... 175

Figure 5.1 NASA's Advanced Resistive Exercise Device (ARED) for the International Space Station (ISS). Adapted from NASA. 188

Figure 5.2 Hydrostatic pressure gradients standing on Earth, during head-down bed rest (HDBR), and weightlessness. Adapted from Gradwell and Rainford (2016)..... 190

Figure 5.3 Lower-body negative pressure (LBNP) device, also called the Chibis, on board the International Space Station (ISS). Adapted from Roscosmos. 192

Figure 5.4 Experimental overview..... 198

Figure 5.5 Protocol duration with constituent tilt / pressure phases. 199

Figure 5.6 Electronic tilt-table experimental setup..... 200

Figure 5.7 Lower-body negative pressure (LBNP) chamber experimental setup..... 201

Figure 5.8 Screenshot from ultrasonography video sequence of the internal jugular vein. 203

Figure 5.9 Mean changes from baseline (BL) for cardiovascular measures in the final minute (min 5) of head-down tilt (HDT, -6 to -24°), supine (0°) and head-up tilt (+12°) with (-40 mmHg) and without (0 mmHg) lower-body negative pressure (LBNP). 207

Figure 5.10 Mean changes from baseline (BL) for parameters in the lower-limb of the final minute (min 5) of head-down tilt (HDT, -6 to -24°), supine (0°) and head-up tilt (+12°); with (-40 mmHg) and without (0 mmHg) lower-body negative pressure (LBNP). 209

Figure 5.11 Mean absolute internal jugular vein cross-sectional area (CSA, left and right) of the final minute (min 5) of head-down tilt (HDT, -6 to -24°), supine (0°) and head-up tilt (+12°); with (-40 mmHg) and without (0 mmHg) lower-body negative pressure (LBNP). 211

Figure 5.12 Mean difference in absolute cross-sectional area of the right (CSA-R) and left (CSA-L) internal jugular veins in the final minute (min 5) of head-down tilt (HDT, -6 to -24°), supine (0°) and head-up tilt (+12°); with (-40 mmHg) and 213

Figure 5.13 Mean changes from baseline (BL) for near-infrared spectroscopy (NIRS) measured prefrontal cortex cerebral tissue saturation index (ΔcTSI) in the final minute (min 5) of head-down tilt (HDT, -6 to -24°), supine (0°) and head-up tilt (+12°); with (-40 mmHg) and without (0 mmHg) lower-body negative pressure (LBNP). 214

Figure 5.14 Mean changes from baseline (BL) for transcranial Doppler (TCD) measured middle cerebral artery blood flow velocity (ΔcBFV) in the final minute (min 5) of head-down tilt (HDT, -6 to -24°), supine (0°) and head-up tilt (+12°); with (-40 mmHg) and without (0 mmHg) lower-body negative pressure (LBNP). 215

Figure 5.15 Mean changes from baseline (BL) for calculated cerebrovascular conductance (ΔCVC; flow/pressure) in the final minute (min 5) of head-down tilt (HDT, -6 to -24°), supine (0°) and head-up tilt (+12°); with (-40 mmHg) and without (0 mmHg) lower-body negative pressure (LBNP). 216

Figure 5.16 Mean changes from baseline (BL) for middle cerebral artery blood flow velocity (ΔcBFV) during five minutes head-up tilt (HUT, +12°), supine (0°), and head-down tilt (HDT, -6 to -24°) with (-40 mmHg) and without (0 mmHg) lower-body negative pressure (LBNP), and recovery (RR, 0° and 0 mmHg). 219

Figure 5.17 Mean changes from baseline (BL) for systemic, peripheral and cerebral hemodynamic measures during five minutes head-down tilt (HDT, -12°) with (-40 mmHg) and without (0 mmHg) lower-body negative pressure (LBNP), and recovery (0°, 0 mmHg). 222

Figure 5.18 Individual participant changes from baseline (BL) for middle cerebral artery blood flow velocity (ΔcBFV) during five minutes head-down tilt (HDT, -12°) with (-40 mmHg) and without (0 mmHg) lower-body negative pressure (LBNP), and recovery (0°, 0 mmHg). 223

Figure 5.19 Relationship plots between mean changes from baseline (BL) for delta heart rate (ΔHR) and pre-frontal cortex cerebral tissue saturation index (ΔcTSI), against delta calf circumference (ΔCC) in the final minute (min 5) of head-down tilt (HDT, -6 to -24°) with (-40 mmHg) and without (0 mmHg) lower-body negative pressure (LBNP). 225

Figure 5.20 Relationship plots between mean changes from baseline (BL) for delta middle cerebral artery blood flow velocity (ΔcBFV) against mean delta calf circumference (ΔCC) in the final minute (min 5) of head-down tilt (HDT, -6 to -24°) with (-40 mmHg) and without (0 mmHg) lower-body negative pressure (LBNP). 226

Figure 5.21 Hypothesised space obstructive syndrome (SOS) cascade phenomenon adapted from Wiener (2012). 233

Figure 6.1 Schematic representation of expected hydrostatic gradients within the arterial and venous vasculature under different conditions. 242

LIST OF TABLES

Table 1.1 Comparison of physiological deconditioning in spaceflight and head-down bed rest (HDBR). Adapted from Nicogossian *et al.* (1994). 38

Table 2.1 German Aerospace Center (DLR) short-arm human centrifuge (SAHC) dimensions and performance. 57

Table 2.2 Implausible physiological data limits of all measured parameters; for data processing, using a custom-made Matlab script. 83

Table 3.1 Participant individual data. 93

Table 3.2 Participant absolute mean baseline (BL) values for all parameters. 101

Table 3.3 Relative estimations of peripheral fluid shifts based on previously published data. 107

Table 4.1 Participant individual data. 138

Table 4.2 Effective g-level and gradient for participant at 2.4 +Gz. 140

Table 4.3 Participant absolute mean baseline (BL) values for all parameters. 147

Table 4.4 Effects and their standard errors of cardiovascular variables as a result of time, position and g-level. 149

Table 4.5 Effects and their standard errors of calf circumference (CC) as a result of time, position and g-level. 154

Table 4.6 Effects and their standard errors of prefrontal cortex cerebral tissue saturation index (cTSI) as a result of time, position and g-level (fixed effects). 156

Table 4.7 Effects and their standard errors of hemodynamic variables as a result of time, and gender (fixed effects). 168

Table 5.1 Individual participant data. 197

Table 5.2 Participant absolute mean baseline (BL) values for all parameters. 205

LIST OF EQUATIONS

Equation 1.1 Equations for forces generated during short-arm human centrifugation (SAHC). 43

Equation 2.1 Equations of optical density and chromophore concentration for calculating near-infrared spectroscopy (NIRS) measurements. 68

Equation 2.2 Calculation of volumetric peripheral fluid displacement percentage increase from calf circumference percentage increase. 73

LIST OF ABBREVIATIONS

+Gz	Head to foot g-level (G)
AC	Alternating current
AG	Artificial gravity
AGREE	Artificial Gravity with Ergometric Exercise
ANOVA	Analysis of variance
ARED	Advanced Resistive Exercise Device
AV	Atrioventricular
BL	Baseline
BMI	Body mass index
BP	Blood pressure
CA	Carotid artery
CAD	Computer aided design
CBF	Cerebral blood flow
cBFV	Cerebral blood flow velocity
CC	Calf circumference
CCW	Counter-clockwise
CEVIS	Cycle Ergometer with Vibration Isolation and Stabilization
cNIRS	Cerebral near-infrared spectroscopy
CO	Cardiac output
COLBERT	Combined Operational Load Bearing External Resistance Treadmill
CPR	Cardiopulmonary resuscitation
CSA	Cross-sectional area
cTSI	Prefrontal cortex cerebral tissue saturation index
CVP	Central venous pressure
CW	Clockwise
DBP	Diastolic blood pressure
DC	Direct current
DLR	German Aerospace Centre
DPF	Differential pathlength factor
ECG	Electrocardiogram
ESA	European Space Agency
EVA	Extravehicular activity
FAI	Fédération Aéronautique Internationale
GFR	Glomerular filtration rate
GLOC	Gravitational loss of consciousness
Hb	Hemoglobin
HDBR	Head-down bed rest
HDL	High density lipoprotein
HDT	Head-down tilt
HHb	Deoxyhemoglobin
HIV	Human immunodeficiency virus
HL	Heart-level
HR	Heart rate

HSD	Honestly significant difference
HUT	Head-up tilt
ICP	Intracranial pressure
IJV	Internal jugular vein
IOP	Intraocular pressure
ISS	International Space Station
LAHC	Long-arm human centrifugation
LBNP	Lower body negative pressure
LDL	Low density lipoprotein
LME	Linear mixed effect
MAP	Mean arterial pressure
MCA	Middle cerebral artery
mNIRS	Calf muscle near-infrared spectroscopy
MNSA	Muscle sympathetic nervous activity
MRI	Magnetic resonance imaging
mTSI	Calf muscle tissue saturation index
NASA	National Aeronautics and Space Administration
NE	Norepinephrine
O_2Hb	Oxyhemoglobin
OI	Orthostatic intolerance
PMM	Permanent multipurpose module
PMMA	Polymethyl methacrylate
PP	Pulse pressure
PSS	Presyncopal symptoms
PVCs	Premature ventricular contractions
RAP	Rotational axis position
Roscosmos	Roscosmos State Corporation for Space Activities
RPM	Revolutions per minute
RR	Recovery period
SAHC	Short-arm human centrifugation
SBP	Systolic blood pressure
SCM	Sternocleidomastoid muscle
SGOT	Serum glutamic oxaloacetic transaminase
SGP	Strain gauge plethysmography
SGPT	Serum glutamic pyruvic transaminase
SNS	Sympathetic nervous system
SOS	Space obstructive syndrome
STS	Sit-to-stand
SV	Stroke volume
TCD	Transcranial Doppler
THb	Total haemoglobin
TPR	Total peripheral resistance
VCO	Venous cuff occlusion
VIIP	Visual impairment and intracranial pressure
VO_2 max	Maximal aerobic capacity
γ-GT	Serum gamma glutamyl transferase

1 GENERAL INTRODUCTION

1.1 Spaceflight deconditioning

There are a multitude of risks associated with human spaceflight from the high g-forces experienced during vehicle launch and psychological isolation, to cosmic radiation and weightlessness. Extensive knowledge has been gained over the last 56 years humans have been travelling into space, since the first manned launch of Russian cosmonaut Yuri Gagarin into orbit on 12th August 1961 to current day International Space Station (ISS) operations. Since Gagarin's successful 108 minute orbit of our planet much research has been conducted on the almost 600 subsequent individuals who have gone into space. The Fédération Aéronautique Internationale (FAI) defines a spacefarer as anybody whose flight exceeds an altitude of 100 km (62 mi) Kármán line, but not necessarily achieve orbit, and may be as short as 15 minutes sub-orbital. Except for the launch and re-entry, it is longer-term spaceflight that poses the greatest risk physiologically, with the body continually unloaded.

In general, alterations in different body systems reach a point of general adaptation around one and a half months into a mission (Figure 1.1A). However, this is not the case for radiation exposure (Chancellor *et al.*, 2014), bone loss (Sibonga, 2013), and visual problems (Mader *et al.*, 2011). Future missions, of longer duration, are required to fully examine the implications of periods in weightlessness exceeding the current 6-month standard ISS on-board stay. Health effects of prolonged spaceflight duration, exceeding the current 438 consecutive day record by Russian cosmonaut Valeri Polyakov in 1994-5, are unknown.

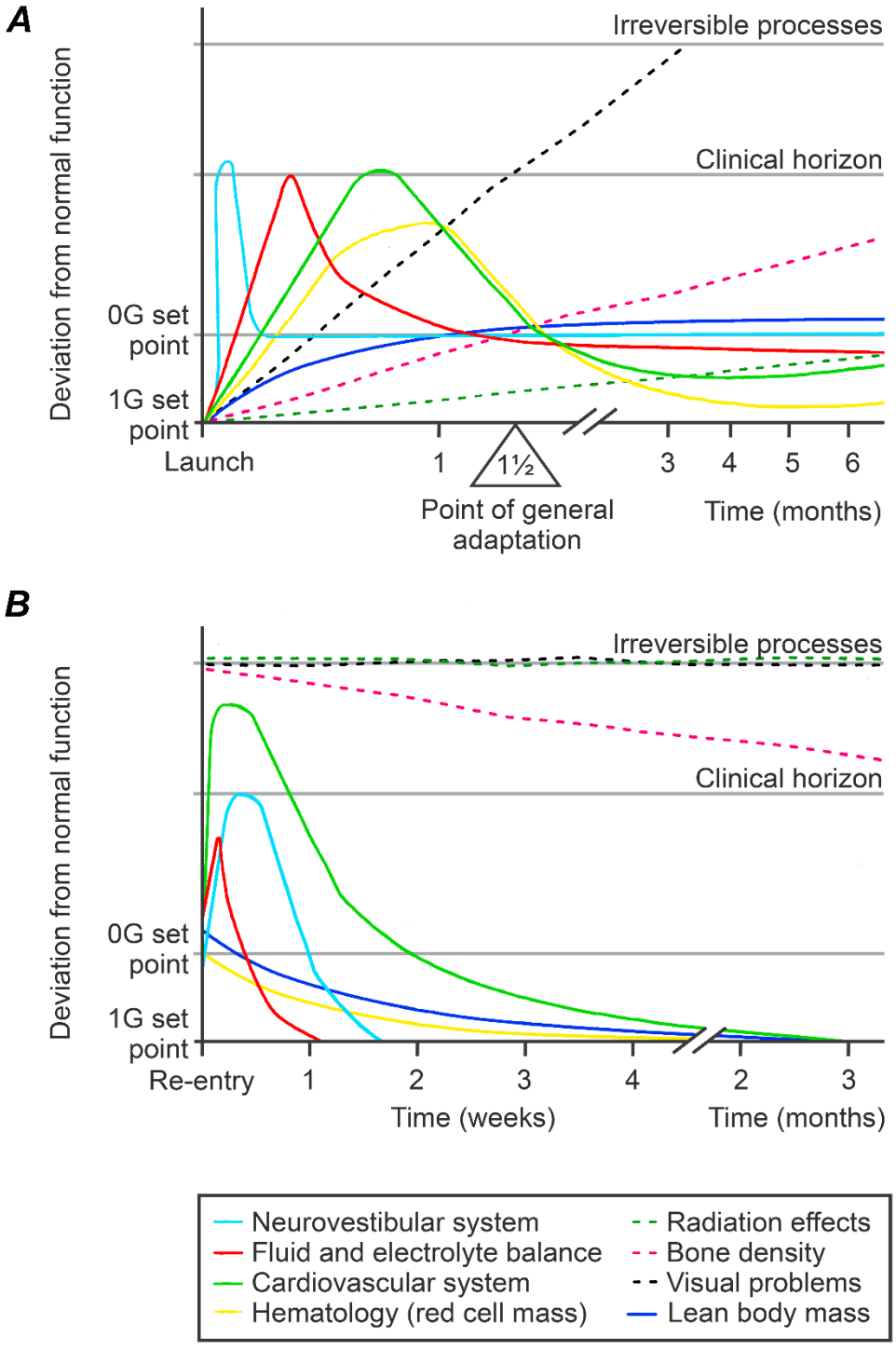

Figure 1.1 Spaceflight adaptations, on multiple organ systems, over the course of a 6-month mission. Adapted from Davis *et al.* (2008)

A, Inflight deviations from normal function (0-6 months); and
B, post-flight recovery (up to 3 months).

Even though the body may adapt well and rapidly to the new environment of space problems are seen on return when re-entering and experiencing gravitational loading once again (Buckey Jr *et al.*, 1996; Baisch & Beck, 1997; Tank *et al.*, 2011). Furthermore, longer periods of unloading require more time in which to reach a pre-flight baseline, and parameters such as visual acuity may never fully recover (Marshall-Bowman *et al.*, 2013) (Figure 1.1B). Astronauts returning to Earth in a deconditioned state are immediately attended to by large rescue crews, consisting of doctors, engineers, and scientists; mitigating any immediate health risk (Clément, 2011). However, the same will not be true for a future visit to the Marian surface and, although the gravity on Mars is only one third of that on Earth, an autonomous spacecraft egress would present a substantial challenge.

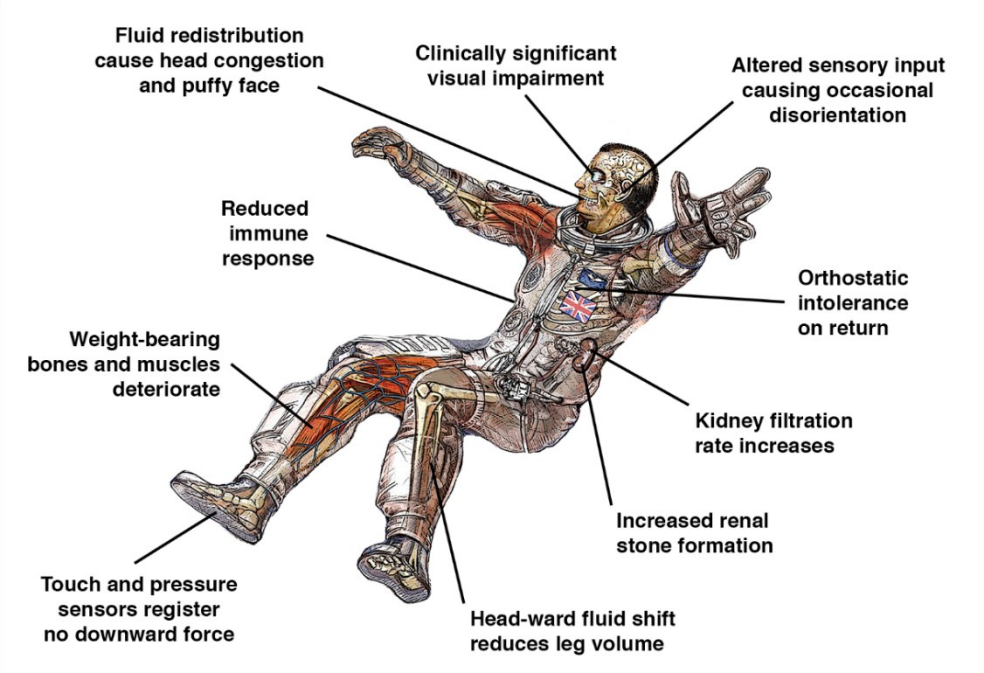

Figure 1.2 Microgravity deconditioning, on multiple organ systems. Adapted from beaudaniels.com.

NASA have current plans for a manned mission to Mars in the 2030s (NASA, 2015b), with an estimated round-trip duration, dependant on trajectory opportunities, of between 16-42 months (Tito *et al.*, 2013). In order for manned interplanetary travel to be realised, the microgravity induced health implications affecting almost all body systems (Figure 1.2) must be studied, understood, and mitigated against. The focus of this research was the cardiovascular system.

1.1.1 Cardiovascular deconditioning

The cardiovascular system is immediately affected upon entering weightlessness, demonstrating a headward fluid shift that increases central volume (Diedrich *et al.*, 2007) and cause the cardiac chambers to distend (Buckey *et al.*, 1996a). The system responds with a cascade to bring about a total reduction in circulating blood volume by 10-17% after 14 days (Alfrey *et al.*, 1996). Within the first two weeks these changes stabilise and a new "space normal" is reached; however, the sudden reintroduction of gravity on return to Earth can manifest itself as orthostatic intolerance (OI) (Buckey Jr *et al.*, 1996; Baisch & Beck, 1997). Around half of all returning astronauts suffer from OI (Lee *et al.*, 2015); which is characterised by an inability to sufficiently maintain stroke volume, blood pressure, and ultimately cerebral perfusion (Maillet *et al.*, 1993; Maillet *et al.*, 1995).

Cardiovascular deconditioning is a major concern, not just on return but also during a mission, where the ability of an astronaut to respond in an emergency situation may be impeded (Greenleaf *et al.*, 1989; Convertino & Sandler, 1995). Additionally, current missions on-board the ISS usually require bouts of strenuous, prolonged exertion in the

form of extravehicular activity (EVA) or spacewalks (Moore Jr *et al.*, 2008). It is therefore crucial cardiovascular function, and specifically maximal aerobic capacity (VO_2 max), is maintained through suitable exercise countermeasures in order to mitigate any potential risk or unforeseen situation during and post-flight. Other spaceflight physiological adaptations include reductions in the functioning of the vestibular otolith organs; with this deconditioning also thought to contribute to post-flight astronaut OI (Hallgren *et al.*, 2016). Considerable evidence has been conducted on human subjects demonstrating that otolith receptor inputs participate in blood pressure regulation (Shortt & Ray, 1997; Hume & Ray, 1999; Ray, 2000; Ray & Monahan, 2002). Furthermore, prior research has shown that the vestibulosympathetic reflex and the baroreceptor reflex interact and are mediated by common neuronal circuitry (Yates *et al.*, 1991; Yates *et al.*, 1995). Current countermeasures are primarily used to prevent muscle atrophy, bone loss, and maintain aerobic capacity (Loehr *et al.*, 2015). However, the high incidence of OI in returning astronauts suggests current exercise regimes could benefit from improvement.

OI is characterised by a diminished venous return, leading to inadequate cardiac pre-load and inability to maintain stroke volume (SV); however, the specific causative factor, as a result of spaceflight, remains unclear. Significant cardiac muscle atrophy has been shown to occur with only two weeks of unloading in simulated microgravity (Levine *et al.*, 1997) and, coupled with muscle atrophy and associated vascular compliance increases (Convertino *et al.*, 1989), demonstrates the importance of maintaining muscle mass and function during a mission. The effectiveness of the leg muscle-pump may also be diminished as weight-bearing muscles atrophy in space

(LeBlanc *et al.*, 1995; LeBlanc *et al.*, 2000); potentially lessening their role, on deep peripheral venous contractions, aiding venous return. A reduced blood volume is thought to be linked to OI and ingestion of a large volume of saline immediately before re-entry has been shown to increase astronaut orthostatic tolerance (Bungo *et al.*, 1985). However, a more recent pharmacological intervention with fludrocortisone, restoring post-flight plasma levels to those pre-flight, did not change OI incidence (Shi *et al.*, 2004); suggesting that both centrally available blood volume, as well as cardiac contractility are essential (Jeong *et al.*, 2012).

Prolonged exposure to periods of increased central volume, induced by head-down bed rest (HDBR), may desensitise stretch baroreceptors (Fritsch *et al.*, 1992; Fritsch-Yelle *et al.*, 1994) tasked with providing short-term control of blood pressure. However, Di Rienzo *et al.* (2008) measured no deconditioning of baroreceptor control of the heart after a 16-day short-duration spaceflight. Nevertheless, more recent research has shown agreement with HDBR data with Eckberg *et al.* (2010) observing impairment of vagal baroreflex function in space after 10-days. Increased baroreceptor sensitivity occurs in the initial microgravity exposure, perhaps due to the centralisation of circulating fluid (Eckberg *et al.*, 2010); however, longer-term data are less clear. It seems likely that an immediate sensitivity peak, upon entering weightlessness, then diminishes as exposure time increases; yet whether or not that proceeds to insignificance, from pre-flight baroreceptor functions, remains to be seen.

Under significant orthostatic stress, the total peripheral resistance (TPR) of an individual increases whilst the mean arterial pressure (MAP) remains relatively unchanged. It has been postulated that blood pressure is maintained, in part, by an

enhancement of the carotid baroreceptor reflex in the presence of a challenge (Cooper & Hainsworth, 2001). Furthermore, subsequent research suggests this positive mechanism augmentation may be occurring due to an increase in carotid baroreceptor sensitivity; and a failure to do so may lead to a reduced orthostatic tolerance (Cooper & Hainsworth, 2002). A predisposition to orthostatic intolerance, as observed in returning astronauts, may be affected by other baroreceptor factors such as reduced sensitivity in aerobically fit individuals (Ogoh *et al.*, 2003); or a currently unknown interaction between cardiopulmonary and carotid baroreceptors.

Recently, vision impairment in astronauts has been observed during spaceflight (Mader *et al.*, 2011) that persists after return to Earth (Stenger *et al.*, 2016). The so-called visual impairment and intracranial pressure (VIIP) syndrome has led some to call it the first true "space sickness", as current attempts to maintain astronaut health have not reduced occurrence (Wiener, 2012). Increased intraocular pressure (IOP), choroidal folds, optic disc edema and globe flattening have all been observed during long-duration missions; with spinal fluid opening pressure also found increased in a number of astronauts post-flight (Mader *et al.*, 2011). It is therefore suggested that elevated intracranial pressure (ICP) may be responsible for reduced visual acuity. Several working hypotheses on the cause of VIIP have been and are currently being investigated; including (i) elevated spacecraft CO_2 levels (Ursino & Lodi, 1997; Ainslie & Duffin, 2009); (ii) high salt diet (Fogarty *et al.*, 2011); (iii) excessive resistive exercise (Fogarty *et al.*, 2011); (iv) venous congestion (Wiener, 2012); and (v) a genetic predisposition (Kramer *et al.*, 2012). However, the initiating factor behind VIIP, regardless of the exact mechanism of

action, is considered by many to be directly related to the pronounced headward fluid shifts in weightlessness (Fogarty *et al.*, 2011; Mader *et al.*, 2011; Kramer *et al.*, 2012).

1.1.2 Spaceflight fluid shifts

Humans have evolved, as bipedal animals on Earth, with an innate ability to maintain suitable blood pressure and cerebral perfusion, despite rapid postural changes on a daily basis affecting pressure along the vascular column (Gradwell & Rainford, 2016). The hydrostatic gradient was recognised over 100 years ago as integral to cardiovascular control by providing a natural pressure reference (Blumberg, 1885; Wagner, 1886) and led to the development of simple physical models of the hydrostatic indifference concept (Gauer & Thron, 1965). However, significant alterations, to gravitational force and direction across the body, may bring the validity of these historical models into question.

Exposure to weightlessness removes the hydrostatic gradient completely, as venous and arterial pressures roughly equalise across the body; and blood volume, normally present in the peripheral and splanchnic regions (Petersen *et al.*, 2011), is shifted into the thorax and towards the head (Figure 1.3A to B). Astronauts often report a feeling of "facial fullness" similar to the common cold and have been described as having a "puffy face" and "chicken legs" (Thornton *et al.*, 1977). It is normal for these initial symptoms to subside after a few days of adaptation as aortic and carotid stretch receptors upregulate the glomerular filtration rate (GFR), increasing excretion and thus reduce circulating volume (Norsk, 1992) (Figure 1.3C).

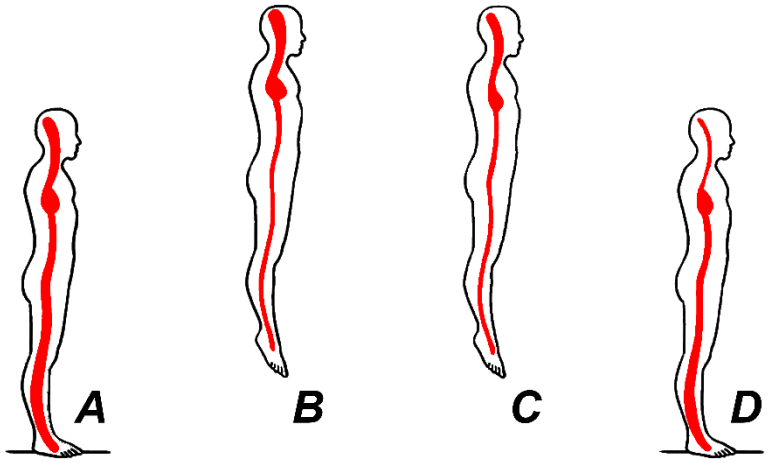

Figure 1.3 Schematic representation of blood volume fluid shift on Earth and in space. Adapted from Clément (2011).

A, Earth (pre-flight): with blood pooling in the lower extremities; **B**, Microgravity (immediate): fluid shifted towards the head; **C**, Microgravity (prolonged): overall volume reduced, relieving headward pressure; and **D**, Earth (post-flight): reduced volume shifted to the periphery.

Interestingly, a decrease in central venous pressure (CVP) has been observed despite a concurrent increase in left atrial diameter (Buckey *et al.*, 1996a). Subsequent research by Videbaek and Norsk (1997) demonstrated, during transient periods of microgravity, that interpleural pressure decreased to a greater extent than CVP; suggesting transmural CVP increases are in fact causing cardiac chamber distension. Furthermore, these increases may explain increased in-flight cardiac output (CO) of up to 41%, in adherence to the Frank-Starling law (Norsk *et al.*, 2015).

Spaceflight fluid shifts eventually reach a euvolemic state appropriate for weightlessness, where the rate of change subsides (Davis *et al.*, 2008) (Figure 1.1A); with little known about time-course of adaption during longer duration flights (> 6-months). Nevertheless, with the re-introduction of Earth's gravity after long-term

spaceflight, previous clinically irrelevant in-flight alterations now appear maladaptive (Figure 1.3D). Recent research has shown elevated headward pressures may, despite stabilised blood redistribution, induce irreversible pathological changes affecting visual acuity (Mader *et al.*, 2011). Additionally, microgravity-induced pressure increases, concurrent in venous and arterial vasculature, may affect cerebral hemodynamics; specifically, through an irreversible venous congestion initiated pathology cascade in space (Wiener, 2012).

1.1.3 Jugular venous congestion

Blood congestion in the jugular veins, as a direct result of hydrostatic gradient abolition in space, and the ensuing cephalic fluid shift, has been measured through quantification of internal jugular vein (IJV) distension in many astronauts (Grigoriev *et al.*, 2011; Arbeille *et al.*, 2015) (Figure 1.4). It has been suggested that microgravity induced venous congestion is the start of a cascade phenomenon, leading to increases in intracranial pressure (ICP) and intraocular pressure (IOP), and directly related to VIIP. Specifically, the mismatch between the two during spaceflight may be of importance to the aetiology of VIIP (Rowell, 1993; Watenpaugh & Hargens, 1996; Zhang, 2013). Approximately two thirds of returning astronauts have experienced degradation in visual acuity following long-term spaceflight; whilst, only one third have reported problems after a short-term flight (≤ 16 days) (Mader *et al.*, 2011). In general, astronaut visual problems get worse as a function of time spent in space; however, the role of venous congestion, and the effect this has on cerebral hemodynamics, and more specifically ICP and IOP remains unclear. Ground-based spaceflight analogues may

prove useful in elucidating the underlying mechanisms of VIIP; with previous research unable to replicate degradation in visual acuity on Earth.

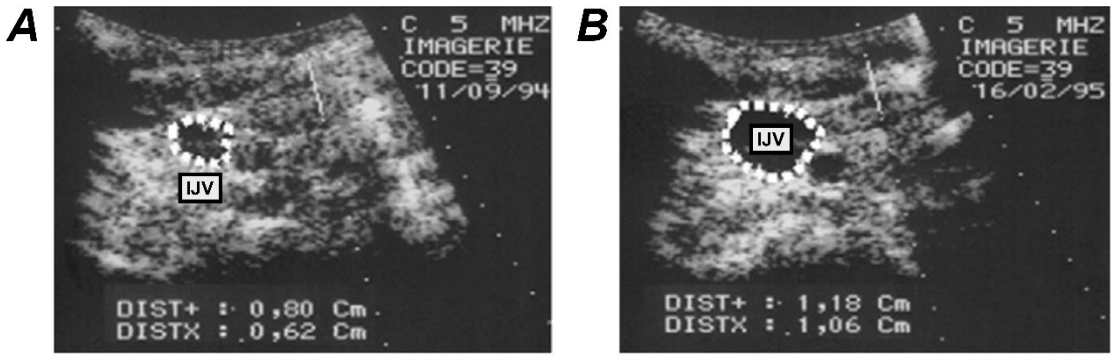

Figure 1.4 Ultrasound of right internal jugular vein (IJV) cross-sectional area (CSA) pre- and during spaceflight. Adapted from Grigoriev *et al.* (2011).

A, pre-flight recording; and **B**, during spaceflight (launch + 5 months). **IJV**, internal jugular vein. Russian cosmonaut data.

1.2 Spaceflight analogues

Access to space remains limited and to date there have been less than 600 astronauts in space examined physiologically (Clément, 2011). Mechanisms of spaceflight deconditioning can be simulated on Earth in order to investigate microgravity effects. However, no method is entirely effective without the universal unloading of weightlessness. Common techniques in humans include water immersion (Figure 1.5D), favoured by the Roscosmos State Corporation for Space Activities (Roscosmos), and head-down bed rest (HDBR) studies (Figure 1.5F) favoured by the National Aeronautics

and Space Administration (NASA) and the European Space Agency (ESA) (Watenpaugh, 2016).

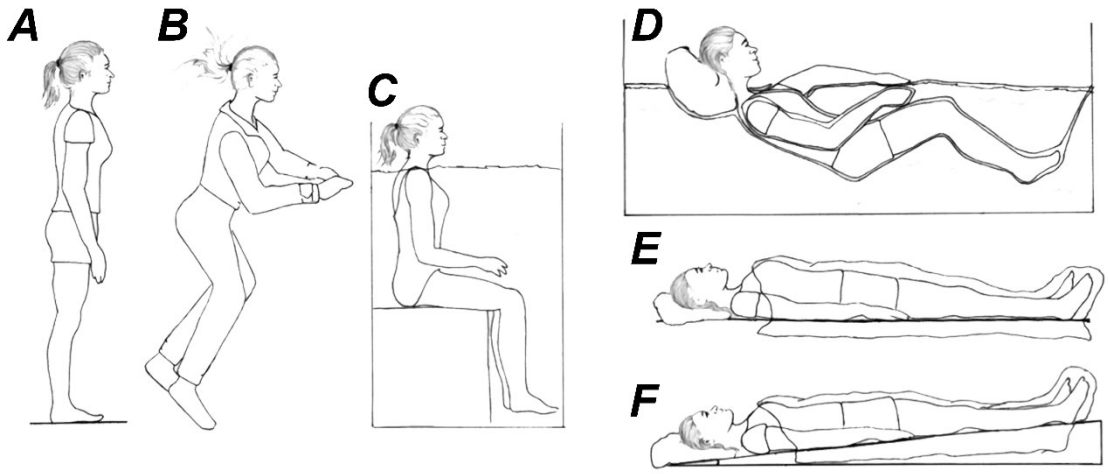

Figure 1.5 Different methodologies of simulated and actual weightlessness exposure. Adapted from Watenpaugh (2016).

A, upright standing posture on Earth; **B**, weightlessness in space; **C**, water immersion; **D**, dry immersion; **E**, horizontal bed rest; and **F**, -6° head-down bed rest (HDBR).

1.2.1 Head-down bed rest (HDBR)

Unloading achieved through bed rest is effective, at removing the daily gravitational forces experienced on weight bearing limbs, resulting in significant reductions in muscle mass (Akima *et al.*, 1997; Akima *et al.*, 2000; Kawakami *et al.*, 2000; Akima *et al.*, 2003) and bone density (Watanabe *et al.*, 2004; Rittweger *et al.*, 2005) in a similar manner to spaceflight. Headward fluid shifts are replicated by head-down tilt (HDT) and now specifically standardised to -6° HDT (Sundblad & Orlov, 2015). Combined

HDT and bed rest (HDBR) followed observations of a Russian scientist in returning cosmonauts who complained of a feeling they were “slipping off the foot of the bed” when lying down (Pavy-Le Traon *et al.*, 2007). Cosmonauts were tilted head-down in order to feel more comfortable when sleeping and it was thought perhaps HDBR was a better simulation of spaceflight. Research conducted at various HDT angles (-5 to -15°) concluded -6° was a suitable compromise between the most comfortable tilt with an acceptable magnitude of response similar to spaceflight (At'kov & Bednenko, 1992).

HDBR reduces muscle mass, aerobic capacity and plasma volume to a similar degree when compared to microgravity (Table 1.1). Therefore, the HDBR model is thought to simulate the physiological effects of spaceflight very well and remains the most common experimental technique with international standardisation guidelines in order to compare and contrast different HDBR datasets (Sundblad & Orlov, 2015). However, observations of VIIP syndrome during spaceflight have so far not been replicated by HDBR and it is postulated that a -6° tilt may be insufficient to replicate fluid shifts in totality. Furthermore, the discrepancy between HDBR and actual microgravity, in relation to visual acuity degradation, may prove useful in the discovery of new targets for improved spaceflight countermeasures.

Table 1.1 Comparison of physiological deconditioning in spaceflight and head-down bed rest (HDBR). Adapted from Nicogossian *et al.* (1994).

	Weightlessness (μG)	*Head-down bed rest (HDBR)*
Height	↑ ± 1.3 cm	↑ ± 1.0 cm
Body mass / weight	↓ 3-4 %	↓ 2-4 %
Maximal aerobic capacity	↓ 17-24 %	↓ 25 %
Plasma volume	↓ 10-15 %	↓ 10-15 %
Muscle mass	↓	↓
Muscle Strength	↓	↓
Nausea (mild to severe)	65%	10%
Visual problems (VIIP)	**50%**	**None**

1.3 Spaceflight countermeasures

On-board the ISS an intensive workout program is scheduled for each astronaut consisting of two hours aerobic/resistive exercise each day (Figure 1.6); however, significant reductions in muscular (Gopalakrishnan *et al.*, 2010), skeletal (Orwoll *et al.*, 2013), and aerobic capacity (Moore Jr *et al.*, 2014) have all been recently been observed. Current exercise regimes were developed with the aim of targeting specific weight bearing muscle groups, provide a re-introduction of ground-reaction forces, and maintain VO_2 max (Loehr *et al.*, 2015). However, spaceflight countermeasures on-board the ISS fail to directly reverse the cephalic fluid shift present in microgravity. It is postulated that combining current exercises, with a method to specifically reverse fluid shifts, would provide a holistic, and more efficient approach. Crucially, it may allow for reduced exercise duration, freeing up valuable crew time, with no degradation in physiological function.

Figure 1.6 Current spaceflight countermeasures on-board the International Space Station (ISS). Adapted from NASA (2013).

A, Combined Operational Load Bearing External Resistance Treadmill (COLBERT); **B,** Cycle Ergometer with Vibration Isolation and Stabilization System (CEVIS); **C,** Advanced Resistive Exercise Device (ARED).

Several other countermeasures have been explored in the past including thigh cuffs to prevent headward fluid shifts (Arbeille *et al.*, 1995; Herault *et al.*, 2000), altered nutrition to increase protein consumption (Lane *et al.*, 2013), fluid-loading before re-entry (Bungo *et al.*, 1985), pharmacological interventions to reduce bone loss (Leblanc *et al.*, 2013), and various in-flight suits to promote venous return (Kozlovskaya *et al.*, 1995) and prevent spinal elongation (Carvil *et al.*, 2017). Crucially, these countermeasures specifically target a particular body system/mechanism, when an integrated approach may be more resourceful and beneficial.

There is a growing trend for increased spaceflight duration that is evident from the recent one-year mission launched in March 2015 to the ISS (NASA, 2015a) and NASA's strategy of sending humans to Mars in the 2030s (NASA, 2015b). The inadequacies of current exercise regimes are likely to become more apparent with

increasing mission duration; and improved countermeasures with a holistic approach, such as artificial gravity (AG) may increase effectiveness.

1.4 Artificial gravity (AG)

The conceptual idea of AG has been around as long as the idea of manned spaceflight itself; with several futuristic suggestions on how gravitational forces can be created when absent, long before spaceflight negative health effects were fully known. In 1883 Konstantin Tsiolkovsky, the influential Russian space visionary, sketched a design for a "space vehicle" with AG created when running along the internal walls. Additionally, Tsiolkovsky discussed the possibility of "spinning space vehicles"; however, never lived to see his designs materialise. In the 1970s NASA commissioned an artist to visualise a "self-sustaining habitat with gravitational forces in space", with the result being a large rotating torus in which inhabitants lived on the outer edges (Figure 1.7). Current technological limitations render this concept virtually impossible; however, the basic principle of achieving gravitational force through centrifugation has persisted (Clement & Pavy-Le Traon, 2004). The use of a short-arm human centrifuge (SAHC, ~ < 3 m radius) is currently the most technically feasible, as opposed to long-arm human centrifugation (LAHC) in order to achieve AG in space, with all required hardware possible to launch in one payload (Clément & Bukley, 2007).

Figure 1.7 Artist's impression inside the Stanford Torus with a diameter of 1.8 km. Adapted from NASA (1976).

1.4.1 Short-arm human centrifugation (SAHC)

Centrifugal force generated by rotation during SAHC is likely to be used as an intermittent spaceflight countermeasure, in contrast to continual AG, and specifically tailored to an individual's orthostatic tolerance (Goswami *et al.*, 2015b). Repeated SAHC exposure has been shown to improve orthostatic tolerance on Earth (Iwasaki *et al.*, 1998) with similar expected observations in-orbit; however, empirical data confirming this has not yet been collected.

1.4.1.1 Force generation

SAHC presents a unique challenge to the body, with a smaller distance from the centre of rotation, leading to a greater difference in g-level between the head and foot. For a

SAHC of approximately 2 m radius the g-level would be ~0 +Gz at the head when ~2 +Gz is experienced at the feet; resulting in a gravitational gradient of >100% (Figure 1.8). Spaceflight headward fluid shift reversal can be elicited through generation of AG/centrifugal force (Yang *et al.*, 2007); however, the use of SAHC means greater angular velocity is required to achieve the same g-level (Equation 1.1i). Greater angular velocity increases the magnitude of Coriolis forces (Equation 1.1ii), which have been shown to induce neurovestibular disturbances and negatively affect g-tolerance (Hargens *et al.*, 2013). However, with the head at the centre of rotation and with no linear velocity ($v = 0$ m.s^{-1}) the Coriolis force is 0 G, despite a >100% g-level gradient ($G_{gradient}$) experienced across the body (Equation 1.1iii).

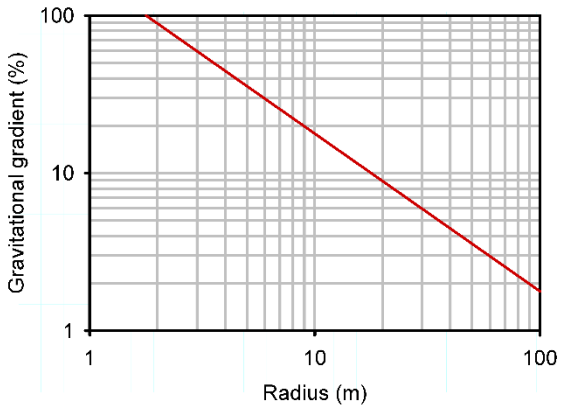

Figure 1.8 Gravitational gradient as a function of rotational axis position (RAP).

Radius from centre of rotation to foot (m). Plotted for average individual of 173 cm height with feet positioned outwards and expressed as a gradient from head to foot g-level.

$$AG_{foot} = \omega^2 r_{foot} \quad \text{(i)}$$

$$F_{Coriolis} = 2m\omega v \quad \text{(ii)}$$

$$G_{gradient} = 1 - \frac{\alpha_{head}}{\alpha_{foot}} = 1 - \frac{\omega^2 r_{head}}{\omega^2 r_{foot}} = 1 - \frac{r_{head}}{r_{foot}} \quad \text{(iii)}$$

Equation 1.1 Equations for forces generated during short-arm human centrifugation (SAHC).

Where $\mathbf{AG_{foot}}$, artificial gravity level at foot (+Gz); $\boldsymbol{\omega}$, angular velocity (rad.s^{-1}); $\mathbf{r_{foot}}$, radius to foot (m); $\mathbf{v}$, linear velocity (m.s^{-1}); and $\mathbf{r_{head}}$, radius to head (m).

1.4.1.2 Future implementation

Various proposals have been made to implement SAHC in space, including the most recent Artificial Gravity with Ergometric Exercise (AGREE) project (Figure 1.9). However, prohibitive costs and insufficient vibration isolation disruption in the microgravity environment has meant no SAHC has ever flown (Clément & Bukley, 2007).

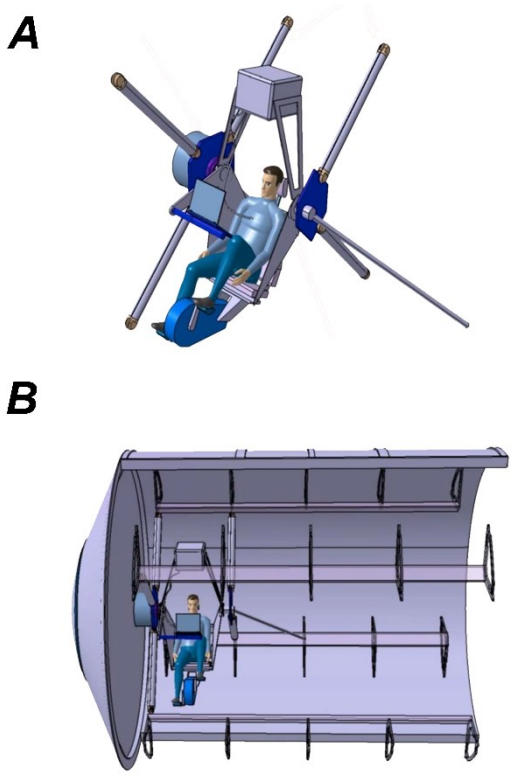

Figure 1.9 Proposed Artificial Gravity with Ergometric Exercise (AGREE) project in the permanent multipurpose module (PMM). Adapted from ESA (2011).

A, AGREE hardware segment; **B,** installed into one of four slots in the PMM.

The potential countermeasure benefit of SAHC in space would likely be further increased when combined with daily exercise. Specifically, exposing weight-bearing limbs to gravitational loading, with concurrent fluid shifts, may prove synergistic; and lower-limb muscle-pump activation would increase venous return, g-tolerance, and thus safety (Diaz *et al.*, 2015).

1.5 Orthostatic challenge

Any prolonged orthostatic challenge inducing central hypovolemia will eventually lead to syncope. This remains the case so long as the legs are passive and fluid shifted to the periphery is allowed to accumulate free from activation of the lower limb muscle-pump (Miller *et al.*, 2005). When blood is redistributed in healthy individuals towards the legs, there is a decrease in cardiac return (cardiac pre-load), cardiac filling pressure and cardiac output (CO). With normal regulatory capability, arterial pressure at heart-level remains unaltered or even slightly increased. Cerebral autoregulation acts to prevent hyper- or hypo-perfusion of the cerebral tissue under differing orthostatic challenge. For mean arterial pressure (MAP) changes within the 50-150 mmHg range, cerebral perfusion remains relatively constant. However, prolonged orthostatic challenge is likely to disrupt the normal regulatory capabilities (Claydon *et al.*, 2005). Once disrupted, relatively small changes in MAP may have a greater effect on cerebral perfusion and thus lead to pre- or total syncope.

There are several ways to elicit varying degrees of central hypovolemia experimentally. These include the following orthostatic challenges: (i) venous cuff occlusion (VCO; simulated); (ii) long- and short- arm human centrifugation (L- and SAHC), also termed artificial gravity (AG); (iii) head-up tilt (HUT); and (iv) lower-body negative pressure (LBNP).

1.5.1 Hydrostatic gradients

On Earth, venous and arterial pressures vary greatly across the body and with postural changes (Figure 1.10); and, immediately upon entering microgravity the hydrostatic gradient is abolished.

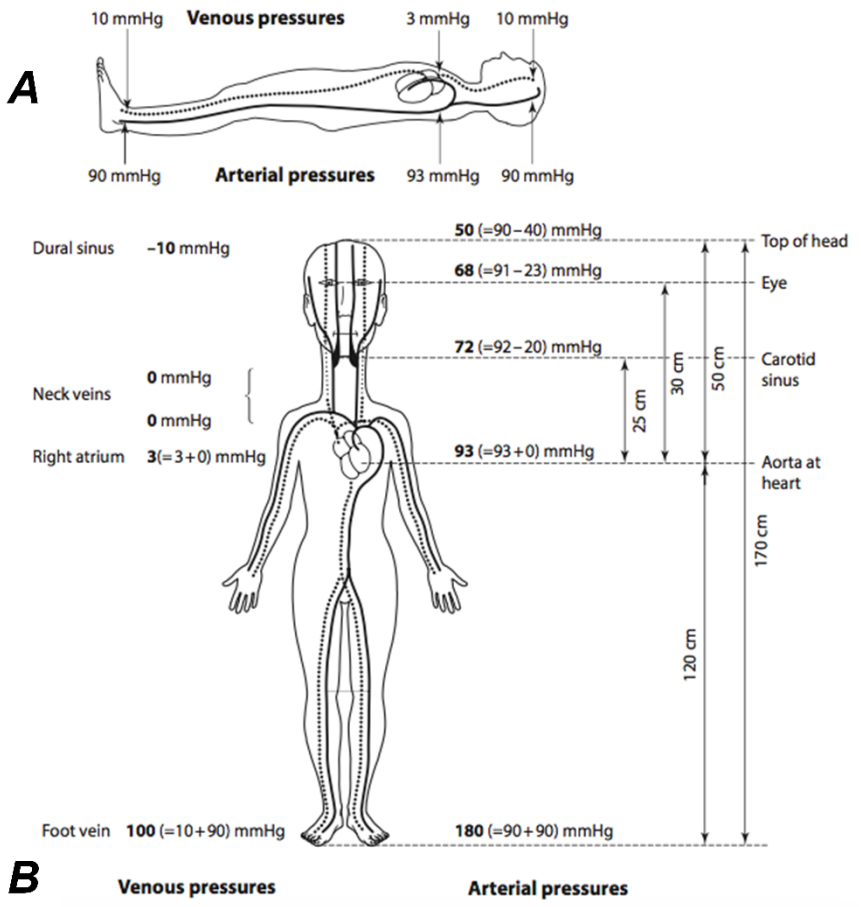

Figure 1.10 Venous and arterial pressures across the body when standing and supine. Adapted from Gradwell and Rainford (2016).

A, supine; and **B,** standing. **Solid line**, arterial vasculature; and **dotted lines**, venous vasculature.

Without gravity acting on the central blood column, arterial pressure equalises in a similar manner to supine; however, pressure changes on the venous side are less clear and provide topic for debate. Central venous pressure (CVP) has been shown to decrease in the initial moments of microgravity exposure despite a concurrent increase atrial diameter (Buckey *et al.*, 1996a); potentially explained by a greater comparative interpleural pressure decrease (Videbaek & Norsk, 1997). Cardiac chamber distension, as a result of this increased transmural CVP, has been shown to increase microgravity stroke volume (SV) (Norsk *et al.*, 2015). Paradoxically, spaceflight sympathetic nervous activity does not change (Levine *et al.*, 2002; Christensen *et al.*, 2005) or is even increased (Norsk *et al.*, 2015), despite an immediate decrease in systemic vascular resistance (Norsk & Christensen, 2009) increasing systemic vasodilation (Norsk *et al.*, 2006). Furthermore, the role of hydrostatic gradient removal is not fully understood but, with the cephalic fluid shift and increased CO, may exacerbate venous congestion and have a disruptive effect on cerebral hemodynamics.

1.5.2 Cerebral hemodynamics

Little research exists into the effect of spaceflight on cerebral hemodynamics and in particular the regulation of cerebral blood flow (CBF). CBF is measured using a transcranial Doppler (TCD) device, typically measuring flow in the middle cerebral artery (MCA) of both or one cerebral hemisphere. There are several conflicting findings with regards to CBF and cerebral blood blow velocity (cBFV). Data from astronauts early on in flight have shown no change in cBFV (Bagian & Hackett, 1991; Iwasaki *et al.*, 2007). Similar observations were made by Arbeille *et al.* (2001) and also a concurrent increase in common carotid artery blood flow; however, after 1 week and 3

months in space, cBFV was found to be no different from pre-flight values. It is likely CBF increases at the start of spaceflight, returning to pre-flight values after 1-week, assuming cerebral vasculature remains constant. However, there has been no research directly measuring cerebral blood vessel diameter in spaceflight and it is likely significant changes occur which may affect cerebral autoregulation.

Cerebral autoregulation acts to maintain suitable cerebral blood flow (CBF) despite altered cerebral perfusion pressure (CPP) (Strandgaard & Paulson, 1984; Aaslid *et al.*, 1989; Paulson *et al.*, 1989; Panerai, 1998). Specifically, a change in mean arterial blood pressure (MAP), within a normal range of 50-150 mmHg (Figure 1.11), has been shown to elicit a rapid autoregulatory response within 2-5 seconds, in order to maintain CBF (Folino, 2007; Gradwell & Rainford, 2016). Therefore, suitable cerebral perfusion, despite postural changes possibly transiently affecting MAP, can be maintained.

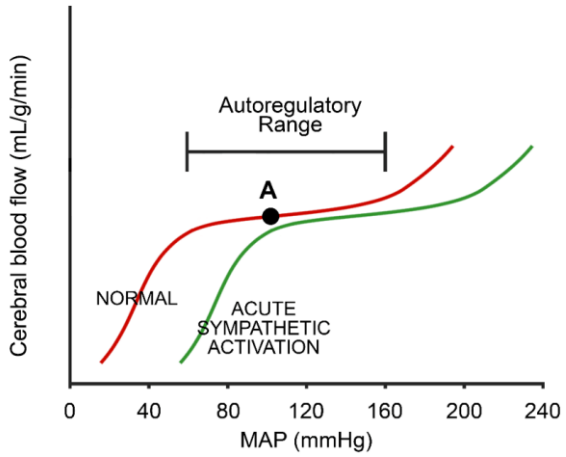

Figure 1.11 Cerebral autoregulation curve. Adapted from Lassen (1959)

Red line, representing normal cerebral autoregulation to changing mean arterial pressure (MAP); **green line,** autoregulatory curve shifted to the right with acute sympathetic activation. This shift helps to protect the brain from the damaging effects of elevated pressure; and **A**, normal physiological operating point.

More generally, the control of CBF is complex and multifactorial (Willie *et al.*, 2014). In addition to cerebral autoregulation, where CBF is buffered with changes in blood pressure (Lassen, 1959), two other contributory concepts have been suggested. Firstly, the metabolic regulation of CBF which is centred on the high sensitivity of brain perfusion to altered arterial partial pressures of CO_2 (P_aCO_2). Research using transcranial Doppler (TCD) of the middle cerebral artery (MCA) shows an approximate 3-6% increase and/or 1-3% decrease to increasing/decreasing P_aCO_2, respectively (Ide *et al.*, 2003; Battisti-Charbonney *et al.*, 2011). Finally, the role of the sympathetic nervous system (SNS), with the entire cerebrovasculature innervated by adrenergic and cholinergic fibres throughout (Willie *et al.*, 2014). Research has shown the extensive sympathetic activation of the larger cerebral arteries is especially important in providing sufficient buffering to large transient increases in perfusion pressure (Cassaglia *et al.*, 2008a, b; Ainslie, 2009; Tzeng *et al.*, 2010).

Surprisingly, Iwasaki *et al.* (2007) demonstrated preservation of human cerebral autoregulation, in six astronauts following a 16-day mission, with a suggestion it may even have been improved. However, a caveat to these findings was that all astronauts tested did not experience post-flight OI; and the implication of these findings on common post-flight development of OI remains unclear. More recent research has shown that microgravity exposure may possibly disrupt cerebral autoregulation and it has been suggested impairment may explain a greater incidence of OI in returning astronauts (Blaber *et al.*, 2011; Zuj *et al.*, 2012). Blaber *et al.* (2011) examined 27 astronauts from shuttle missions lasting 8 to 16 days and crucially examined autoregulatory response in two groups: (i) astronauts able to complete a 10 min post-

flight stand test; and (ii) those unable. It was found astronauts unable to complete a stand test, indicative of post-flight OI, displayed impaired cerebral autoregulation; perhaps contributing to the reduced orthostatic tolerance. Nevertheless, these findings were during short-term missions and the effects of altered cerebral hemodynamics during long-term spaceflight requires further research.

Different orthostatic challenges elicit various degrees of fluid shifts, through several possible mechanisms, and it is postulated that autoregulation may be differentially affected by orthostatic challenge type. When taken in isolation, VCO reduces lower-limb outflow whilst arterial inflow is maintained; thus, increasing localised peripheral fluid shifts with minimal systemic primary stimulus. This is in contrast to SAHC which involve changes to the gravitational gradient across the body. Therefore, altered hydrostatic gradients, within the arterial and venous vasculature, are likely to have a resultant effect on cerebral autoregulation. Specifically, it is postulated discrepancies in fluid shift mechanisms, between spaceflight and HDT, may differentially affect emergence of internal jugular vein (IJV) congestion; with a significant effect on cerebral hemodynamics (Figure 1.12).

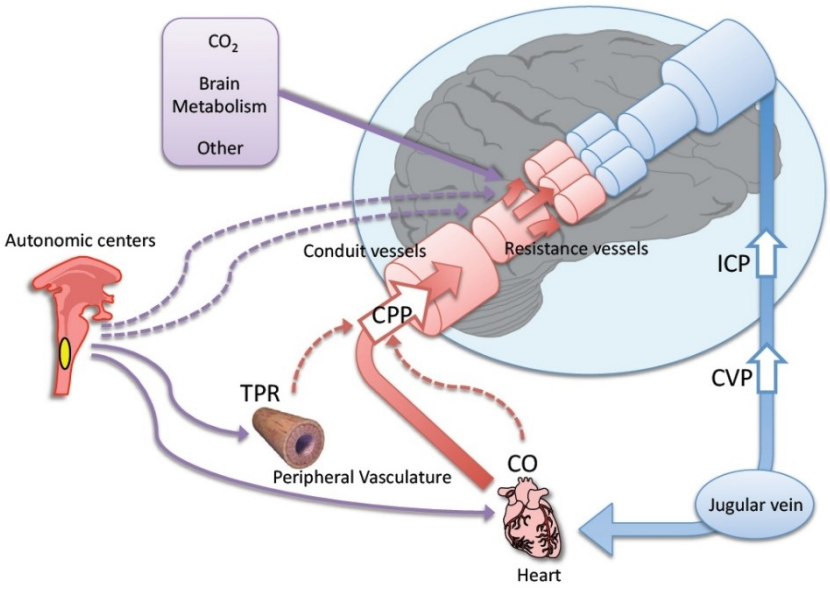

Figure 1.12 Schematic overview of cerebral autoregulation cascade.

ICP, intracranial pressure; **CVP**, central venous pressure; **CPP**, cerebral perfusion pressure; **TPR**, total peripheral resistance; and **CO**, cardiac output. Adapted from Tzeng (2012).

Transient microgravity with parabolic flight has been shown to immediately increase CBF and it is postulated that changes in systemic arterial resistance and/or increased intracranial pressure (ICP) may contribute to greater CBF (Bondar *et al.*, 1990). Additionally, elevated ambient pCO^2 levels in the confined environment of a spacecraft may have a contributory role in increased CBF, through altered ICP (Hughson *et al.*, 2016).

There is less agreement in the literature for HDT research. CBF during -6° HDT has both been shown to increase (Kawai *et al.*, 1993), decrease (Frey *et al.*, 1993; Arbeille *et al.*, 2001; Hirayanagi *et al.*, 2005; Sun *et al.*, 2005), and stay the same (Zhang *et al.*, 1997; Arbeille *et al.*, 2001; Traon *et al.*, 2002). It has been suggested measured CBF

variances are due to different HDT durations (Blaber *et al.*, 2013b); however, we postulate that interindividual anatomical differences in venous vasculature, and specifically the IJV, possibly exhibit a causative effect. Anatomical differences may place an individual under greater susceptibility due to an inflow/outflow mismatch (Wilson *et al.*, 2011). Little is known about venous drainage of cerebral tissue; however, idiopathic intracranial hypertension, with visual acuity degradation similar to VIIP (Suzuki *et al.*, 2001), exhibit similar venous insufficiencies akin to congestion (Wilson *et al.*, 2011). There is an indication of a link between peripheral and central fluid shifts to venous congestion and cerebral hemodynamics; however, direct concurrent measurements during orthostatic challenge have yet to be made.

1.6 Aims and hypothesis

The principle objective of this thesis is to characterise the role of orthostatic challenge induced blood volume shifts on central, peripheral, and cerebral hemodynamics; and based on this, to assess the suitability of future holistic spaceflight countermeasures.

Experiments detailed in this thesis will use four types of orthostatic challenge, namely venous cuff occlusion (VCO); short-arm human centrifugation (SAHC); head-down tilt (HDT); and lower-body negative pressure (LBNP) to manipulate circulating volume from central to peripheral compartments and vice versa. VCO induced fluid shifts will be determined in relation to orthostatic challenge magnitude. SAHC, with multiple rotational axis positions (RAP) across the body, will be investigated in an attempt to understand whether an altered hydrostatic gradient affects systemic response, and cerebral hemodynamics.

In addition, due to the lack of knowledge of venous congestion importance in cerebral hemodynamics, this thesis will investigate headward fluid shifts on Earth in an attempt to understand the underlying mechanisms involved in venous congestion associated visual acuity pathology in space.

Hence, the studies reported in this thesis aim to investigate: (i) VCO induced fluid shift effects, on systemic cardiovascular response, and quantifying central blood relocation importance to orthostatic challenge; (ii) to determine the effect of an altered gravitational gradient, as an orthostatic challenge, on central, peripheral, and cerebral response; and finally (iii) to evaluate the importance of venous congestion in microgravity and spaceflight analogues; and assess suitable amelioration methods.

The unifying hypothesis of these studies is:

Orthostatic challenge induced peripheral fluid shifts offer protection to headward pressure increases and cerebral hemodynamics, by restoring hydrostatic gradients to Earth-like upright norms.

2 MATERIAL AND METHODS

2.1 Experimental methods

The focus of this thesis is the headward and peripheral fluid shifts that occur in response to different simulated and actual orthostatic challenges. Several differing methodologies were employed to manipulate participant compartmental fluid shifts (central and peripheral), with the associated systemic, peripheral, and cerebral hemodynamic responses recorded.

2.1.1 Bilateral lower-limb venous cuff occlusion (VCO)

Manufacturer: SC12D (13 x 85 cm), Hokanson Inc., Bellevue, WA, USA.

Venous cuff occlusion (VCO) sequentially reduces venous outflow with increasing pressures whilst arterial inflow is maintained. As a non-invasive method, this posed minimal risk to the subjects and, whilst participants were asked to remain still and silent throughout, they were also encouraged to vocalise any discomfort felt (see section 2.5.1).

VCO is a mechanical method to shift fluid to the periphery and can be classed as a 'simulated' orthostatic challenge. Namely, VCO has the ability to alter hemodynamics independent of postural or gravitational changes across the body. External pressure was applied to both limbs, at the proximal end of the thigh (Figure 2.1), using a 13 cm lower-limb cuff and digitally controlled pressure valve for accuracy. Use of a high-pressure gas canister ensured each VCO level could be delivered rapidly (< 10 s) and safely. Furthermore, incremental cuff pressures were used to stratify volume shifted to the periphery.

Figure 2.1 Example bilateral lower-limb venous cuff occlusion (VCO) applied to the proximal end of the thigh. Credit: occlusioncuff.com.

Additionally, cuff size has been shown important (Loenneke *et al.*, 2011) and in the present study kept the same for all individuals, as was the positions at the most proximal end of the thigh.

2.1.2 Short-arm human centrifugation (SAHC)

Manufacturer: Custom-built, AMST Systemtechnik GmbH, Ranshofen, Austria.

The German Aerospace Center (DLR) custom-built short-arm human centrifuge (SAHC) was completed in 2013 (Figure 2.2). After operational, safety, and functional tests the research carried out as part of this thesis was the first full-scale utilization of the newly built hardware. The unique modular design allowed for an increase in the mass capacity of measurement devices and made SAHC experimentation with large mass devices possible. Furthermore, maximum angular velocity was 38 rpm allowing for a sufficient g-level to be delivered, to the feet when supine, even with a small radius

(Table 2.1). An ability to alter the center of rotation, and thus the gravitational gradient experienced across the body, was crucial to this part of data collection.

Figure 2.2 Short-arm human centrifuge (SAHC) at the German Aerospace Center (DLR) :envihab in Cologne.

Table 2.1 German Aerospace Center (DLR) short-arm human centrifuge (SAHC) dimensions and performance.

G, g-level; **CW**, clockwise; **CCW**, counter-clockwise; **AC**, alternating current; and **DC**, direct current.

Radius	0 – 380 cm (at outside perimeter)
Radial acceleration	6 G (maximum)
Angular velocity	4 rad/s (~ 38 rpm)
Maximum angular acceleration	0.133 rad/s^2 from 0 – 6 G in 30 s
Spinning direction	CW and CCW
Noise level	< 40 dBA
Power distribution	115 / 230 V (AC) and 12 / 24 V (DC)

The participant was secured safely to the centrifuge by a parachute harness and suspended on the nacelle in a bicycle seat to ensure they remained as passive as possible, without lower-limb 'muscle-pump' activation.

2.1.2.1 Associated risks

The centrifuge run, at the maximum g-levels used (2.4 +Gz) can potentially cause orthostatic hypotension. If so, the test can lead to a fall in heart rate and blood pressure, paleness, sweating, and sometimes also to nausea, vomiting and in rare cases gravitational loss of consciousness (GLOC) (Whinnery & Whinnery, 1990). An altered gravitational gradient, due to a change in rotation axis position (RAP), produces a unique orthostatic challenge across to the body. This stimulus, and the specific hemodynamic response to it, forms the focus of part of the research; with a greater challenge likely providing a clearer difference between changing gravitational gradients. However, challenge intensity must be balanced against participant safety and complete hemodynamic collapse. The present SAHC experimental set-up and profiles are based on an extensive literature review and own investigations within our research group and institute.

During prolonged SAHC, the response of the autonomic nervous system is not sufficient to prevent a peripheral fluid shift, maintain venous return to the heart, cardiac output and ultimately cerebral perfusion (Grasser *et al.*, 2009). Present research is aimed to specifically determine the limitations of SAHC protocols, and response to differing gravitational gradients, that could be used in future spaceflight settings.

Should hypotension or one of the termination criteria (see section 2.1.5) occur the centrifuge would be immediately stopped, which promptly normalises the circulation state. The test will also be aborted with the emergence of a severe presyncopal episode, based on the professional opinion of the study physician. However, if need be, measures necessary to maintain cardiorespiratory function during these experiments can be carried out, with reanimation facilities on standby. Additionally, heart rate and blood pressure were continuously monitored and trained personnel, together with a physician skilled in cardiopulmonary resuscitation (CPR), were present if needed.

Prior to experimentation on the centrifuge a venous cannula was inserted into the arm of each participant in case of an emergency. Whilst no specific protocols involving the venous cannula were planned, this pre-emptive measure allowed for a faster emergency response time, by negating the need to locate a vein, if intravenous fluids were required.

2.1.2.2 Additional SAHC measurements

The integrity of the expected g-level was monitored using a tri-directional accelerometer at foot level (SS26LB, Biopac Systems, Goleta, CA, USA), with specific heart-level +Gz values calculated for each participant. Integral hardware monitoring produced data files at the end of experimentation which included centrifuge revolutions per minute (RPM), temperature, and mechanical torque produced.

At all times an infrared camera was pointed at the participant's head, chest, and face to monitor signs of presyncope, continuous blood pressure device placement, and leg muscle-pump activation, respectively. All camera feeds were recorded and catalogued for further analysis if the collection of anomalous data warranted it.

2.1.2.3 Operational personnel

During experimentation the participant was sealed and safety locked inside the centrifuge spin area. Lights were turned off and the participant monitored on infrared camera by personnel in the adjacent control room (Figure 2.3). All experimental hardware was either fixed onto multiple shelves in the moving centrifuge arm or wirelessly connected through Bluetooth to the control room.

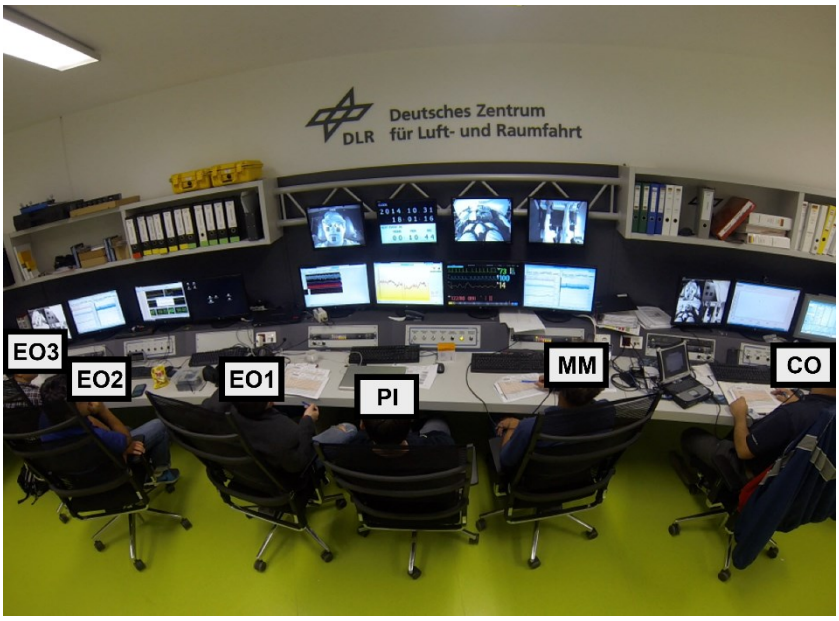

Figure 2.3 Short-arm human centrifuge (SAHC) control room with operator stations for scientists, doctors, and engineers.

EO1-3, experimental operators 1 to 3; **PI**, principal investigator; **MM**, medical monitor (physician); and **CO**, centrifuge operator.

2.1.3 Electronic head-down/up tilt-table (HDT and HUT)

Manufacturer: Custom-built, Medical University Graz, Graz, Austria.

The electronic tilt-table at *:envihab* German Aerospace Center (DLR; Figure 2.4) is fully programmable to deliver precise, reproducible angles of tilt in a desired timeframe. Participants were sufficiently held in place due to the ribbed, rubberized surface, preventing slippage during angles of head-down tilt (HDT) to -30°. Furthermore, the ability to tilt without any harness prevents shoulder discomfort and potential interference of physiological responses.

Figure 2.4 Electronic tilt table installed at :envihab German Aerospace Center (DLR) in Cologne. Credit: DLR, 2014.

2.1.3.1 Associated risks

HDT, especially at steeper angles, may produce discomfort and an unusual feeling of "facial fullness" and it was possible participants would have experienced a mild

headache. However, upon returning to a supine position this sensation was expected to resolve itself and any HDT was immediately terminated if requested. During other studies within our research group, severe back pain has been experienced but for a much longer duration (up to four hours) than the current study duration. It was therefore anticipated at a maximum HDT of -24° for five minutes would be tolerable. The maximum angle of tilt is an increased divisible multiple of the currently used -6° HDT. -18° was deemed sufficient from the literature but -24 tested to ensure a further response could be quantified; whether that was an expected plateau, in terms of fluid shifted from the periphery, or an increase in the headward fluid shift.

2.1.3.2 Additional HDT/HUT measurements

Each protocol on the electronic tilt table was fully programmed prior to experimentation and a record of each profile catalogued for further use. Additionally, room temperature, precise tilt angle and time were synchronised for reference.

2.1.4 Lower-body negative pressure (LBNP) chamber

Manufacturer: Custom-built, German Aerospace Center (DLR), Cologne, Germany.

The lower-body negative pressure (LBNP) chamber is a custom-built, temperature, humidity, and pressure-controlled device. This hardware is integrated for use with the electronic tilt-table simultaneously and was run from the same programmable script. Participants were inserted into the chamber and distance/height adjusted to ensure a comparable portion of the body was exposed to the pressure and therefore response; as this has been shown to affect cardiovascular response (Goswami *et al.*, 2009).

Participants were sealed into place using a neoprene 'skirt' to achieve a suitable pressure seal and lower-body movements could be visually monitored through the transparent Perspex dome (Figure 2.5).

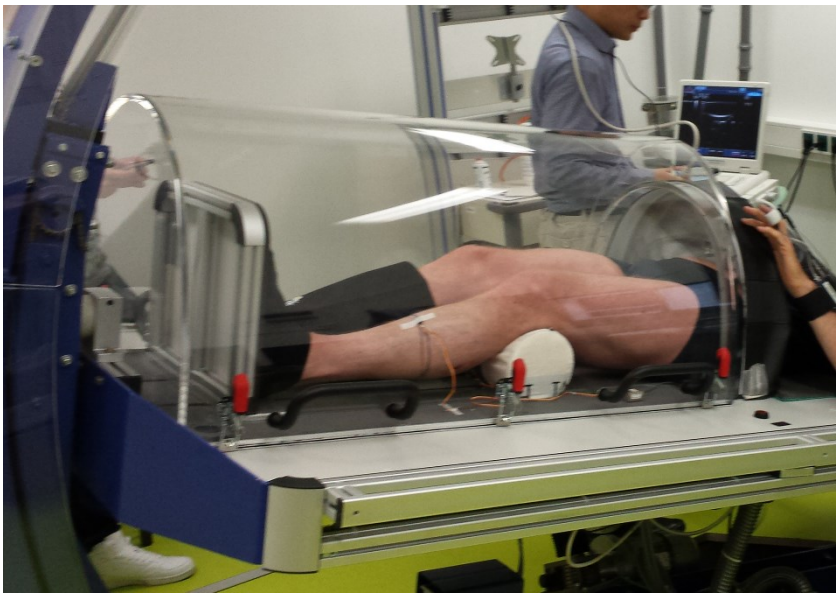

Figure 2.5 Lower-body negative pressure (LBNP) transparent Perspex chamber.

2.1.4.1 Associated risks

The LBNP device run can potentially cause orthostatic hypotension. Prolonged LBNP may lead to a fall in heart rate and blood pressure, paleness, sweating, and sometimes also to nausea, vomiting and in rare cases (at only -40 mmHg) loss of consciousness. Due to the reduced pressure in the periphery, and a localised stimulus, the response of the autonomic nervous system may eventually lead to a failure in maintaining venous return to the heart, cardiac output and ultimately cerebral perfusion (Levine *et al.*,

1994). However, the experimental set-up is based on an extensive literature review, and current research group experience in the institute, further minimising the risks.

If hypotension or one of the termination criteria (see section 2.1.5) occur the LBNP device would be immediately stopped and the tilt table angle returned to supine, which would promptly normalises the circulation state (Van Lieshout *et al.*, 2003). Additionally, any test would be aborted if the medical doctor deemed it necessary through the emergence of a visible presyncopic episode. Measures necessary to maintain cardiorespiratory function during these experiments can be carried out with reanimation facilities on standby. Furthermore, heart rate and blood pressure were continuously monitored by trained personnel, together with a physician skilled in cardiopulmonary resuscitation (CPR), to perform any medical interventions if needed.

2.1.4.2 Additional LBNP measurements

Similar data to the electronic tilt table is collected and catalogued on the same file, but with the addition of LBNP chamber temperature, humidity, and pressure at a given time.

2.1.5 Orthostatic challenge termination criteria

Unless the subject directly requests the cessation of centrifugation/LBNP, the medical monitor will determine a stopping point if the subject displays presyncopal signs. These signs could be subjective: grey-out, head vacuum feeling, daze feeling, omnidirectional vertigo, sudden sensation of heat, nausea, sweating, non-responsiveness; as well as objective: a systolic blood pressure drop-off > 15mmHg, and/or a sudden decline in heart rate > 15 bpm, or a sustained tachycardia > 1 min > 90% maximum age-predicted

heart rate. An overview of the termination criteria in which the medical doctor on duty will follow is outlined and summarised below in three main classes:

2.1.5.1 Significant cardiac arrhythmia

a. Supraventricular or ventricular tachycardia;
b. Indication of atrioventricular node conduction blockade (AV-blockade > Degree I);
c. Premature ventricular contractions (PVCs) that correspond to any one of the following criteria:
    i. 6 or more PVCs per minute;
    ii. Prematurity index $[(Q_{Normal\ beat} - Q_{PVC})/QT\ time_{Normal\ beat}] < 0.9$ (R-on-T phenomenon);
    iii. PVCs which occur repeatedly ($> 2\times$) in couplets or in salvos (≥ 3);
    iv. Polymorphous PVCs.

2.1.5.2 Haemodynamic criteria

a. Decrease in the continuously recorded mean arterial blood pressure by 40% of the baseline value in supine position or to values < 60 mmHg without increase in heart rate within 10-sec;
b. Increase in heart rate to > 70% of the maximum heart rate over 10-sec;
c. Decrease in heart rate to < 50% of the plateau heart rate in the first minute after the tilt maneuver or to rates of < 50/min over 10-sec;
d. A continuous decrease in heart rate and mean arterial blood pressure over 15-sec or the achievement of a minimum value for one or both parameters.

2.1.5.3 Clinical criteria

a. Nausea, pronounced sweating, paleness, dizziness, paraesthesias;
b. Angina pectoris;
c. Slow auditory response.

2.2 Cerebral measurements

2.2.1 Transcranial Doppler (TCD)

Manufacturer: DWL Multi-Dop T digital, Compumedics GmbH, Singen, Germany.

Transcranial Doppler (TCD) ultrasound provides a non-invasive method for examination of the intracranial arteries measuring the velocity of blood flowing through the cerebral vasculature. The TCD device was securely attached to the participant's forehead (via an elastic strap) causing no discomfort (Figure 2.6).

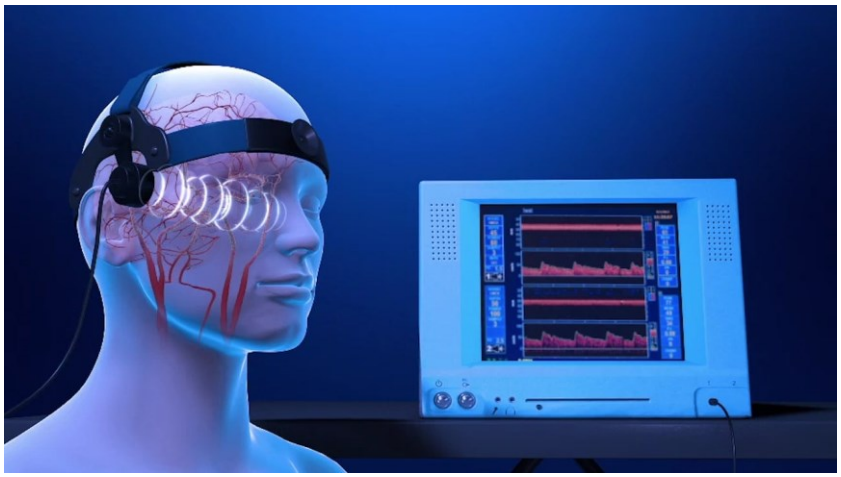

Figure 2.6 Transcranial Doppler (TCD) device focused on the middle cerebral artery (MCA) to determine cerebral blood flow velocity (cBFV). Credit: Cedars-Sinai Medical Center.

Mean cerebral blood flow velocity (cBFV) of the middle cerebral artery (MCA) was measured, through either the right or left temporal window, with 4 MHz pulsed transcranial Doppler ultrasound (Compumedics GmbH, Singen, Germany). A major

limitation of the TCD method is that the measured velocity being used to provide an inference on cerebral flow is based on an assumption of constant/unchanging diameter of the MCA (Purkayastha & Sorond, 2012).

The temporal window was determined to produce the best signal during pre-testing and used on all test days. The analogue signals from these devices were recorded simultaneously, with other synchronised data, using multi-channel hardware and software (MP100, Biopac System Inc., CA, USA). Beat-by-beat analysis of these data was performed offline.

2.2.2 Cerebral near-infrared spectroscopy (cNIRS)

Manufacturer: PortaLite, Artinis Medical Systems, Einsteinweg, The Netherlands.

The PortaLite device, uses near-infrared spectroscopy (NIRS) to measure local cerebral tissue saturation as well as oxyhemoglobin (O_2Hb), deoxyhemoglobin (HHb), and total hemoglobin (THb) concentrations. Jobsis (1977) demonstrated that biological tissues were relatively transparent to near-infrared light (700-1300 nm) making it possible to non-invasively measure changes in the light absorption properties of hemoglobin as the main innate chromosphere. If the absorption is known, the chromosphere's absorption can be calculated using the Beer-Lambert law (Equation 2.1i). However, this applies only to a transparent non-scattering medium and a correction factor must be applied for a scattering medium. A modification of the Beer-Lambert law, using a differential pathlength factor (DPF), allows for the increase in optical pathlength as a result of scattering that occurs in body tissue (Equation 2.1ii). Equation 2.1ii remains valid for a

medium consisting of one chromophore; however, when measuring O_2Hb, HHb, and THb several wavelengths need to be utilised concurrently (Figure 2.7).

$$OD_\lambda = \log\left(\frac{I_o}{I}\right) = \varepsilon_\lambda \cdot c \cdot L \qquad \text{(i)}$$

$$\Delta c = \frac{\Delta OD_\lambda}{\varepsilon_\lambda \cdot L \cdot DPF} \qquad \text{(ii)}$$

Equation 2.1 Equations of optical density and chromophore concentration for calculating near-infrared spectroscopy (NIRS) measurements.

(i), Lambert-Beer law; and **(ii)**, Lambert-Beer law for a scattering medium. Where $\mathbf{OD_\lambda}$ is the optical density of the medium; $\mathbf{I_o}$ is the incident light; **I**, transmitted light; $\boldsymbol{\varepsilon_\lambda}$ the chromophore extinction coefficient (in $\mu M^{-1}.cm^{-1}$); **c**, chromophore concentration (μM); **L**, distance between entry and exit points (cm); and **λ** wavelength used (nm).

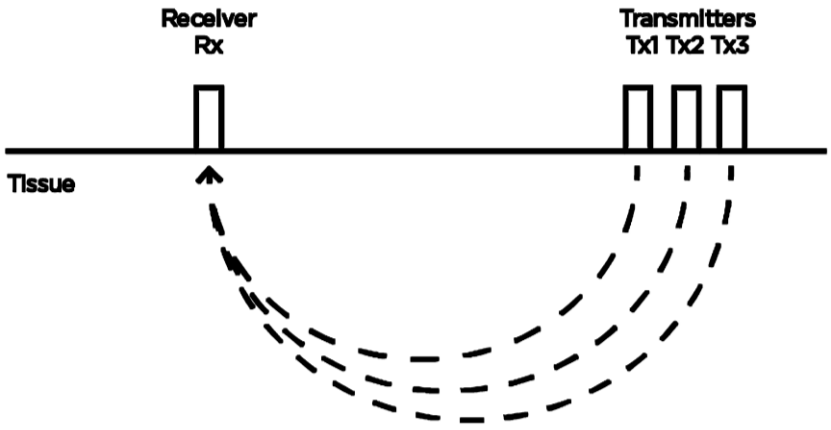

Figure 2.7 Schematic of transmission and absorption, of near-infrared light wavelengths (700-1300 nm), in a scattering medium. Adapted from Artinis Medical Systems.

The PortaLite separated probe is small, non-invasive and easy to attach (Figure 2.8) and operated using dedicated Oxysoft software (V6.0, Artinis Medical Systems, The Netherlands). It was attached to the participant's forehead on the right-side, using adhesive tape, and prior to fixation the area was cleaned with a mild abrasive and alcohol. At the start of experimentation the Oxysoft software allowed for the real-time quality check of signal integrity and the input of participant age, which has been shown to affect cranium thickness (Yoshitani *et al.*, 2007) and therefore NIRS readings. The PortaLite has three light sources and is therefore capable of measuring tissue saturation index (TSI), which is an absolute measure of O_2Hb and the favoured overall measure in previous studies (Matcher *et al.*, 1995; Naulaers *et al.*, 2007; Murkin & Arango, 2009).

Figure 2.8 Prefrontal cortex cerebral near-infrared spectroscopy (NIRS) consisting of emitter and receiver attached to the participant forehead. Credit: Artinis Medical Systems.

This method requires accurate measurement of rapid changes in arterial O_2Hb concentrations by a NIR spectrometer; with limitations of this monitor contributing to errors in measurement of perfusion and the calculated TSI (Elwell *et al.*, 1992). Additionally, measured changes in O_2Hb concentration do not differentiate between arterial inflow and venous outflow and there is an assumption of a steady-state in O_2 consumption of the cerebral tissue being measured (Pellicer & del Carmen Bravo, 2011). Reproducibility of measured results is highly dependent on placement of the light probes; with pictures taken between measurements on different days and placement of the probe on one day was unmoved to mitigate against this. An index of perfusion (TSI) was used to measure changes experienced over a given period as opposed to absolute values.

2.2.3 Internal jugular vein (IJV) cross-sectional area (CSA) ultrasonography

Manufacturer: MyLab Gamma, Esoate SpA, Genoa, Italy.

Ultrasonography is a common imaging technique used across medical fields to image organs and tissues. Boundaries between tissues, using high frequency sound waves and their echoes, can be imaged; as can changes in venous cross-sectional area (CSA) (Bellazzini *et al.*, 2009). Ultrasound was performed on the internal jugular vein (IJV) to evaluate venous distention through CSA quantification as evidence of congestion (Figure 2.9).

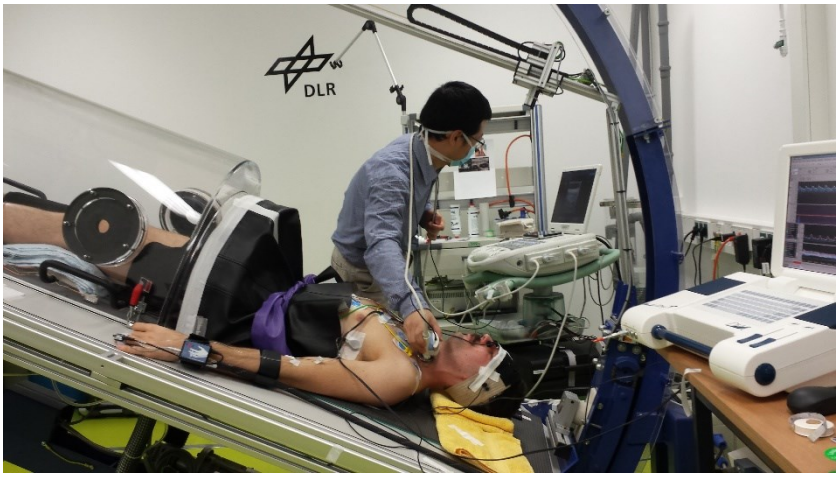

Figure 2.9 Internal jugular vein (IJV) cross-sectional area (CSA) determination using ultrasonography.

The jugular vein section was measured on B-mode echographic transversal views of the neck at the cricoid level parallel to the clavicle. The probe was placed at an angle of approximately 90° on the participant's neck as lightly as possible and large amounts of ultrasonic gel was used to avoid significant venous compression and/or change the shape and dimension of the vein. The use of surplus gel also ensured the absence of black cones and dark areas in the images. Short video sequences were stored and offline measurements, of the pulse-triggered maximal right and left IJV-CSA, were made using the manual area trace function of the machine (MyLab Gamma, Esoate SpA, Genoa, Italy).

2.3 Peripheral measurements

2.3.1 Strain gauge plethysmography (SGP)

Manufacturer: SC6 with Indium-Gallium gauges, Hokanson Inc., Bellevue, WA, USA.

To date, strain gauge plethysmography (SGP) is a valuable non-invasive, practical and low-cost tool for assessing volumetric changes, for instance during venous compliance and orthostatic testing experiments. In the present study, strain gauges were fixed around the calf midpoint (directly between the tibiae tuberosity and medial malleolus bony prominences) and then stretched to a standard tension, so that any increases in circumference would be encompassed within the linear part of the strain gauge range (Figure 2.10).

Changes in calf volume result in a corresponding change in calf circumference and thus strain gauge length, which is detected as an alteration in electrical resistance of the gauge and thus potential difference. Since the gauge length is made equal to the resting circumference of the limb, any changes in gauge resistance are related to the changes in limb volume during orthostatic challenge (Equation 2.2). Crucially, the strain gauges used were calibrated using the custom-built calibration tool described below.

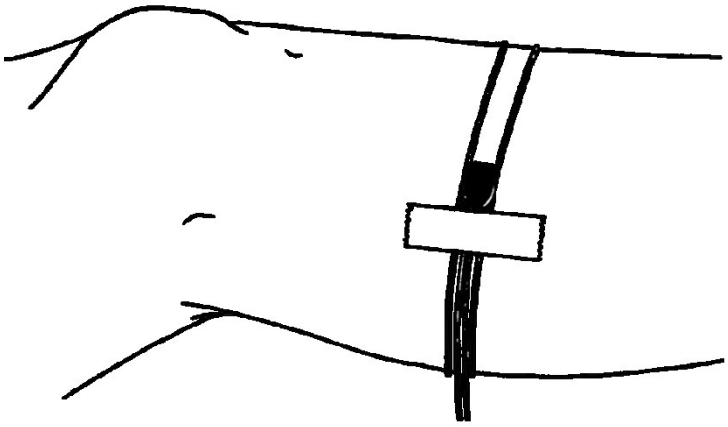

Figure 2.10 Strain gauge plethysmography (SGP) attached to calf mid-point. Credit: Hokanson Inc.

$$V_1 = \pi \left(\frac{1}{2\pi}\right)^2 h \qquad \text{(i)}$$

$$V_2 = \pi \left(\frac{1+C}{2\pi}\right)^2 h \qquad \text{(ii)}$$

$$\frac{V_2 - V_1}{V_1} = \frac{\left(\pi \left(\frac{1+C}{2\pi}\right)^2 - 0.0796\right).100}{1} \qquad \text{(iii)}$$

Equation 2.2 Calculation of volumetric peripheral fluid displacement percentage increase from calf circumference percentage increase.

(i), leg volume before VCO; **(ii)**, leg volume after VO; and **(iii)**, leg volume percentage increase due to VCO. Where ***C*** is the measured percentage increase in calf circumference.

2.3.1.1 Gauge calibration

Manufacturer: Custom-built, German Aerospace Center (DLR), Cologne, Germany.

The gauge calibration device was designed to encompass all calf circumferences to provide a specific two point calibration for each participant. Additionally, 26 grooves were milled 13 mm apart and to a depth of 3 mm, matching precisely the diameter of the Indium-Gallium gauges (Figure 2.11). Each milled groove was of a known circumference and, based on machine precision (German Aerospace Center, Cologne, Germany), accurate to the nearest one hundredth of a millimeter (± 0.01 mm).

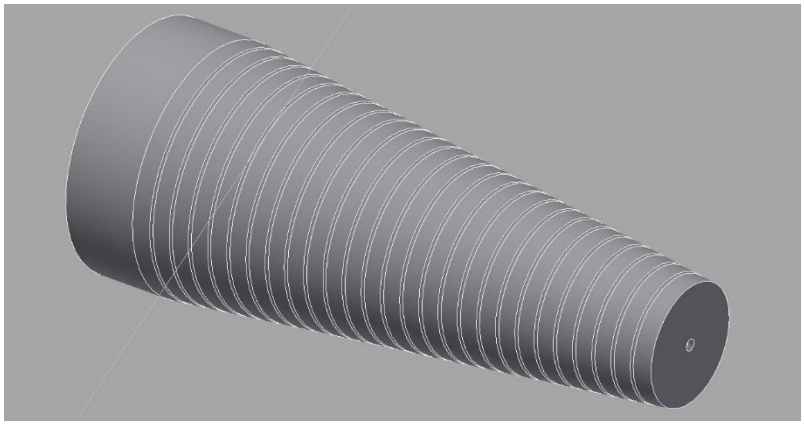

Figure 2.11 Custom-built strain gauge plethysmography (SGP) calibration device for absolute circumference determination.

Computer aided design (CAD) with decreasing circumference (of known size) up the funnel shaped rod. Final device was precision cut on a lathe out of Polymethyl methacrylate (PMMA) acrylic cylinder (diameter: 200 x width: 400 cm).

On experimentation day each participant's calf midpoint was roughly determined using a standard tape measure and two circumferences on the calibration tool selected for the two point calibration. After calibration, the gauge was transferred to the participant for the duration of testing. Finally, following experimentation the gauge was transferred back to the cone to ensure there had been no deviation in the initial calibration.

2.3.2 Muscle near-infrared spectroscopy (mNIRS)

Manufacturer: PortaMon, Artinis Medical Systems, Einsteinweg, The Netherlands.

Muscle NIRS (mNIRS) was used to assess localised calf tissue saturation index (TSI) and relied upon similar technology described in section 2.2.2. The PortoMon is a slightly larger device, than what was used to assess cerebral TSI, and without the corrective algorithm for cranium thickness (Yoshitani *et al.*, 2007). The device was fixed to the medial head of the gastrocnemius muscle belly using adhesive tape and a light-blocking, black covering. Prior to fixation the area was shaved, cleaned with a mild abrasive, and rubbed with alcohol. Data was continuously collected using Oxysoft software (V6.0, Artinis Medical Systems, The Netherlands), with cNIRS as an additional channel, and synchronised by networked time to other parameters.

2.4 Systemic measurements

2.4.1 Heart rate and continuous blood pressure

Manufacturer: Finometer, Finapres Medical Systems, Enschede, The Netherlands.

Systolic, diastolic and mean arterial blood pressure (MAP) and pulse pressure (PP) were measured using the Finometer device. The Finometer is a non-invasive device for measuring continuous blood pressure on the second phalanx of the second and/or third finger of either hand. The current systolic/diastolic pressures were measured with the help of a cuff containing an integrated pressure and volume sensor placed on the finger phalanx. As part of this process a pulse pressure graph was recorded, the maxima and minima of which correspond to the systolic and diastolic blood pressures. Specifically, the volume of blood in the finger arteries, over the entire cardiac cycle, was determined by a cuff pulse oximeter and kept constant by a matched resultant counter-pressure (Figure 2.12). Constant blood volume over time results in a finger cuff pressure that equals the intra-arterial pressure and can be corroborated by a standard medical sphygmomanometer.

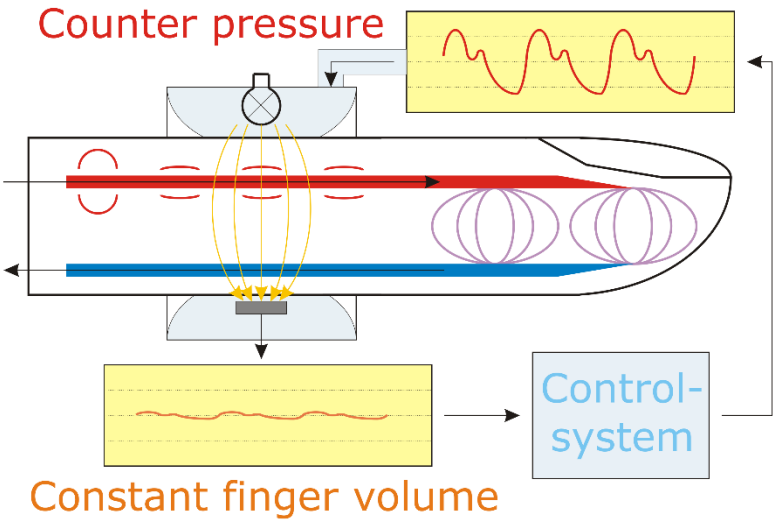

Figure 2.12 Vascular unloading technique used by the Finometer device to measure continuous beat-by-beat blood pressure and heart rate. Credit: ProfBondi CC-BY-SA 3.0.

2.4.2 Additional measurements

From the continuous signal, beat-to-beat systolic, diastolic, pulse pressure and mean blood pressure was recorded, as well as model flow estimates for beat-to-beat cardiac output (CO), stroke volume (SV) and total peripheral resistance (TPR), as described by Wesseling *et al.* (1993).

2.5 Discomfort and presyncopal symptoms (PSS)

2.5.1 Discomfort definition

At any point during bilateral lower-limb venous cuff occlusion (VCO) each participant was encouraged to remain still and silent unless experiencing discomfort. Any instance of participant registering pain associated to the occlusion pressure was recorded.

Participants were separated into those experiencing discomfort (PAIN+) and those not (PAIN-), at a particular VCO level.

2.5.2 PSS definition

During each SAHC run, a participant was classified as having experienced presyncopal symptoms (PSS+) if, during the run or post-run offline analysis, they satisfied any one or more of the criteria in sections 2.5.2.1 and 2.5.2.2. However, a participant was recorded as not having experienced presyncopal symptoms (PSS-) if none of the five conditions were met.

2.5.2.1 Hemodynamic criteria (post-run, offline script)

a. MAP decrease >40% of baseline supine value;
b. MAP <60 mmHg without HR increase in 10 s;
c. Continuous decrease in HR and MAP over 15 s.

2.5.2.2 Clinical criteria or participant withdrawal (during-run, recorded)

a. Nausea, pronounced sweating, paleness, dizziness, paresthesia;
b. Immediately on participant request.

2.6 Participant selection & medical monitoring

2.6.1 Participant selection

A total of 45 participants (23 male; 22 female) were recruited and took part in at least one of the main studies and gave their written informed consent to participate. Selected participants were physically active, healthy, non-smoking and normotensive and required to pass a medical screening for participant safety reasons. The medical

screening process is outlined below and similar to that of a commercial pilot (see section 2.6.1.1); with participants also required to satisfy the following inclusion (see section 2.6.1.2) and exclusion criteria (2.6.1.3).

2.6.1.1 Medical screening

The medical screening examination consists of a clinical-chemical blood analysis consisting of: glucose, creatinine, urea, uric acid, serum glutamic oxaloacetic transaminase (SGOT), serum glutamic pyruvic transaminase (SGPT), serum gamma glutamyl transferase (γ-GT), total cholesterol (high density lipoprotein, HDL; and low density lipoprotein, LDL), and haematology (blood count). Further analysis included: urine (glucose, protein, urobilinogen), resting electrocardiogram (ECG), adapted Bruce Protocol with cycle ergometry to verify appropriate aerobic fitness (for age and gender) and cardiac function (Bruce *et al.*, 1963), standing test for orthostatic tolerance assessment, and a medical history. Female volunteers additionally had to test negative on a standard pregnancy test before each experiment.

Tests for HIV and hepatitis B and C were carried out. Before these tests, all participants were advised about the possible consequences of a positive test result. In the case of a hepatitis infection (in Germany), we would present a report including the name of the participant to the Health Department. In the case of an HIV infection, an anonymous report would be submitted and affected participants advised to seek further guidance from their regular doctor.

2.6.1.2 Inclusion criteria

All of the following inclusion criteria were satisfied in order to participate:

a. Healthy male or female participants aged between 20 and 45 years old;
b. Mass: 65-85 kg;
c. Height: 158-190 cm;
d. Body Mass Index (BMI) of 20-26 kg/m^2;
e. Not a competitive athlete;
f. Non-smoker, for at least six months before the start of the study;
g. In the position to participate in the complete study;
h. Demonstrable social insurance and official certificate of absence of criminal record;
i. Successful completion of screening examination;
j. Provision of Declaration of Consent at the start of the study.

2.6.1.3 Exclusion criteria

If any one of the following conditions were true then a participant was excluded:

a. Drug or alcohol abuse (regular consumption of 20-30 g alcohol / day);
b. Smoking;
c. Obesity (BMI > 26);
d. Diabetes mellitus;
e. Muscle or joint diseases;
f. Herniated disc;
g. History of epileptic seizures;
h. Heart disease or a cardiac pacemaker;
i. Severe orthostatic intolerance or impaired neurovestibular function;
j. Chronic back pain;
k. Pregnancy;
l. Any other condition deemed unsuitable by the Medical Director for study inclusion.

2.6.2 Medical monitoring

Throughout the experiment, intervallic systolic (SBP) and diastolic blood pressure (DBP) was measured by oscillometry (IntelliVue MMS X2, Amsterdam, Netherlands) on the upper arm. The blood pressure measurements served to medically monitor all participants.

Continuous recording of the ECG and heart rate were made via a 3-lead attached to the chest. Participants were observed throughout by the medical monitor who observed strict adherence to the defined orthostatic challenge termination criteria (see section 2.1.5).

2.7 Data handling

2.7.1 General study design

The VCO study (first) consisted of incrementally increasing occlusion pressures with the repetition of -60 mmHg, at the end, to assess reproducibility. However, the SAHC and HDT±LBNP studies (second and third) were entirely randomised (random.org, 2016) meaning experimental conditions experienced were completely different between participants. All experiments within this thesis took the format of an orthostatic challenge, of various types and length, followed by a recovery period in order for hemodynamic responses to return to baseline. The parameters outlined above fall into one of three categories: cerebral, peripheral, and systemic hemodynamic measures; and all were continuously recorded during baseline, challenge and recovery.

Data for each main study were collected on one session apart from the second study (SAHC) which was spread over two months. Multiple sessions were exactly one month apart to ensure responses to the orthostatic challenge were unaffected by women participant's menstrual cycle. Additionally, all studies as part of this thesis conformed to the declaration of Helsinki and was approved by the Ethics Committee of the North Rhine Medical Association in Düsseldorf, Germany (lfd. Nummer 2014123 and 2015381).

2.7.2 Statistical approaches

*Software:G*Power (Erdfelder et al., 1996); R (R Foundation for Statistical Computing, Vienna, Austria) and lme4 (Bates et al., 2012); and Matlab (R2015a, The Mathworks Inc., MA, USA).*

Power calculations, with cerebral tissue saturation index (cTSI) as the key end-point, were carried out using G*Power. After data collection, all continuously recorded data were analysed and processed in accordance with a custom Matlab script. Specifically, the following processes were carried out: (i) removal of implausible physiological data points (Table 2.2); (ii) removal of maximal percentage change in relation to the standard deviation of the signal; and (iii) data resampled at 4Hz (piecewise cubic spline interpolation) assuming >95% data integrity.

R (R Foundation for Statistical Computing, Vienna, Austria) and *lme4* (Bates *et al.*, 2012) were used to perform linear mixed effect (LME) analysis of the relationship between cardiovascular parameters and the time course of each orthostatic challenge. Furthermore, 2 and 3-way interactions were entered into the model with intercepts for

each participant as a random effect, with secondary models incorporating participant sex to explore gender effects. P-values were obtained by likelihood ratio tests of the full model with the effect in question, against the model without that effect.

Table 2.2 Implausible physiological data limits of all measured parameters; for data processing, using a custom-made Matlab script.

TCD, transcranial Doppler: cerebral blood flow velocity; **cNIRS**, cerebral near-infrared spectroscopy (NIRS): cerebral tissue saturation index; **SGP**, strain-gauge plethysmography: calf circumference; **mNIRS**, calf muscle NIRS: muscle tissue saturation index; **HR**, heart rate; **MAP**, mean arterial pressure; **SV**, stroke volume; and **TPR**, total peripheral resistance.

	Lower limit	Upper limit
Central		
TCD	> 5 $cm.s^{-1}$	< 100 $cm.s^{-1}$
cNIRS	> 50 %	< 100 %
Peripheral		
SGP	> 100 mm	< 400 mm
mNIRS	> 50 %	< 100 %
Systemic		
HR	> 20 bpm	< 220 bpm
MAP	> 20 mmHg	< 155 mmHg
SV	> 20 mL	< 200 mL
TPR	> 300 $dyn.s.cm^{-5}$	< 3000 $dyn.s.cm^{-5}$

Matlab (R2015a, The Mathworks Inc., MA, USA) was also used to perform statistical analysis. Visual inspection of residual plots did not reveal any obvious deviations from homoscedasticity or normality of residuals. The tests applied were one-way analysis of variance (ANOVA, repeated measures), post hoc tests with preventative post hoc control of the type I error rate (Tukey's Honestly Significant Difference, HSD) and t-

test (independent, by groups). Linear and non-linear regression analysis was used to estimate the relationships among variables. Additionally, hemodynamic responses between groups were compared, for all participants, using Bland-Altman plots (Bland & Altman, 1986) and reproducibility was quantified as the standard deviation of the difference between both groups. The data are presented as mean (±SEM) unless otherwise stated with the level of significance set at $p \leq 0.05$.

3 BILATERAL LOWER-LIMB VENOUS CUFF OCCLUSION AS A SIMULATED ORTHOSTATIC CHALLENGE AND ITS EFFECT ON CENTRAL HYPOVOLEMIA AND CEREBRAL TISSUE OXYGENATION

3.1 Introduction

Fluid shifted to the lower extremities, coupled with insufficient venous return, gives rise to orthostatic intolerance (OI) which is characterised as an inability to maintain adequate cerebral perfusion (Van Lieshout *et al.*, 2003). Healthy individuals during a prolonged orthostatic challenge, or those with a deconditioned cardiovascular system, are most susceptible to OI. Around half of all returning astronauts suffer from OI on return to Earth's gravity (Buckey *et al.*, 1996b) due to one of the four following hypotheses: (i) reduced circulating blood volume; (ii) increased vascular compliance; (iii) cardiac hypo-function; and (iv) alterations in baroreflex function. Additionally, reduced functioning of the otolith system has been shown to prevent blood pressure stability during an orthostatic challenge (Hallgren *et al.*, 2015); and this presents as a potential target, as a driver of the autonomic reflex, to mitigate OI (Yates & Bronstein, 2005). Periodic exposure to venous cuff occlusion (VCO) may ameliorate OI if it is able to effectively challenge the cardiovascular system and thus prevent deconditioning. An orthostatic challenge without a sufficient response will lead to eventual syncope, thus repeated challenge to the cardiovascular system must be balanced against a safe level of exposure.

VCO is routinely used diagnostically to assess reactivity of vasculature, through altered perfusion pressures of occluded limbs, and evaluate general health of blood vessels (Hull *et al.*, 1976; Wilkinson & Webb, 2001). Occlusion with plethysmography is a well-established technique, capable of detecting small volume increases to accurately record blood flow non-invasively (Litter & Wood, 1954). Limiting venous blood flow,

whilst maintaining unaltered arterial flow, leads to an increase in volume of the occluded limb which can be measured using a fluid filled plethysmograph (Figure 3.1).

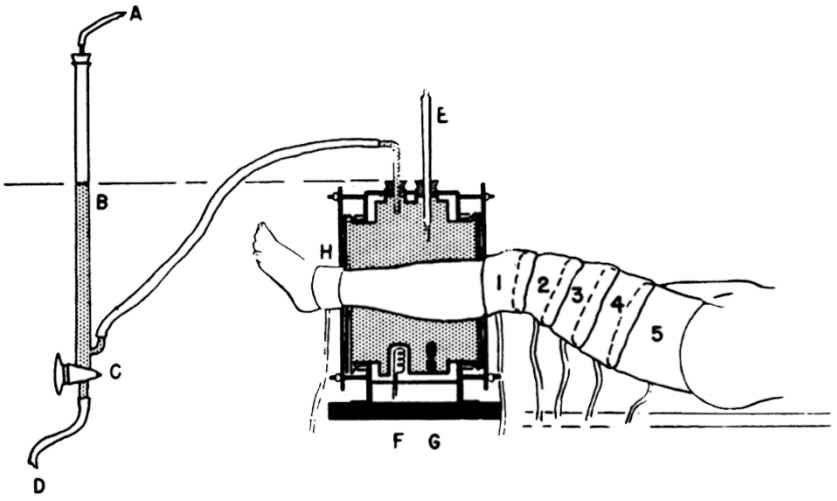

Figure 3.1 The Burette-plethysmograph apparatus used by Litter and Wood (1954) to explore the effects of graded external pressure on volume and distribution of blood in the leg.

A, pressurising valve; **B**, water fluid column; **C**, opening stopcock; **D**, drainage tube; **E**, thermometer, **F**, electric heater; **G**, propeller, **H**, narrow blood pressure cuff; and **1,2,3** and **4**, multiple pressure cuffs along thigh.

VCO elicits a mechanical movement of blood without an actual change in position or force along the limbs or body. As such, VCO may be used to experimentally simulate an orthostatic challenge, with minimal systemic influences, by rapid fluid relocation. Sarin *et al.* (1992) demonstrated a mean external cuff pressure of ~110 mmHg was required to entirely occlude both deep and superficial venous vasculature; even though internal venous pressures were likely much lower. However, Groothuis *et al.* (2003) suggested external occlusion pressures from 30 mmHg to expected diastolic pressure

(80 mmHg) elicited the greatest arterial inflow; with pressures above this potentially also compressing arteries.

Factors shown to affect internal pressures, elicited by VCO, include calf circumference (Loenneke *et al.*, 2011) and cuff width (Loenneke *et al.*, 2012); with other research suggesting inter-individual differences can be resolved by basing occlusion pressures on individual systolic blood pressure (SBP) (Cook *et al.*, 2007). Utilisation of VCO, as a simulated orthostatic challenge, requires the consideration of potential diminished internal pressures from externally applied VCO. Therefore, VCO pressures required to elicit total venous occlusion are likely greater than the measured mean resting lower-limb venous pressure of ~95 mmHg; which has also been shown to have large inter-individual variability (Kügler *et al.*, 2001). VCO pressures from 0 to above, and not far beyond 95 mmHg, are likely to sequentially affect arterial filling in all individuals. Specifically, for the purposes of attempting to simulate an orthostatic challenge, an upper occlusion pressure must not exceed the limiting point where arterial flow begins to be impeded.

3.1.1 Orthostatic challenge

Whilst VCO is not an orthostatic challenge *per se* it affords the ability to shift fluid, in a similar manner to alterations of body position from lying to upright, from one body compartment to another (central to peripheral). Healthy individuals maintain suitable blood pressure during an orthostatic challenge through sensitive baroreceptors feedback response to small changes in blood pressure affecting the stretch stress of carotid and aortic regions (Gabrielsen *et al.*, 1996; Pump *et al.*, 2001). Crucially acting to maintain

blood pressure within acceptable parameters (50-150 mmHg) and ensuring sufficient cerebral perfusion is achieved in agreement with the cerebral autoregulation curve (Figure 1.11). However, Giller *et al.* (1992) demonstrated a significant reduction in cerebral blood flow during, lower-body negative pressure (LBNP) induced, normotensive central hypovolemia. It is clear the relationship between mean arterial pressure (MAP) and cerebral blood flow is important; however, the autoregulatory response may not entirely explain the complex relationship between blood pressure and cerebral hemodynamics during orthostatic challenge.

Disruption of this innate process directly challenges the limits of individual homeostatic capability. VCO as a localised challenge elicits peripheral fluid shifts to the detriment of central blood volume; and central hypovolemia, without other systemic mechanisms playing a part, is likely to affect cerebral hemodynamics. Any deviations, from expected cerebral autoregulatory responses, may provide an insight into the ability of VCO to simulate an orthostatic challenge.

3.1.2 Peripheral fluid displacement

Blood shifted outside of the central compartment, sequestered in the periphery or splanchnic circulation, has been shown to impede mechanisms responsible for maintaining sufficient cerebral tissue oxygenation (Van Lieshout *et al.*, 2003). A universal characteristic of an orthostatic challenge is progressive central hypovolemia; however, the role of the splanchnic circulation in this fluid relocation shows a diametric response between LBNP and HUT (Taneja *et al.*, 2007). Taneja *et al.* (2007) demonstrated splanchnic blood pooling and emptying during HUT and LBNP

respectively but, despite these findings, both postural challenges resulted in similar reductions in central volume. Similarly, increased sympathetic outflow has been shown during both long- and short-arm human centrifugation (LAHC and SAHC) leading to splanchnic bed constriction (Blomqvist & Stone, 1983). These findings demonstrate a corrective mechanistic response to prevent clinically significant central hypovolemia, maintain blood pressure, and ultimately preserve cerebral perfusion.

Within the literature, peripheral fluid shifts were estimated and compared based on published individual mean data (Clauser *et al.*, 1969); with an assumption of total circulating blood volume (~5000 mL) segmented with 15% in the lower periphery (Karpeles & Huff, 1955) and 30% in the central compartment (Nylin & Celander, 1950). Several studies and methodologies, reporting percentage change in fluid volume in either region, were compiled and calculated based on the mean individual assumption.

The estimations of fluid shifted to the periphery, during different orthostatic challenges, revealed similar values between altered challenge magnitudes in a sit-to-stand (STS) test, head-up tilt (HUT), and graded SAHC with cycle ergometry. Fluid displacement from central to peripheral compartments was measured by thoracic impedance and estimated at: ~217 mL following 5 min STS (Frey *et al.*, 1994), ~192 mL after 30 min HUT to 53° (Laszlo *et al.*, 2001), and ~203 mL after 25 min 1.2 +Gz graded SAHC with exercise (Iwase, 2005).

The volumes of fluid shifted under different orthostatic challenges differ greatly from one another as does tolerance (Watenpaugh *et al.*, 2004); however as shown,

comparable fluid shifts may be elicited when exposure magnitude is adjusted between differing challenge types. These calculated estimations indicate either: (i) volume shifted is more important than challenge type; or (ii) large changes in fluid displacement, along with challenge type, is affecting tolerance.

VCO involves a purely passive mechanical stimulus whereby fluid accumulation is elicited without concurrent input from other body systems. Specifically, blood redistribution occurs without any altered forces across the body or postural change. A better understanding of VCO induced hemodynamic responses, and the role of fluid displacement, on Earth may prove beneficial in the development of future effective and safe occlusion-based spaceflight countermeasures. However, the effect of VCO induced peripheral fluid shifts on cerebral hemodynamics remain unclear.

3.1.3 Cerebral hemodynamics

During an orthostatic challenge fluid is shifted towards the periphery and, under insufficient cardiovascular control eventual, syncope occurs. Immediately prior presyncopal symptoms are experienced, which are characterised by a significant drop in cerebral blood flow and localised cerebral oxygenation.

Cerebral hemodynamics are measured in many ways including transcranial Doppler (TCD), magnetic resonance imaging (MRI), and transcranial cerebral near-infrared spectroscopy (cNIRS). cNIRS is outlined in several studies as an appropriate key measure indicating orthostatic tolerance in healthy participants (Krakow *et al.*, 2000) and patients with sympathetic failure (Harms *et al.*, 2000). In normal healthy individuals, cerebral hemodynamics should remain fairly constant; however, under

significant challenge or prolonged central hypovolemia clinically relevant and measurable cerebral oxygenation reductions occur (Van Lieshout *et al.*, 2003).

The present non-invasive study was conducted in order to contribute towards a better understanding of cardiovascular responses to a simulated orthostatic challenge of VCO (up to 120 mmHg); with an inference on its suitability as an intermittent spaceflight countermeasure. Fluid shifted to the periphery is discussed considering the relationship between systemic and cerebral hemodynamics, and contrasted to previously published classical orthostatic challenge responses.

3.1.4 Aims

The aim of this study was to assess the effect and reproducibility of bilateral lower-limb venous cuff occlusion (VCO), at pressures up to 120 mmHg (0, 20, 40, 60, 80, 100 and 120 mmHg), in simulating an orthostatic challenge whilst supine. Changes in systemic (heart rate, HR; and mean arterial pressure, MAP), peripheral (calf circumference, CC; and calf muscle tissue oxygenation, mTSI), and cerebral (cerebral oxygenation, cTSI) measurements, to increasing occlusion pressures, were compared to baseline (BL, 0 mmHg). To assess reproducibility of VCO responses, specific occlusion pressure measurements were performed twice.

3.1.5 Hypothesis

It was hypothesised that five minutes bilateral lower-limb VCO would show a directly proportional relationship, of significant increases, in systemic cardiovascular response and fluid shifted to the periphery. Secondly, cerebral tissue oxygenation would reduce

in response to increasing occlusion pressures and be proportional to fluid shifted to the periphery. Furthermore, it was postulated that VCO induced responses would be reproducible in relation to systemic, peripheral, and cerebral hemodynamics.

3.2 Methods

3.2.1 Study design and participants

Nine (5 male) healthy normotensive, non-smoking participants (Table 3.1) gave written informed consent to participate in the study that conformed to the declaration of Helsinki and was approved by the Ethics Committee of the North Rhine Medical Association in Düsseldorf, Germany.

Table 3.1 Participant individual data.

Age on first experimental day; height and weight measured immediately before centrifuge run.

	Sex	*Age (yrs)*	*Height (m)*	*Weight (kg)*	*BMI (kg/m²)*
P01	M	25.8	1.83	76	22.7
P02	F	26.7	1.69	56	19.5
P03	M	28.5	1.79	80	25.1
P04	F	27.1	1.61	62	23.7
P05	F	23.8	1.70	59	20.4
P06	M	25.3	1.78	75	23.7
P07	M	18.5	1.74	64	21.1
P08	M	28.4	1.66	62	22.4
P09	F	26.2	1.71	64	21.9
Mean ± SD	-	25.6 ± 3.1	1.72 ± 0.07	66 ± 9	22.3 ± 1.8

3.2.2 Experimental protocol

Prior to testing each participant was familiarized with all aspects of the study, including the methodology, experimental setup, and personnel involved (Figure 3.2A). Participants underwent passive rapid inflation bilateral lower-limb venous cuff occlusion (VCO, 13 cm width, Hokanson Stopler E-20, Bellevue, WA, USA) in the supine position (Figure 3.2B) at increasing external pressures of 0, 20, 40, 60 (repeated), 80, 100, and 120 mmHg for a period of five minutes with rest periods (cuff deflation) of at least ten minutes between occlusions (Figure 3.3A). All participants were tested in the same conditions either in the morning (from 0900) or afternoon (from 1300). Prior to venous occlusion participants were instructed to eat a light breakfast or lunch one hour before and, in the preceding 24-hour period, consume no alcohol or caffeine. Participants were asked to remain silent and completely still throughout and asked after each run if they had experienced pain (PAIN+) or not (PAIN-).

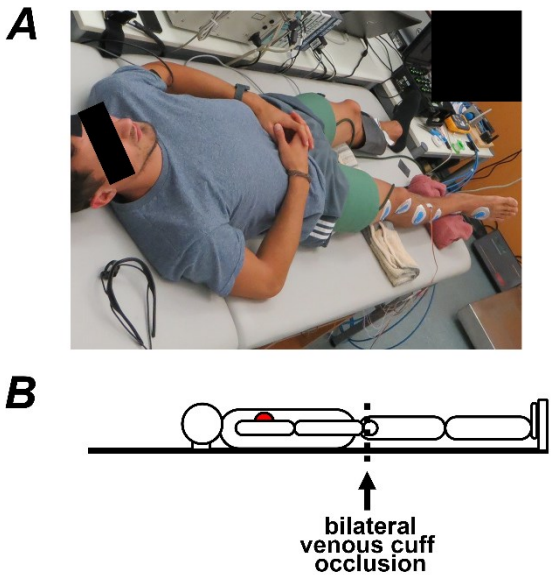

Figure 3.2 Experimental overview.

A, Temperature controlled physiology lab with testing table (DLR, Cologne, Germany); **B**, Bilateral lower-limb venous cuff occlusion (VCO) position to the end of the thigh, as proximal as possible.

Each of the seven occlusions consisted of three phase: (i) five minute baseline immediately before, (ii) five minute cuff inflation (occlusion), and (iii) five minute recovery where the cuff was rapidly deflated (Figure 3.3B). The 60 mmHg pressure was repeated, between the 100 mmHg and 120 mmHg levels, to assess if there was an altered response to the same pressure at different points in the protocol.

Thirty minutes prior to the start of the first baseline recording subjects positioned themselves in the supine position (0°) with arms and legs 10° and 20° abducted from the body, respectively. Previous research has shown thirty minutes to be sufficient for fluid redistribution to occur in the body following postural change (Drummer *et al.*, 2000).

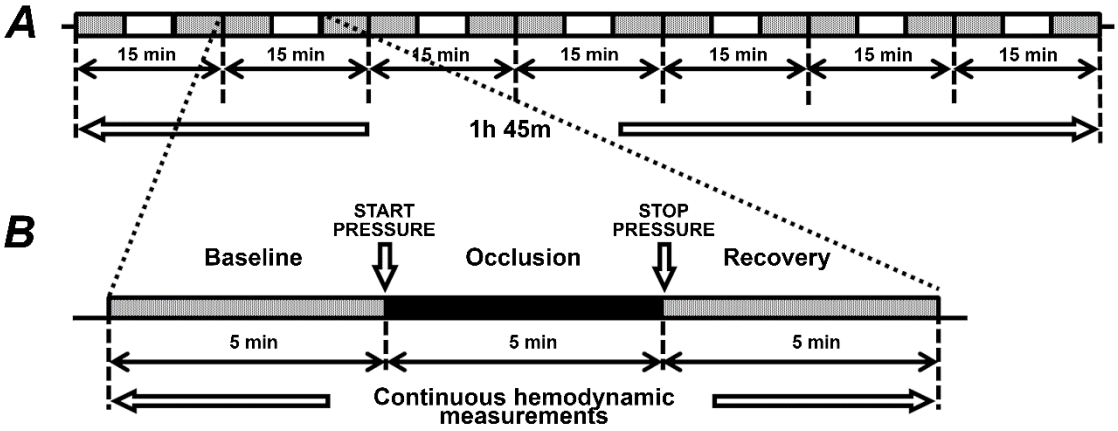

Figure 3.3 Protocol duration with constituent occlusion, baseline and recovery phases.

A, protocol consisting of five randomised occlusion profiles (15 min each), with no less than 10 min rest between them, thus constituting a protocol of 1 h 45 min; **B**, single profile over 15 min consisting of three phases: baseline, occlusion, and recovery.

3.2.2.1 Systemic cardiovascular measurements

Continuous beat-by-beat heart rate (HR) via a standard 3-lead electrocardiogram (ECG; Biopac Systems, Goleta, CA, USA) and mean arterial finger blood pressure (MAP) were recorded with a Finometer (Finapres Medical Systems, Amsterdam, The Netherlands). The Finometer finger cuff was placed around the third finger of the right hand and kept at heart-level relative to the supine participant (Figure 3.4E). Finometer BP measurements were corroborated with absolute arterial BP measurements obtained by an automated sphygmomanometer (Intellivue MMS X2, Philips, Best, The Netherlands) prior to starting the profile. Stroke volume (SV) and total peripheral

resistance (TPR) were estimated from the arterial BP waveform using the Modelflow method (Leonetti, *et al.* 2004) via Beatscope software (TNO-TPD, Biomedical Instrumentation, Amsterdam, The Netherlands).

3.2.2.2 Peripheral fluid displacement

A Burette-plethysmograph (Figure 3.1) effectively measures limb volume increases up to the point where the equivalent cuff pressure in the limb equals the localised venous pressure. However, nowadays it is more common to use VCO with small indium-gallium-filled silicon tube strain gauge plethysmography (SGP) which still measures fluid displacement but is technically very different from a large water filled chamber (Pointel *et al.*, 1981; Roberts *et al.*, 1986; Altenkirch *et al.*, 1989b; Hiatt *et al.*, 1989).

Therefore, movement of fluid to the lower extremities, and away from the central compartment, was quantified using SGP (EC6 Strain Gauge Plethysmograph, Hokanson Inc., Bellevue, WA, USA); positioned around the calf midpoint (directly between the tibiae tuberosity and medial malleolus bony prominences) of each participant (Figure 3.4D).

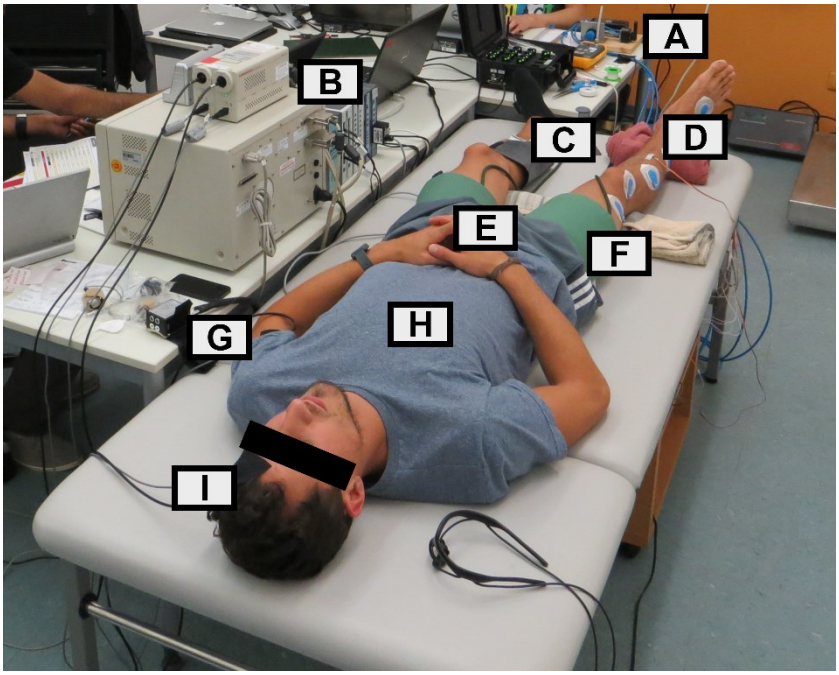

Figure 3.4 Experimental setup.

A, electronically controlled pressure gauge; **B**, data acquisition hardware; **C**, near infrared spectroscopy (NIRS) of the calf muscle; **D**, strain gauge plethysmography around the mid-calf; **E**, Finapres continuous blood pressure monitor; **F**, bilateral lower-limb venous occlusion cuffs; **G**, NIRS control arm muscle; **H**, 3 lead electrocardiogram (ECG); and **I**, prefrontal cortex cerebral NIRS.

3.2.2.3 Cerebral perfusion

Cerebral near-infrared spectroscopy of the left prefrontal cortex immediately below the forehead hairline of each participant (cNIRS; PortaLite, Artinis Medical Systems, The Netherlands; Figure 3.4I) was used to determine the absolute ratio of oxy- (O_2HB) and deoxyhemoglobin (HHb). Taking into account participant frontal cranium thickness, based on age and gender, the cerebral tissue saturation index (cTSI) was deduced (Lynnerup *et al.*, 2005) providing a measure of global cerebral perfusion (Weiss *et al.,* 2005).

3.2.2.4 Estimation of peripheral fluid shifts

Peripheral fluid shift estimations were based on expected circulating blood volume (~5000 mL) with 15% in the lower limbs and 30% in the thoracic compartment (Clauser *et al.*, 1969). A direct relationship was assumed between altered thoracic impedance (Ω) and fluid displacement (Mohapatra & Arenson, 1979; Taneja *et al.*, 2007); with uniform inflation assumed based on measured calf circumference and a simple cylindrical model (Heymsfield *et al.*, 2008). Estimations were calculated based on percentage change in circumference of the idealised cylindrical model (Equation 2.2).

3.2.3 Statistical analysis

All continuously recorded data were analysed in 10 s frames and artefacts removed with a Matlab (R2015a, The Mathworks Inc., MA, USA) function using the following criteria (i) conservative and plausible physiological limits (Table 2.2); and (ii) maximal percentage of change in relation to the standard deviation of the signal. Data was resampled at 4Hz (piecewise cubic spline interpolation) as long as >95% of data were valid yielding 9 complete sets of data for further analysis.

Firstly, occlusion effects are presented as changes from a last minute baseline (BL) mean to the last minute (min 5) at each occlusion pressure (0-120 mmHg). Therefore, pressure effects on response, with the assumption of the largest response following the greatest period of occlusion, were determined. Secondly, the time course responses of the highest occlusion pressure, in which no participant experienced pain (100 mmHg), are presented. Specifically, changes from a last minute BL mean, to each 1 min mean of

all 10 min measurements (5 min occlusion; and 5 min recovery) following the start of occlusion.

Matlab (R2015a, The Mathworks Inc., MA, USA) was used to perform statistical analysis. Visual inspection of residual plots did not reveal any obvious deviations from homoscedasticity or normality of residuals. The tests applied were one-way analysis of variance (ANOVA, repeated measures), post hoc tests with preventative post hoc control of the type I error rate (Tukey's Honestly Significant Difference, HSD) and t-test (independent, by groups). Two-way ANOVA for unbalanced design were performed to explore the main effect of pain related responses to occlusion pressure and any interaction between them. Linear regression analysis was used to estimate the relationships among variables. Hemodynamic responses from the first and second 60 mmHg VCO (min 5) were compared for each participant using Bland-Altman plots (Bland & Altman, 1986) and reproducibility was quantified as the standard deviation of the difference between the first and second. The data are presented as mean (±SEM) unless otherwise stated with the level of significance set at $p \leq 0.05$.

3.3 Results

Nine participants completed all bilateral lower-limb venous cuff occlusion (VCO) pressures (0 to 120 mmHg); with four participants expressing pain at the highest pressure used (120 mmHg). However, all participants were able to tolerate 120 mmHg for the entire five minutes. Baseline values, prior to the start of experimentation, for all participants are outline in

Table **3.2**.

Table 3.2 Participant absolute mean baseline (BL) values for all parameters.

Measured BL is a mean of the last minute immediately before start of the experiment in all participants (n=9).

HR, heart rate; **SV**, stroke volume; **TPR**, total peripheral resistance; **MAP**, mean arterial pressure; **CC**, calf circumference; **mTSI**, muscle tissue saturation index; **cTSI**, cerebral tissue saturation index.

Parameter	*Absolute mean baseline (BL) ± SEM*
HR	66 ± 2 bpm
SV	72.4 ± 5.7 mL
TPR	1562 ± 126 dyn.s.cm^{-5}
MAP	81± 2 mmHg
CC	326 ± 5 mm
mTSI	71.05 ± 0.42 %
cTSI	72.03 ± 1.10 %

3.3.1 Occlusion pressure effect on cardiovascular response

The effect of pressure was significantly positive for the changes from baseline (BL) in mean heart rate (ΔHR: $F_{(6,54)}$=2.44, p=0.036; Figure 3.5A), and total peripheral resistance (ΔTPR: $F_{(6,54)}$=3.29, p=0.008; Figure 3.5D); and significantly negative for mean stroke volume (ΔSV: $F_{(6,54)}$=2.60, p=0.027; Figure 3.5C). No significant differences were observed for changes from BL in mean arterial pressure (ΔMAP) across VCO pressures ($F_{(6,54)}$=1.06, p=0.399; Figure 3.5B). Absolute MAP of all participants was 82 ± 9 mmHg (at BL) to 87 ± 6 mmHg (at 120 mmHg VCO). Systolic blood pressure (SBP) was 118 ± 18 mmHg (at BL) to 137 ± 12 mmHg (at 120 mmHg

VCO); and diastolic blood pressure (DBP) was 66 ± 9 mmHg (at BL) to 72 ± 6 mmHg (at 120 mmHg VCO).

Post hoc analysis revealed ΔHR was no different compared to BL up to 100 mmHg VCO ($0.082<p<0.949$), but significantly positive in the final minute of 120 mmHg VCO (7 ± 2 bpm, $p=0.020$; Figure 3.5A). ΔSV was no different compared to BL up to 100 mmHg VCO ($0.052<p<0.608$), but significantly negative during 120 mmHg VCO (-20.3 ± 4.9 mL, $p=0.014$; Figure 3.5C). Conversely, ΔTPR was significantly positive at 100 and 120 mmHg ($p<0.026$) compared to BL with the greatest significance at 120 mmHg (366 ± 91 dyn.s.cm^{-5}, $p=0.016$; Figure 3.5D).

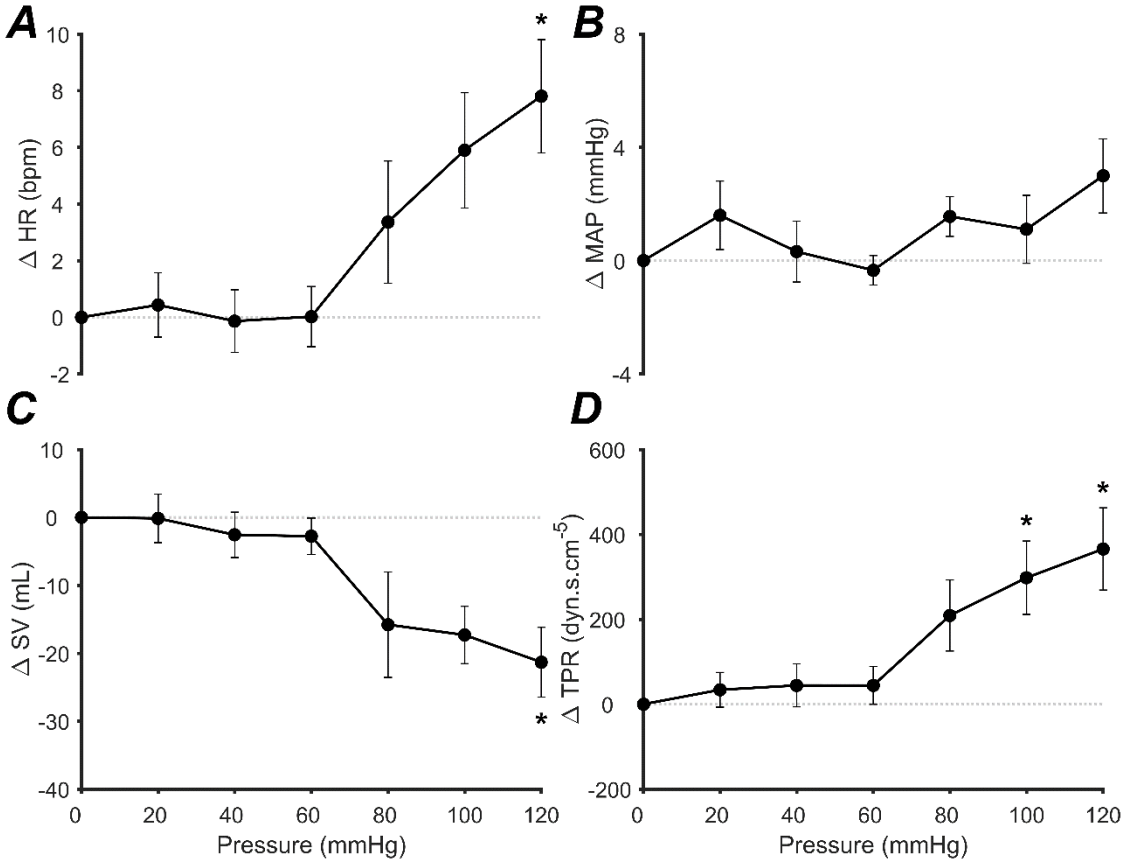

Figure 3.5 Mean (±SEM) changes from baseline (BL) for cardiovascular measures in the final minute (min 5) of bilateral lower-limb venous cuff occlusion (VCO, 0 to 120 mmHg).

A, mean heart rate (ΔHR); **B**, averaged mean arterial pressure (ΔMAP); **C**, mean stroke volume (ΔSV); and **D**, mean total peripheral resistance (ΔTPR).

Mean at each pressure calculated as a final minute (min 5) delta from the final minute (min 5) mean of the baseline (BL) immediately before each respective occlusion. *vs. Baseline*: * $p < 0.05$, $n = 9$.

3.3.2 Peripheral fluid displacement

An analysis of variance showed that the effect of pressure was significant for the changes from baseline (BL) in calf circumference (ΔCC: $F_{(6,54)}$=8.96, p<0.001; Figure 3.6A) and near-infrared spectroscopy (NIRS) measured calf muscle tissue saturation index (ΔmTSI: $F_{(6,54)}$=7.18, p<0.001; Figure 3.6B).

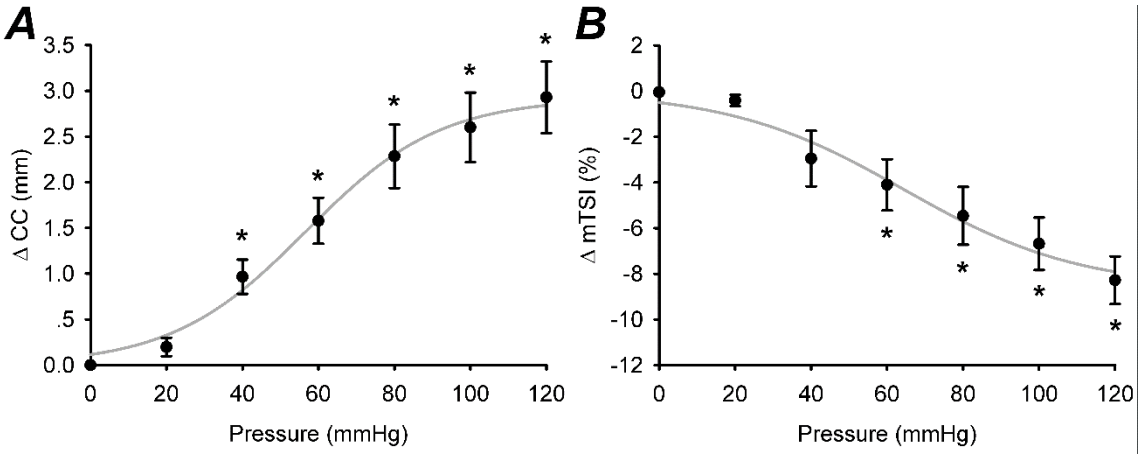

Figure 3.6 Mean (±SEM) changes from baseline (BL) for calf circumference (ΔCC) and mean calf muscle tissue saturation index (ΔmTSI) in the final minute (min 5) of bilateral lower-limb venous cuff occlusion (VCO, 0 to 120 mmHg).

A, mean calf circumference (ΔCC); **B**, near-infrared spectroscopy (NIRS) measured calf muscle tissue saturation index (ΔmTSI).

Mean at each pressure calculated as a final minute (min 5) delta from the final minute (min 5) mean of the baseline (BL) immediately before each respective occlusion. **Grey line**, nonlinear regression sigmoidal (f = a/(1+exp(-(x-x0)/b))). *vs. Baseline*: * p < 0.05, n = 9.

Post hoc analysis revealed ΔCC during all VCO pressures at 40 mmHg and above were significantly positive compared to BL ($p<0.05$) with the largest delta recorded at the highest occlusion pressure (120 mmHg: 2.9 ± 0.4 mm, $p=0.001$). No significant differences in ΔCC were measured at 20 mmHg VCO ($p=0.210$). A significant (0-120 mmHg: $R^2=0.99$, $F_{(6,54)}=239.6$, $p<0.001$) positive non-linear sigmoidal model was observed as the best fit between ΔCC and VCO pressure (Figure 3.6A).

Conversely, ΔmTSI at 60 mmHg VCO and above was significantly negative ($p<0.05$) with the largest delta also recorded at the highest occlusion pressure (120 mmHg: -8.28 ± 1.04 %, $p=0.002$). At 40 mmHg VCO and below no significant differences compared to BL were measured (0-40 mmHg: $0.042<p<0.715$). Despite this, a significant ($R^2=0.99$, $F_{(6,54)}=68.6$, $p<0.001$) negative non-linear sigmoidal model was observed as the best fit between ΔmTSI and all VCO pressures (0-120 mmHg; Figure 3.6B). Additionally, as ΔCC increased, a negative linear relationship to ΔmTSI was observed ($R^2=0.99$, $F_{(6,54)}=337.47$, $p<0.001$; Figure 3.7).

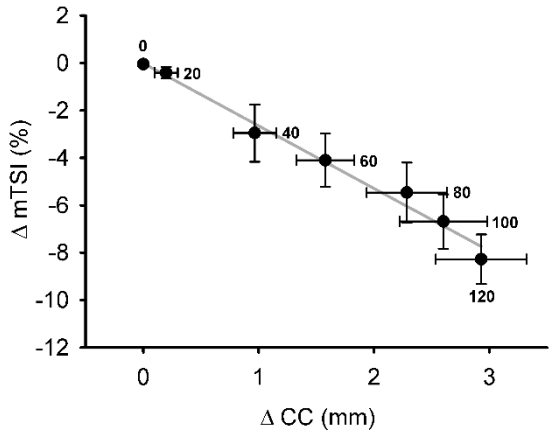

Figure 3.7 Linear relationship between changes from baseline (BL) in mean calf muscle tissue saturation index (ΔmTSI) and mean calf circumference (ΔCC) in the final minute (min 5) of bilateral lower-limb venous cuff occlusion (VCO) pressures up to 120 mmHg.

Mean at each pressure (± SEM) calculated as a final minute (min 5) delta from the final minute (min 5) mean of the baseline (BL) immediately before each respective occlusion. Each point with labelled VCO pressure (mmHg). **Grey line**, linear regression (f = y0+a*x). n = 9.

3.3.2.1 Estimated peripheral fluid shifts

Orthostatic challenge data was tabulated and the volume of peripheral fluid shifts were calculated for: (i) venous cuff occlusion (VCO) during spaceflight (Thornton & Hoffler, 1974); (ii) sit-to-stand (STS) tests (Frey et al., 1994); (iii) head-up tilt (HUT) tests (Laszlo et al., 2001); (iv) lower-body negative pressure (LBNP) (Lundvall et al., 1993); (v) short-arm human centrifugation (SAHC) (Iwase, 2005); and (vi) VCO on Earth in the present study (Table 3.3).

Table 3.3 Relative estimations of peripheral fluid shifts based on previously published data.

VCO, venous cuff occlusion; **STS**, sit-to-stand test; **HUT**, head-up tilt; **LBNP**, lower-body negative pressure; and **SAHC**, short-arm human centrifugation. Experimental methodology include: **(i)**, Increased flow and percentage change in limb size measured by strain gauge plethysmography; and (**ii**), percentage change in central/thoracic volume measure by bioelectrical impedance.

Research paper	*Thornton and Hoffler (1974)*	*Frey et al. (1994)*	*Laszlo et al. (2001)*	*Lundvall et al. (1993)*	*Iwase (2005)*	*Present study*
Orthostatic challenge type	VCO during spaceflight	STS	HUT	LBNP	SAHC	VCO
No. of participants (n)	3	47	7	16	12	9
Magnitude	30 > 50 mmHg	Sit > stand	$0^0 > 12^0 > 30^0 > 53^0 > 70^0$	-70 mmHg	1.2 +Gz at heart (not passive)	20 > 40 > 60 > 80 > 100 > 120 mmHg
Duration	5 min	5 min	30 min	10 min	25 min	5 min
Method	Strain gauge plethysmography (flow)	Thoracic bioelectrical impedance	Thoracic bioelectrical impedance	Strain gauge plethysmography (flow)	Thoracic bioelectrical impedance	Strain gauge plethysmography (Δ%)
Measured difference	+8% > +15%	-10% > -14%	0% > -2% > -7% > -12% > -16%	+69%	-13%	+0.1 > +0.3 > +0.5 > +0.7 > +0.8 > +0.9 %
Peripheral fluid displacement estimation (~mL)	**288 > 326**	**157 > 217**	**-7 > 34 > 117 > 192 > 249**	**710**	**203**	**7 > 41 > 73 > 115 > 135 > 158**

3.3.3 Cerebral tissue oxygenation

An analysis of variance showed that the effect of pressure was non-significant for the changes from baseline (BL) in NIRS measured prefrontal cortex cerebral tissue saturation index (ΔcTSI; 0-120 mmHg: $F_{(6,54)}$=1.36, p=0.248; Figure 3.8).

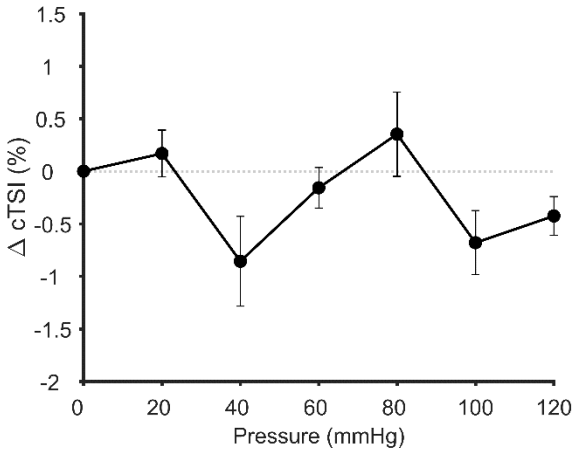

Figure 3.8 Mean (±SEM) changes from baseline (BL) for prefrontal cortex cerebral tissue saturation index (ΔcTSI) in the final minute (min 5) of bilateral lower-limb venous cuff occlusion (VCO, 0 to 120 mmHg).

Mean at each pressure calculated as a final minute (min 5) delta from the final minute (min 5) mean of the baseline (BL) immediately before each respective occlusion. *vs. Baseline*: * p < 0.05, n = 9.

3.3.4 Pain related responses

The main effect of experiencing pain during occlusion was significantly positive in ΔHR ($F_{(6,54)}$=6.34, p=0.045; Figure 3.9A), and ΔTPR ($F_{(6,54)}$=5.23, p=0.048; Figure 3.9D); whilst ΔSV ($F_{(6,54)}$=9.33, p=0.022; Figure 3.9C) was significantly negative. Experiencing pain had no effect on ΔMAP ($F_{(6,54)}$=0.15, p=0.711; Figure 3.9D).

An analysis between occlusion pressure and incidence of pain revealed significant interaction effects (*Pressure:Pain*±) in ΔHR ($F_{(6,54)}$=2.44, p=0.041; Figure 3.9A); but none in ΔMAP ($F_{(6,54)}$=0.28, p=0.944; Figure 3.9B), ΔSV ($F_{(6,54)}$=1.21, p=0.321; Figure 3.9D), and ΔTPR ($F_{(6,54)}$=1.45, p=0.216; Figure 3.9D).

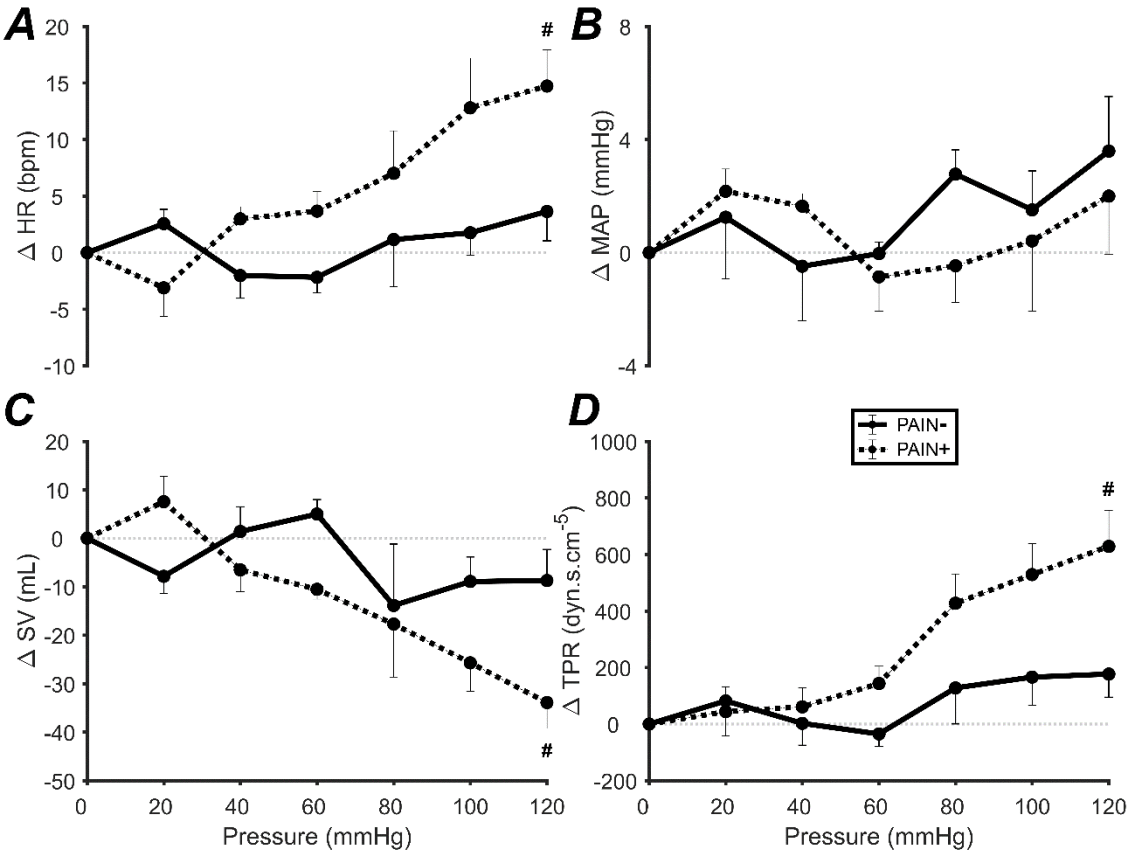

Figure 3.9 Comparison of mean (±SEM) changes from baseline (BL) for cardiovascular measures in the final minute (min 5) of bilateral lower-limb venous cuff occlusion (VCO, 0 to 120 mmHg) in participants verbally reporting pain and not (PAIN+ *vs.* PAIN-).

A, mean heart rate (ΔHR); **B**, averaged mean arterial pressure (ΔMAP); **C**, mean stroke volume (ΔSV); and **D**, mean total peripheral resistance (ΔTPR).

Mean at each pressure calculated as a final minute (min 5) delta from the final minute (min 5) mean of the baseline (BL) immediately before each respective occlusion. **Solid line**, no pain verbally reported; **dotted line**, pain verbally reported. *PAIN+ vs. PAIN-:* # p < 0.05, PAIN+: n = 4; and PAIN-: n=5.

Post hoc analysis revealed, in participants experiencing pain compared to those not (PAIN+ *vs.* PAIN-), significantly greater ΔHR (15 ± 2 *vs.* 4 ± 2 bpm, p=0.029; Figure 3.9A) and ΔTPR (629 ± 128 *vs.* 177 ± 82 dyn.s.cm^{-5}, p=0.035; Figure 3.9D) during 120 mmHg VCO. Conversely, ΔSV was significantly lower in PAIN+ (-9 ± 6 *vs.* -33 ± 5 mL, p=0.049; Figure 3.9C).

3.3.5 Insufficient simulated orthostatic challenge and duration

Occlusion pressures up to 120 mmHg were used; however, due to the pain experienced by almost half of participants at the highest level, 100 mmHg has been selected as the highest pressure tolerated by all without pain. Further minute-by-minute analysis was conducted during the entire ten minute profile (VCO: min 0-5; and recovery, RR: min 5-10) in all participants.

3.3.5.1 Cardiovascular

No significant differences were found in changes from baseline (BL) of ΔHR and ΔMAP at the mean final minute (min 5) during 100 mmHg occlusion; however, during the entire ten minute profile (min 0-10) significant differences in ΔHR ($F_{(10,88)}$=2.56, p=0.009, Figure 3.10A) were observed. Across all minutes (min 0-10) no significant differences were found in ΔMAP ($F_{(10,88)}$=0.80, p=0.625,Figure 3.10B). Post hoc analysis revealed ΔHR was significantly positive in the last minute of VCO (min 5: p=0.030) compared to BL but no different during the rest of the profile (0.082<p<0.923; Figure 3.10A).

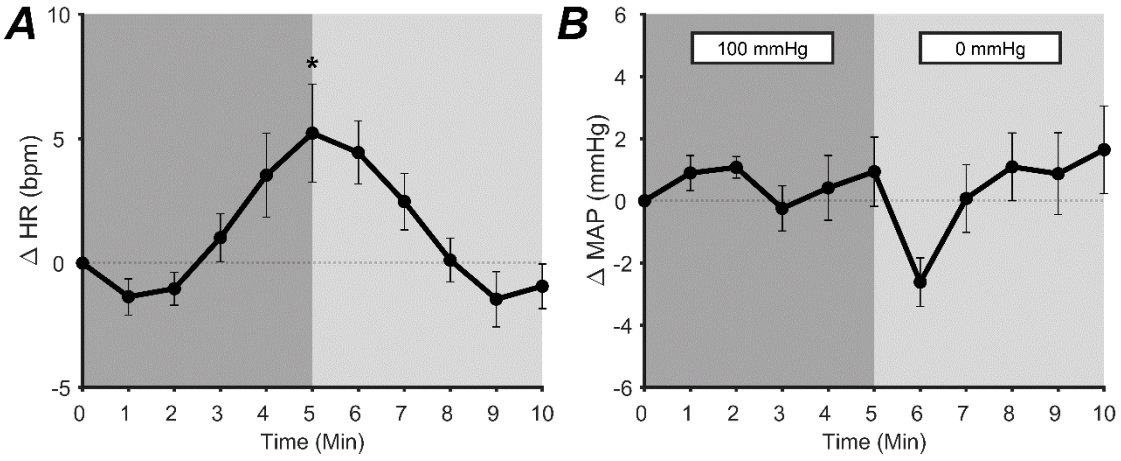

Figure 3.10 Mean (±SEM) changes from baseline (BL) for heart rate (ΔHR) and averaged mean arterial pressure (ΔMAP) during five minutes bilateral lower-limb venous cuff occlusion (VCO: min 0-5, 100 mmHg) and recovery (RR: min 5-10, 0 mmHg).

A, mean heart rate (ΔHR); and **B**, averaged mean arterial pressure (ΔMAP).

Each 60 s data point is a mean delta from the final minute (min 5) mean of the baseline (BL) immediately before 100 mmHg occlusion. **Dark grey**, during 100 mmHg VCO; **light grey**, recovery (RR) immediately following VCO (0 mmHg). *vs. Baseline*: * $p < 0.05$, n = 9.

3.3.5.2 Increased peripheral fluid displacement

Significant differences during the entire ten minute 100 mmHg VCO profile (min 0-10) were observed in changes from baseline (BL) of calf circumference (ΔCC; $F_{(10,88)}$11.79, $p<0.001$; Figure 3.11A) and NIRS measured calf muscle tissue saturation index (ΔmTSI: $F_{(10,88)}=10.32$, $p<0.001$; Figure 3.11B).

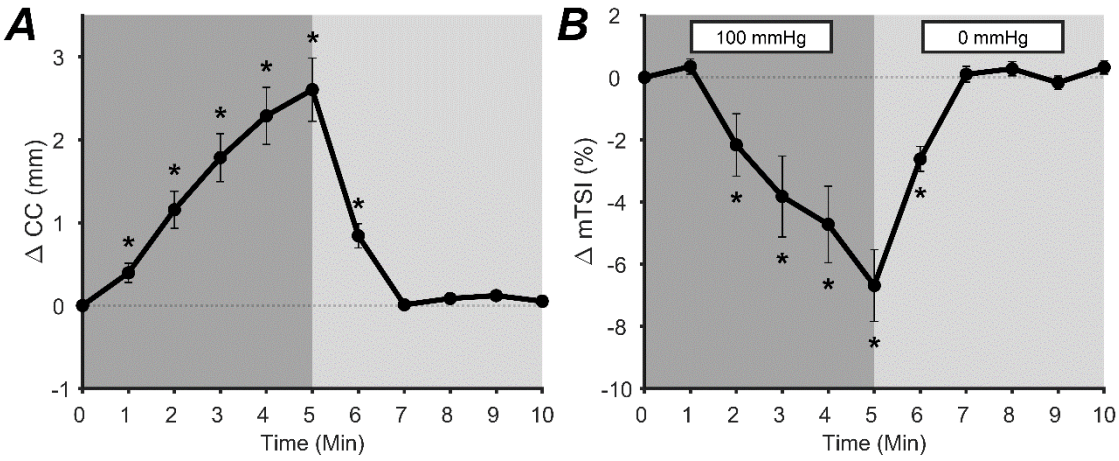

Figure 3.11 Mean (±SEM) changes from baseline (BL) for calf circumference (ΔCC) and calf muscle tissue saturation index (ΔmTSI) during five minutes bilateral lower-limb venous cuff occlusion (VCO: min 0-5, 100 mmHg) and recovery (RR: min 5-10, 0 mmHg).

A, mean calf circumference (ΔCC); and **B**, mean calf muscle tissue saturation index (ΔmTSI).

Each 60 s data point is a mean delta from the final minute (min 5) mean of the baseline (BL) immediately before 100 mmHg occlusion. **Dark grey**, during 100 mmHg VCO; **light grey**, recovery (RR) immediately following VCO (0 mmHg). *vs. Baseline*: * $p < 0.05$, n = 9.

Post hoc analysis revealed ΔCC was significantly positive at min 1-6 ($p<0.046$) with the greatest difference compared to BL in the final minute of VCO (min 5: 2.6 ± 0.4 mm, $p=0.002$); with ΔCC from min 7-10 no different from BL ($0.137<p<0.876$; Figure 3.11A). Conversely, ΔmTSI was significantly negative at min 2-6 ($p<0.05$) with the greatest difference compared to BL also in the final minute of VCO (min 5: -6.69 ± 1.15 %, $p=0.002$); with ΔmTSI from min 7-10 no different from BL ($0.403<p<0.708$; Figure 3.11B).

3.3.5.3 Unchanged cerebral perfusion

No significant differences during the entire ten minute 100 mmHg VCO profile (min 0-10) were observed in changes from baseline (BL) of prefrontal cortex cerebral tissue saturation index (ΔcTSI: $F_{(10,88)}$=1.02, p=0.435; Figure 3.12).

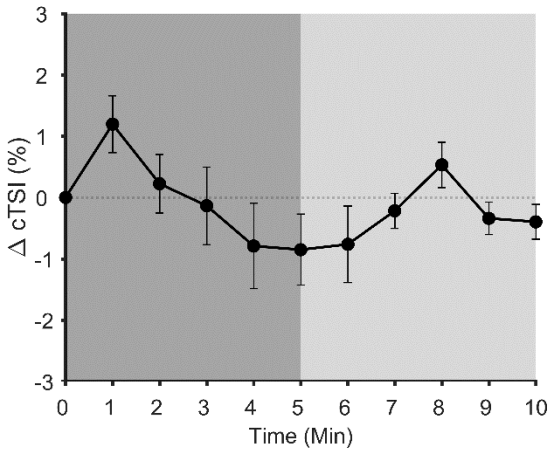

Figure 3.12 Mean (±SEM) changes from baseline (BL) for near-infrared spectroscopy (NIRS) pre-frontal cortex cerebral tissue saturation index (ΔcTSI) during five minutes bilateral lower-limb venous cuff occlusion (VCO: min 0-5, 100 mmHg) and recovery (RR: min 5-10, 0 mmHg).

Each 60 s data point is a mean delta from the final minute (min 5) mean of the baseline (BL) immediately before 100 mmHg occlusion. **Dark grey**, during 100 mmHg VCO; **light grey**, recovery (RR) immediately following VCO (0 mmHg). *vs. Baseline*: * $p < 0.05$, n = 9.

3.3.6 Test-retest reproducibility of 60 mmHg VCO

A comparison of changes from BL, at the last minute of occlusion (min 5), between the first and second 60 mmHg VCO revealed a moderate correlation in ΔHR (R^2=0.42, $F_{(1,7)}$=4.98, p=0.061; Figure 3.13A). There was a strong correlation between ΔcTSI (R^2=0.66, $F_{(1,7)}$=13.66, p=0.008; Figure 3.16A) and ΔCC (R^2=0.99, $F_{(1,7)}$=1787, p<0.001; Figure 3.15A) measurements; however no correlation between ΔMAP (R^2=0.02, $F_{(1,7)}$=0.14, p=0.718; Figure 3.14A).

Bland-Altman plots (Bland & Altman, 1986) of the difference between the two delta values *vs*. the mean of both are displayed (Figure 3.13B; Figure 3.14B; Figure 3.15B; and Figure 3.16B). The standard deviation of the difference between measurements for the two occlusions was large in ΔHR (4 bpm), ΔMAP (3 mmHg), and ΔcTSI (0.45 %) compared to the respective mean changes from BL during 60 mmHg (ΔHR: 1 bpm; ΔMAP: 0 mmHg; and ΔcTSI: -0.28 %). However, this value in ΔCC (0.4 mm) was relatively low compared to the mean delta during 60 mmHg (1.6 mm).

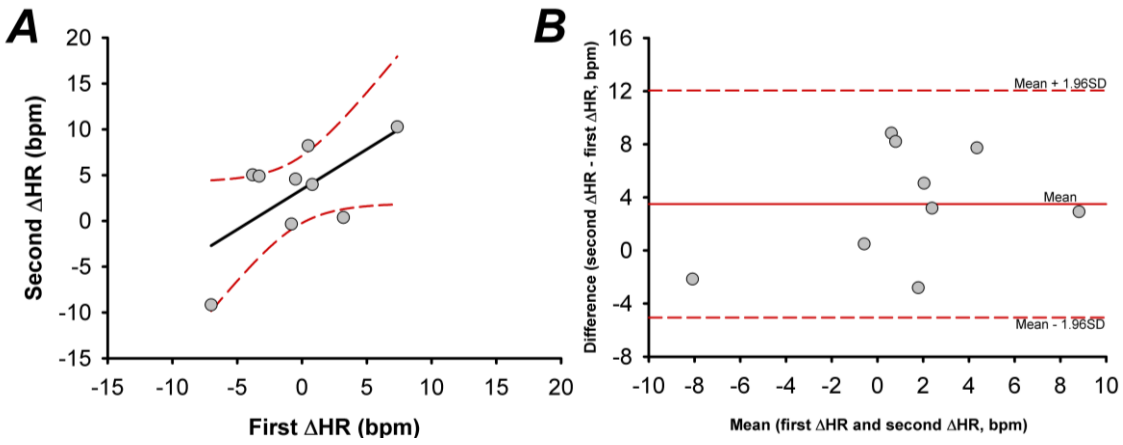

Figure 3.13 A, Relationship between changes from baseline (BL) in heart rate (ΔHR) during first and second 60 mmHg bilateral lower-limb venous cuff occlusion (VCO) in the final minute (min 5); and **B**, Bland-Altman plot of paired differences in ΔHR against a mean of both, in all participants (n=9).

Black line, linear regression (f = y0+a*x); **dotted red line**, *upper*: mean +1.96 SD; *lower*: mean -1.96 SD, each with 95% CI. n = 9.

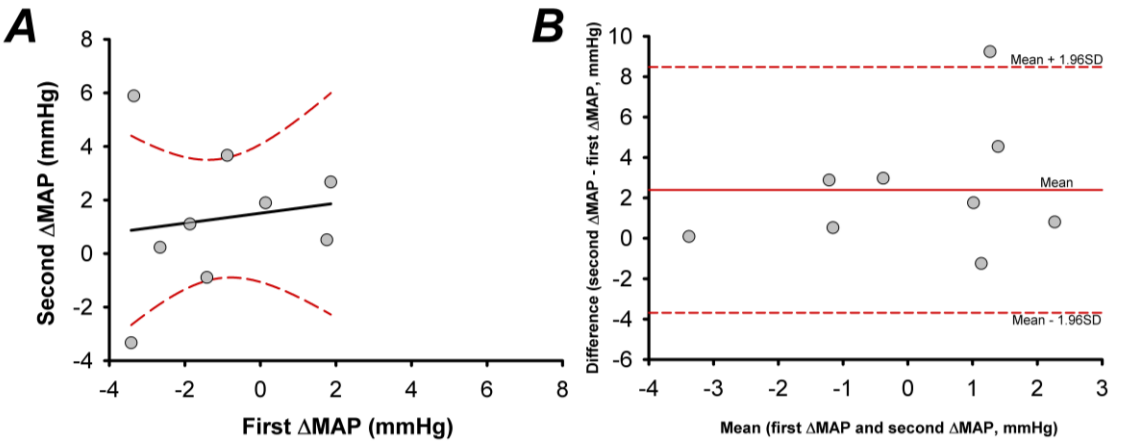

Figure 3.14 A, Relationship between changes from baseline (BL) in mean arterial pressure (ΔMAP) during first and second 60 mmHg bilateral lower-limb venous cuff occlusion (VCO) in the final minute (min 5); and **B**, Bland-Altman plot of paired differences inΔMAP against a mean of both, in all participants (n=9).

Black line, linear regression (f = y0+a*x); **dotted red line**, *upper*: mean +1.96 SD; *lower*: mean -1.96 SD, each with 95% CI. n = 9.

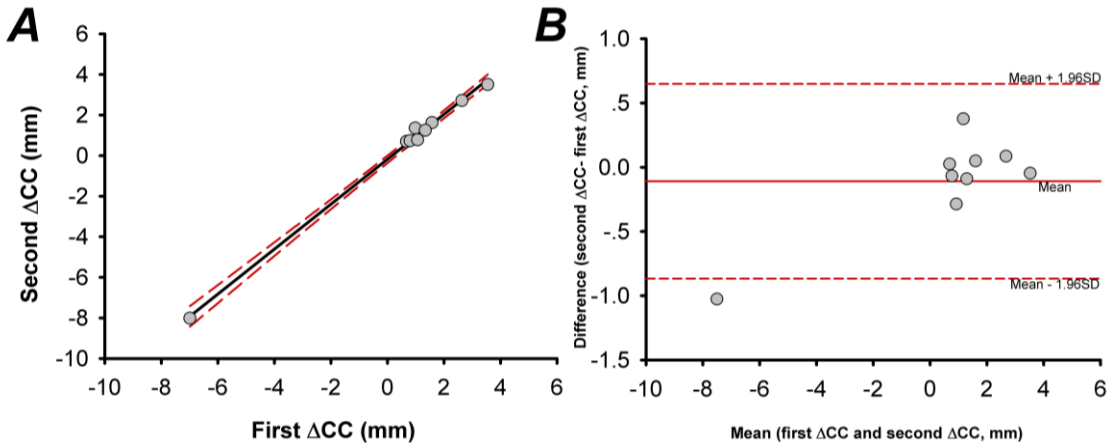

Figure 3.15 A, Relationship between changes from baseline (BL) in calf circumference (ΔCC) during first and second 60 mmHg bilateral lower-limb venous cuff occlusion (VCO) in the final minute (min 5); and **B**, Bland-Altman plot of paired differences in ΔCC against a mean of both, in all participants (n=9).

Black line, linear regression (f = y0+a*x); **dotted red line**, *upper*: mean +1.96 SD; *lower*: mean -1.96 SD, each with 95% CI. n = 9.

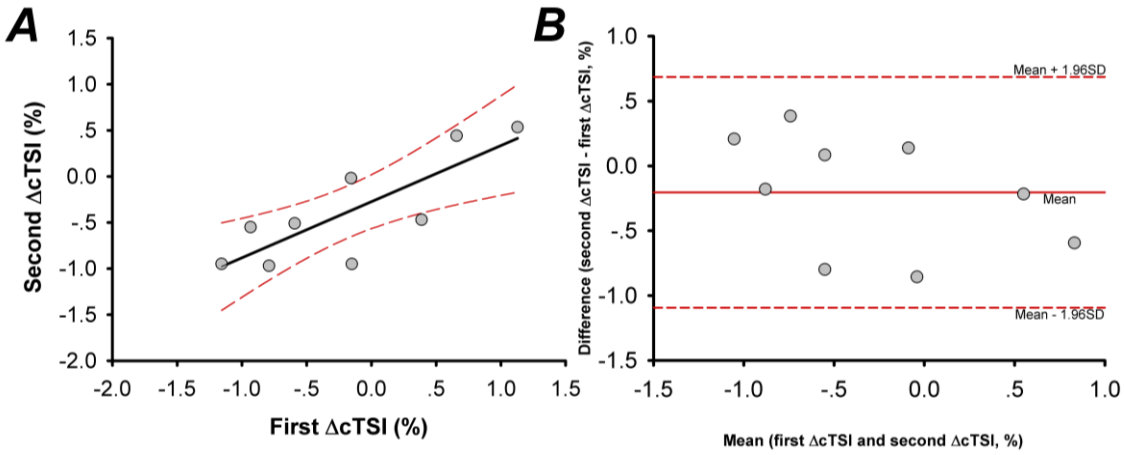

Figure 3.16 A, Relationship between changes from baseline (BL) in prefrontal cortex cerebral tissue saturation index (ΔcTSI) during first and second 60 mmHg bilateral lower-limb venous cuff occlusion (VCO) in the final minute (min 5); and **B**, Bland-Altman plot of paired differences in ΔcTSI against a mean of both, in all participants (n=9).

Black line, linear regression (f = y0+a*x); **dotted red line**, *upper*: mean +1.96 SD; *lower*: mean -1.96 SD, each with 95% CI. n = 9.

3.3.7 Invalid simulated orthostatic challenge

There was a moderate effect size between fluid shifted to the periphery, measured by changes from baseline (BL) in mean calf circumference (ΔCC) and mean heart rate (ΔHR, R^2=0.61, $F_{(5,48)}$=9.36, p=0.041; Figure 3.17A).

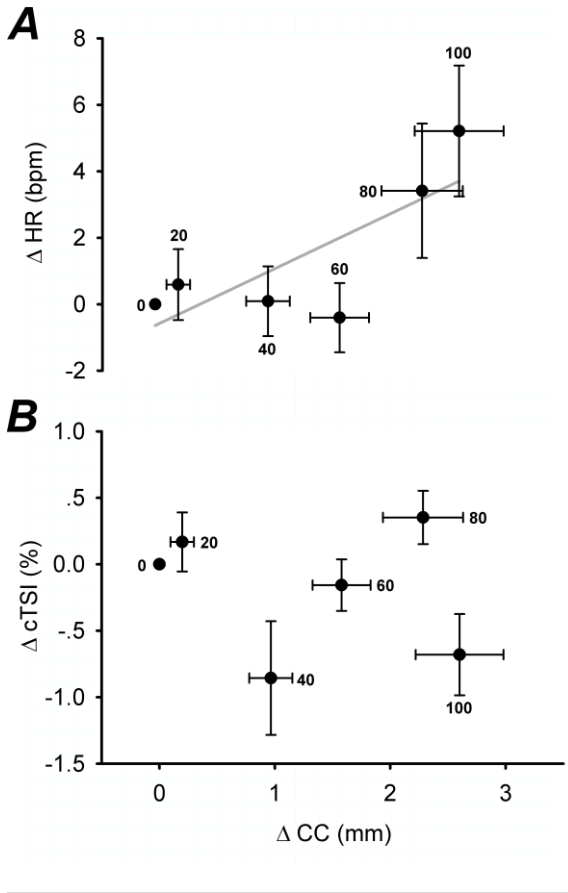

Figure 3.17 Non-existent relationship between changes from baseline (BL) in mean heart rate (ΔHR) and mean prefrontal cortex cerebral tissue saturation index (ΔcTSI), and mean delta calf circumference (ΔCC) in the final minute (min 5) of bilateral lower-limb venous cuff occlusion (VCO) pressures up to 100 mmHg.

A, mean heart rate (ΔHR) *vs.* mean calf circumference (ΔCC); and **B**, mean pre-frontal cortex cerebral tissue saturation index (ΔcTSI) *vs.* ΔCC.

Mean at each pressure (±SEM) calculated as a final minute (min 5) delta from the final minute (min 5) mean of the baseline (BL) immediately before each respective occlusion. Each point with labelled VCO pressure (mmHg). **Grey line**, linear regression (f = y0+a*x). n = 9.

Surprisingly, there was no relationship between ΔCC and cerebral tissue oxygenation, measured by prefrontal cortex cerebral tissue saturation (ΔcTSI, R^2=0.04, $F_{(5,48)}$=0.17, p=0.703, p=0.557; Figure 3.17B).

In general, bilateral lower-limb venous cuff occlusion (VCO) significantly shifted fluid to the periphery at occlusion pressure 40 mmHg and above. However, unexpectedly this significant fluid shift had only a moderate effect on systemic cardiovascular response (ΔHR) and no effect on cerebral perfusion (ΔcTSI).

3.4 Discussion

The main findings of the study were that venous occlusion pressure had no significant effect on systemic cardiovascular response until 120 mmHg; despite significant increases in peripheral fluid displacement from 40 mmHg. A significant positive linear relationship between systemic cardiovascular responses (heart rate, HR) and decreasing central volume (peripheral fluid displacement to calf circumference, CC) was observed. However, there was no significant relationship between cerebral tissue oxygenation (cTSI) and CC.

3.4.1 Bilateral lower-limb venous cuff occlusion pressures

VCO had no significant effect, on all measured cardiovascular parameters, up to an externally applied pressure of 100 mmHg; apart from a positive change from baseline (BL) in total peripheral resistance (ΔTPR) in the last minute of occlusion. Similarly, ΔTPR and heart rate (ΔHR) at 120 mmHg were significantly positive, whilst stroke volume (ΔSV) was negative with respect to BL.

Research has shown large external VCO pressures at the skin translate to significantly reduced pressure exerted on the deep venous structures (Shaw & Murray, 1982; Partsch & Partsch, 2005). In fact, external VCO pressures of 80 mmHg to 140 mmHg were required to entirely occlude the popliteal and great saphenous vein (Sarin *et al.*, 1992). Large inter-individual differences, between externally applied cuff and known internal venous pressures of 80-100 mmHg, are thought to arise due to anthropometric differences of the lower-limb; and anatomical position of the venous vasculature (Keen, 1961; Altenkirch *et al.*, 1988). This presumably caused external pressure, applied to the

proximal end of the thigh, to be significantly larger than those exerted on internal venous structures in the present study. Furthermore, internal pressure differences are likely to vary widely between individuals (of differing age, height, and weight), with leg muscle mass and inter-individual anatomical differences in deep venous structures thought to play a role (Kügler *et al.*, 2001). Participants of the present study were all around the same age, height, and weight (Table 3.1); thus, diminishing the possibility of differing individual anthropometric measurements affecting results. Nevertheless, the lack of significant systemic response in ΔHR, ΔMAP, ΔSV, and ΔTPR may be explained by varied resting venous pressures, and greater leg muscle mass preventing correct VCO pressure application and complete occlusion.

It is postulated that an increase in ΔHR, ΔMAP, ΔSV, and ΔTPR response to 120 mmHg (except mean arterial pressure, ΔMAP) can be explained by substantial sympathetic activation as a result of the pain experienced by four participants. Muscle sympathetic nervous activity (MSNA) has been shown to be significantly correlated to TPR (Charkoudian *et al.*, 2005) and, in the present study, it was significantly higher at 100 mmHg and 120 mmHg. Furthermore, ΔHR was significantly higher and ΔSV lower in participants who verbally expressed pain, compared to those who did not at 120 mmHg. Additionally, only four individuals verbally reported pain and it is likely all experienced reduced comfort as VCO pressures increased. It is also interesting to note that, whilst pain was only ever registered at 120 mmHg, a divergence in response can be seen at lower VCO pressures. In particular ΔHR and ΔTPR were significantly higher in participants experiencing pain; however, it was only significant at 120 mmHg. In addition, an interaction effect between pressure and pain (*Pressure:Pain*±) was only significant in ΔHR.

The highest level of bilateral lower-limb VCO tested, in which all participants experienced no pain, was 100 mmHg. Strain gauge plethysmography measured calf circumference demonstrated arterial inflow was not impeded at the measured pressures; and the rate of calf inflation only started to decrease following a period of venous pooling, even at 100 mmHg. At this level ΔHR in the last minute (min 5) was significantly positive (with respect to BL). Increased HR has been observed to be rapidly induced (~1-2 beat) by central hypovolemia (*i.e.* significant loss of fluid), such as in haemorrhagic shock sympathetic compensation (Cooke *et al.*, 2004). ΔCC in the present study was significantly positive from the first minute of 100 mmHg VCO onwards (Figure 3.11A) with concurrent increases in ΔHR anticipated. However, ΔHR was no different than BL up until the last minute of 100 mmHg. It is postulated during VCO challenge blood is being sequestered elsewhere, such as the splanchnic circulation (Taneja *et al.*, 2007); leading to the discrepancy of response between ΔCC and ΔHR in the first four minutes of 100 mmHg occlusion.

3.4.2 Peripheral fluid displacement

Changes from BL in calf circumference (ΔCC), induced by graded VCO, followed a sigmoidal curve from BL to 120 mmHg. A reduction in the slope was observed at VCO pressures above 100 mmHg and demonstrate venous filling was nearing capacity, in agreement with the pressure-volume curve (Guyton, 1965). A similar observation was made in calf muscle tissue oxygenation (ΔmTSI); but instead decreasing as occlusion pressure increased. Furthermore, a significant correlation between ΔCC and ΔmTSI is indicative of either measure being a good indicator of central to peripheral relocation of blood. Similarly, previous research has shown strain gauge plethysmography

measurements of flow to have a strong correlation to Doppler measures of blood velocity when undergoing limb occlusion (Tschakovsky *et al.*, 1995).

The majority of fluid shifted to the periphery, at VCO levels of 20-100 mmHg, can be attributed to deep venous filling (Buckey *et al.*, 1988). Furthermore, it is postulated five minute VCO was short enough to prevent significant fluid movement into the interstitial space; with a longer duration orthostatic challenge, demonstrating a greater volume accumulation, attributed to this compartment (Fortney, 1991).

Research has shown that calf circumference is an important determining factor of suitable pressures for occlusion (Loenneke *et al.*, 2011) and even the width of the VCO cuff itself (Loenneke *et al.*, 2012); whilst other research has still based suitable occlusion pressure selection on individual systolic blood pressure (SBP) (Cook *et al.*, 2007). Further research is required to determine the influence of resting blood pressure, apparatus used, and lower-limb size on venous occlusion. However, in the present study, the same equipment and pressures were tested and was deemed sufficient in order to examine orthostatic challenge capacity of VCO, in all participants.

Fluid accumulation reveals an indication of orthostatic challenge magnitude and a comparative analysis with VCO may reveal its effectiveness as a simulated orthostatic challenge. Orthostatic challenges sit-to-stand (STS) (Levine *et al.*, 1994), head-up tilt (HUT) (Madsen *et al.*, 1995), lower-body negative pressure (LBNP), and short-arm human centrifugation (SAHC) (Smith *et al.*, 2013) all exhibit significant fluid shifted to the periphery with systemic hemodynamic responses; and crucially, significant alterations in cerebral hemodynamics. In the present study, the peripheral fluid displacement estimated (Table 3.3) was between ~7-158 mL at VCO pressure of 0-120

mmHg; with a comparable estimated fluid shift, in healthy individuals, of ~157 mL in a STS test during 5 min sit (Frey *et al.*, 1994) and greater than the ~117 mL estimated volume during HUT to 30° for 30 min (Laszlo *et al.*, 2001) (Table 3.3). Prolonged orthostatic challenge, leading to eventual syncope, involves significant movement of fluid to the periphery to bring about central hypovolemia (Cooke *et al.*, 2004). However, the precise role of smaller initial volumes of fluid shifted to the periphery is unclear; and specifically, the effect on significant changes in systemic and cerebral hemodynamics.

3.4.3 Cerebral hemodynamics

Surprisingly, no significant difference was measured in changes from BL in prefrontal cortex cerebral tissue saturation index (ΔcTSI), a good indicator of overall cerebral blood flow (Kirkpatrick *et al.*, 1998; Hirofumi *et al.*, 2003). A significant reduction, during a prolonged orthostatic challenge, would have been expected. The fact that no such reduction was measured suggests either: (i) insufficient fluid was shifted to the periphery to elicit a response; (ii) fluid shifted was sufficient but other compensatory mechanisms were involved; or (iii) ΔcTSI as a measure of localised cerebral perfusion was unable to measure globalised changes present during VCO.

In fact, it appears likely that fluid volume shifted to the periphery was insufficient to elicit changes in cerebral hemodynamics. In the present study, cerebral oxygenation (cTSI) was measured using near-infrared spectroscopy (NIRS) and research has shown this to correlate well to cerebral blood flow velocity (cBFV) during surgery (Kurth *et al.*, 1995; Pigula *et al.*, 2000). Rickards *et al.* (2015) demonstrated that 1000 mL blood volume removed directly from the antecubital vein (equating to a 150 mL peripheral

fluid shift, ~15% total) over a 15 min period, did not lead to significant differences in middle cerebral artery (MCA) blood flow velocity (cBFV; 69.5 ± 5.1 *vs.* 66.6 ± 5.2 cm/s, $p>0.05$). However, during the same protocol cBFV was shown to decrease from baseline after 5 min LBNP at -45 mmHg (70.0 ± 4.2 *vs.* 61.5 ± 5.8 cm/s, $p<0.05$) with an estimated peripheral fluid shift of ~ 450 mL.

A limitation of this study is that end-tidal CO_2 ($P_{ET}CO_2$) was not measured as a potential influencing factor on cerebral perfusion. Previous research has shown that carotid baroreceptor reflex control not only acts to maintain blood pressure but is a potent regulator of ventilator response in dogs (Brunner *et al.*, 1982) and humans (Stewart *et al.*, 2011). In addition, Stewart *et al.* (2011) showed that ventilator baroreceptor sensitivity is not modulated by chemoreceptor activation; but rather increases/decreases in MAP resulted in decreased/increased ventilator response, respectively. The current study results show MAP remains unchanged so it is unlikely to have had an effect on $P_{ET}CO_2$ through any ventilatory baroreceptor activation; however, future studies would benefit from this consideration and measuring either ventilation rate or $P_{ET}CO_2$.

Unaltered cerebral hemodynamics in the present study may also be explained by the role of the splanchnic circulation as a buffer to central and peripheral fluid displacement (Fu *et al.*, 2005). Research has shown emptying and pooling of the splanchnic circulation in response to LBNP and HUT, respectively (Taneja *et al.*, 2007); however, the precise role of this region in VCO is unknown. It is postulated that unaffected cerebral tissue oxygenation, may be due to systemic compensatory mechanisms constricting peripheral vasculature, aiding venous return and maintaining cerebral tissue oxygenation.

3.4.4 Reproducability

ΔHR, ΔMAP, and ΔcTSI after VCO testing does not have short-term test-retest reproducibility within the current participant cohort of nine. However, results indicate a far better reproducibility of ΔCC measurements in individuals when exposed to repeated VCO at 60 mmHg. This study demonstrates the ability of VCO to elicit reproducible shifts of fluid to the periphery measured by ΔCC; however, calls into question the benefit when ΔHR, ΔMAP, and ΔcTSI differ greatly between identical VCO occlusion pressures.

Our results indicate that hemodynamic variables (ΔHR, ΔMAP, and ΔcTSI) were not reproducible when measured twice at 60 mmHg VCO; however, ΔCC was. Research has shown that different occlusion cuff width significantly alter the response to VCO between individuals (Loenneke *et al.*, 2012) and disregarding this finding is likely to impede the reproducibility of results on different days and between individuals. However, in the present study this is not applicable as all testing was completed in one day and expressed as delta values. Additionally, cuff inflation was automated and this is likely to have also reduced the error. Research has shown a high degree of reproducibility when measuring occlusion and calf blood flow (Kooijman *et al.*, 2007); however, earlier research has shown the opposite (Altenkirch *et al.*, 1989a). It is likely the findings of Altenkirch *et al.* (1989a) are mirrored in the current research; namely, that low reproducibility was due to a high degree of random biological variability.

Baseline periods between testing, set at 10 min for each 5 min occlusion, may not have been of sufficient duration to allow for a complete return to pre-occlusion values. Previous research has set sufficient initial baseline duration of >30 min quiet rest in the

supine position and at 1-2 times the period of orthostatic challenge (Fu *et al.*, 2005; Rickards *et al.*, 2015; Patel *et al.*, 2016). The present study adhered to this methodological commonality; however, the reproducibility of measured hemodynamic responses in future VCO studies may benefit from an increased recovery phase duration. Thus, negate the possibility of a cumulative effect on measured responses, due to an incomplete return to BL, following occlusion (Linden & Mary, 1982; Tonino & Driscoll, 1988; Bootsma *et al.*, 1996).

3.4.5 Insufficient simulated orthostatic challenge

It is proposed there is a diminished mechanistic response to VCO in comparison to STS, HUT, LBNP or SAHC orthostatic challenges; and, as previous discussed, the role of the splanchnic circulation is heavily implicated. From a purely mechanical point of view this seems logical as VCO elicits a fluid shift passively without the recruitment or stimulus to other body systems. Perhaps the greatest distinguishing factor is the presence of high pressure cuffs at the proximal end of both legs having only an isolated effect of fluid accumulation. In contrast to HUT and SAHC, which involve a changing gravitational vector, producing a holistic challenge and greater resultant systemic response.

Nevertheless, the positive linear relationship between ΔHR and ΔCC in the current research demonstrates a close link between central hypovolemia and systemic response. This suggests fluid shifted to the periphery, during VCO, is directly related to fluid removed from the central compartment. This observation suggests the role of the splanchnic circulation in VCO is independent of occlusion pressure; however, further research is required.

The present research outlines VCO as an insufficient orthostatic challenge; however, within the literature attempts have been made with the VCO technique to alter central and cerebral circulation by the periphery fluid shift. VCO has also been used in space on board Salyut-6/Soyuz in an attempt to prevent the headward fluid shift seen in microgravity. An occlusion cuff applied to the upper thigh and worn for twenty minutes at 40 to 60 mmHg was shown to decrease the sensation of "head pulsation" providing an early indication of this method as a potential spaceflight countermeasure (Matsnev *et al.*, 1983; Gorgiladze & Bryanov, 1989). However, these reports were lacking objective data and, to our knowledge, no further work on intermittent spaceflight VCO as an effective countermeasure has been conducted with data collection. Additionally, past VCO spaceflight-related use includes assessment of calf compliance during weightlessness (Watenpaugh *et al.*, 2001) and also during 18 days of bed rest (Bleeker *et al.*, 2004).

Furthermore, continuous daytime occlusion cuff wearing by astronauts, between 1995 and 1999 on-board the Russian space station MIR station, was shown to have a beneficial effect on reduced facial oedema and loss of vascular tone (Arbeille *et al.*, 1995; Herault *et al.*, 2000). However, vascular deconditioning was not tested and adherence to the experimental protocol, with exact durations of time worn, were not reported.

In the present study, results suggest an insufficient fluid shift is the likely factor in VCO as a poor simulated orthostatic challenge. However, any attempt to increase fluid displacement, through increased occlusion pressure, would prove counterproductive due to diminished arterial flow caused by partial occlusion (Greenfield *et al.*, 1963).

ΔMAP changes from BL were not significant during VCO and recovery. This is in contrast to several occlusion studies that show an immediate significant reduction of 15-22 mmHg following cessation of VCO (Tiecks *et al.*, 1995; Jünger *et al.*, 1997; White & Markus, 1997). It is possible that the smaller than expected drop in MAP, immediately following VCO, was due to a reduced demand on the autoregulatory system further discreditng VCO as a sufficent orthostatic challenege in the participants tested.

3.4.6 Conclusion

Our results suggest that bilateral lower-limb VCO at external pressures up to 120 mmHg, at the proximal end of the thigh, were insufficient at eliciting an increased and comparable response to HUT/HDT, and low-level LBNP and LAHC/SAHC. Specifically, in relation to the magnitude of cerebral tissue oxygenation decrease, peripheral, and systemic hemodynamic response. In addition, hemodynamic responses without significant pain during VCO (up to 100 mmHg) were even less capable of simulating an orthostatic challenge. Further research into the external/internal cuff pressure relationship, on VCO-induced fluid shifts and resultant hemodynamic response, may better characterise VCO orthostatic challenge potential.

The change in peripheral fluid displacements (ΔCC) during VCO were significant and reproducible but there were no notable changes from baseline in cerebral tissue oxygenation. Furthermore, ΔHR, ΔMAP, and ΔcTSI responses were not reproducible within the nine participants at 60 mmHg VCO. To our knowledge, this is the first study to: (i) investigate cardiovascular responses and cerebral tissue oxygenation to increasing levels of bilateral lower-limb VCO; and (ii) provide results that demonstrate the

insufficiencies of VCO as a simulated orthostatic challenge, and to elicit a reproducible systemic response, despite comparable peripheral fluid shifts.

Previous research suggest daily intermittent VCO, on the proximal end of the thighs, as a potential spaceflight countermeasure (Matsnev *et al.*, 1983; Gorgiladze & Bryanov, 1989). However, in the present study, we demonstrate VCO is unlikely to provide any physiological benefit, due to an insufficient orthostatic challenge devoid of any potential training effect, during intermittent use in spaceflight.

4 EFFECT OF NOVEL SHORT-ARM HUMAN CENTRIFUGATION INDUCED GRAVITATIONAL GRADIENTS UPON CARDIOVASCULAR RESPONSE, CEREBRAL TISSUE OXYGENATION AND OVERALL ORTHOSTATIC TOLERANCE

4.1 Introduction

Exposure to microgravity induces a number of deleterious effects on humans as a result of gravitational unloading; including muscle atrophy (Aaslid *et al.*, 1989), bone loss (Mack & LaChance, 1967), and cardiorespiratory deconditioning (Trappe *et al.*, 2006). In addition to unloading, such effects may also relate to a headward fluid shift following the negation of the normal hydrostatic pressure gradient (Hargens & Richardson, 2009). In fact, astronauts are often referred to be suffering from "puffy face" (Figure 4.1B) and "skinny leg" syndrome which is not only associated with sinus congestion (Greenleaf, 1984), but has recently been implicated in visual impairment and intracranial pressure (VIIP) syndrome (Donoviel & Sutton, 2013; Marshall-Bowman *et al.*, 2013).

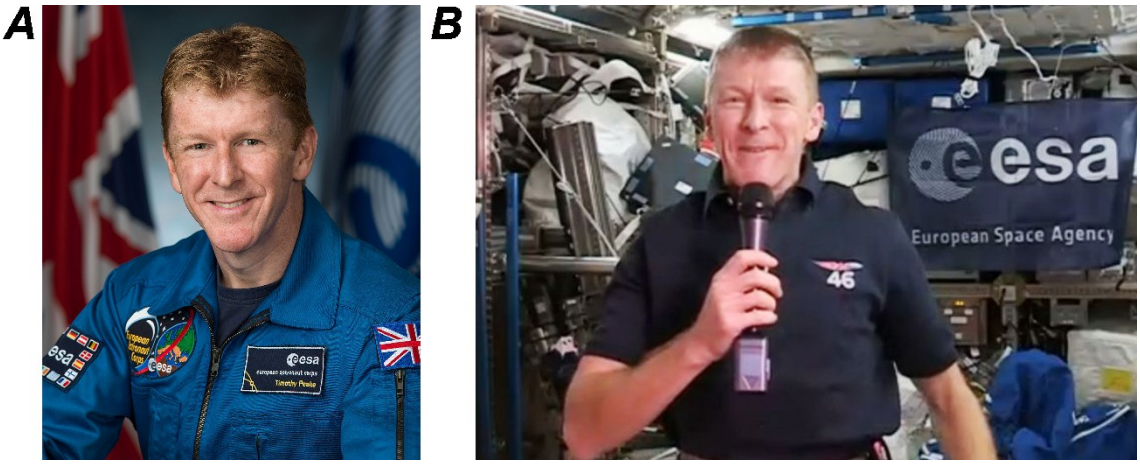

Figure 4.1 A, astronaut Timothy Peake before his space mission on Earth; and **B**, during 6 month mission to the International Space Station showing fluid shift seen here by facial edema. Adapted from European Space Agency (ESA).

4.1.1 Spaceflight countermeasures

Current spaceflight countermeasures on-board the International Space Station (ISS) attempt to ameliorate the effects of gravitational unloading through an extensive daily exercise program (Clément, 2011). Training consists of treadmill running, cycle ergometry and resistive exercise, which has been shown to be effective at reducing loss of muscle mass (Trappe *et al.*, 2009), bone density (Shackelford *et al.*, 2004) and cardiorespiratory function (Loehr *et al.*, 2011). However, despite such current countermeasures, typically 30-50% of all returning astronauts demonstrate orthostatic intolerance (OI) on return (Moore *et al.*, 1996; Blaber *et al.*, 2011). It is postulated that high OI incidence arises from current countermeasures targeting gravitational unloading without concurrent headward fluid shift reversal and combining the two may prove synergistic.

4.1.1.1 Artificial gravity

Long arm human centrifuges (LAHC) and high-performance aircraft g-exposure research has shown a relatively predictable dose-dependent effect of +Gz upon the cardiovascular system and thus g-tolerance, which is limited by the ability to maintain cerebral perfusion when coupled with a foot-ward fluid shift (Scott *et al.*, 2007). Repeated exposure to LAHC can improve orthostatic tolerance (Scott *et al.*, 2013) but remains impractical for an artificial gravity (AG) application during spaceflight due to technical limitations (Clement & Pavy-Le Traon, 2004).

Prolonged exposure to LAHC is associated with OI but this is without a g-gradient (*i.e.* almost constant gravitational forced experienced at head and feet). This is whilst short-

arm human centrifugation (SAHC) leads to a g-gradient where a far greater +Gz level is experienced at the feet in comparison to the head (Clement & Pavy-Le Traon, 2004). Recent research on Earth has shown that periodically shifting central blood volume to the periphery, via SAHC at 2.4 +Gz, leads to significant improvements in subsequent standing orthostatic tolerance (Goswami *et al.*, 2015b). However, whilst these results are promising, benefits need to be balanced against the risk of mild central hypovolemia and syncope during SAHC.

For LAHC and SAHC the orthostatic challenge is commonly defined in the literature as the g-level experienced at the feet for a particular duration. However, a third factor of body position with respect to the axis of rotation (rotational axis position; RAP) differs between LAHC and SAHC, leading to greater g-gradients in the latter. For instance the g-gradient, defined as the percentage difference between g-level at the head and feet, is approximately +22% for an 8 m radius LAHC and +72% (Figure 1.8) for the 2.4 m radius SAHC at the German Aerospace Center (DLR) in Cologne.

4.1.2 Hydrostatic gradient

Gravitational forces significantly alter the cardiovascular system even during every day postural movements. However, centrifugal force elicits an additional challenge, to a suitable cardiovascular response, through variations in the g-level experienced across the length of the body. On Earth there is a large pressure gradient from the head to the feet and this is almost entirely removed upon entering space; in a similar manner to supine (Figure 4.2).

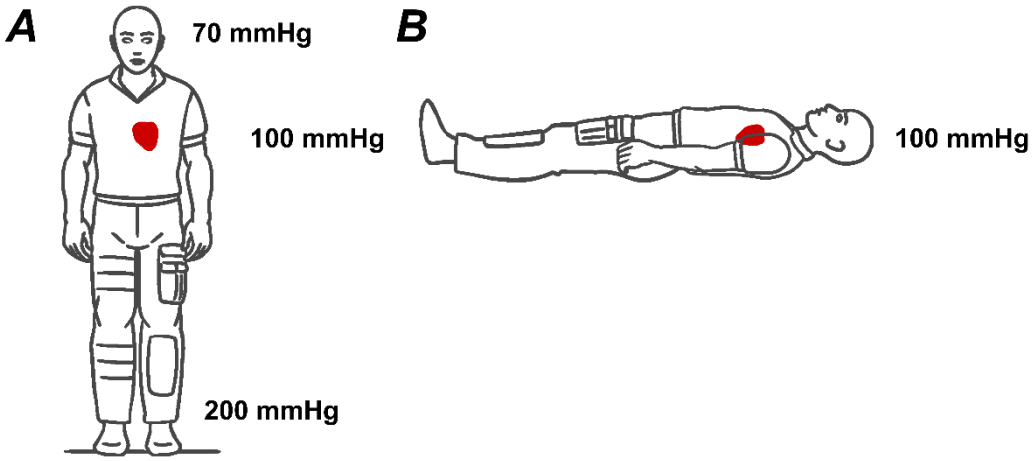

Figure 4.2 Hydrostatic pressure gradient from head to foot on Earth when **A**, standing and; **B**, supine. Adapted from (Clément, 2011).

Veins in the lower-limbs experience pressure of ~200 mmHg. Transition into weightlessness abolished the effective gradient, similar to what is observed when supine.

The hydrostatic gradient under constant 1 +Gz on Earth is fundamental to maintaining cardiovascular homeostasis and cardiopulmonary and carotid baroreceptors play an important role (Gabrielsen *et al.*, 1996; Pump *et al.*, 2001). Cardiovascular mechanisms evolved under a constant g-level and the resultant hydrostatic pressure changes across the body, from standing to supine on Earth, pose no significant orthostatic challenge to healthy individuals. Interestingly, during SAHC the pressures across the body are changed in a new way not seen in standing or supine on Earth, or in weightlessness. It is postulated that the differential hydrostatic pressures, between aortic and carotid regions, is critical to appropriate hemodynamic control. SAHC, with the ability to alter the hydrostatic gradient, may prove useful as a novel experimental paradigm in cardiovascular research. Specifically, SAHC presents an opportunity to examine the

interrelationship between different baroreceptors and the resultant hemodynamic response.

4.1.3 Gender effects

Several studies have shown a significantly different response between genders in response to an orthostatic stress. Convertino *et al.* (1998) showed woman had a greater heart rate (HR) response during LAHC with other research recording an overall reduced tolerance to SAHC (Fong *et al.*, 2007). Similarly, a greater HR response to LBNP in females, leading to reduced tolerance, has been reported (Montgomery *et al.*, 1977; Frey & Hoffler, 1988; White *et al.*, 1996). Research shows marked gender differences to an orthostatic challenge exist; however, anthropometrical differences between sexes has been shown as a non-contributory factor in LBNP (Lawler *et al.*, 1998). An observed reduced tolerance to an orthostatic stress has been attributed to females having a lower sympathetic outflow to peripheral vasculature (Shoemaker *et al.*, 2001) with Convertino (1998) demonstrating a reduced elevation of circulating norepinephrine (NE) in women, during orthostatic challenge, compared to men. Nevertheless, specific data pertaining to SAHC gender differences remain unclear.

4.1.4 Hemodynamic measurements

A large study by Weiss *et al.* (2005) showed measured differences in cerebral tissue saturation index (cTSI), measured by near-infrared spectroscopy (NIRS), correlated significantly to accurate changes in arterial oxygen saturation, arteriovenous oxygen extraction, and central venous oxygen saturation. If one assumes a constant cerebral metabolic rate, NIRS-derived cerebral perfusion presents as a useful tool in differentiating physiological response to an orthostatic challenge; where a drop below a

measured threshold leads to pre- and eventual syncope (Van Lieshout *et al.*, 2003). In addition, strain gauge plethysmography (SGP) remains the gold standard for quantification of peripheral limb volume changes and a surrogate to understand the extent of volume removed from the central circulation (Joyner *et al.*, 2001). Similarly, heart rate (HR) and blood pressure (BP) are accurate for quantifying overall systemic cardiovascular response and observations of presyncopal symptoms (PSS) in individuals can be used as an indicator of (reduced) g-tolerance.

Thus, in the present study, we investigated the effect of a shift in RAP (and resultant g-gradients) upon systemic cardiovascular response using HR and BP, peripheral fluid displacement using SGP, cerebral perfusion with NIRS, and orthostatic tolerance by observing PSS on the newly-constructed SAHC at the German Aerospace Centre (DLR, Cologne, Germany; Figure 2.2).

4.1.5 Aims

The aim of the study was to conduct a systematic comparative analysis of three standardised g-gradients (RAPs) to provide context, with the two extremities (*P1 vs. P3*) being used for comparative purposes. Specifically, to assess significant differences in cardiovascular responses, as a result of g-gradients. In addition, gender variances were examined to ascertain if RAP specific changes in hemodynamic response were affected by sex.

In general, the present study set out to characterise hemodynamic response to altered hydrostatic gradients during SAHC. Specifically, to provide a better insight for future artificial gravity (AG) research by investigating the third variable in human

centrifugation studies; namely g-gradient in addition to duration and magnitude of exposure.

4.1.6 Hypothesis

We hypothesized that RAP shift from the head to heart (altered g-gradient) during SAHC, with a comparable g-level at the feet, would improve g-tolerance through a reduction of peripheral fluid shifts, supported cerebral perfusion and thus attenuated systemic cardiovascular response.

4.2 Methods

4.2.1 Study design and participants

Twenty (10 male) healthy normotensive, non-smoking participants (Table 4.1) gave written informed consent to participate in the study that conformed to the declaration of Helsinki and was approved by the Ethics Committee of the North Rhine Medical Association in Düsseldorf, Germany.

Table 4.1 Participant individual data.

Age on first experimental day; height and weight measured immediately before centrifuge run.

	Sex	*Age (yrs)*	*Height (m)*	*Weight (kg)*	*BMI (kg/m^2)*
P01	M	24.1	1.75	65	21.2
P02	F	28.0	1.60	57	22.3
P03	F	26.4	1.71	64	21.9
P04	F	23.6	1.68	72	25.5
P05	F	21.8	1.64	70	26.0
P06	F	26.5	1.70	58	20.1
P07	F	29.4	1.61	51	19.7
P08	F	20.5	1.70	65	22.5
P09	F	26.4	1.60	60	23.4
P10	M	35.9	1.86	80	23.1
P11	M	22.5	1.73	69	23.1
P12	M	23.5	1.81	75	22.9
P13	F	24.1	1.73	65	21.7
P14	F	31.6	1.70	67	23.2
P15	M	33.2	1.85	82	24.0
P16	M	25.6	1.78	73	23.0
P17	M	29.2	1.75	75	24.5
P18	M	26.3	1.84	87	25.7
P19	M	21.7	1.75	65	21.2
P20	M	25.9	1.72	68	23.0
Mean ± SD	-	26.3 ± 4.0	1.73 ± 0.08	68 ± 9	22.9 ± 1.7

Before being enrolled into the study, all participants underwent medical screening which consisted of a clinical-chemical blood analysis described in detail in section 2.6.1.1. Further inclusion tests included: a resting electrocardiogram (ECG), adapted Bruce Protocol with cycle ergometry to verify appropriate aerobic fitness (for age and gender) and cardiac function (Bruce *et al.*, 1963), standing test for orthostatic tolerance assessment, and a medical history. Female participants additionally had to test negative on a urine-based pregnancy test before each session. Prior to testing each participant was familiarized with all aspects of the study, including the methodology, personnel involved and the short-arm human centrifuge (SAHC; Figure 4.3A).

4.2.2 Experimental protocol

Participants underwent ten passive 10 min SAHC runs over two experimental sessions on separate days (2 months apart) with rest phases of at least 25 min between each of the five runs per day (Figure 4.4). Each participant was tested on both occasions either in the morning (0900-1300) or afternoon (1300-1700). Prior to centrifugation participants were instructed to eat a light breakfast, or lunch 1 h before and, in the preceding 24 h period, consume no alcohol or caffeine. Participants were fixed to the centrifuge, in the supine position feet facing outwards, with an adjustable parachute harness and bicycle saddle. Centrifugation took place in the dark with participants asked to remain silent and completely still throughout unless experiencing discomfort. Monitoring took place via several infrared cameras on the face, chest and legs.

Each centrifuge run was performed at one of three centres of rotation an identical distance apart (above the head, *P1*; apex of the head, *P2* and at the heart, *P3*) thereby generating three differing g-gradients across the body, standardised against the

anatomical position of the heart (fourth intercostal space), in each participant. Gz forces were measure directly using a tri-axial accelerometer (SS26LB, Biopac Systems, Goleta, CA, USA) at the feet and heart-level. G-gradients are expressed as the percentage difference of g-level at the head in relation to g-level at the feet. At 2.4 +Gz at the feet the g-level at the head is +0.5 at *P1*, 0.0 at *P2* and -0.7 Gz at *P3*. These give rise to differences of +1.9, +2.4 and +3.1 Gz (*P1*, *P2* and *P3* respectively) and g-gradients of +81 %, *P1*; +100 %, *P2*; and +130 %, *P3* (Table 4.2; and grey shaded area, Figure 4.3B). In addition, three standardised g-levels at the feet (1.0 +Gz, 1.7 +Gz and 2.4 +Gz) were tested in a random combination and order for nine total centrifuge profiles with the addition of a tenth familiarisation run at the start.

Table 4.2 Effective g-level and gradient for participant at 2.4 +Gz.

P1, above head; ***P2***, head apex; and ***P3***, heart-level. **G-gradient**, defined as the percentage difference between g-level at the head and feet at 2.4 +Gz.

	G-level at Head (+/-Gz)	*G-level at Feet (+Gz)*	*Delta G-level (+Gz)*	*G-gradient (%)*
P1	+0.5	+2.4	+1.9	**+81**
P2	+0.0	+2.4	+2.4	**+100**
P3	-0.7	+2.4	+3.1	**+130**

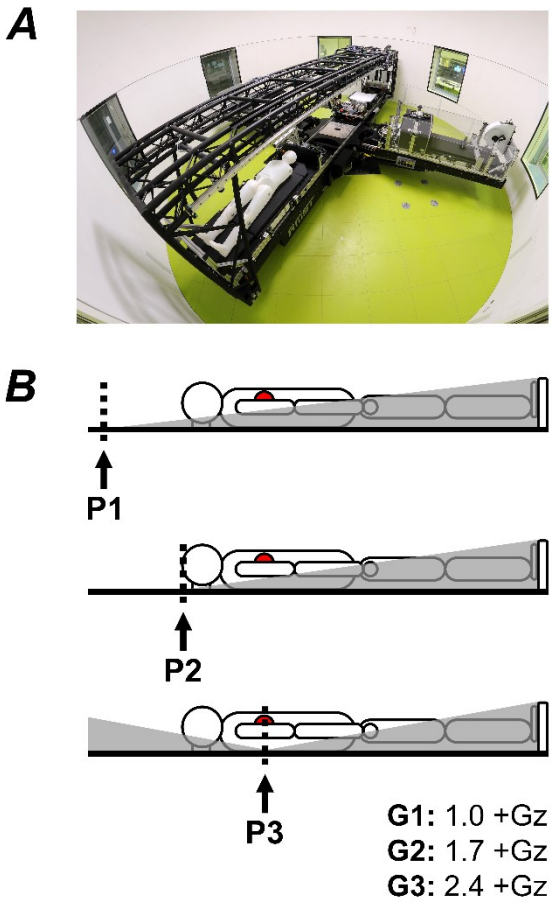

Figure 4.3 Protocol overview.

A, short-arm human centrifuge (SAHC) with unique capability to alter rotational axis position and thus g-gradient (at DLR, Cologne, Germany); **B**, Nine centrifuge profiles in total (3x3) - three centres of rotation: *P1*, above the head; *P2*, apex of head; and *P3* at heart-level and three g-levels at the feet: G1, 1.0 +Gz; G2, 1.7 +Gz; and G3, 2.4 +Gz.

Grey shaded area, altered g-gradient across the body at each rotational axis position: *P1*, +81 %; *P2*, +100 %; and *P3*, +130 % (at 2.4 +Gz; Table 4.2).

Each of the two testing days consisted of five centrifuge profiles (Figure 4.4A), randomly assigned with an online randomizer (random.org, 2016). Each centrifuge profile was split into five distinct phases (Figure 4.4B) with a fixed ramp-up and -down time (120 s) irrespective of g-level. Comparable physiological responses relating to g-tolerance have been shown to be dependent on the g-onset time (Whinnery & Forster,

2013) and the approach taken in this study removes the prospect of this having an influencing factor.

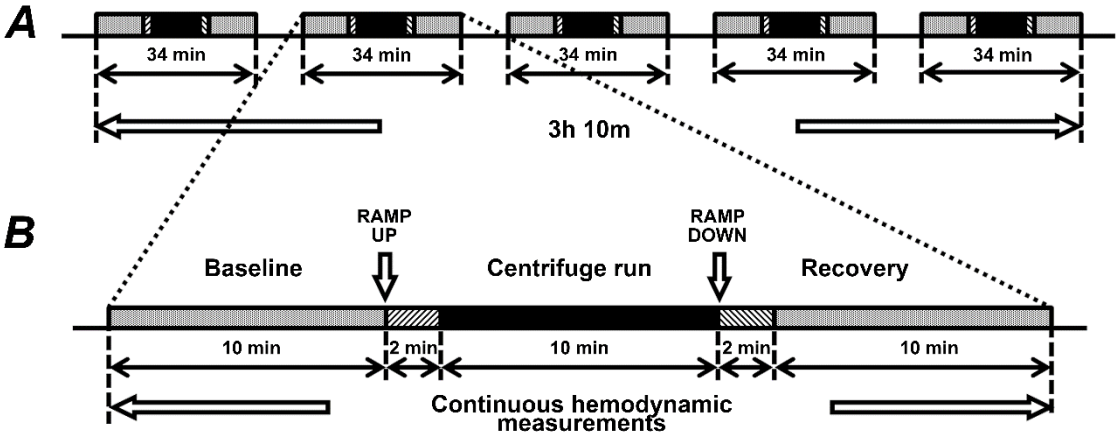

Figure 4.4 Protocol duration with constituent centrifuge profile phases

A, protocol consisting of five randomised centrifuge profiles (34 min each), with no less than 25 min rest between them, thus constituting a protocol of 3 h 10 min; **B**, single profile over 34 min consisting of five phases: baseline, ramp-up, centrifuge run, ramp-down and recovery.

4.2.2.1 Cerebral perfusion

Cerebral near-infrared spectroscopy of the left prefrontal cortex immediately below the forehead hairline of each participant (cNIRS; PortaLite, Artinis Medical Systems, The Netherlands; Figure 4.5C) was used to determine the absolute ratio of oxy- (O_2Hb) and deoxyhemoglobin (HHb). Taking into account participant frontal cranium thickness, based on age and gender, the cerebral tissue saturation index (cTSI) was deduced (Lynnerup *et al.*, 2005), which has been shown to correlate well to prefrontal cortex cerebral perfusion (Weiss *et al.,* 2005).

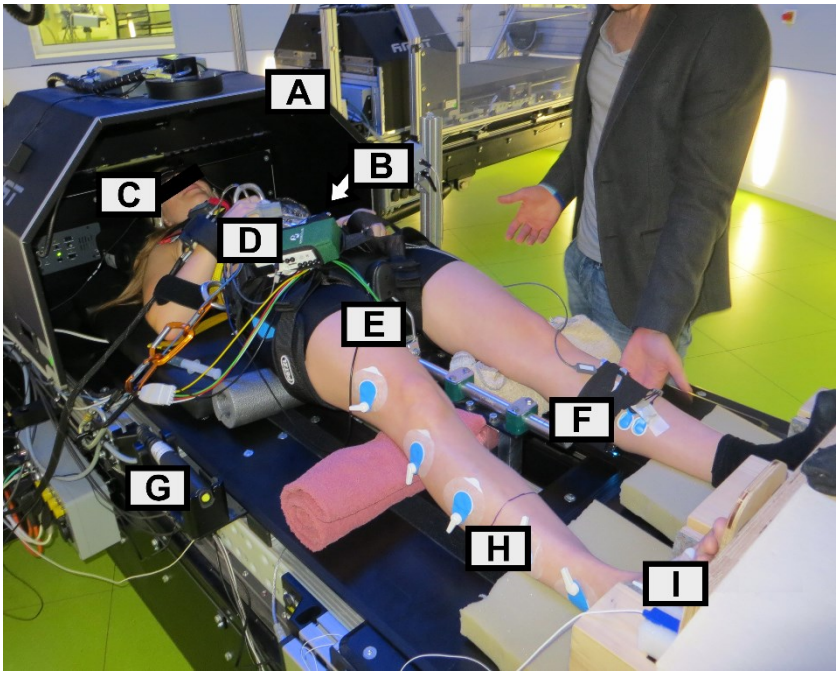

Figure 4.5 Experimental setup.

A, centrifuge cover hood with mounted infrared camera; **B**, blood pressure cuff for medical monitoring; **C**, near infrared spectroscopy (NIRS) of the prefrontal cortex; **D**, Finapres continuous blood pressure monitor; **E**, participant 'seated' in a bicycle saddle to prevent muscle pump activation; **F**, NIRS of the calf muscle; **G**, emergency alarm for participant safety; **H**, strain gauge plethysmography of the calf; and **I**, Accelerometer measuring accurate +Gz level at the feet.

4.2.2.2 Peripheral fluid displacement

Movement of fluid to the lower extremities, and away from the central compartment, was quantified using strain gauge plethysmography (SGP; EC6 Strain Gauge Plethysmograph, Hokanson Inc., Bellevue, WA, USA); positioned around the calf midpoint (directly between the tibiae tuberosity and medial malleolus bony prominences) of each participant (Figure 4.5H). Claydon and Hainsworth (2005) demonstrated individuals with orthostatic intolerance (OI) exhibited subconscious

strategies in which venous return was improved. As such, a bike saddle was installed on the centrifuge to limit leg 'muscle-pump' activation (Figure 4.5E).

4.2.2.3 Systemic cardiovascular measurements

Continuous beat-by-beat heart rate (HR) via a standard 3-lead electrocardiogram (ECG; Biopac Systems, Goleta, CA, USA) and mean arterial finger blood pressure (MAP) was recorded with a Finometer (Finapres Medical Systems, Amsterdam, The Netherlands). The Finometer finger cuff was placed around the third finger of the right hand and fixed by a sling at the level of the fourth intercostal space at the level of the heart (Figure 4.5D). Finometer BP measurements were corroborated with absolute arterial BP measurements obtained by an automated sphygmomanometer (Intellivue MMS X2, Philips, Best, The Netherlands) prior to starting the profile. Stroke volume (SV) and total peripheral resistance (TPR) were estimated from the arterial BP waveform using the Modelflow method (Leonetti, *et al.* 2004) via Beatscope software (TNO-TPD, Biomedical Instrumentation, Amsterdam, The Netherlands).

4.2.2.4 Presyncopal symptoms (PSS)

Participants were retrospectively classified as experiencing presyncopal symptoms (PSS+) or not (PSS-) when one (or more) of the following was observed: (i) continuous HR and BP decrements for longer than 15 s; (ii) nausea, paleness, dizziness; and/or (iii) participant requested run termination.

4.2.3 Statistical analysis

Following a pilot study of the measures used in this paper in which fluid shifts were induced, an error probability (α) of 0.05, power ($1 - \beta$) of 0.80 with an average effect

size (d) of 0.05, power calculation, using G* Power (Erdfelder, Faul, & Buchner, 1996), yielded a participant number of 15. However, due to the challenging nature of the experiment an additional 25% were recruited to mitigate any attrition.

All continuously recorded data were analysed in 10 s frames and artefacts were removed offline with a custom made Matlab (R2015a, The Mathworks Inc., MA, USA) script using the following criteria: (i) conservative and plausible physiological limits (Table 2.2); and (ii) maximal percentage of change in relation to the standard deviation of the signal. Data was resampled at 4Hz (piecewise cubic spline interpolation) as long as >95% of data were valid yielding 15 complete sets of data for further analysis. Data presented are delta values of each 1 min mean of the 24 min measurements following ramp-up from mean of the last fives minutes of the 10 min baseline immediately before each corresponding profile.

R (R Foundation for Statistical Computing, Vienna, Austria) and *lme4 (Bates et al., 2012)* were used to perform linear mixed effect (LME) analysis of the relationship between each cardiovascular parameter and the time course of each centrifuge run. Time, position and g-level at the feet (with 2 and 3-way interactions) were entered into the model with intercepts for each participant as a random effect, with a second model incorporating participant sex to explore gender effects. Visual inspection of residual plots did not reveal any obvious deviations from homoscedasticity or normality of residuals. P-values were obtained by likelihood ratio tests of the full model with the effect (time, position and g-level at the feet) in question, against the model without that effect.

To reduce complexity of the models, a secondary analysis was performed with data both averaged for each 2 min increment of centrifugation and compared for differences arising due to position at that moment. To evaluate the specific differences induced (*P1* vs. *P3*; and male vs. female), one-way analysis of variance (ANOVAs) were conducted, followed by post hoc tests with preventive post hoc control of the type I error rate (Tukey's Honestly Significant Difference, HSD).

Linear regression analysis was used to estimate the relationships among hemodynamic variables and a chi-square test of independence was used to estimate equality of proportions between RAP, and gender. The data are presented as mean (±SEM) unless otherwise stated with the level of significance set at $p \leq 0.05$.

4.3 Results

Twenty participants completed all short-arm human centrifuge (SAHC) profiles, during g-levels from 1.0 to 2.4 +Gz at the feet in position 1 (*P1*, above head), position 2 (*P2*, head-apex), and position 3 (*P3*, heart-level). The greatest difference in cardiovascular response occurred at the highest g-level (2.4 +Gz) with the largest attenuations observed between SAHC in *P1* and *P3*. Initially data are presented for all g-gradients (*P1-3*) and g-levels (1.0-2.4 +Gz) with further analysis consisting of *P1/P3* time-course comparisons across the whole 24 min run (ramp-up, centrifugation, ramp-down, and recovery). Baseline values, prior to the start of experimentation, for all participants are outline in

Table 4.3.

Table 4.3 Participant absolute mean baseline (BL) values for all parameters.

Measured BL is a mean of the last minute immediately before start of the experiment in all participants (n=20).

HR, heart rate; **SV**, stroke volume; **TPR**, total peripheral resistance; **MAP**, mean arterial pressure; **CC**, calf circumference; **mTSI**, muscle tissue saturation index; **cTSI**, cerebral tissue saturation index.

Parameter	*Absolute mean baseline (BL) ± SEM*
HR	65 ± 2 bpm
SV	86.8 ± 3.6 mL
TPR	1181 ± 73 dyn.s.cm^{-5}
MAP	74 ± 2 mmHg

CC	338 ± 3 mm
mTSI	64.78 ± 0.90 %
cTSI	68.20 ± 1.77 %

4.3.1 G-level / g-gradient effect on cardiovascular response

G-level (+Gz) as a fixed effect was shown by the linear mixed effects model to be highly significant for changes from baseline (BL) in mean heart rate (ΔHR), averaged mean arterial pressure (ΔMAP), mean stroke volume (ΔSV), and mean total peripheral resistance (ΔTPR; Table 4.4A). Significant main effects of rotation axis position (RAP), giving rise to a specific g-gradient (*P1-3*), were found in ΔHR, ΔMAP, ΔSV and ΔTPR (Table 4.4A) with several two and three-way interactions between variables also observed (*Time:Position:G-level;* Table 4.4B).

Table 4.4 Effects and their standard errors of cardiovascular variables as a result of time, position and g-level.

A, main effects tabulated linear mixed effects statistics; and **B**, interaction effects.

HR, heart rate; **SV,** stroke volume; **TPR,** total peripheral resistance; **MAP,** mean arterial pressure.
Time, measured in seconds from the start of the centrifuge phase; **position,** expressed as multiple of the distance from heart-level to the apex of the head (in relation to the rotational axis); **g-level,** +Gz experienced during each profile at the feet.

A

		(Intercept)			**Time (s)**			**Position (HL)**			**G-level (+Gz)**		
	n	*Effect ± SE*	*F-value*	*p-value*	*Effect ± SE*	*F-value*	*p-value*	*Effect ± SE*	*F-value*	*p-value*	*Effect ± SE*	*F-value*	*p-value*
ΔHR (bpm)	20	-8.98 ± 1.77	54.0	< 0.001	0.009 ± 0.004	658	< 0.05	-2.63 ± 0.60	6365	< 0.001	3.53 ± 0.80	13038	< 0.001
ΔSV (mL)	20	17.4 ± 2.1	409	< 0.001	-0.015 ± 0.005	78.6	< 0.001	-9.70 ± 0.85	1949	< 0.001	-16.6 ± 1.15	3037	< 0.001
ΔTPR (dyn.s.cm^{-5})	20	-239.2 ± 51.1	136	< 0.001	0.241 ± 0.135	44.1	< 0.001	199.0 ± 20.9	678	< 0.001	222.7 ± 28.1	14.6	< 0.001
ΔMAP (mmHg)	20	-9.56 ± 1.39	3.65	0.056	0.011 ± 0.003	3.58	0.058	3.13 ± 0.53	3537	< 0.001	1.48 ± 0.71	196	< 0.001

B

		Time (s) : Position (HL)			**Time (s) : G-level (+Gz)**			**Position (HLs) : G-level (+Gz)**			**Time (s) : Position (HL) : G-level (+Gz)**		
	n	*Effect ± SE*	*F-value*	*p-value*	*Effect ± SE*	*F-value*	*p-value*	*Effect ± SE*	*F-value*	*p-value*	*Effect ± SE*	*F-value*	*p-value*
ΔHR (bpm)	20	-0.010 ± 0.002	221	< 0.001	-0.008 ± 0.002	277	< 0.001	4.30 ± 0.36	1782	< 0.001	0.011 ± 0.001	112	< 0.001
ΔSV (mL)	20	0.011 ± 0.002	27.5	< 0.001	-0.010 ± 0.003	44.4	< 0.001	3.52 ± 0.51	12.3	< 0.001	-0.009 ± 0.001	35.0	< 0.001
ΔTPR (dyn.s .cm^{-5})	20	-0.040 ± 0.061	0.221	0.638	-0.195 ± -.081	24.9	< 0.001	-75.1 ± 12.5	122	< 0.001	0.019 ± 0.037	0.258	0.611
ΔMAP (mmHg)	20	-0.002 ± 0.002	0.001	0.982	-0.007 ± 0.002	32.4	< 0.001	0.772 ± 0.318	53.5	< 0.001	0.001 ± 0.001	2.07	0.151

Specific baseline (BL) changes: Post hoc analysis revealed SAHC at *P1* resulted in positive changes from BL in ΔHR across all g-levels (1.0-2.4 +Gz: $p<0.01$-0.001); with a similar observation at *P2* during 1.7 +Gz ($p<0.001$) and 2.4 +Gz ($p<0.001$) but not 1.0 +Gz ($p=0.110$; Figure 4.6A). ΔHR at *P3* compared to BL was only significantly positive at the highest g-level (1.0 +Gz: $p=0.318$; 1.7 +Gz: $p=0.169$; and 2.4 +Gz: $p<0.001$; Figure 4.6A). ΔMAP at *P1* was significantly positive during 1.0 +Gz ($p=0.018$) and 1.7 +Gz ($p<0.001$) but not at 2.4 +Gz ($p=0.071$) compared to BL; whilst at *P2* ΔMAP was unchanged during all g-levels (1.0-2.4 +Gz: $0.292<p<0.612$; Figure 4.6B). ΔMAP at *P3* was unchanged during 1.0 +Gz ($p=0.135$) but significantly negative at 1.7 +Gz ($p=0.017$) and 2.4 +Gz ($p<0.001$; Figure 4.6B).

In all positions (*P1-3*) and across all g-levels (1.0-2.4 +Gz) ΔSV was significantly negative compared to BL ($p<0.01$-0.001; Figure 4.6C). Conversely, in all positions (*P1-3*) and across all g-levels (1.0-2.4 +Gz) ΔTPR was significantly positive compared to BL ($p<0.05$-0.001; Figure 4.6D).

Rotational axis position comparison (RAP, P_{n1} vs. P_{n2}): Post hoc analysis revealed ΔHR was no different at *P1* compared to *P2* (*P1 vs. P2*) during 1.0 +Gz ($p=0.949$) but significantly greater at 1.7 +Gz ($p<0.001$) and 2.4 +Gz ($p<0.001$; Figure 4.6A). Similarly, ΔHR was significantly greater at *P2* compared to *P3* (*P2 vs. P3*) during 1.7 +Gz ($p=0.001$) and 2.4 +Gz ($p<0.001$) but not 1.0 +Gz ($p=0.059$; Figure 4.6A). During all g-levels at *P1*, ΔHR was significantly higher compared to *P3* (*P1 vs. P3*, 1.0-2.4 +Gz: $p<0.05$-0.001) with the greatest difference during 2.4 +Gz (45 ± 4 *vs.* 8 ± 2 bpm, $p<0.001$; Figure 4.6A).

ΔMAP was no different at *P1* compared to *P2* (*P1 vs. P2*) during all g-levels (1.0-2.4 +Gz: 0.096<p<0.306; Figure 4.6B). However, ΔMAP was significantly greater at *P2* compared to *P3* (*P2 vs. P3*) during 1.7 +Gz (p=0.025) and 2.4 +Gz (p=0.014) but not 1.0 +Gz (p=0.143; Figure 4.6B). During all g-levels at *P1*, ΔMAP was significantly higher compared to *P3* (*P1 vs. P3*, 1.0-2.4 +Gz: p<0.05-0.001) with the greatest difference during 1.7 +Gz (6 ± 1 *vs.* -5 ± 2 mmHg, p<0.001; Figure 4.6B).

ΔSV was no different at *P1* compared to *P2* (*P1 vs. P2*) during all g-levels (1.0-2.4 +Gz: 0.128<p<0.647; Figure 4.6C). However, ΔSV was significantly lower at *P2* compared to *P3* (*P2 vs. P3*) during 1.0 +Gz (p=0.011) and 2.4 +Gz (p=0.007) but not 1.7 +Gz (p=0.206; Figure 4.6C). During all g-levels at *P1*, ΔSV was significantly lower compared to *P3* (*P1 vs. P3*, 1.0-2.4 +Gz: p<0.05-0.001) with the greatest difference during 2.4 +Gz (-34.7 ± 2.4 *vs.* -19.2 ± 1.6 mL, p<0.001; Figure 4.6C).

ΔTPR was no different at *P1* compared to *P2* (*P1 vs. P2*; 0.309<p<0.879), or *P2* compared to *P3* (*P2 vs. P3*; 0.153<p<0.381) during all g-levels (1.0-2.4 +Gz; Figure 4.6D). Similarly, ΔTPR at *P1* compared to *P3* (*P1 vs. P3*) during 1.0 +Gz and 2.4 +Gz showed no difference (1.0 +Gz: p=0.065; and 2.4 +Gz: p=0.312) but was significantly greater during 1.7 +Gz (346 ± 67 *vs.* 153 ± 38 dyn.s.cm^{-5}, p=0.040; Figure 4.6D).

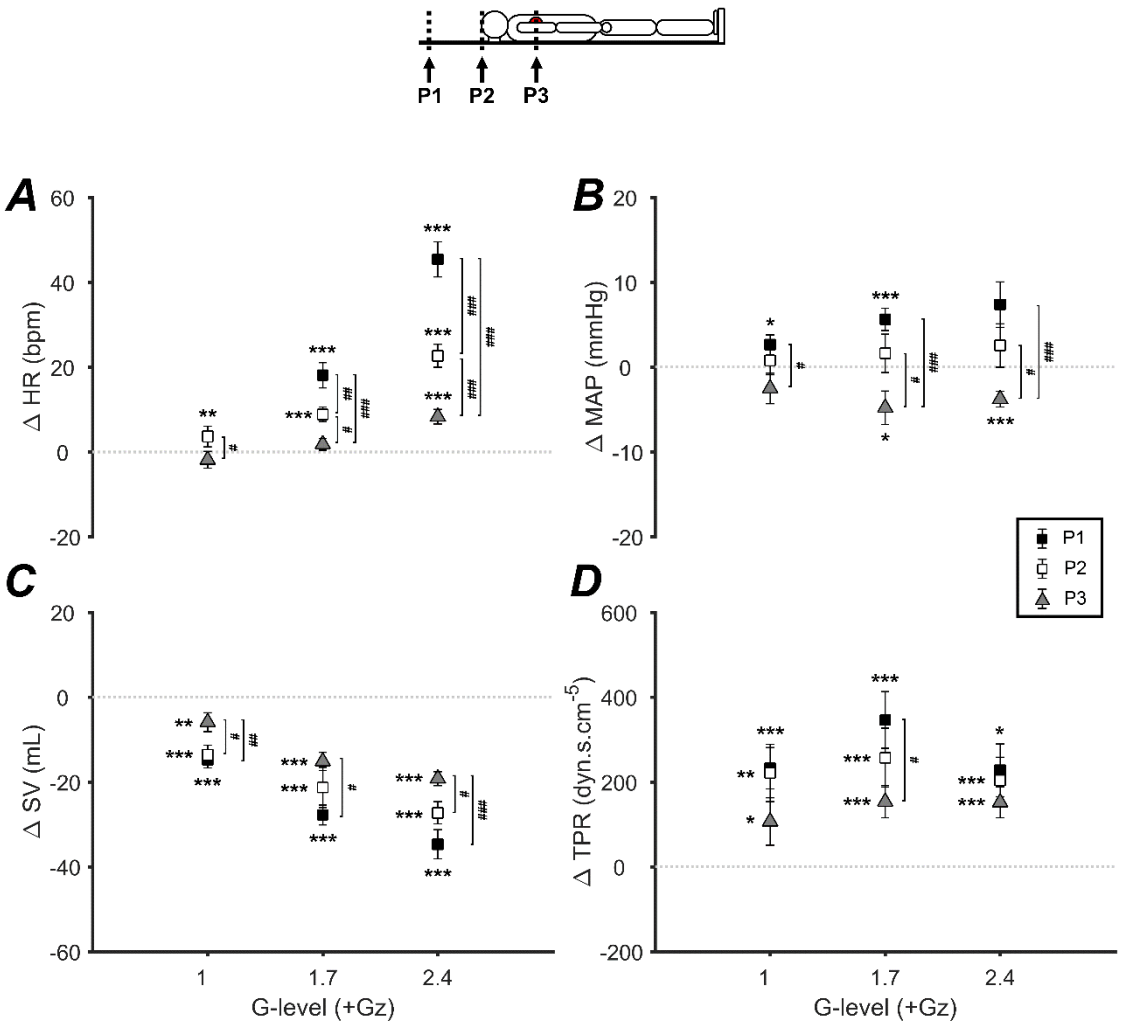

Figure 4.6 Mean changes from baseline (BL) for cardiovascular measures in the final minute (min 10) of short-arm human centrifugation (SAHC, 1.0 to 2.4 +Gz) at position 1 (*P1*, above the head), position 2 (*P2*, apex of head), and position 3 (*P3*, heart-level).

A, changes from baseline (BL) in mean heart rate (ΔHR); **B**, changes from BL in averaged mean arterial pressure (ΔMAP); **C**, changes from BL in mean stroke volume (ΔSV); and **D**, changes from BL in mean derived total peripheral resistance (ΔTPR).

Mean at each g-level (± SEM) is calculated as a final minute (min 10) mean delta from the final minute (min 10) mean of the baseline (BL) immediately before each respective centrifuge run. **Black square**, at position 1 ($P1$, above head); **white square**, at position 2 ($P2$, apex of head); and **grey triangle**, at position 3 ($P3$, heart-level). Baseline (*): * $p < 0.05$, ** $p < 0.01$, *** $< p < 0.001$. Position (#): # $p < 0.05$, ## $p < 0.01$, ### $p < 0.001$. n = 20.

4.3.2 G-level / g-gradient effect on lower-limb peripheral fluid displacement

G-level (+Gz) as a fixed effect was shown by the linear mixed effects model to be highly significant for changes from baseline (BL) in calf circumference (ΔCC; Table 4.5A). Significant main effects of rotation axis position (RAP), giving rise to a specific g-gradient (*P1-3*), were also found in ΔCC with significant two and three-way interactions also observed (*Time:Position:G-level;* Table 4.5B).

Specific baseline (BL) changes: Post hoc analysis revealed SAHC in all positions (*P1-3*) and across all g-levels (1.0-2.4 +Gz) ΔCC was significantly positive compared to BL ($p<0.01$-0.001; Figure 4.7).

Rotational axis position comparison (RAP, P_{n1} vs. P_{n2}): Post hoc analysis revealed ΔCC was no different at *P1* compared to *P2* (*P1 vs. P2*) during all g-levels ($0.191<p<0.429$; Figure 4.7). However, ΔCC was significantly greater at *P2* compared to *P3* (*P2 vs. P3*) during 1.0 +Gz ($p=0.035$) and 2.4 +Gz ($p=0.038$) but not 1.7 +Gz ($p=0.741$; Figure 4.7). ΔCC at *P1* was significantly higher compared to *P3* (*P1 vs. P3*) only at the highest g-level (2.4 +Gz: 5.2 ± 0.6 *vs.* 3.0 ± 0.4 mm, $p=0.005$; Figure 4.7).

Table 4.5 Effects and their standard errors of calf circumference (CC) as a result of time, position and g-level.

A, main effects tabulated linear mixed effects statistics;
B, interaction effects tabulated linear mixed effects statistics.

Time, measured in seconds from the start of the centrifuge phase; **position,** expressed as multiple of the distance from heart-level to the apex of the head (in relation to the rotational axis); **g-level,** +Gz experienced during each profile at the feet.

A

		(Intercept)			**Time (s)**			**Position (HL)**			**G-level (+Gz)**		
	n	*Effect ± SE*	*F-value*	*p-value*	*Effect ± SE*	*F-value*	*p-value*	*Effect ± SE*	*F-value*	*p-value*	*Effect ± SE*	*F-value*	*p-value*
ΔCC (mm)	20	0.102 ± 0.431	32.0	< 0.001	0.001 ± 0.001	1793	< 0.001	-0.112 ± 0.115	1035	< 0.001	0.379 ± 0.155	2938	< 0.001

B

		Time (s) : Position (HL)			**Time (s) : G-level (+Gz)**			**Position (HLs) : G-level (+Gz)**			**Time (s) : Position (HL) : G-level (+Gz)**		
	n	*Effect ± SE*	*F-value*	*p-value*	*Effect ± SE*	*F-value*	*p-value*	*Effect ± SE*	*F-value*	*p-value*	*Effect ± SE*	*F-value*	*p-value*
ΔCC (mm)	20	-0.001 ± 0.000	175	< 0.001	0.000 ± 0.000	291	< 0.001	0.156 ± 0.069	262	< 0.001	0.001 ± 0.000	45.8	< 0.001

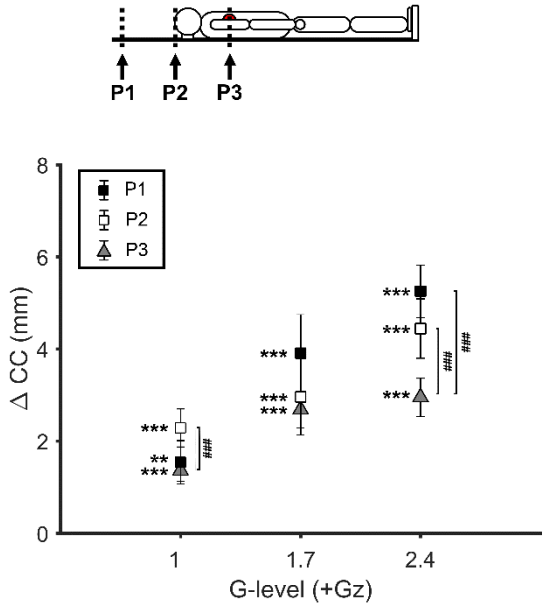

Figure 4.7 Mean changes from baseline (BL) for calf circumference (ΔCC) in the final minute (min 10) of short-arm human centrifugation (SAHC, 1.0 to 2.4 +Gz) at position 1 (*P1*, above the head), position 2 (*P2*, apex of head), and position 3 (*P3*, heart-level).

Mean at each g-level (± SEM) calculated as a final minute (min 10) mean delta from final minute (min 10) mean of the baseline (BL) immediately before each respective centrifuge run. **Black square**, at position 1 (*P1*, above head); **white square**, at position 2 (*P2*, apex of head); and **grey triangle**, at position 3 (*P3*, heart-level). Baseline (*): * $p < 0.05$, ** $p < 0.01$, *** $< p < 0.001$. Position (#): # $p < 0.05$, ## $p < 0.01$, ### $p < 0.001$. n = 20.

4.3.3 G-level / g-gradient effect on cerebral perfusion

G-level (+Gz) as a fixed effect was shown by the linear mixed effects model to be highly significant for changes from baseline (BL) in prefrontal cortex cerebral tissue saturation index (ΔcTSI; Table 4.6A). Significant main effects of rotation axis position (RAP), giving rise to a specific g-gradient (*P1-3*), were also found in ΔcTSI with significant two and three-way interactions also observed (*Time:Position:G-level;* Table 4.6B).

Table 4.6 Effects and their standard errors of prefrontal cortex cerebral tissue saturation index (cTSI) as a result of time, position and g-level (fixed effects).

A, main effects tabulated linear mixed effects statistics;
B, interaction effects tabulated linear mixed effects statistics.

Time, measured in seconds from the start of the centrifuge phase; **position,** expressed as multiple of the distance from heart-level to the apex of the head (in relation to the rotational axis); **g-level,** +Gz experienced during each profile at the feet.

A

		(Intercept)			**Time (s)**			**Position (HL)**			**G-level (+Gz)**		
	n	*Effect ± SE*	*F-value*	*p-value*	*Effect ± SE*	*F-value*	*p-value*	*Effect ± SE*	*F-value*	*p-value*	*Effect ± SE*	*F-value*	*p-value*
ΔcTSI (%)	20	2.42 ± 0.33	18.8	< 0.001	-0.002 ± 0.001	6.55	<0.05	-0.66 ± 0.12	1194	< 0.001	-1.46 ± 0.16	2452	< 0.001

B

		Time (s) : Position (HL)			**Time (s) : G-level (+Gz)**			**Position (HLs) : G-level (+Gz)**			**Time (s) : Position (HL) : G-level (+Gz)**		
	n	*Effect ± SE*	*F-value*	*p-value*	*Effect ± SE*	*F-value*	*p-value*	*Effect ± SE*	*F-value*	*p-value*	*Effect ± SE*	*F-value*	*p-value*
ΔcTSI (%)	20	0.002 ± 0.000	7.56	< 0.01	0.002 ± 0.000	20.1	< 0.001	0.120 ± 0.70	45.2	< 0.001	-0.001 ± 0.000	34.5	< 0.001

Specific baseline (BL) changes: Post hoc analysis revealed SAHC at *P1* resulted in negative changes from BL in ΔcTSI during only the highest g-level (1.0 +Gz: p=0.504; 1.7 +Gz: p=0.091; and 2.4 +Gz: p=0.001); with a similar observation at *P2* (1.0 +Gz: p=0.160; 1.7 +Gz: p=0.964; and 2.4 +Gz: p<0.001); and *P3* 1.0 +Gz: p=0.158; 1.7 +Gz: p=0.698; and 2.4 +Gz: p=0.003; Figure 4.8).

Rotational axis position comparison (RAP, P_{n1} vs. P_{n2}): Post hoc analysis revealed ΔcTSI was no different at *P1* compared to *P2* (*P1 vs. P2*) during 1.0 +Gz (p=0.544) and 1.7 +Gz (p=0.213) but significantly lower at 2.4 +Gz (p=0.011; Figure 4.8). Similarly, ΔcTSI was significantly lower at *P2* compared to *P3* (*P2 vs. P3*) during 1.0 +Gz (p=0.046) only and not 1.7 +Gz (p=780) or 2.4 +Gz (p=0.130; Figure 4.8). ΔcTSI at *P1*was significantly lower compared to *P3* (*P1 vs. P3*) at the highest g-level only (2.4 +Gz: -3.54 ± 0.50 *vs.* -0.96 ± 0.31 %, p<0.001; Figure 4.8).

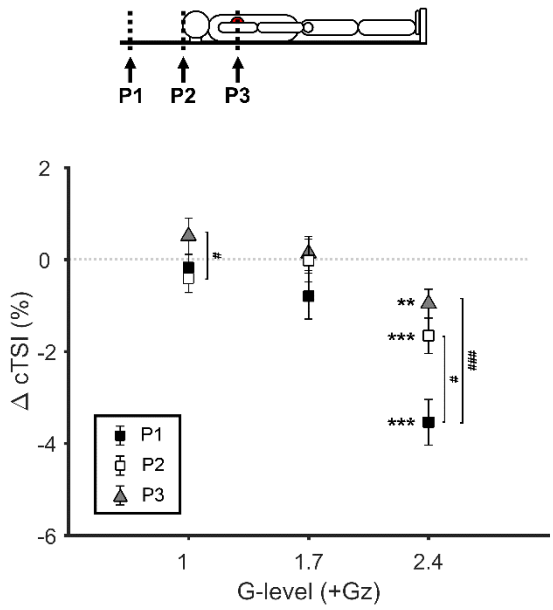

Figure 4.8 Mean changes from baseline (BL) for near-infrared spectroscopy (NIRS) measured prefrontal cortex cerebral tissue saturation index (ΔcTSI) in the final minute (min 10) of short-arm human centrifugation (SAHC, 1.0 to 2.4 +Gz) at position 1 (*P1*, above the head), position 2 (*P2*, apex of head), and position 3 (*P3*, heart-level).

Mean at each g-level (± SEM) calculated as a final minute (min 10) mean delta from final minute (min 10) mean of the baseline (BL) immediately before each respective centrifuge run. **Black square**, at position 1 (*P1*, above head); **white square**, at position 2 (*P2*, apex of head); and **grey triangle**, at position 3 (*P3*, heart-level). Baseline (*): * $p < 0.05$, ** $p < 0.01$, *** $< p < 0.001$. Position (#): # $p < 0.05$, ## $p < 0.01$, ### $p < 0.001$. n = 20.

4.3.4 Attenuated cardiovascular response and duration

Time (s) as a fixed effect was shown by the linear mixed effects model to be highly significant for changes from baseline (BL) in mean heart rate (ΔHR), mean stroke volume (ΔSV), and mean total peripheral resistance (ΔTPR) but not averaged mean arterial pressure (ΔMAP; Table 4.4A).

Specific baseline (BL) changes: Post hoc analysis revealed ΔHR was significantly positive at *P1* (above head) during all 2.4 +Gz 10 min short-arm human centrifugation (SAHC) compared to baseline (BL, min 0-10, $p<0.05$); as was ΔHR at position 3 (*P3*) but to a lesser extent (BL, min 0-10, $p<0.05$; Figure 4.9A). During ramp-down and recovery (RR: min 10-22), ΔHR at *P1* was significantly negative compared to BL (min 14-22: $p<0.05$), and unchanged from min 14-22 at *P3* ($0.081<p<0.978$; Figure 4.9A)

ΔMAP was significantly positive during min 1-5 of SAHC compared to baseline (BL, $p<0.05$); conversely, at *P3* ΔMAP was significantly negative (min 0-10, $p<0.05$; Figure 4.9B). During RR, ΔMAP at *P1* was unchanged as was *P3* compared to BL (min 14-22; Figure 4.9B).

ΔSV was significantly negative at *P1* during min 1-11 SAHC compared to baseline (BL, $p<0.05$) as was ΔSV at *P3* but to a lesser extent (BL, min 0-11, $p<0.05$; Figure 4.9C). During RR, ΔSV at *P1* was unchanged apart for a significant increase at min 15 compared to BL ($p<0.05$); however, at *P3* ΔSV was completely unchanged (Figure 4.9C). ΔTPR was significantly positive at *P1* during min 0-8 SAHC compared to baseline (BL, $p<0.05$) as was ΔTPR at *P3* at min -1, 1-10 ($p<0.05$; Figure 4.9D). During RR, ΔTPR at *P1* was unchanged; however, min 13 at *P3* was significantly negative compared to BL (Figure 4.9D).

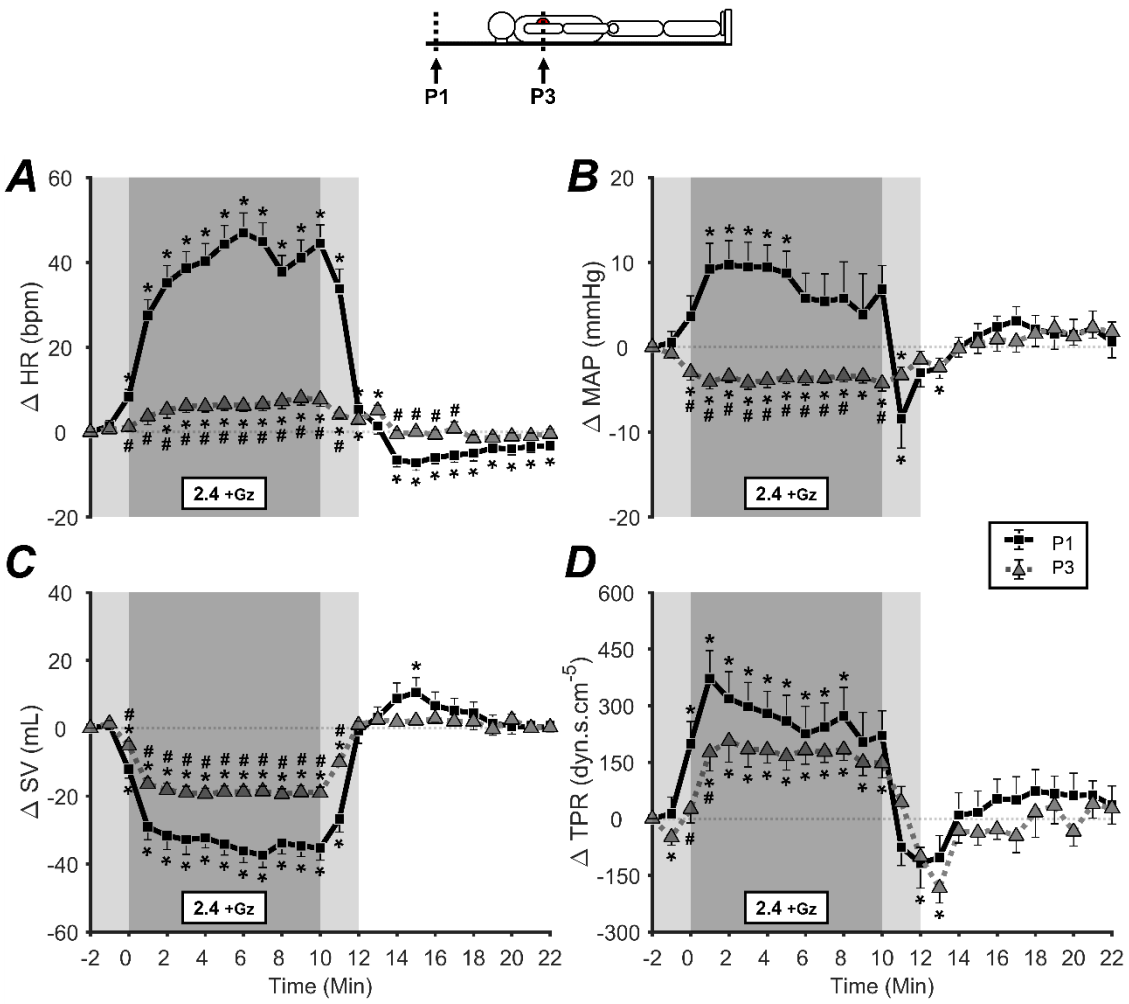

Figure 4.9 Mean changes from baseline (BL) for cardiovascular measures during ten minutes short-arm human centrifugation (SAHC, 2.4 +Gz) with two minutes ramp-up and –down; and recovery (RR, 10 min).

A, changes from baseline (BL) in mean heart rate (ΔHR); **B**, changes from BL in averaged mean arterial pressure (ΔMAP); **C**, changes from BL in mean derived stroke volume (ΔSV); and **D**, changes from BL in mean derived total peripheral resistance (ΔTPR).

Mean ± SEM is 60 s mean delta from final minute (min 10) mean of the baseline (BL) before each respective centrifuge run. **Black square**, at position 1 (*P1*, above head); **grey triangle**, at position 3 (*P3*, heart-level). Shaded areas: **light grey**, two minute centrifuge ramp-up and -down (min -2 to 0 and 10 to 12); **dark grey**, ten minutes centrifugation (SAHC: min 0-10); **white**, ten minutes recovery (RR: min 12-22). Baseline (*): * $p < 0.05$. Position (#): # $p < 0.05$. n = 20.

Rotational axis position comparison (RAP, P_{n1} vs. P_{n2}): Post hoc analysis revealed ΔHR at *P3* was significantly lower than *P1* (*P3 vs. P1*) during 2.4 +Gz SAHC (min 0-11, $p<0.05$) and significantly higher during RR (min 14-17, $p<0.05$) with the greatest difference at min 6 (6 ± 1 *vs.* 47 ± 5 bpm, $p<0.001$; Figure 4.9A). Similarly, ΔMAP at *P3* was significantly lower than *P1* (*P3vs. P1*) during SAHC (min 0-9 and 10, $p<0.05$) with the greatest difference at min 4 (-4 ± 1 *vs.* 9 ± 3 mmHg, $p<0.001$); but no difference during RR (min 12-22: $0.233<p<0.973$; Figure 4.9B).

ΔSV at *P3* was significantly higher than *P1* (*P3 vs. P1*) during SAHC at min 0-11 ($p<0.05$) with the greatest difference at min 7 (-18.6 ± 1.6 *vs.* -37.5 ± 3.6 mL, $p<0.001$; but no difference during RR (min 12-22: $0.135<p<0.978$; Figure 4.9C). Conversely, ΔTPR at *P3* was significantly lower than *P1* (*P3 vs. P1*) only at the start of SAHC (min 0-1: $p<0.05$) with the greatest difference at min 0 (25 ± 37 *vs.* 199 ± 59 dyn.s.cm^{-5}, $p=0.013$; and no difference during RR (min 12-22: $0.154<p<0.888$; Figure 4.9D).

4.3.5 Reduced peripheral fluid displacement and duration

Time (s) as a fixed effect was shown by the linear mixed effects model to be highly significant for changes from baseline (BL) in mean calf circumference (ΔCC; Table 4.5).

Specific baseline (BL) changes: Post hoc analysis revealed ΔCC was significantly positive at *P1* (above head) during min 3-12 of 2.4 +Gz short-arm human centrifugation (SAHC) compared to baseline (BL, $p<0.05$); similarly, at *P3* ΔCC was significantly positive but to a lesser degree (min 0-12, $p<0.05$; Figure 4.10). During recovery (RR),

ΔCC at *P1* remained significantly positive (min 12-21, $p<0.05$); however, at *P3* compared to BL there was no difference (min 14-22; Figure 4.10).

Rotational axis position comparison (RAP, P_{n1} vs. P_{n2}): ΔCC at *P3* was significantly lower than *P1* (*P3 vs. P1*) during SAHC (min 5-10, $p<0.05$) and also significantly lower during RR (min 12-21) with the greatest difference in the final minute of SAHC (min 10: 2.9 ± 0.4 *vs.* 5.8 ± 0.4 mm, $p<0.001$; Figure 4.10).

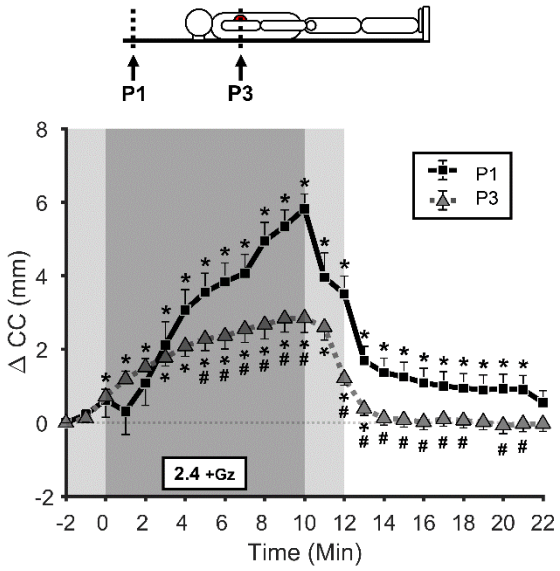

Figure 4.10 Mean changes from baseline (BL) for calf circumference (ΔCC) during ten minutes short-arm human centrifugation (SAHC, 2.4 +Gz) with two minutes ramp-up and -down; and recovery (RR, 10 min).

Mean ± SEM is 60 s mean delta from final minute (min 10) mean of the baseline (BL) before each respective centrifuge run. **Black square**, at position 1 (*P1*, above head); grey triangle, at position 3 (*P3*, heart-level). Shaded areas: **light grey**, two minute centrifuge ramp-up and -down (min -2 to 0 and 10 to12); **dark grey**, ten minutes centrifugation (SAHC: min 0-10); **white**, ten minutes recovery (RR: min 12-22). Baseline (*): * $p < 0.05$. Position (#): # $p < 0.05$. n = 20.

4.3.6 Ameliorated cerebral perfusion and time-course

Time (s) as a fixed effect was shown by the linear mixed effects model to be highly significant for changes from baseline (BL) in prefrontal cortex cerebral tissue saturation index (ΔcTSI; Table 4.6).

Specific baseline (BL) changes: ΔcTSI was significantly negative at *P1* (above head) during min 1-11 of 2.4 +Gz short-arm human centrifugation (SAHC) compared to baseline (BL, $p<0.05$); similarly, at *P3* ΔcTSI was significantly negative but to a lesser degree (min 1-11, $p<0.05$; Figure 4.11). During recovery (RR), ΔcTSI at *P1* was unchanged as was *P3* compared to BL (min 12-22; Figure 4.11).

Rotational axis position comparison (RAP, P_{n1} vs. P_{n2}): ΔcTSI at *P3* was significantly higher than *P1* (*P3 vs. P1*) during SAHC (min 1-11, $p<0.05$) with the greatest difference at min 5 (-0.72 ± 0.38 *vs.* -3.61 ± 0.58 %, $p<0.001$; but no significant difference during RR (min 12-22; Figure 4.11).

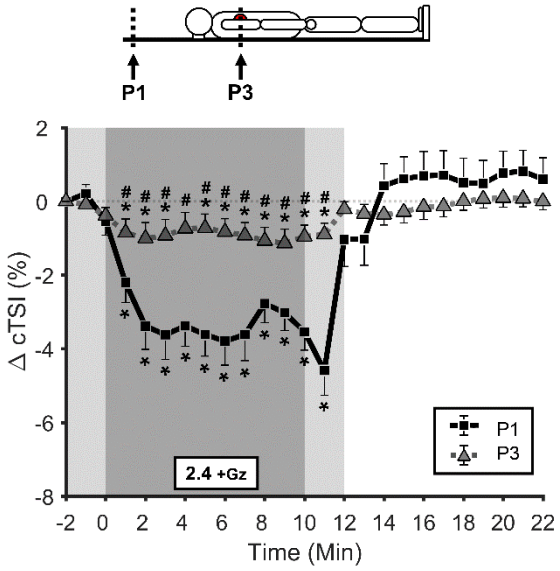

Figure 4.11 Mean changes from baseline (BL) for near-infrared spectroscopy (NIRS) measured prefrontal cortex cerebral tissue saturation index (ΔcTSI) during ten minutes short-arm human centrifugation (SAHC, 2.4 +Gz) with two minutes ramp-up and -down; and recovery (RR, 10 min).

Mean ± SEM is 60 s mean delta from final minute (min 10) mean of the baseline (BL) before each respective centrifuge run. **Black square**, at position 1 (*P1*, above head); grey triangle, at position 3 (*P3*, heart-level). Shaded areas: **light grey**, two minute centrifuge ramp-up and -down (min -2 to 0 and 10 to12); **dark grey**, ten minutes centrifugation (SAHC: min 0-10); **white**, ten minutes recovery (RR: min 12-22). Baseline (*): * $p < 0.05$. Position (#): # $p < 0.05$. n = 20.

4.3.7 Individual responses to altered g-gradients

Individual changes from baseline (BL) in heart rate (ΔHR) at 2.4 +Gz in position 1 (*P1*, above head) show a majority of participants display large positive changes from BL with large interindividual variability (Figure 4.12A). Conversely, individual ΔHR at 2.4 +Gz in position 3 (*P3*, heart-level) shows a majority of participants display small positive changes from BL; with reduced interindividual variability (Figure 4.12B).

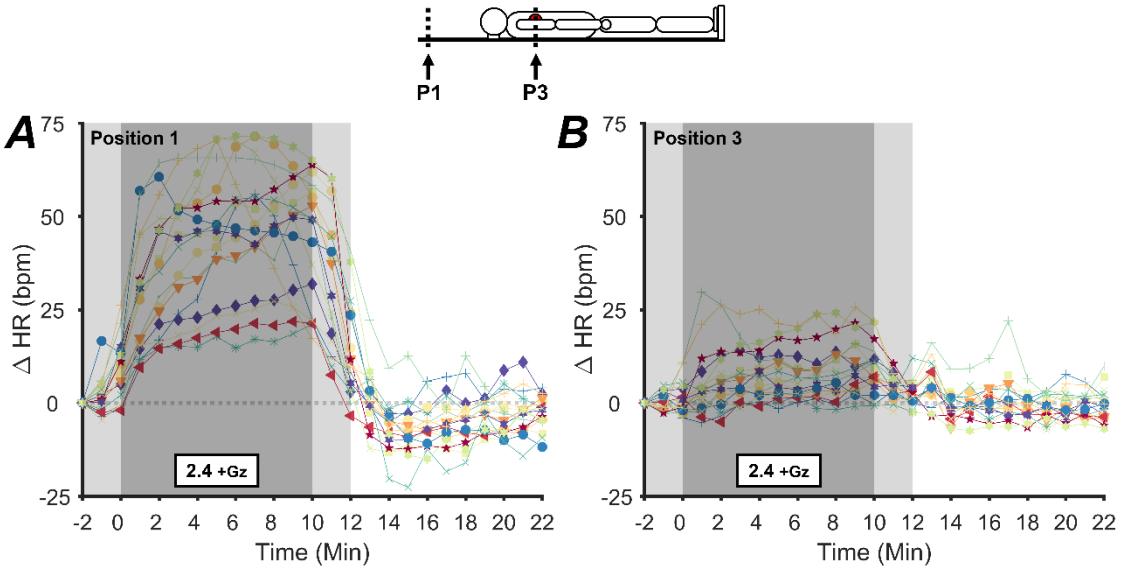

Figure 4.12 Individual participant changes from baseline (BL) for heart rate (ΔHR) during ten minutes short-arm human centrifugation (SAHC, 2.4 +Gz) with two minutes ramp-up and –down; and recovery (RR, 10 min).

Individual mean at each data point is calculated as a 60 s mean delta from the final minute (min 10) mean of the baseline (BL) immediately before each respective centrifuge run. Shaded areas: **light grey**, two minute centrifuge ramp-up and -down (min -2 to 0 and 10 to 12); **dark grey**, ten minutes centrifugation (SAHC: min 0 to 10); **white**, ten minutes recovery (RR: min 12 to 22); n = 20.

Individual changes from baseline (BL) in calf circumference (ΔCC) at 2.4 +Gz in position 1 (*P1*, above head) shows a majority of participants display large positive changes from BL with large interindividual variability (Figure 4.13A). However, individual ΔCC at 2.4 +Gz in position 3 (*P3*, heart-level) shows a majority of participants display small positive changes from BL; with reduced interindividual variability (Figure 4.13B).

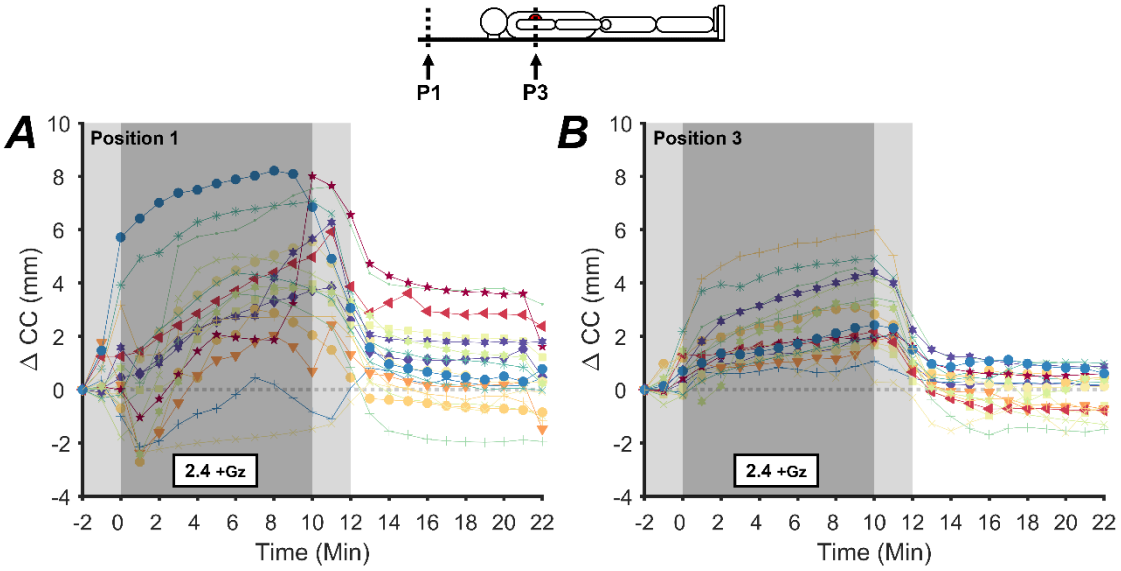

Figure 4.13 Individual participant changes from baseline (BL) for calf circumference (ΔCC) during ten minutes short-arm human centrifugation (SAHC, 2.4 +Gz) with two minutes ramp-up and –down; and recovery (RR, 10 min).

Individual mean at each data point is calculated as a 60 s mean delta from the final minute (min 10) mean of the baseline (BL) immediately before each respective centrifuge run. Shaded areas: **light grey**, two minute centrifuge ramp-up and -down (min -2 to 0 and 10 to 12); **dark grey**, ten minutes centrifugation (SAHC: min 0 to 10); **white**, ten minutes recovery (RR: min 12 to 22); n = 20.

Individual changes from baseline (BL) in prefrontal cortex cerebral tissue saturation index (ΔcTSI) at 2.4 +Gz in position 1 (*P1*, above head) shows a majority of participants display large negative changes from BL with large interindividual variability (Figure 4.14A). Individual ΔcTSI at 2.4 +Gz in position 3 (*P3*, heart-level) shows a majority of participants display small negative changes from BL; with reduced interindividual variability (Figure 4.14A).

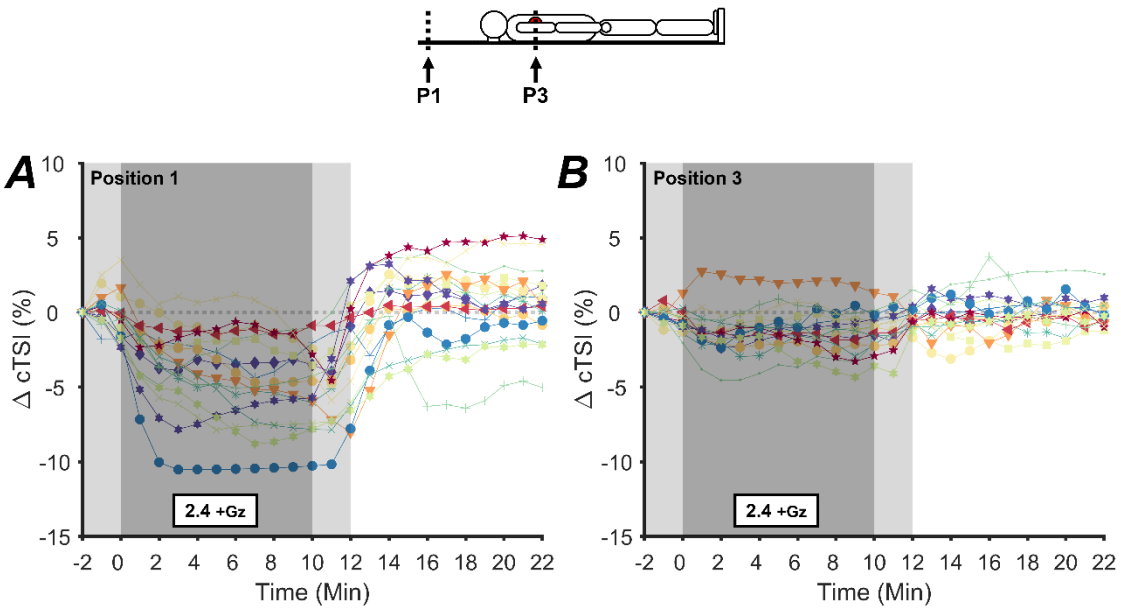

Figure 4.14 Individual participant changes from baseline (BL) for near-infrared spectroscopy (NIRS) measured prefrontal cortex cerebral tissue saturation index (ΔcTSI) during ten minutes short-arm human centrifugation (SAHC, 2.4 +Gz) with two minutes ramp-up and –down; and recovery (RR, 10 min).

Individual mean at each data point is calculated as a 60 s mean delta from the final minute (min 10) mean of the baseline (BL) immediately before each respective centrifuge run. Shaded areas: **light grey**, two minute centrifuge ramp-up and -down (min -2 to 0 and 10 to 12); **dark grey**, ten minutes centrifugation (SAHC: min 0 to 10); **white**, ten minutes recovery (RR: min 12 to 22); n = 20.

4.3.8 Gender variances in hemodynamic response

Gender as a fixed effect was shown by the linear mixed effects model to not be significant for changes from baseline (BL) in mean heart rate (ΔHR), averaged mean arterial pressure (ΔMAP), mean stroke volume (ΔSV), mean total peripheral resistance (ΔTPR), or mean cerebral tissue saturation index (ΔcTSI); but highly significant in delta mean calf circumference (ΔCC; Table 4.7).

Table 4.7 Effects and their standard errors of hemodynamic variables as a result of time, and gender (fixed effects).

Time, in seconds from the start of the centrifuge phase;
gender, expressed as binary integer for male and female;

cTSI, cerebral tissue saturation index; **CC,** calf circumference - strain gauge plethysmography; **HR,** heart rate; **SV,** stroke volume; **TPR,** total peripheral resistance; **MAP,** mean arterial pressure.

		(Intercept)			Time (s)			Gender (M/F)		
	n	*Effect* ± *SE*	*F-value*	*p-value*	*Effect* ± *SE*	*F-value*	*p-value*	*Effect* ± *SE*	*F-value*	*p-value*
ΔHR (bpm)	20	3.91 ± 5.04	54.5	< 0.001	0.011 ± 0.001	255	< 0.001	2.63 ± 2.36	1.23	0.282
ΔSV (mL)	20	-15.5 ± 4.4	338	< 0.01	-0.006 ± 0.001	77.9	< 0.001	-0.760 ± 2.068	0.135	0.718
ΔTPR (dyn.s.cm^{-5})	20	136.0 ± 90.9	128	< 0.001	-0.111 ± 0.014	59.4	< 0.001	36.5 ± 42.6	0.734	0.404
ΔMAP (mmHg)	20	-5.00 ± 3.01	2.96	0.085	-0.002 ± 0.000	19.7	< 0.001	2.45 ± 1.42	3.00	0.102
ΔCC (mm)	20	-1.60 ± 1.31	37.5	< 0.001	0.003 ± 0.000	1112	< 0.001	1.39 ± 0.66	5.03	< 0.05
ΔcTSI (%)	20	-1.58 ± 0.58	20.1	< 0.001	0.000 ± 0.000	1.77	0.183	0.422 ± 0.386	1.17	0.295

4.3.8.1 Central hemodynamics

Specific baseline (BL) changes: Post hoc analysis revealed ΔHR was significantly positive in males at positions 1, 2, and 3 (*P1-3*) during 2.4 +Gz short-arm human centrifugation (SAHC) compared to baseline (BL; *P1*, *P3*, and *P3*, p<0.05-0.001); and also in females (*P1-3*: p<0.05-0.001; Figure 4.15A). However, ΔMAP was significantly positive in males only at position 1 during 2.4 +Gz SAHC compared to baseline (BL; *P1*, p=0.039; *P2*, p=0.193; and *P3*, p=0.147); but significantly negative in females only at *P3* (*P1*, p=0.831; *P2*, p=0.997; and *P3*, p<0.001; Figure 4.15B).

ΔSV was significantly positive in males at all positions during 2.4 +Gz SAHC compared to baseline (BL; *P1*, *P3*, and *P3*, p<0.05-0.001); and also in females (*P1-3*: p<0.05-0.001; Figure 4.15C). Similarly, ΔTPR was significantly positive in males at all positions during 2.4 +Gz SAHC compared to baseline (BL; *P1-3*, p<0.05); and also in females (*P1-3*: p<0.05-0.01; Figure 4.15D).

Gender comparison (Male vs. Female): Post hoc analysis revealed ΔHR in males was no different than females (male *vs.* female) at all positions (*P1*: p=0.139; *P2*: p=0.222; and *P3*: p=0.215; Figure 4.15A). However, ΔMAP in males was significantly greater than females (male *vs.* female) at *P1* (16 ± 2 *vs.* 1 ± 2 mmHg, p=0.020) and *P3* (-2 ± 1 *vs.* -5 ± 1 mmHg, p=0.045) but not *P2* (p=0.314; Figure 4.15B).

ΔSV in males was no different than females (male *vs.* female) at all positions (*P1*: p=0.071; *P2*: p=0.425; and *P3*: p=0.857; Figure 4.15C). Similarly, ΔTPR in males was no different than females (male *vs.* female) at all positions (*P1*: p=0.927; *P2*: p=0.906; and *P3*: p=0.928; Figure 4.15D).

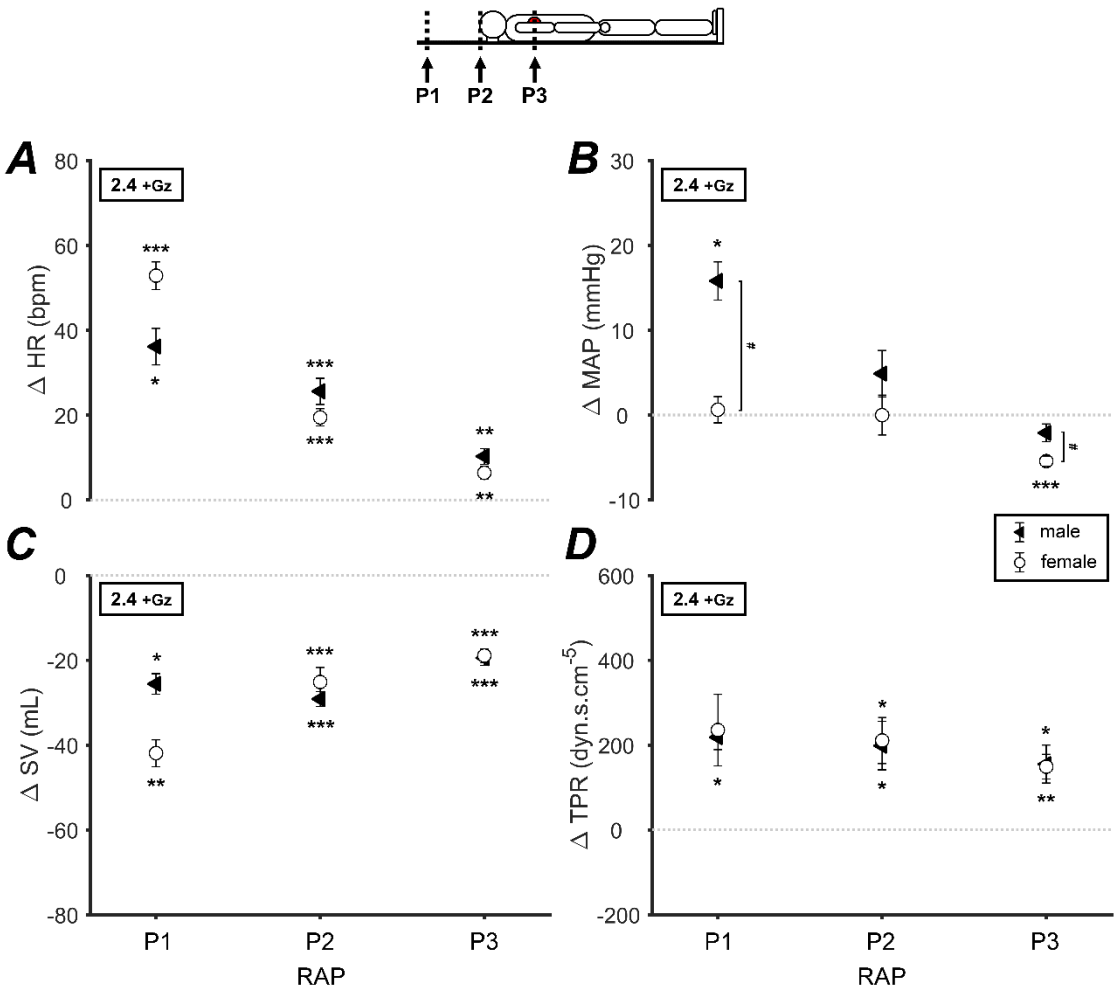

Figure 4.15 Mean changes from baseline (BL) for cardiovascular measures in the final minute (min 10) of 2.4 +Gz short-arm human centrifugation (SAHC) at rotational axis position (RAP) 1 (*P1*, above the head), position 2 (*P2*, apex of head), and position 3 (*P3*, heart-level) between males and females.

A, changes from baseline (BL) in mean heart rate (ΔHR); **B**, changes from BL in averaged mean arterial pressure (ΔMAP); **C**, changes from BL in mean stroke volume (ΔSV); and **D**, changes from BL in mean derived total peripheral resistance (ΔTPR).

Mean at each g-level (± SEM) is calculated as a final minute (min 10) mean delta from the final minute (min 10) mean of the baseline (BL) immediately before each respective centrifuge run. **Black triangle**, males; and **white circle**, females. Baseline (*): * $p < 0.05$, ** $p < 0.01$, *** $p < 0.001$. Gender (#): # $p < 0.05$, ## $p < 0.01$, ### $p < 0.001$; n = 20 (10 male).

4.3.8.2 Peripheral fluid displacement

Specific baseline (BL) changes: Post hoc analysis revealed ΔCC was significantly positive in males at all positions during 2.4 +Gz SAHC compared to baseline (BL; *P1-3*, p<0.01-0.001); and also in females (*P1-3*, p<0.05-0.001; Figure 4.16).

Gender comparison (Male vs. Female): Post hoc analysis revealed ΔCC in males was significantly greater than females (male *vs.* female) at *P3* (3.8 ± 0.4 *vs.* 2.2 ± 0.3 mm, p=0.027); with no difference at *P1* (p=0.482) and *P2* (p=0.105; Figure 4.16).

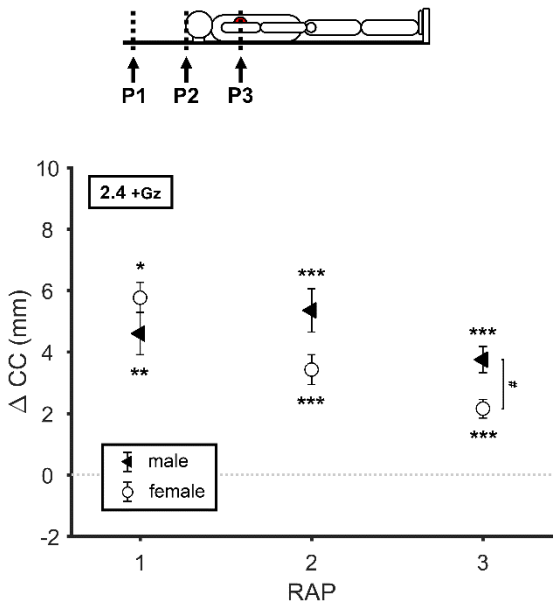

Figure 4.16 Mean changes from baseline (BL) in calf circumference (ΔCC) in the final minute (min 10) of short-arm human centrifugation (SAHC, 1.0 to 2.4 +Gz) at rotational axis position (RAP) 1 (*P1*, above the head), position 2 (*P2*, apex of head), and position 3 (*P3*, heart-level) between males and females.

Mean at each g-level (± SEM) is calculated as a final minute (min 10) mean delta from the final minute (min 10) mean of the baseline (BL) immediately before each respective centrifuge run. **Black triangle**, males; and **white circle**, females. Baseline (*): * p < 0.05, ** p < 0.01, *** p <0.001. Gender (#): # p < 0.05, ## p < 0.01, ### p < 0.001; n = 20 (10 male).

4.3.8.3 Cerebral perfusion

Specific baseline (BL) changes: Post hoc analysis ΔcTSI was significantly negative in males at all positions during 2.4 +Gz SAHC compared to baseline (BL; *P1-3*, p<0.05-0.01); and also in females (*P1-3*: p<0.05; Figure 4.17).

Gender comparison (Male vs. Female): Post hoc analysis ΔcTSI in males was no different than females (male *vs.* female) at all positions (*P1*: p=0.151; *P2*: p=0.730; and *P3*: p=0.902; Figure 4.17).

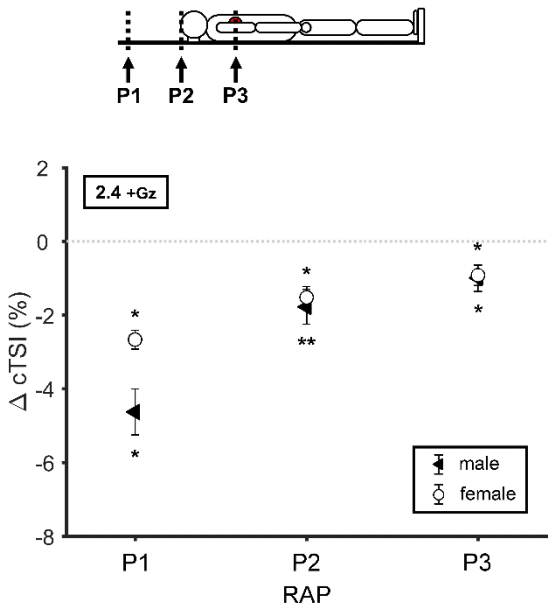

Figure 4.17 Mean changes from baseline (BL) for near-infrared spectroscopy (NIRS) measured prefrontal cortex cerebral tissue saturation index (ΔcTSI) in the final minute (min 10) of short-arm human centrifugation (SAHC, 1.0 to 2.4 +Gz) at rotational axis position (RAP) 1 (*P1*, above the head), position 2 (*P2*, apex of head), and position 3 (*P3*, heart-level) between males and females.

Mean at each g-level (± SEM) is calculated as a final minute (min 10) mean delta from the final minute (min 10) mean of the baseline (BL) immediately before each respective centrifuge run. **Black triangle**, males; and **white circle**, females. Baseline (*): * p < 0.05, ** p < 0.01, *** p <0.001. Gender (#): # p < 0.05, ## p < 0.01, ### p < 0.001; n = 20 (10 male).

4.3.8.4 Presyncopal symptoms

The proportion of male participants experiencing presyncopal symptoms (PSS+) compared to females was statistically no different at *P1*: $\chi^2(1, n=10)=2.31$, p=0.129; *P2*: $\chi^2(1, n=10)=0.35$, p=0.554; or *P3*: $\chi^2(1, n=10)=$NaN, p=1.000 across all g-levels (Figure 4.18).

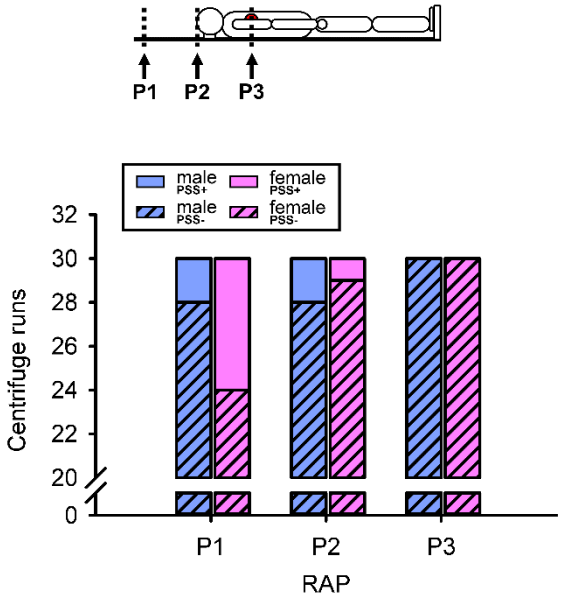

Figure 4.18 G-tolerance in each rotational axis position (RAP, *P1-3*) across all short-arm human centrifugation (SAHC) foot g-levels (1.0, 1.7 and 2.4 +Gz) in males and females.

Male and female participants were exposed to nine centrifuge profiles giving rise to 90 separate centrifuge runs in each gender group, consisting of 30 in each position: ***P1***, rotational axis position (RAP) above head; ***P2***, RAP head apex; ***P3***, RAP heart-level.

Participants classified as having experienced presyncopal symptoms (PSS+, **white**) or not experiencing PSS (PSS-, **black**). male: n = 10; female: n = 10.

4.3.9 Increased overall g-tolerance

The proportion of participants experiencing presyncopal symptoms (PSS+) was significantly higher at *P1* compared to *P3* across all g- levels: $\chi^2(1, n=20)=8.57$,

p=0.003; but not compared to *P2*: $\chi^2(1, n=20)=3.08$, p=0.079; or *P2 vs. P3*: $\chi^2(1, n=20)=2.50$, p=0.114 (Figure 4.19).

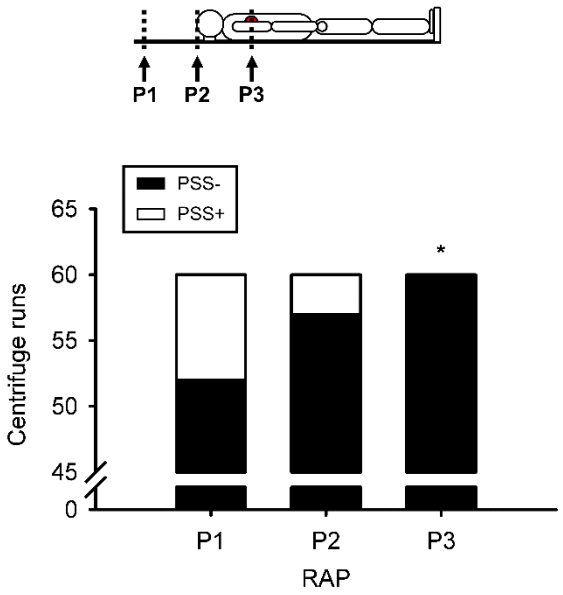

Figure 4.19 G-tolerance in each rotational axis position (RAP, *P1-3*) across all short-arm human centrifugation (SAHC) foot g-levels (1.0, 1.7 and 2.4 +Gz) in all participants.

All participants were exposed to nine centrifuge profiles giving rise to 180 separate centrifuge runs, consisting of 60 in each position: ***P1***, rotational axis position (RAP) above head; ***P2***, RAP head apex; ***P3***, RAP heart-level.

Participants classified as having experienced presyncopal symptoms (PSS+, **white**) or not experiencing PSS (PSS-, **black**). Chi-squared, * $p < 0.05$; n = 20.

4.3.10 Unsupported cerebral perfusion

The relationship between ΔHR and ΔCC, at increasing +Gz levels, shows a strong positive linear relationship unaffected by changing position (Figure 4.20A), conversely, the relationship between ΔcTSI and ΔCC, whilst unaffected by position, demonstrated a negative relationship but also unaffected by position changes demonstrated by an unchanging slope gradient in *P1-3* (Figure 4.20B).

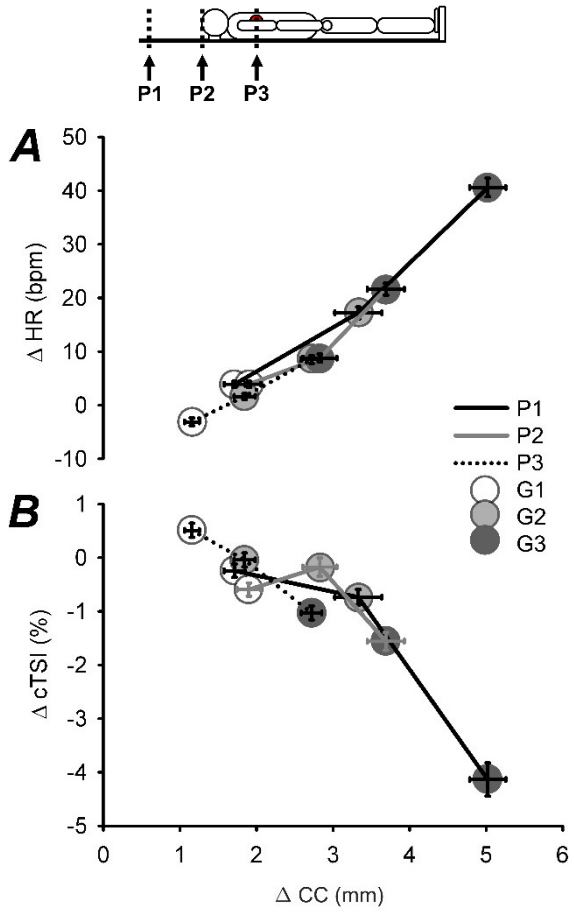

Figure 4.20 Relationship between mean changes from baseline (BL) in heart rate (Δ HR) and prefrontal cortex cerebral tissue saturation index (ΔcTSI) vs. calf circumference (Δ CC) during centrifugation at all g-levels (1.0-2.4 +Gz) and positions (*P1-3*).

A, mean changes from baseline (BL) in heart rate (ΔHR) against calf circumference (ΔCC); **B**, mean changes from baseline (BL) in prefrontal cortex cerebral tissue saturation index (ΔcTSI) against ΔCC.

Mean at each g-level and position (± SEM) is calculated as a final minute (min 10) mean delta from the final minute (min 10) mean of the baseline (BL) immediately before each respective centrifuge run. **Black line**: rotational axis position above head (*P1*); **grey line**: rotational axis position at apex of head (*P2*); **dotted line**: rotational axis position at heart-level (*P3*); **white circle**: g-level 1.0 +Gz at feet (G1); **light grey circle**: g-level 1.7 +Gz at feet (G2); **dark grey circle**: g-level 2.4 +Gz at feet (G3). n = 20.

4.4 Discussion

The purpose of this study was to investigate the effect of induced g-gradients, across the body during short-arm centrifugation, upon cardiovascular regulation and orthostatic tolerance. Specifically, we aimed: (i) to determine physiological differences, in response to g-gradients, by measuring cerebral tissue oxygenation, peripheral fluid displacement, systemic cardiovascular responses and the emergence of presyncopal symptoms (PSS); and (ii) provide a better insight for future artificial gravity (AG) research by characterising a third variable of human centrifugation studies; namely g-gradient in addition to duration and magnitude of exposure. All participants included in analysis were able to tolerate the three g-gradients (*P1-P3*) at 2.4 +Gz with none experiencing any neurovestibular disturbances leading to motion sickness.

We observed that shifting the centre of centrifugal force to heart-level helped maintain cerebral perfusion, as estimated by cNIRS, whilst attenuating the increase in HR and occurrence of PSS. In general, this research provides strong evidence of the significant effect increasing g-gradient, by moving rotational axis position (RAP) towards the body, has on reducing cardiovascular response and increasing overall g-tolerance. To our knowledge, this is the first study to: (i) investigate the cardiovascular and cerebral responses to an altered g-gradient during short-arm human centrifugation (SAHC); and (ii) place the centre of rotation within the body whilst measuring cardiovascular and cerebral responses in addition to indicators of g-tolerance (*i.e.* PSS).

4.4.1 G-level response

Significant main effects of increasing levels of +Gz were revealed in the present study. Specifically, increases in heart rate (ΔHR), total peripheral resistance (ΔTPR), mean arterial pressure (ΔMAP), as well as calf circumference (ΔCC) were observed in agreement with previous research (Goswami *et al.*, 2015a). Conversely, stroke volume (ΔSV) and prefrontal cortex cerebral tissue saturation index (ΔcTSI) were significantly lower with increasing +Gz, which was also in agreement with recent studies (Iwasaki *et al.*, 2012; Smith *et al.*, 2013). The time-course response of ΔCC (slow) and ΔHR (fast) differed greatly; suggesting the baroreceptor response to the future central hypovolemia were occurring through central pathways subserving feed-forward or 'central command' responses (Dampney *et al.*, 2002).

At the highest g-level (2.4 +Gz), ΔCC was unchanged by position in the initial stages up until minute five (Figure 4.10), whilst ΔcTSI was significantly lower in *P1* than *P3* from the first minute onwards (Figure 4.11). Thus, cerebral perfusion was attenuated earlier in the centrifuge run than ΔCC, presumably due to a varied peripheral vascular response to early orthostatic stimulation (Watenpaugh *et al.,* 2004). By the last minute, a concurrent ΔCC increase with ΔcTSI decrease was observed providing evidence of a simple measure of peripheral fluid shifts having utility as a proxy of cerebral hemodynamics during SAHC.

4.4.2 Attenuated fluid displacement

Based on previous research, a strong consequential systemic response to calf pooling, and thus decreased cardiac return (pre-load), filling pressure, and increased HR, was expected (Rowell *et al.*, 1996). In the present study, and in agreement, a robust strong

relationship between peripheral displacement (ΔCC) and systemic response (ΔHR), was observed. Research has demonstrated that deep veins of the lower extremities can hold large volumes of blood (Gunga *et al.*, 2016); however, it remains unclear how this anatomy affects calf circumference to sequential filling. Nevertheless, the unaffected association between ΔCC and ΔHR suggests that peripheral displacement was quantified in its entirety by calf circumference; and not sequestered elsewhere, during orthostatic challenge, such as the splanchnic circulation. A comparable relationship was presented by Hachiya *et al.,* (2010) during LBNP; however, modulation of splanchnic region constriction led to differences in tolerance ('right-ward shift') and intolerance ('left-ward shift') of HR responses when compared to CC (Figure 4.20).

Previous research has shown the importance of splanchnic region vasoconstriction in response to an orthostatic challenge (Hinghofer-Szalkay *et al.*, 2008); and the buffering role of splanchnic vascular beds to fluid shifts has been demonstrated (Blaber *et al.*, 2013a). However, in the present study a strong relationship between ΔCC and ΔHR was observed that was unaffected by g-level or g-gradient. This apparent contradiction to the published literature indicates the splanchnic region may have less of an effect, on hemodynamic response to SAHC, than anticipated. Furthermore, ΔCC may be a reasonable surrogate measure of central hypovolemia during SAHC and current data indicates support for a simplistic two compartment model of fluid shifts.

4.4.3 Unsupported cerebral tissue oxygenation

It was hypothesized that cerebral perfusion would be supported to a greater extent at *P3* than *P2* and *P1* with a smaller reduction in cTSI for a given increase in CC; however, this was not the case in the present study. One possible explanation is that increased

arterial headward pressure results in venous congestion (Davis *et al.,* 2008), thereby limiting cerebral blood flow and hence cerebral oxygenation. Further work is required to confirm this and to determine the relationship between cerebral venous drainage (*e.g.* jugular vein congestion) and cerebral hemodynamics.

Additionally, attention must be brought to the limitations of the NIRS measurement. This method requires accurate measurement of rapid changes in arterial O_2Hb concentrations by a NIR spectrometer; with limitations of this monitor contributing to errors in measurement of perfusion and the calculated TSI (Elwell *et al.*, 1992). Measured changes in O_2Hb concentration do not differentiate between arterial inflow and venous outflow and there is an assumption of a steady-state in O_2 consumption of the cerebral tissue being measured (Pellicer & del Carmen Bravo, 2011). Reproducibility of measured results is highly dependent on placement of the light probes; with pictures taken between measurements on different days and placement of the probe on one day unmoved to mitigate against this. An index of perfusion (TSI) was used to measure changes experienced over a given period as opposed to absolute values.

The classical view of cerebral autoregulation is that for a MAP between 50-150 mmHg CBF is maintained (Lassen, 1959); however, the measured responses in relation to MAP and TSI do not line up with this. Willie *et al.* (2014) stated that CBF control is more complex and multifactorial than the parochial cerebral autoregulation model. Results from the current research seem to suggest other factors for TSI change should be considered, such as: i) potential increased/decreased arterial CO_2 (P_aCO_2) levels, which have been shown to increase/decrease CBF, respectively (Ide *et al.*, 2003; Battisti-Charbonney *et al.*, 2011); ii) the role of the sympathetic nervous system (SNS), where

research has shown extensive sympathetic activation of the larger cerebral arteries is especially important in providing sufficient buffering to large transient increases in cerebral perfusion pressure (Cassaglia *et al.*, 2008a, b; Ainslie, 2009; Tzeng *et al.*, 2010). Whilst not directly measured/addressed in this study; future research would benefit from considering these additional factors.

4.4.4 Gravitational tolerance

The 'total gravitational exposure' across the body changes with rotational position despite a comparable +Gz level at the feet. It is known that the hydrostatic gradient is of great importance in determining an orthostatic challenge, particularly during a passive stress (Hinghofer-Szalkay, 2011). Thus, resultant modification of aortic and carotid baroreceptor feedback may explain similar cardiovascular responses at *P3* and *P1,* during a high and low +Gz level, respectively. Similarly, research by Hallgren *et al.* (2016) demonstrating reduced otolith system input on an increased OI occurrence in returning astronauts can be compared to the differential inputs to the otolith organs expected at both *P3* and *P1* in the current study. Collectively, *P3* has been shown to reduce the overall orthostatic challenge through a significantly reduced proportion of participants exhibiting PSS+ to those not (PSS-). Thus, the g-gradient of *P3* was shown to increase g-tolerance despite g-level at the feet remaining the same (2.4 +Gz) for a set duration of ten minutes.

Significant attenuations in cerebral perfusion, central hypovolemia and systemic cardiovascular response occurred at *P3*, the most prominent of which was ΔHR. Interestingly, it has been postulated that the hydrostatic gradient between the carotid and aortic baroreceptors is a potent determinant of HR responses to orthostatic challenge

(Ferguson *et al.*, 1985). At *P3* in the present study the hydrostatic gradient was reversed, suggesting (in isolation) that bradycardia should ensue. However, ΔHR at *P3* represented a 'dampened' increase, likely due to the removal of central blood volume having an opposing effect on ΔHR. Whilst not explored in the present study, this working hypothesis could be tested by prevention of the fluid shift during centrifugation via use of anti-g trousers.

Large inter-individual differences were present during 2.4 +Gz in ΔHR, ΔCC, and ΔcTSI; with the greatest deviation between participants during SAHC at *P1*. A large variation in HR response and the mechanisms involved during an orthostatic stress have been implicated in reduced tolerance to LBNP (Convertino *et al.*, 2012), and SAHC (Goswami *et al.*, 2015a). Hachiya *et al.* (2012) suggested reduced tolerance in woman was due to a diminished sympathetic outflow to the periphery; with men demonstrating comparatively less calf blood pooling. In addition, Goswami *et al.* (2015b) demonstrated the benefits of individualised centrifuge training which supports the idea of a large range of responses between individuals. It is postulated that participants who exhibit a faster HR response, in which the peak was achieved sooner, reached their so-called 'orthostatic challenge capacity' earlier on and placed them at a greater risk of hemodynamic collapse (Stewart, 2013). In general, it is postulated that centrifuge training improves orthostatic tolerance through a combination of decreased vascular resistance and enhanced cardiac function (Evans *et al.*, 2004; Stenger *et al.*, 2007).

Several studies have explored gender inconsistencies of systemic response, with various explanations offered as the reason for and observed reduced orthostatic tolerance in women. Shoemaker *et al.* (2001) postulated gender differences could be explained by a

reduced sympathetic outflow to the peripheral vasculature in women causing a reduced tolerance. Additionally, a reduction in circulating norepinephrine (NE) was shown during an orthostatic challenge when comparing men to women (Convertino, 1998). There is also pharmacological evidence to suggest that women display a greater responsiveness to cardiac β-adrenoceptors (Convertino, 1998; Phillips, 2010) and this may be a contributory factor. Differences in the elevation of HR are obviously not enough to predict orthostatic tolerance and it has been suggested that women also display a lower venous return and cardiac filling compared to males (Fu *et al.*, 2004).

However, significant gender differences during SAHC in ΔHR, ΔMAP, ΔSV, ΔTPR, and ΔcTSI were not observed in the present study. Only ΔCC was significantly greater in men. The difference in ΔCC between genders is likely explained by anthropometric differences where a larger mean muscle mass in men is capable of greater fluid displacement than a smaller one. Furthermore, Russomano *et al.* (2015) postulated increased lower-limb venous compliance amongst females was a contributory factor in gender-dependant tolerance. Nevertheless, significant differences in peripheral fluid shift between genders had no significant effect on systemic and cerebral hemodynamics in the current cohort. These findings seemingly contradict the literature which suggest fundamental differences in cardiovascular response to an orthostatic challenge between men and women (Montgomery *et al.*, 1977; Frey & Hoffler, 1988; White *et al.*, 1996; Convertino, 1998; Fong *et al.*, 2007); and that any observed differences to LBNP were not due to anthropometric variations (Lawler *et al.*, 1998). However, it is postulated that significant alterations to the g-gradient may explain previously reported differences observed during SAHC. Changing the RAP whilst maintaining the g-level at the feet was shown to have a significant effect on systemic, peripheral and cerebral

hemodynamics. Past SAHC research reporting g-level at the heart (Iwase, 2005; Goswami *et al.*, 2015b) neglects to report the RAP meaning g-level at the feet will differ greatly between participants.

It is believed a paradigm shift in what constitutes the magnitude of g-level, during SAHC, is required. Current research outlines the significance of distance from the centre of rotation on hemodynamic response. Furthermore, it is suggested that total gravitational exposure across the body is a better determinant of orthostatic challenge to SAHC than magnitude of g-level at a specific point. Therefore, it seems reasonable to assume men and women, typically of differing average heights, would therefore actually experience a different magnitude of exposure to the currently standardized g-level. It is postulated that past observations of gender based differences to SAHC exposure may arise due to anthropometric differences (specifically height) currently not taken into account during experimental design. Thus, it is suggested that differences in hemodynamic response arise as a result of insufficient SAHC standardisation, instead of gender. There was no significant height difference or cardiovascular response between genders in the present study; however, further research is required to explore this specific hypothesis.

4.4.5 Future application

A key theme in SAHC research is ensuring any "cure is not worse than the disease" (Aubert *et al.*, 2016); and with this consideration the present research outlines a promising case for SAHC as a future spaceflight countermeasure. It was found that, for the same +Gz level delivered to the feet of participants, an increased g-tolerance could be achieved. Thus, the significance of this observation means an associated high

stimulus, to the muscle and bones of the legs, can be delivered without the risk of syncope. Research has shown that the higher the g-level delivered the greater the potential 'training benefit' consisting of an enhanced cardiac function and reduced vascular resistance (Evans *et al.*, 2004). Therefore, if this experimental paradigm was combined with exercise a higher g-level could be administered and a greater potential benefit to the musculoskeletal system could be achieved. Future direction for this research could explore the same hemodynamic parameters but, instead of passive SAHC, with the addition cycle ergometry or sliding plate squats. Several SAHCs around the world now have the ability to exercise during exposure, including resistive exercise, supine squats (Frett *et al.*, 2014) and self-powered cycling (Diaz *et al.*, 2015). SAHC at *P3* has been shown to be a reduced orthostatic challenge, in relation to attenuated hemodynamic response, despite the foot g-level remaining unaltered. However, the physiological training value of this potential countermeasure must be tested on its ability to maintain cardiovascular function in the face of unloading; and determine if any benefit, through orthostatic intolerance (OI) reduction, can be achieved.

4.4.6 Conclusion

Our results suggest that rotational axis position, and thus g-gradient warrants further investigation. Currently, magnitude of centrifugation as an index of g-stress is commonly quantified by +Gz level experienced at a specific point (*i.e.* the feet or heart) for a specific period (Caiozzo *et al.*, 2004; Smith *et al.*, 2013; Diaz *et al.*, 2015). However, in addition to g-level magnitude and duration (Clément & Bukley, 2007), we present physiological data demonstrating g-gradient as an important third factor.

Standardisation of short- and long-arm centrifugation studies would benefit from the above findings in order for physiological data to be comparable. Furthermore, the unique and quantifiable orthostatic challenge, presented by a changing gravitational gradient, could be used to better explore and understand the interrelationship between carotid and aortic baroreceptor control.

5 LOWER-BODY NEGATIVE PRESSURE EFFECTS ON PERIPHERAL AND CEREBRAL HEMODYMANICS DURING HEAD-DOWN TILT INDUCED JUGULAR VENOUS CONGESTION

5.1 Introduction

Current spaceflight countermeasure regimes targeting the negative physiological effects of unloading are now relatively effective in maintaining muscle mass (Akima *et al.*, 2000; Mulder *et al.*, 2006) and bone density (Leblanc *et al.*, 2013) within healthy levels. Increased intensity, nutritional supplementation, and pharmacological interventions are all additional methods in which countermeasure regime effectiveness has been improved (Hargens *et al.*, 2013). Thus, potentially decreasing the need to schedule up to 2 hours exercise a day (Clément, 2011), freeing up crew time without any negative physiological consequence. However, potentially mission critical deleterious effects are still observed despite substantial crew time devoted to preserving physiological function. Specifically, the increased incidence of orthostatic intolerance (OI) on return (Buckey Jr *et al.*, 1996; Blaber *et al.*, 2011) and the emergence of Visual impairment and intracranial pressure (VIIP) syndrome (Polk, 2009); which has been termed the first true 'space sickness' (Michael & Marshall-Bowman, 2015).

Cycling (Cycle Ergometer with Vibration Isolation and Stabilization, CEVIS), running (Combined Operational Load Bearing External Resistance Treadmill, COLBERT), and resistive exercise (Advanced Resistive Exercise Device, ARED) form the core hardware for astronaut exercise regimes on board the International Space Station (ISS) (Clément, 2011). These countermeasures individually act to maintain the load-bearing muscle size, aerobic capacity, and other specific muscles through resistive training. Collectively they are termed specific countermeasures, which act on singular body systems, in contrast to a holistic approach acting on multiple. Crucially, current countermeasures provide the reintroduction of a force, absent in weightlessness, whilst failing to directly counteract

increased cephalic volume. It is postulated that a present failure to reverse headward fluid shifts in space is leading to the high incidence of VIIP (Wiener, 2012). It is also postulated that intermittent exercise, coupled with inadvertent transient peripheral fluid shifts, may exacerbate the problem by daily preventing a 'long-term protective' adaptation. Thus, increased exercise intensity may ameliorate muscle and bone loss but to the detriment of visual acuity. It has also been suggested that high levels of resistive exercise, specifically using ARED (Figure 5.1), may exacerbate VIIP (Fogarty *et al.*, 2011); however, the precise contributory role remains unclear.

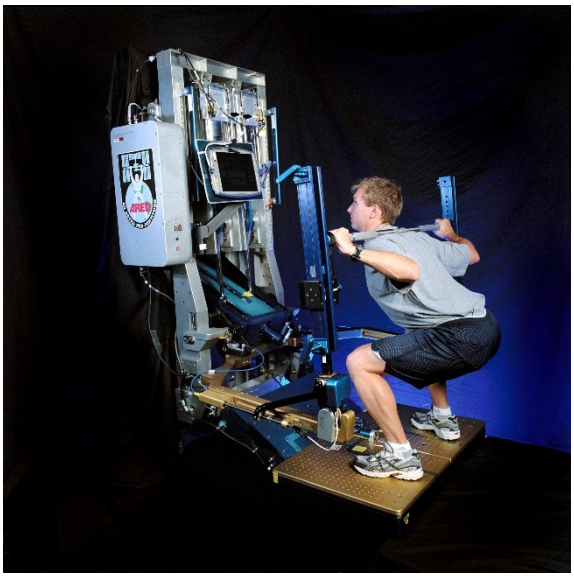

Figure 5.1 NASA's Advanced Resistive Exercise Device (ARED) for the International Space Station (ISS). Adapted from NASA.

ARED uses vacuum cylinders to simulate free weights for resistive exercise to maintain muscle and bone strength while in space.

Since humans first went into space in 1961 there have been just under 600 astronauts exposed to the harsh conditions of spaceflight (NASA, 2017). Over the past 50 years,

ample evidence has been obtained, and knowledge gained, to the precise physiological effects of weightlessness. At the birth of human spaceflight it was clear, early on, that unloading had a significant effect on the body. However, relatively new observations of deleterious adaptations have been made, such as the discovery of VIIP syndrome within the last 10 years (Polk, 2009; Mader *et al.*, 2011). Access to human spaceflight data remains limited, as do the types of experiment that can be performed due to technological restrictions. However, some mechanisms involved in spaceflight effects can be replicated on Earth to increase the number of observations and data collected. Specifically, spaceflight analogues can be used to gain a better understanding, of human physiology in microgravity, without ever leaving the Earth's surface.

5.1.1 Spaceflight analogues

Ground based studies, such as head-down bed rest (HDBR), are a useful tool for exploring physiological deconditioning and in particular muscle atrophy, bone loss, and reduced baroreceptor function among others (Pavy-Le Traon *et al.*, 2007). However, past spaceflight analogue research has been unable to experimentally replicate clinically significant vision problems, experienced by astronauts in space, here on Earth (Taibbi *et al.*, 2013) (Table 1.1). Previous bed rest studies use a standardized methodology (Sundblad & Orlov, 2015) in order to recreate the unloading and headward fluid shifts seen in weightlessness. A precise head-down tilt (HDT) angle of -6° is commonly used in an attempt to replicate spaceflight fluid shifts and a lack of gravitational force along the main column of blood (Kakurin *et al.*, 1976). Hydrostatic forces can be estimated through calculations; however, a precise comparable force in HDBR is unachievable due the persistence of a hydrostatic gradient (Figure 5.2B).

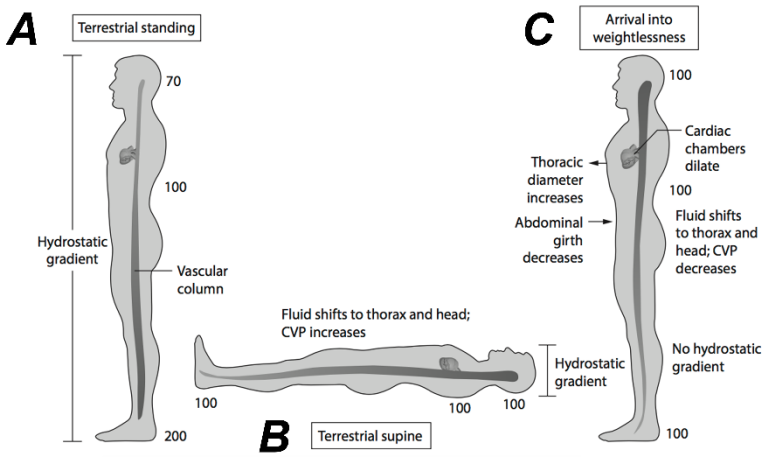

Figure 5.2 Hydrostatic pressure gradients standing on Earth, during head-down bed rest (HDBR), and weightlessness. Adapted from Gradwell and Rainford (2016).

A, standing on Earth; **B**, head-down bed rest (HDBR) spaceflight analogue; and **C**, initial weightlessness.

CVP, central venous pressure. Mean arterial pressures (MAP) expressed in mmHg.

Wiener (2012) suggested internal jugular vein (IJV) compression, leading to venous congestion, as a contributing factor in spaceflight induced VIIP. An absence of congestion during -6° HDT bed rest supports this hypothesis where it is likely not enough fluid is displaced. It is postulated that fluid shifted from the periphery toward the head at -6° does not reach a threshold in which venous congestion occurs on Earth. HDBR at greater angles of HDT is likely required to elicit a fluid shift inducing venous congestion comparable to that observed during spaceflight. The precise reason for this discrepancy remains unclear; however, a better understanding of the role venous congestion during HDT may prove beneficial to elucidating the unknown mechanisms involved in VIIP.

5.1.2 Fluid displacement

A significant cephalic fluid shift in space brings about a multitude of responses immediately upon entering microgravity. Specifically, astronauts experience a feeling of facial fullness as a result of "chicken legs" and a "puffy face" (Aubert *et al.*, 2016). Paradoxically, central venous pressure (CVP) in weightlessness, during the immediate short-term, has been shown to actually decrease despite concurrent atrial diameter increases (Buckey *et al.*, 1996a). However, measurements of interpleural pressure during parabolic flight demonstrated greater decreases than CVP. Thus, suggesting transmural CVP increased during short periods of microgravity (Videbaek & Norsk, 1997). Cardiovascular adaptations to microgravity occur readily within the first few weeks, the most prominent of which is a significant reduction in circulating blood volume (Johnston & Dietlein, 1977). During spaceflight, hemodynamic functional adaptation was thought to reach a steady state within a few days and remain broadly and clinically insignificant thereafter (Charles & Lathers, 1991); however, the emergence of VIIP (Mader *et al.*, 2011) and high incidence of OI in returning astronauts (Buckey Jr *et al.*, 1996; Blaber *et al.*, 2011) seem to suggest otherwise.

Previous research has demonstrated the ability of periodically shifting fluid to the periphery at improving orthostatic tolerance (Goswami *et al.*, 2015b). However, the degree to which this can improve physiological function in space, and specifically ameliorate against VIIP, is still to be elucidated. LBNP as a spaceflight countermeasure (Figure 5.3) is currently being investigated on board the International Space Station (ISS), in an experiment called 'Fluid Shifts' (Stenger *et al.*, 2016).

Figure 5.3 Lower-body negative pressure (LBNP) device, also called the Chibis, on board the International Space Station (ISS). Adapted from Roscosmos.

Russian Cosmonaut Yuri Malenchenko wears the Chibis device.

This experiment aims to explore the precise role of fluid redistribution, measured using tracer dilution techniques (deuterium oxide, $^{2}H_2O$; and sodium bromide, NaBr); and ultrasound quantified venous congestion, on the emergence of VIIP. Pre-, flight-, and post-data collection, over three 6-month missions, is ongoing with the last results expected in September 2017 (Stenger *et al.*, 2016). Similarly, investigating the association of fluid displacement, from the peripheral to central compartments, with indicators of jugular venous congestion has not been systematically tested on Earth. Nevertheless, a spaceflight analogue experiment exploring the association between venous congestion and immediate peripheral fluids may provide an insight into the causal mechanisms of VIIP. The cephalic fluid shift experienced in spaceflight (and also with HDT) is opposable by LBNP (Baisch & Petrat, 1993); furthermore, it is likely that great angles of HDT would be proportional to an opposite relocation of fluid with

increasing LBNP values. Similar findings were observed by Hinghofer-Szalkay *et al.* (2004) where the ability of LBNP to neutralize the cardiovascular effects of HDT were demonstrated. Specifically, LBNP levels of -15 to -35 mmHg were shown to correlate to HDT angles of -6 to -24° in heart rate (HR), specific volume regulating hormone aldosterone, and fluid displacement measured by thoracic impedance (Hinghofer-Szalkay *et al.*, 2004).

5.1.3 Venous congestion

Significant increases in cross-sectional area (CSA) of the internal jugular vein (IJV) during spaceflight are typical and have been observed in all astronauts, without exception, when measured (Grigoriev *et al.*, 2011) (Figure 1.4). Increased IJV-CSA occurs as a consequence of the cephalic fluid shift and provides evidence of venous congestion; however, the effect this has on cerebral hemodynamics is less clear.

It is postulated that the emergence of cerebral venous congestion, to headward fluid shift increases, is likely dependent on individual IJV anatomy. Large differences between right and left IJV-CSA have been observed with the maximal right IJV-CSA greater than the left (Lichtenstein *et al.*, 2001) and also larger in males (Maratea *et al.*, 2013). Interestingly, research has shown the incidence of VIIP in men to be around 70% and only 40% in females predominantly in the right eye of both genders (Marshall-Bowman *et al.*, 2013). Female IJV-CSA is smaller than males under the same condition but most probably not disproportionately, and also more variable in size (Maratea *et al.*, 2013). However, greater vascular compliance and higher plasma volume loss have been measured in females (Waters *et al.*, 2002; Fu *et al.*, 2004) and may explain the potential gender variances observed in VIIP.

Asymmetric IJV anatomy and variances in magnitude of peripheral displacement further support the idea of venous congestion as a primary contributing factor to VIIP and key target for any future therapeutic countermeasure. However, whether manipulation of venous congestion has any effect on cerebral hemodynamics remains to be seen. Headward fluid shifts, such as those occurring during HDT and weightlessness, cause a reduced outflow of blood from the head (Gisolf *et al.*, 2005); in space this has been hypothesised to set off a cascade phenomenon termed space obstructive syndrome (SOS) (Wiener, 2012).

Venous and arterial pressures vary greatly across the body and with postural changes (Figure 1.10). In order for a spaceflight analogue to be useful, with respect to simulating spaceflight venous congestion, similar pressures across the body must be recreated. In theory, comparable venous and arterial pressures across the body can be created during HDT. However, the remaining gravitational vector during HDT on Earth is in contrast to the complete absence of a hydrostatic gradient in weightlessness. Nevertheless, during HDT various levels of IJV distension occur and it is postulated, with a sufficient angle of tilt, spaceflight venous congestion can be simulated.

Headward venous and arterial pressure increases occur as a result of HDT leading to a reversal of the standing hydrostatic pressure gradient. However, the angle of tilt in which sufficient fluid is displaced, leading to the emergence of venous congestion remains unknown. The inability of -6° HDBR to replicate the symptoms of spaceflight VIIP (Pavy-Le Traon *et al.*, 2007) could indicate hydrostatic pressures are insufficiently recreated at this level; and provide evidence of the role fluid shifts may play in VIIP. It is postulated an increase in angle of HDT would replicate comparable pressure changes

and emergence of vision problems in the long-term. The precise angle at which venous congestion can be induced by peripheral fluid shifts is unknown; and how this is associated to cerebral hemodynamics remains unclear.

5.1.4 Aims

The aim of this study was to assess the effect of lower-body negative pressure (LBNP at -40 mmHg) on jugular venous congestion induced by angles of tilt from +12° head-up tilt (HUT), 0° supine, to -6°, -12°, -18°, and -24° head-down tilt (HDT). Specifically, to differentiate the effects of arterial and venous pressure increases in the neck upon cerebral autoregulation and tissue oxygenation. It is known HDT elicits a cephalic fluid shift opposable by LBNP; however, the effect this has on venous congestion and cerebral hemodynamics has yet to be fully elucidated.

Changes in systemic (heart rate, HR; and mean arterial pressure, MAP) and peripheral (calf circumference, CC; and calf muscle tissue oxygenation, mTSI) measurements, to increasing angles of tilt, were compared with values at baseline (BL). Additionally, venous congestion was assessed through measurements of the internal jugular vein cross-sectional area (CSA) with (-40 mmHg) and without (0 mmHg) LBNP; and changes from BL in cerebral hemodynamics (cerebral oxygenation, cTSI; and blood flow velocity, cBFV), under all conditions, determined.

5.1.5 Hypothesis

It was hypothesised that venous congestion induced by HDT, and measurable by an increased jugular vein CSA, would be abolished by the addition of LBNP. Secondly, the specific HDT angle, with the emergence of congestion, would be greater than the

currently accepted spaceflight analogue of -6°. Thirdly, the LBNP level required for venous congestion removal would be tilt-dependent and consisting of a suitable pressure/tilt match. Specifically, an unmatched LBNP and tilt, either too great or too small, would be detrimental to appropriate cerebral blood flow.

5.2 Methods

5.2.1 Study design and participants

Sixteen (8 male) healthy normotensive, non-smoking participants (Table 5.1) gave written informed consent to participate in the study that conformed to the declaration of Helsinki and was approved by the Ethics Committee of the North Rhine Medical Association in Düsseldorf, Germany.

Before being enrolled into the study, all participants underwent medical screening which consisted of: clinical-chemical blood analysis described in detail in section 2.6.1.1. Further analysis included: urine (glucose, protein, urobilinogen, drugs); resting electrocardiogram (ECG); adapted Bruce Protocol with cycle ergometry to verify appropriate aerobic fitness (for age and gender) and cardiac function (Bruce *et al.*, 1963); a stand test to assess orthostatic tolerance; and, a complete medical history. Prior to testing each participant was familiarized with all aspects of the study, including the methodology, personnel involved and the electronic tilt-table and lower-body negative (LBNP) chamber (Figure 5.4A).

Table 5.1 Individual participant data.

Age on first experimental day; height and weight measured immediately before centrifuge run.

	Sex	*Age (yrs)*	*Height (m)*	*Weight (kg)*	*BMI (kg/m2)*
P01	M	23.6	1.73	69	23.1
P02	M	37.0	1.86	80	23.1
P03	F	27.6	1.71	64	21.9
P04	F	21.6	1.70	61	21.1
P05	M	27.4	1.84	87	25.7
P06	M	27.2	1.85	75	21.9
P07	M	26.6	1.96	100	26.0
P08	F	27.5	1.60	58	22.7
P09	F	30.5	1.61	51	19.7
P10	F	24.7	1.65	54	19.8
P11	F	22.9	1.64	70	26.0
P12	F	21.2	1.70	60	20.8
P13	F	27.6	1.70	62	21.5
P14	M	25.2	1.76	68	22.0
P15	M	27.0	1.72	73	24.7
P16	M	28.5	1.75	72	23.5
Mean ± SD	-	26.6 ± 3.8	1.74 ± 0.10	69 ± 13	22.7 ± 2.1

5.2.2 Experimental protocol

Participants underwent 5 min tilt-table testing (+12 to -24°) without and with lower-body negative pressure (-40 mmHg; TILT+LBNP) during the experiment with rest phases of at least 10 min between the twelve runs in the session (Figure 5.5). Each participant was tested either in the morning (0900-1200) or afternoon (1300-1600). Prior to experimentation participants were instructed to eat a light breakfast, or lunch 1 h before and, in the preceding 24 h period, consume no alcohol or caffeine. Participants were asked to remain silent and completely still throughout TILT±LBNP unless experiencing discomfort.

Each tilt was performed at one of six angles, including +12° head-up tilt (HUT), supine (0°), and head-down tilt (HDT) in -6° increments from -6 to -24° (Figure 5.4B). Participants were not strapped in but the LBNP seal around the iliac crest provided sufficient stability as did the rubberised table during tilt.

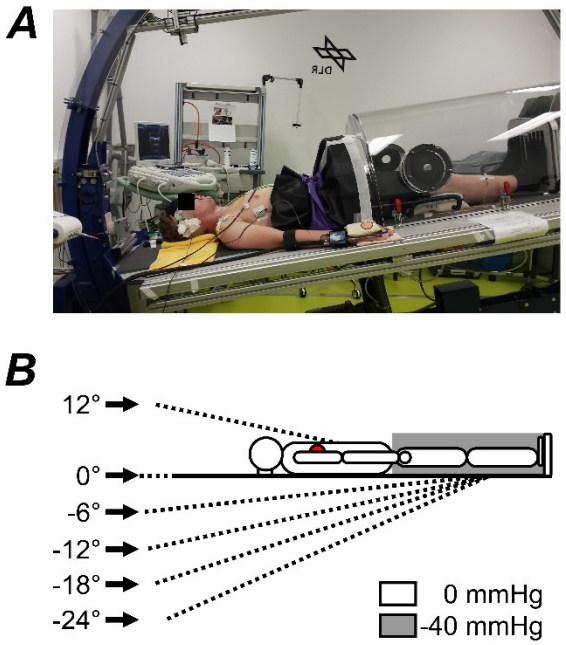

Figure 5.4 Experimental overview.

A, electronic tilt-table with lower-body negative pressure (LBNP) chamber (at DLR, Cologne, Germany); **B**, six angles of tilt (+12 to -24°) without and with -40 mmHg lower-body negative pressure (±LBNP).

Grey shaded area, area of -40 mmHg +LBNP application.

Each experimental day consisted of twelve tilt profiles (Figure 5.5A), randomly assigned with an online randomizer (random.org, 2016). Each tilt profile was split into five phases (Figure 5.5B) with a standardised onset and offset time (60 s) irrespective of tilt angle or ±LBNP.

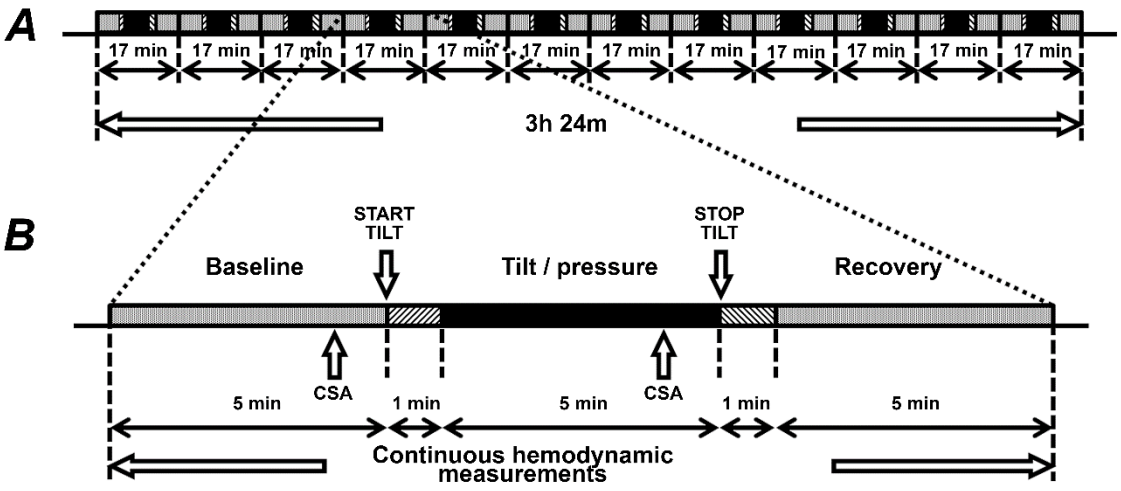

Figure 5.5 Protocol duration with constituent tilt / pressure phases.

A, protocol consisting of twelve randomised tilt / pressure profiles (17 min each), with no less than 10 min rest between them, thus constituting a protocol of 3 h 24 min; **B**, single profile over 17 min consisting of five phases: baseline, start tilt (onset), tilt / pressure, stop tilt (offset), and recovery.

5.2.2.1 Systemic cardiovascular measurements

Continuous beat-by-beat heart rate (HR) via a standard 3-lead electrocardiogram (ECG; Biopac Systems, Goleta, CA, USA) and mean arterial finger blood pressure (MAP) were recorded with a Finometer (Finapres Medical Systems, Amsterdam, The Netherlands). The Finometer finger cuff was placed around the third finger of the left hand (Figure 5.6B) and continuous calibration adjustments at each angle of tilt made using a height correction sensor (Figure 5.6D). Finometer BP measurements were corroborated with absolute arterial BP measurements obtained by an automated sphygmomanometer (Intellivue MMS X2, Philips, Best, The Netherlands) prior to starting each profile. Stroke volume (SV) and total peripheral resistance (TPR) was estimated from the arterial BP waveform using the Modelflow method (Leonetti, *et al.*

2004) via Beatscope software (TNO-TPD, Biomedical Instrumentation, Amsterdam, The Netherlands).

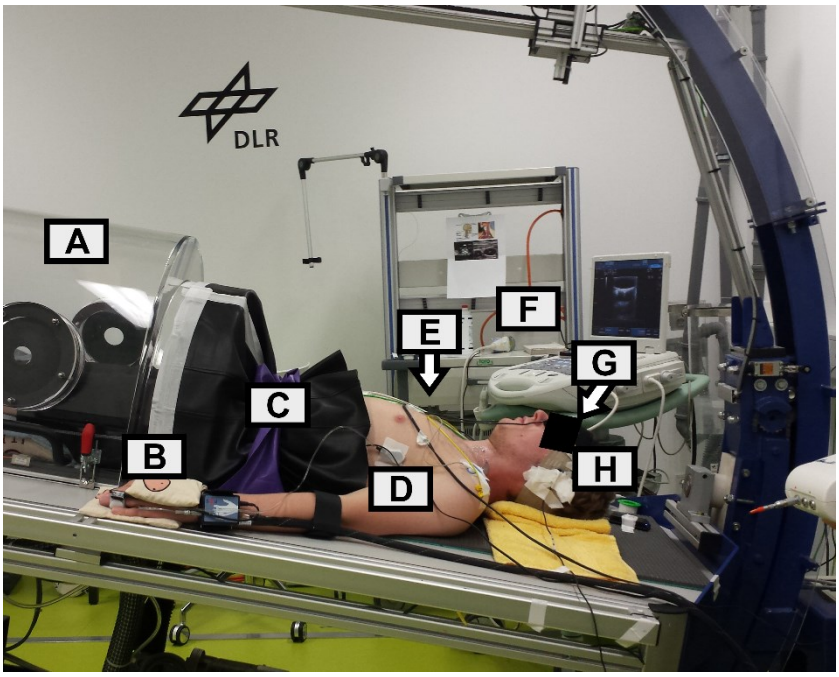

Figure 5.6 Electronic tilt-table experimental setup.

A, lower-body negative pressure (LBNP) chamber (Figure 5.7); **B**, Finapres continuous blood pressure monitor; **C**, LBNP chamber in line with iliac crest and secured to waist; **D**, Finapres height correction for blood pressure; **E**, 3-lead electrocardiogram (ECG); **F**, Ultrasonography for internal jugular vein; **G**, near infrared spectroscopy (NIRS) of the prefrontal cortex; **H**, Transcranial Doppler (TCD) sensor.

5.2.2.2 Peripheral fluid displacement

Lower-limb muscle oxygenation was measured using near-infrared spectroscopy (mNIRS; PortaMon, Artinis Medical Systems, Einsteinweg, The Netherlands) of the calf muscle to obtain the tissue saturation index (mTSI, Figure 5.7C). Movement of fluid to the lower extremities, and away from the central compartment, was quantified

using strain gauge plethysmography (SGP; EC6 Strain Gauge Plethysmograph, Hokanson Inc., Bellevue, WA, USA). In each participant the gauge was positioned around the calf midpoint (directly between the tibiae tuberosity and medial malleolus bony prominences) to record accurate changes in calf circumference (CC, Figure 5.7B).

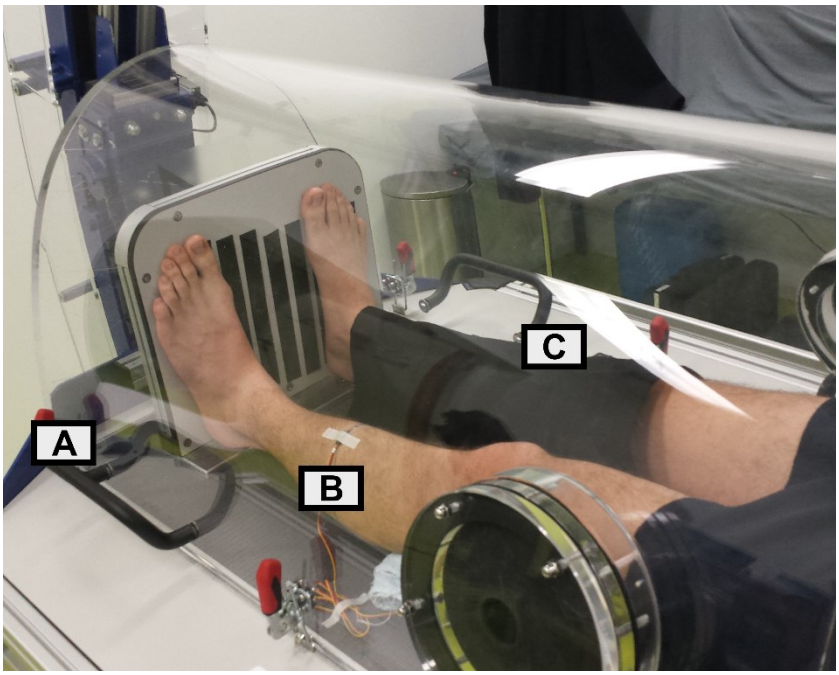

Figure 5.7 Lower-body negative pressure (LBNP) chamber experimental setup.

A, pressure, humidity and temperature sensor; **B**, strain gauge plethysmography; **C**, near infrared spectroscopy (NIRS) of the calf muscle with light shielding.

5.2.2.3 Venous congestion

Right and left internal jugular vein cross-sectional areas (CSA-R and CSA-L) were recorded using ultrasonography (MyLab Gamma, Esoate SpA, Genoa, Italy). The ultrasound probe was placed at an angle of approximately 90° at the cricoid level,

parallel to the clavicle, to obtain transversal views of the neck during baseline and TILT±LBNP phases.

Measurements were made in B-mode (brightness mode) with the probe on the participant's neck with a thick layer of ultrasonic gel; ensuring complete coupling between the transducer and the participant's skin, and thereby exert virtually no compressive force at all. Thus, significant and excessive pressure, potentially changing the shape and dimension of the vein, was avoided; whilst image quality, free from black cones and dark areas, was maintained.

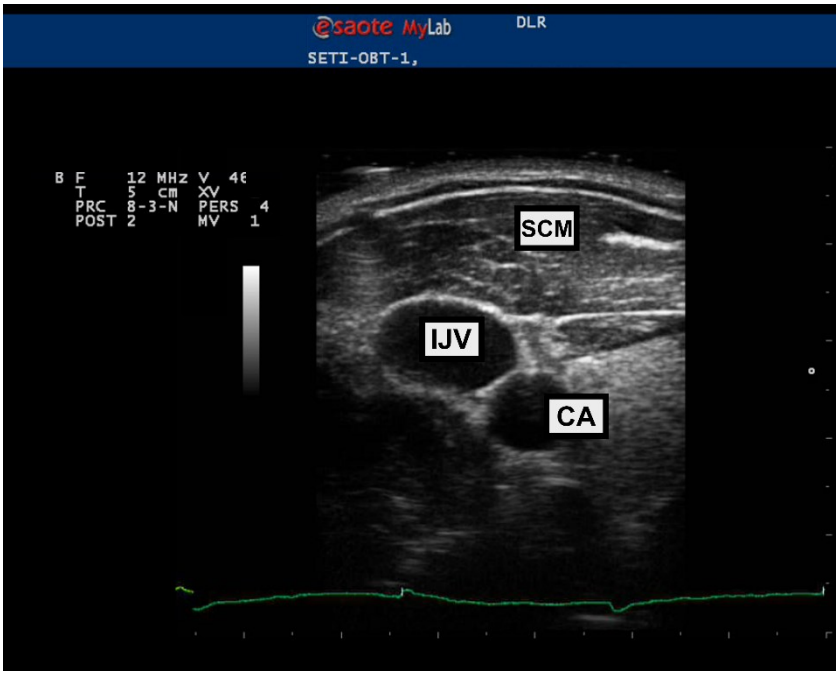

Figure 5.8 Screenshot from ultrasonography video sequence of the internal jugular vein.

SCM, sternocleidomastoid muscle; **IJV**, internal jugular vein; **CA**, carotid artery.

Short video sequences were stored and offline measurements of the pulse-triggered maximal right and left internal jugular vein cross-sectional area were made using the manual area trace function of the machine (Figure 5.8). One operator was used for all measurements, with an average of three screenshots taken for each value, and blinded to the experimental condition.

5.2.2.4 Cerebral perfusion

Cerebral near-infrared spectroscopy of the left prefrontal cortex immediately below the forehead hairline of each participant (cNIRS; PortaLite, Artinis Medical Systems, Einsteinweg, The Netherlands; Figure 5.6B) was used to determine the absolute ratio of

oxy- (O_2Hb) and deoxyhemoglobin (HHb). Taking into account participant frontal cranium thickness, based on age and gender, the cerebral tissue saturation index (cTSI) was deduced (Lynnerup *et al.*, 2005) with an inference on global cerebral perfusion (Weiss *et al.,* 2005).

Cerebral blood flow velocity (cBFV) in the middle cerebral artery (MCA) was continuously measured using transcranial Doppler (TCD; DWL Multi-Dop T digital, Compumedics GmbH, Singen, Germany) attached to the participant's head (Figure 5.6H).

5.2.3 Statistical analysis

Following previous studies of the measures used in this paper in which fluid shifts were induced, an error probability (α) of 0.05, power ($1 - \beta$) of 0.80 with an average effect size (d) of 0.05, power calculation, using G* Power (Erdfelder, Faul, & Buchner, 1996), yielded a participant number of 15.

All continuously recorded data were analysed in 30 s frames and artefacts removed with a custom made Matlab (R2015a, The Mathworks Inc., MA, USA) script using the following criteria: (i) physiologically plausible limits (Table 2.2); and (ii) maximal percentage of change in relation to the standard deviation of the signal. Data was resampled at 4Hz (piecewise cubic spline interpolation) as long as >95% of data were valid yielding 15 complete sets of data for further analysis.

Data at specific tilt angles without and with pressure (TILT±LBNP) were analysed using the changes from the respective last minute baseline (BL) mean to a 1 min mean in the last minute of each TILT±LBNP (min 5). Data presented during the entire run are delta values of each 30 s mean of the 12 min measurements following TILT±LBNP

onset from the last minute BL mean. A mean of the three absolute internal jugular vein cross sectional area measurements were made for the last minute of BL and TILT±LBNP.

Matlab (R2015a, The Mathworks Inc., MA, USA) was used to perform statistical analysis. Visual inspection of residual plots did not reveal any obvious deviations from homoscedasticity or normality of residuals. The tests applied were one-way analysis of variance (ANOVA, repeated measures), post hoc tests with preventative post hoc control of the type I error rate (Tukey's Honestly Significant Difference, HSD) and t-test (independent, by groups). Linear and non-linear peak Gaussian regression analyses were used to estimate the relationships among variables. Furthermore, a test for equality of slopes and intercepts was performed to assess significant difference (Sokal & Rohlf, 1969). The data are presented as mean (±SEM) unless otherwise stated with the level of significance set at $p \leq 0.05$.

5.3 Results

5.3.1 Cardiovascular response

Data below are presented as changes from the baseline (BL) in mean heart rate (ΔHR), averaged mean arterial pressure (ΔMAP), mean stroke volume (ΔSV), and total peripheral resistance (ΔTPR), measured continuously, during all angles and head-down tilt (TILT, +12 to -24°) without lower-body negative pressure (0 mmHg) and with (+-40 mmHg). Baseline values, prior to the start of experimentation, for all participants are outline in

Table **5.2**.

Table 5.2 Participant absolute mean baseline (BL) values for all parameters.

Measured BL is a mean of the last minute immediately before start of the experiment in all participants (n=16).

HR, heart rate; **SV**, stroke volume; **TPR**, total peripheral resistance; **MAP**, mean arterial pressure; **CC**, calf circumference; **mTSI**, muscle tissue saturation index; **cTSI**, cerebral tissue saturation index; **CSA-R_{MAX}**, maximum cross-sectional area of the right jugular vein; **CSA-L_{MAX}**, maximum cross-sectional area of the left jugular vein.

Parameter	*Absolute mean baseline (BL) ± SEM*
HR	65 ± 2 bpm
SV	82.2 ± 3.5 mL
TPR	1402 ± 99 dyn.s.cm^{-5}
MAP	86± 2 mmHg
CC	348 ± 7 mm
mTSI	80.77 ± 1.47 %
cTSI	75.12 ± 2.83 %
CSA-R_{MAX}	86 ± 11 mm^2
CSA-L_{MAX}	71 ± 7 mm^2

Changes from baseline (BL): TILT without LBNP (0 mmHg) resulted in no deviations in ΔHR during all angles of tilt (+12 to -24°: $0.127<p<0.926$; Figure 5.9A). However, ΔMAP without LBNP was significantly positive and negative at +12° and -24° respectively ($p<0.05$) but unchanged at all other angles of tilt ($0.066<p<0.365$; Figure 5.9B). ΔSV without LBNP was no different at all angles of tilt (+12 to -24°: $0.111<p<0.691$; Figure 5.9C) in a similar observation of ΔTPR without LBNP (+12 to -24°: $0.350<p<0.763$; Figure 5.9D)

With the addition of LBNP (-40 mmHg) ΔHR was significantly positive at -12° and above (-12 to +12°, $p<0.05$-0.001; Figure 5.9A). ΔMAP was significantly negative with LBNP at all tilt angles (+12 to -24°, $p<0.05$-0.001; Figure 5.9B) as was ΔSV (+12 to -24°, $p<0.01$-0.001; Figure 5.9C). However, ΔTPR with LBNP was significantly positive (-24 to +12°, $p<0.05$-0.001; Figure 5.9D).

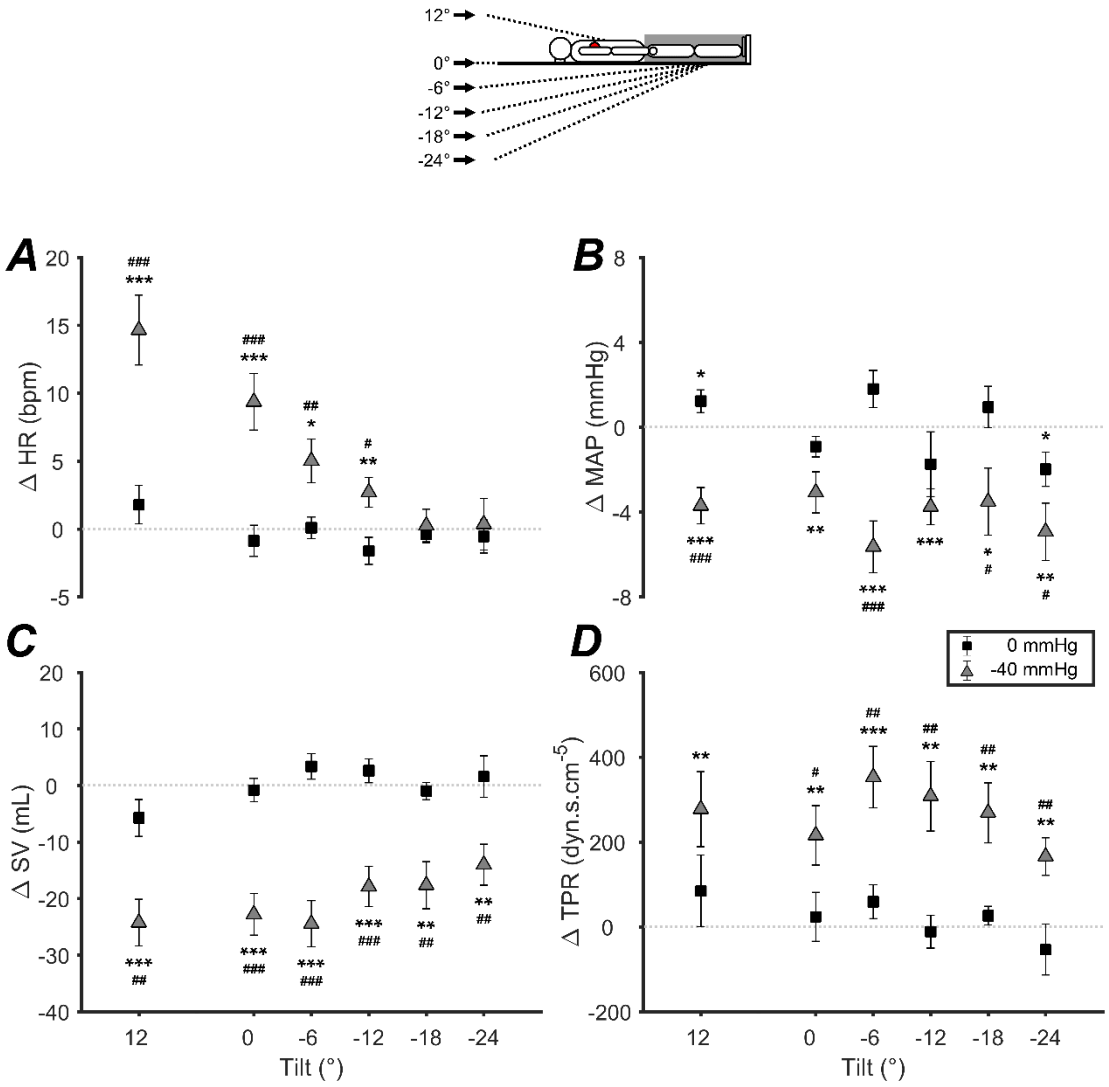

Figure 5.9 Mean changes from baseline (BL) for cardiovascular measures in the final minute (min 5) of head-down tilt (HDT, -6 to -24°), supine (0°) and head-up tilt (+12°) with (-40 mmHg) and without (0 mmHg) lower-body negative pressure (LBNP).

A, changes from baseline (BL) in mean heart rate (ΔHR); **B**, changes from BL in averaged mean arterial pressure (ΔMAP); **C**, changes from BL in mean stroke volume (ΔSV) significantly negative with LBNP (-40 mmHg) at all tilt angles; and **D**, changes from BL in mean total peripheral resistance (ΔTPR).

Mean at each angle (± SEM) is calculated as a final minute (min 5) mean delta from the final minute (min 5) mean of the baseline (BL) immediately before each respective tilt/pressure. **Black square**, without LBNP (0 mmHg); **grey triangle**, with LBNP (-40 mmHg). *vs.* Baseline (*): * $p < 0.05$, ** $p < 0.01$, *** $< p < 0.001$. *vs.* LBNP+/- (#): # $p < 0.05$, ## $p < 0.01$, ### $< p < 0.001$; n = 16.

Pressure comparison (-40 mmHg vs. 0 mmHg): ΔHR with LBNP was significantly greater than without (-40 mmHg *vs.* 0 mmHg) at -12° and above (-12 to +12°, p<0.05-0.001) with the greatest difference at 0° (9 ± 2 *vs.* 1 ± 0 bpm; $F_{(1,30)}$=18.35, p<0.001; Figure 5.9A). However, ΔMAP with LBNP was significantly lower than without at -12° and above (-12 to +12°, p<0.05-0.001) with the greatest difference at -6° (-6 ± 1 *vs.* 2 ± 1 mmHg; $F_{(1,30)}$=22.75, p<0.001; Figure 5.9B).

ΔSV with LBNP was significantly lower than without (-40 mmHg *vs.* 0 mmHg) at all angles (+12 to -24°, p<0.01-0.001) with the greatest difference at -6° (-24.5 ± 4.1 *vs.* 3.4 ± 2.3 mL; $F_{(1,30)}$=11.86, p=0.002; Figure 5.9C). Conversely, ΔTPR with LBNP was significantly greater than without (-40 mmHg *vs.* 0 mmHg) at 0° and below (0 to -24°, p<0.05-0.001) with the greatest difference at -12° (308 ± 82 *vs.* -12 ± 38 dyn.s.cm^{-5}; $F_{(1,30)}$=24.31, p<0.001; Figure 5.9D).

5.3.2 Lower-limb response

Data below are presented as changes from the baseline (BL) in mean calf circumference (ΔCC) and calf muscle tissue saturation index (ΔmTSI), measured continuously, during all angles and head-down tilt (TILT, +12 to -24°) without lower-body negative pressure (0 mmHg) and with (-40 mmHg).

Changes from baseline (BL): TILT without LBNP (0 mmHg) resulted in no deviations in ΔCC during all angles of tilt (+12 to -24°: 0.057<p<0.286; Figure 5.10A); and similar observations were made in ΔmTSI (+12 to -24°: 0.102<p<0.628; Figure 5.10B).

With the addition of LBNP (-40 mmHg) ΔCC was significantly positive at -12° and above (-12 to +12°, p<0.05-0.001) and negative at -24° (p=0.009; Figure 5.10A). ΔmTSI was significantly negative with LBNP at tilt angles above -6 ° (-6 to +12°, p<0.05-0.001); however, no change was measured below (-12 to -24: 0.193<p<0.480); Figure 5.10B).

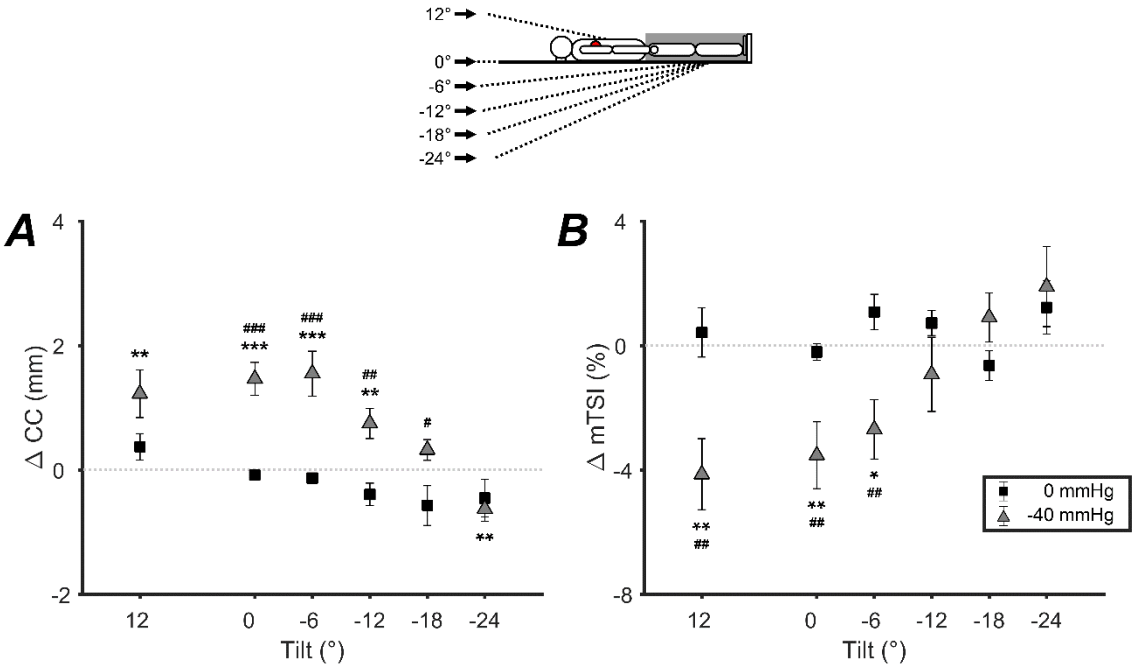

Figure 5.10 Mean changes from baseline (BL) for parameters in the lower-limb of the final minute (min 5) of head-down tilt (HDT, -6 to -24°), supine (0°) and head-up tilt (+12°); with (-40 mmHg) and without (0 mmHg) lower-body negative pressure (LBNP).

A, changes from baseline (BL) in mean calf circumference (ΔCC); and **B**, changes from BL in mean calf muscle tissue saturation index (ΔmTSI).

Mean at each angle (± SEM) is calculated as a final minute (min 5) mean delta from the final minute (min 5) mean of the baseline (BL) immediately before each respective tilt/pressure. **Black square**, without LBNP (0 mmHg); **grey triangle**, with LBNP (-40 mmHg). *vs.* Baseline (*): * p < 0.05, ** p < 0.01, *** < p <0.001. *vs.* LBNP+/- (#): # p < 0.05, ## p < 0.01, ### < p <0.001; n = 16.

Pressure comparison (-40 mmHg vs. 0 mmHg): ΔCC with LBNP was significantly greater than without (-40 mmHg *vs.* 0 mmHg) at -18° to 0° ($p<0.05$-0.001) with the greatest difference at 0° (1.5 ± 0.3 *vs.* -0.1 ± 0.1 mm; $F_{(1,30)}=29.42$, $p<0.001$; Figure 5.10A). However, ΔmTSI with LBNP was significantly lower than without at -6° and above (-6 to +12°, $p<0.01$) with the greatest difference at -6° (-2.70 ± 0.95 *vs.* 1.07 ± 0.57 %; $F_{(1,30)}=10.09$, $p=0.004$; Figure 5.10B).

5.3.3 Emergence and removal of venous congestion

Data below are mean absolute values of internal jugular vein cross-sectional area on the right (CSA-R) and left (CSA-R), taken from three repeated ultrasound measurements in the final minute (min 5), at all angles and head-down tilt (TILT, +12 to -24°) without lower-body negative pressure (0 mmHg) and with (-40 mmHg).

Changes from baseline (BL): CSA-R during TILT without LBNP (0 mmHg) was significantly greater than baseline (BL) at -18° and below (-18 to -24°: $p<0.001$), less at +12° ($p<0.001$) and no change between 0 to -12° ($0.054<p<0.926$; Figure 5.11A). Similarly, CSA-L without LBNP was significantly greater than baseline (BL) at -12° and below (-12 to -24°: $p<0.01$-0.001), less at +12° ($p<0.001$) and no change at 0° and -6° ($0.098<p<0.935$; Figure 5.11B).

With the addition of LBNP (-40 mmHg) CSA-R was significantly lower at -12° and above compared to BL (-12 to +12°, $p<0.05$-0.001) with no change at -18 and -24° ($0.412<p<0.757$; Figure 5.11A). CSA-L was significantly less at -6 ° and above (-6 to +12°, $p<0.001$) compared to BL but no change was measured at -12° and below (-12 to -24: $0.056<p<0.700$); Figure 5.11B).

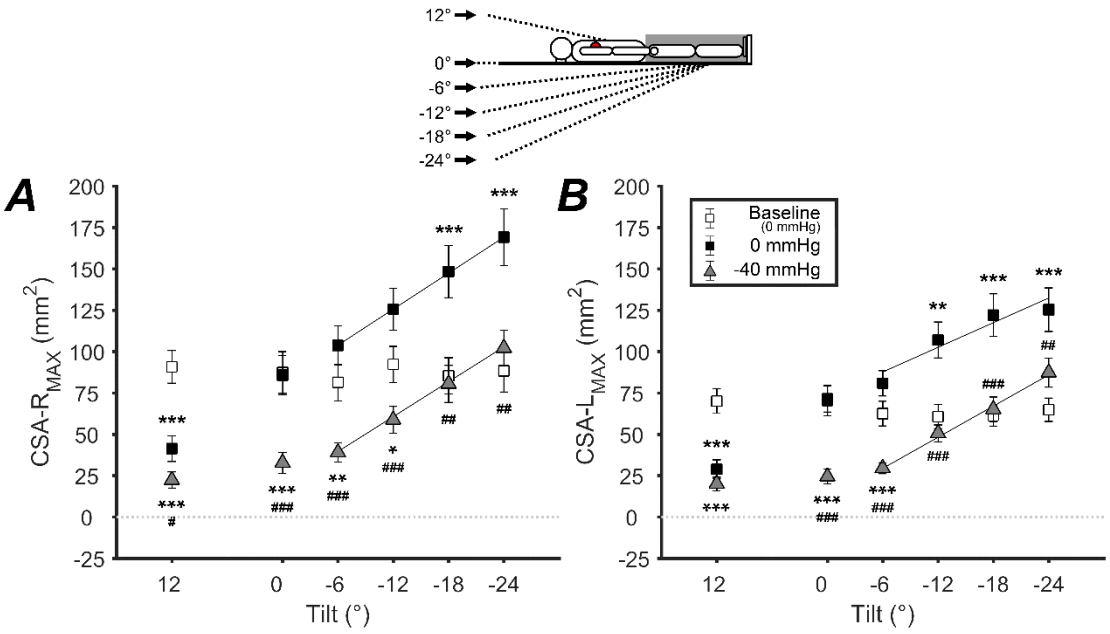

Figure 5.11 Mean absolute internal jugular vein cross-sectional area (CSA, left and right) of the final minute (min 5) of head-down tilt (HDT, -6 to -24°), supine (0°) and head-up tilt (+12°); with (-40 mmHg) and without (0 mmHg) lower-body negative pressure (LBNP).

A, mean absolute right internal jugular vein cross-sectional area (CSA-R); and **B**, mean absolute left internal jugular vein cross-sectional area (CSA-L).

Mean at each angle (± SEM) is calculated as an average of three individual maximum measurements in the final minute (min 5) of each tilt/pressure and the baseline (BL) immediately before each respective tilt/pressure. **Black square**, without LBNP (0 mmHg); **grey triangle**, with LBNP (-40 mmHg). *vs.* Baseline (*): * $p < 0.05$, ** $p < 0.01$, *** $< p < 0.001$. *vs.* LBNP+/- (#): # $p < 0.05$, ## $p < 0.01$, ### $< p < 0.001$; n = 16.
-6 to -24°: Linear regression polynomial (f = y0+a*x).

Pressure comparison (-40 mmHg vs. 0 mmHg): CSA-R with LBNP was significantly lower than without (-40 mmHg *vs.* 0 mmHg) at all tilt angles (+12° to -24°: $p<0.05$-0.001) with the greatest difference at -6° (39 ± 6 *vs.* 104 ± 12 mm^2; $F_{(1,30)}=23.93$, $p<0.001$; Figure 5.11A). Similarly, CSA-L with LBNP was significantly lower than without at 0° and below (0 to -24°, $p<0.01$) with the greatest difference also at -6° (30 ± 3 *vs.* 81 ± 8 mm^2; $F_{(1,30)}=38.01$, $p<0.001$; Figure 5.11B).

CSA-R regression lines with ($R^2=0.999$, $F_{3,32}=3946$, $p<0.001$, $m=-3.52$) and without LBNP ($R^2=0.999$, $F_{3,32}=7047$, $p<0.001$; $m=-3.65$) showed no difference in slope ($F_{1,4}=1.09$, $p=0.356$) but significantly different y-intercepts (82 *vs.* 17 mm^2; $F_{1,4}=13021$, $p<0.001$; Figure 5.11A). Similarly, CSA-L regression lines with ($R^2=141.3$, $p<0.001$, $p=0.003$, $m=-3.13$) and without LBNP ($R^2=0.893$, $F_{3,32}=16.67$, $p=0.045$, $m=-2.48$) also showed no difference in slope ($F_{1,4}=3.53$, $p=0.134$; Figure 5.11B) but significantly different y-intercepts (72 *vs.* 11 mm^2; $F_{1,4}=1.09$, $p=0.356$; Figure 5.11B).

5.3.3.1 Reduction of right-left internal jugular vein asymmetry by LBNP

Differences between right and left internal jugular vein cross-sectional area (ΔR-L CSA) were consistently positive, even at baseline (0°, 0 mmHg). However, there was no significant difference in ΔR-L CSA without LBNP at all angles of tilt apart from -24° significantly positive ($p=0.030$). With the addition of LBNP at -24° compared to without (-40 mmHg *vs.* 0 mmHg) this asymmetry was abolished (43.9 ± 18.3 *vs.* 14.9 ± 9.5 mm^2, $F_{(1,30)=}1.98$, $p=0.170$; Figure 5.12).

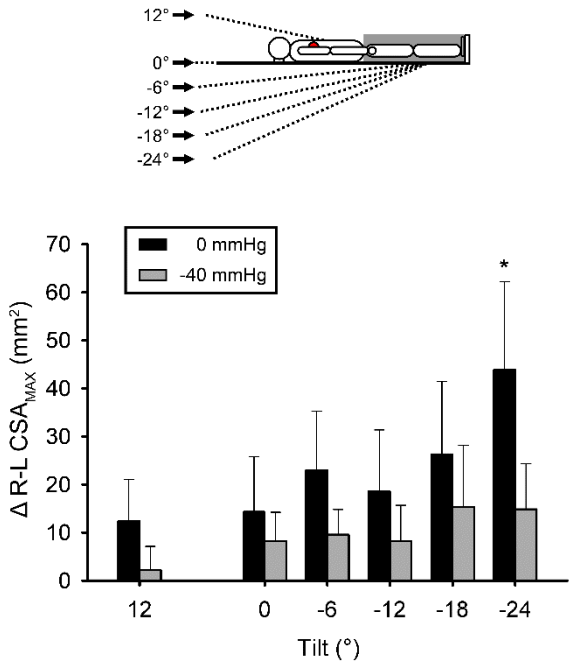

Figure 5.12 Mean difference in absolute cross-sectional area of the right (CSA-R) and left (CSA-L) internal jugular veins in the final minute (min 5) of head-down tilt (HDT, -6 to -24°), supine (0°) and head-up tilt (+12°); with (-40 mmHg) and without (0 mmHg) lower-body negative pressure (LBNP).

Mean at each angle (± SEM) is calculated as an average of three individual maximum ultrasound measurements in the final minute (min 5) of each tilt/pressure and the baseline (BL) immediately before each respective tilt/pressure. Delta is calculated as CSA-R minus CSA-L. **Black**, without LBNP (0 mmHg); **grey**, with LBNP (-40 mmHg). *CSA-R vs.* CSA-L (*): * $p < 0.05$; n = 16.

5.3.4 Cerebral hemodynamics

Data below are presented as changes from the baseline (BL) in mean prefrontal cortex cerebral tissue saturation index (ΔcTSI), mean middle cerebral artery blood flow velocity (ΔcBFV), and calculated changes from baseline in cerebrovascular conductance (ΔCVC; flow/pressure: MAP/cBFV), measured continuously, during all

angles and head-down tilt (TILT, +12 to -24°) without lower-body negative pressure (0 mmHg) and with (-40 mmHg).

Changes from baseline (BL): ΔcTSI during TILT without LBNP (0 mmHg) was no different at all angles of tilt (+12 to -24°: 0.215<p<0.755; Figure 5.13); with the same observation in ΔcBFV (+12 to -24°, 0.125<p<0.736; Figure 5.14).

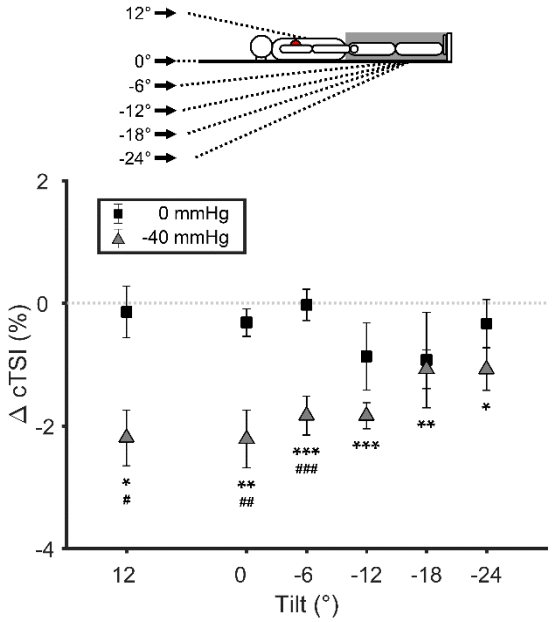

Figure 5.13 Mean changes from baseline (BL) for near-infrared spectroscopy (NIRS) measured prefrontal cortex cerebral tissue saturation index (ΔcTSI) in the final minute (min 5) of head-down tilt (HDT, -6 to -24°), supine (0°) and head-up tilt (+12°); with (-40 mmHg) and without (0 mmHg) lower-body negative pressure (LBNP).

Mean at each angle (± SEM) is calculated as a final minute (min 5) mean delta from the final minute (min 5) mean of the baseline (BL) immediately before each respective tilt/pressure. **Black square**, without LBNP (0 mmHg); **grey triangle**, with LBNP (-40 mmHg). *vs.* Baseline (*): * p < 0.05, ** p < 0.01, *** < p <0.001. *vs.* LBNP+/- (#): # p < 0.05, ## p < 0.01, ### < p <0.001; n = 16.

With the addition of LBNP (-40 mmHg) ΔcTSI was significantly negative at all tilt angles (+12 to -24°, p<0.05-0.001; Figure 5.13); however, no change was measured in ΔcBFV with LBNP apart from -12° significantly positive (p=0.031); Figure 5.14).

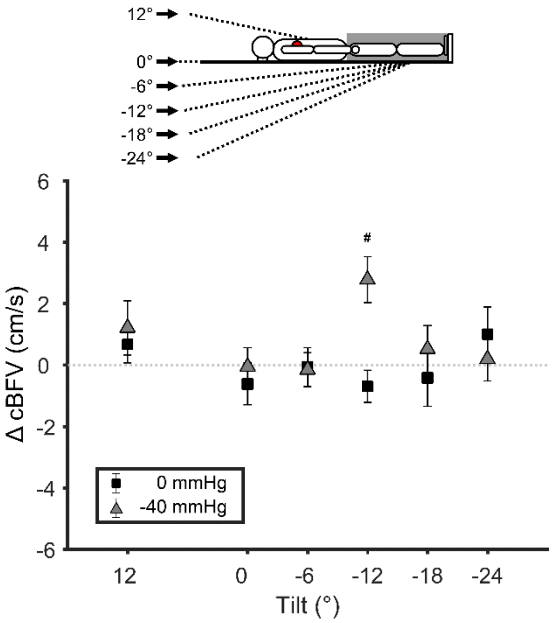

Figure 5.14 Mean changes from baseline (BL) for transcranial Doppler (TCD) measured middle cerebral artery blood flow velocity (ΔcBFV) in the final minute (min 5) of head-down tilt (HDT, -6 to -24°), supine (0°) and head-up tilt (+12°); with (-40 mmHg) and without (0 mmHg) lower-body negative pressure (LBNP).

Mean at each angle (± SEM) is calculated as a final minute (min 5) mean delta from the final minute (min 5) mean of the baseline (BL) immediately before each respective tilt/pressure. **Black square**, without LBNP (0 mmHg); **grey triangle**, with LBNP (-40 mmHg). *vs.* Baseline (*): * p < 0.05, ** p < 0.01, *** < p <0.001. *vs.* LBNP+/- (#): # p < 0.05, ## p < 0.01, ### < p <0.001; n = 16.

Pressure comparison (-40 mmHg vs. 0 mmHg): ΔcTSI with LBNP was significantly lower than without (-40 mmHg *vs.* 0 mmHg) at -6° and above (-6° to +12°: p<0.05-0.001) with the greatest difference at -6° (-1.83 ± 0.32 *vs.* -0.03 ± 0.25 %; $F_{(1,30)}$=16.69, p<0.001; Figure 5.13). ΔcBFV with LBNP was significantly higher than without at -12°

(4.12 ± 1.36 *vs.* -0.71 ± 0.56 cm.s^{-1}; $F_{(1,30)}$=7.37, p=0.013) with no difference at all other angles (+12°: p=0.979; 0°: p=0.397; -6°: p=0.841; -18°: p=0.754; and -24°: p=0.398; Figure 5.14). Similarly, ΔCVC was significantly lower than without LBNP at -18° (1.25 ± 0.74 vs. -0.45 ± 0.42 cm.s^{-1}.mmHg^{-1}; $F_{(1,30)}$=6.24, p=0.045) with no difference at all other angles (Figure 5.15).

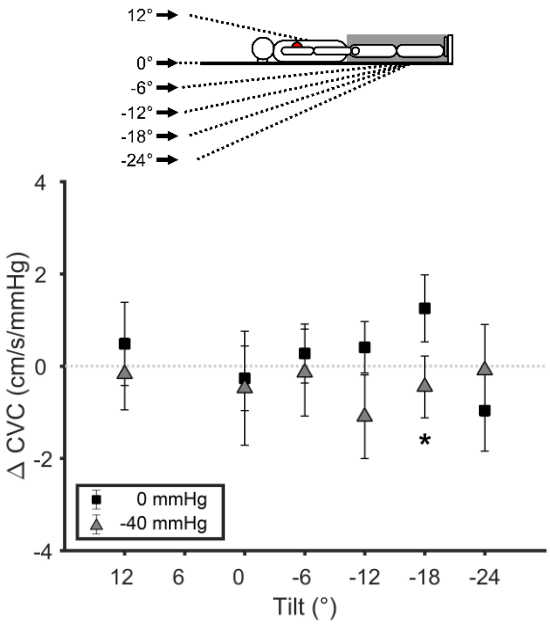

Figure 5.15 Mean changes from baseline (BL) for calculated cerebrovascular conductance (ΔCVC; flow/pressure) in the final minute (min 5) of head-down tilt (HDT, -6 to -24°), supine (0°) and head-up tilt (+12°); with (-40 mmHg) and without (0 mmHg) lower-body negative pressure (LBNP).

Mean at each angle (± SEM) is calculated as a final minute (min 5) mean delta from the final minute (min 5) mean of the baseline (BL) immediately before each respective tilt/pressure. **Black square**, without LBNP (0 mmHg); **grey triangle**, with LBNP (-40 mmHg). *vs.* Baseline (*): * p < 0.05, ** p < 0.01, *** < p <0.001. *vs.* LBNP+/- (#): # p < 0.05, ## p < 0.01, ### < p <0.001; n = 16.

5.3.4.1 Cerebral blood flow time course

The entire 12 minute run profile consisted of: (i) start onset of TILT±LBNP (min -1.0 to 0.0); (ii) orthostatic challenge exposure (TILT±LBNP: min 0.0 to 5.0); (iii) end offset of tilt pressure (min 5.0 to 6.0); and (iv) recovery (RR: min 6.0 to 11.0; Figure 5.16).

Data below are presented as changes from baseline (BL) in continuously measured mean middle cerebral artery blood flow velocity (ΔcBFV) at 30 second intervals across the whole run profile duration (min -1.0 to 11.0). ΔcBFV time course at head-up tilt (HUT, +12°), supine (0°), and head-down tilt (HDT, -6 to -24°) without lower-body negative pressure (0 mmHg) and with (-40 mmHg) are plotted (Figure 5.16).

Changes from baseline (BL): ΔcBFV without LBNP (0 mmHg) during all angles of tilt (TILT, min 0.0-5.0) was no different (+12 to -24), apart from significantly negative in min 0 at +12° ($p=0.013$; Figure 5.16A), 0° ($p=0.004$; Figure 5.16B), and -12° ($p=0.006$; Figure 5.16D).

ΔcBFV without LBNP during ramp-down and recovery (RR, min 5.0-11.0) was unchanged at 0° ($0.086<p<0.901$; Figure 5.16B) and -24° ($0.093<p<0.852$; Figure 5.16F). However, ΔcBFV was significantly negative at +12° (min 9.0-10.0, $p<0.05$; Figure 5.16A), -6° (min 8.5, $p<0.05$; Figure 5.16C), and -12° (min 6, 8.5, 9.5-10.5, $p<0.05$; Figure 5.16D). Conversely, ΔcBFV was significantly positive at -18° (min 8.5, $p<0.05$; Figure 5.16E).

With the addition of LBNP (-40 mmHg) ΔcBFV was no different at all angles of tilt (+12 to -24°, $p<0.05$-0.001) apart from significantly positive at -12° in the final minute of HDT (min 4.5, $p<0.05$; Figure 5.16D). During RR with LBNP, ΔcBFV was

significantly negative during 0° (min 7, $p<0.05$; Figure 5.16B), -6° (min 6.5-9.0, and 10.0-11.0, $p<0.05$; Figure 5.16C), and -24° (min 6.5, $p<0.05$; Figure 5.16F); with no change during +12° ($0.065<p<0.811$, Figure 5.16A), -12° ($0.399<p<0.923$, Figure 5.16D), or -18° ($0.212<p<0.952$, Figure 5.16E).

Pressure comparison (-40 mmHg vs. 0 mmHg): ΔcBFV with LBNP was no different than without (-40 mmHg *vs.* 0 mmHg), across all time points, at +12° ($F_{(24,375)}=0.39$, p=0.536; Figure 5.16A), 0° ($F_{(24,375)}=0.68$, p=0.418; Figure 5.16B), -6° ($F_{(24,375)}=0.66$, p=0.426; Figure 5.16C), -18° ($F_{(24,375)}=0.03$, p=0.864; Figure 5.16E), -24° ($F_{(24,375)}=0.31$, p=0.582; Figure 5.16F). However, at -12°, ΔcBFV was significantly greater with the addition of LBNP to TILT at min 0.0-1.0, 2.5, and 3.5-4.5 ($F_{(24,375)}=5.39$, p=0.031) with the greatest difference in the final minute (min 4.5: 4.12 ± 1.36 *vs.* -0.71 ± 0.56 $cm.s^{-1}$, p=0.013; Figure 5.16D). During RR, ΔcBFV was no different at all angles of tilt.

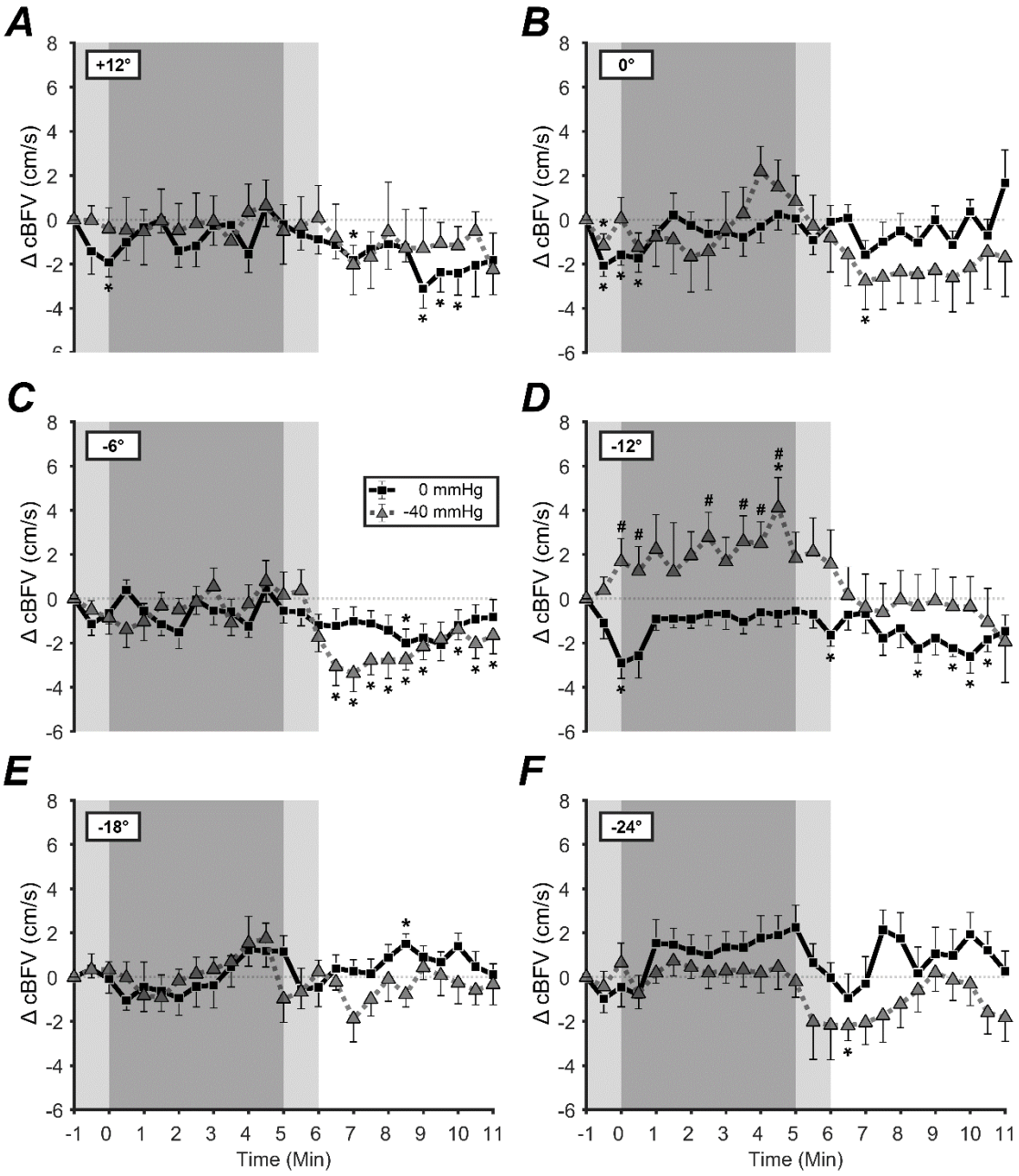

Figure 5.16 Mean changes from baseline (BL) for middle cerebral artery blood flow velocity (ΔcBFV) during five minutes head-up tilt (HUT, +12°), supine (0°), and head-down tilt (HDT, -6 to -24°) with (-40 mmHg) and without (0 mmHg) lower-body negative pressure (LBNP), and recovery (RR, 0° and 0 mmHg).

A, mean middle cerebral artery blood flow velocity (ΔcBFV) during +12° head-up tilt (HUT); **B**, ΔcBFV during 0° supine; **C**, ΔcBFV during -6° head-down tilt (HDT); **D**, ΔcBFV during -12° HDT; **E**, ΔcBFV during -18° HDT; and **F**, ΔcBFV during -24° HDT.

Mean ± SEM is 30 s mean delta from final minute (min 5) mean of each baseline (BL) before tilt. **Black square**, without LBNP (0 mmHg); **grey triangle**, with LBNP (-40 mmHg). Shaded areas: **light grey**, one minute onset of tilt/pressure (min -1.0-0 and 5.0-6.0); **dark grey**, five minutes tilt (HDT: min 0.0-5.0); **white**, five minutes recovery (RR: min 6.0-11.0). *vs.* Baseline (*): * $p < 0.05$. *vs.* LBNP+/- (#): # $p < 0.05$; n = 16.

5.3.5 Time effect at 12° head-down tilt

Data below are presented as changes from baseline (BL) in continuously measured mean heart rate (ΔHR), averaged mean arterial pressure (ΔMAP), mean calf circumference (ΔCC), and prefrontal cortex cerebral tissue saturation index (ΔcTSI) at 30 second intervals across the whole run profile duration (min -1.0 to 11.0). Parameter time course at -12° head-down tilt (HDT) without lower-body negative pressure (0 mmHg) and with (-40 mmHg) are plotted (Figure 5.17).

Changes from baseline (BL): ΔHR without LBNP (0 mmHg) was unchanged during -12° HDT (min 0.0-5.0: $0.127<p<0.997$; Figure 5.17A); as was ΔMAP (min 0.0-5.0: $0.271<p<0.966$; Figure 5.17B).

ΔCC without LBNP (0 mmHg) was no different during -12° HDT apart from significantly negative at min 0.5 ($p<0.05$; Figure 5.17C); whilst ΔcTSI was also significantly negative at min 1.0-1.5 and 3.5-4.5 ($p<0.0.5$; Figure 5.17D).

ΔHR without LBNP during ramp-down and recovery (RR, min 5.0-11.0) was unchanged apart from significantly positive at min 10.0 ($p<0.05$; Figure 5.17A). Similarly, ΔMAP and ΔcTSI changes were insignificant during RR (ΔMAP: $p<0.05$, Figure 5.17B; and ΔcTSI: $p<0.05$, Figure 5.17D). However, ΔCC without LBNP during the final minute of RR was significantly negative (min 11.0, $p<0.05$; Figure 5.17C).

With the addition of LBNP (-40 mmHg) during -12° HDT, ΔHR was significantly positive at min 0.5-5.0 ($p<0.05$; Figure 5.17A); as was ΔCC in the first stages of LBNP (min 0.0-2.0, $p<0.05$; Figure 5.17C). Conversely, ΔMAP and ΔcTSI were both significantly negative with the addition of LBNP during -12° HDT (ΔMAP: min 0.5, and 1.5-2.5, $p<0.05$, Figure 5.17B; and ΔcTSI: min 1.0-4.0, and 5.0, $p<0.05$, Figure 5.17D).

During RR with LBNP, ΔHR was significantly negative (min 8.5, 10.0-11.0, $p<0.05$; Figure 5.17A), but ΔMAP and ΔcTSI were significantly positive (ΔMAP: min 7.5, 8.5 and 10.0-10.5, $p<0.05$, Figure 5.17B; and ΔcTSI: min 6.5-8.5, $p<0.05$, Figure 5.17D). However, ΔCC during this RR period was no different from BL ($0.490<p<0.931$; Figure 5.17C).

Pressure comparison (-40 mmHg vs. 0 mmHg): ΔHR with LBNP was significantly greater than without (-40 mmHg *vs.* 0 mmHg) at -12° HDT in min 0.5-5.0 ($F_{(24,375)}=7.83$, $p=0.009$) with the greatest difference at min 4.5 (7 ± 1 *vs.* 0 ± 1 bpm; $p<0.001$; Figure 5.17A); however, ΔMAP and ΔcTSI were no different (ΔMAP: $F_{(24,375)}=2.36$, $p=0.135$, Figure 5.17B; and ΔcTSI: $F_{(24,375)}=0.13$, $p=0.723$; Figure 5.17D). ΔCC was significantly greater with the addition of LBNP to HDT at min 0.0-3.0 ($F_{(24,375)}=6.29$, $p=0.019$) with the greatest difference at min 1.5 (0.9 ± 0.2 *vs.* -0.4 ± 0.2 mm; $p<0.001$; Figure 5.17C). During RR, only ΔHR and ΔMAP were significantly lower and greater respectively when comparing 0 to -40 mmHg; with the greatest difference in ΔHR at min 10 (-3 ± 1 *vs.* 3 ± 1 bpm; $p=0.003$; Figure 5.17A) and in ΔMAP at min 10.5 (3 ± 1 *vs.* -1 ± 1 mmHg; $p=0.021$; Figure 5.17B).

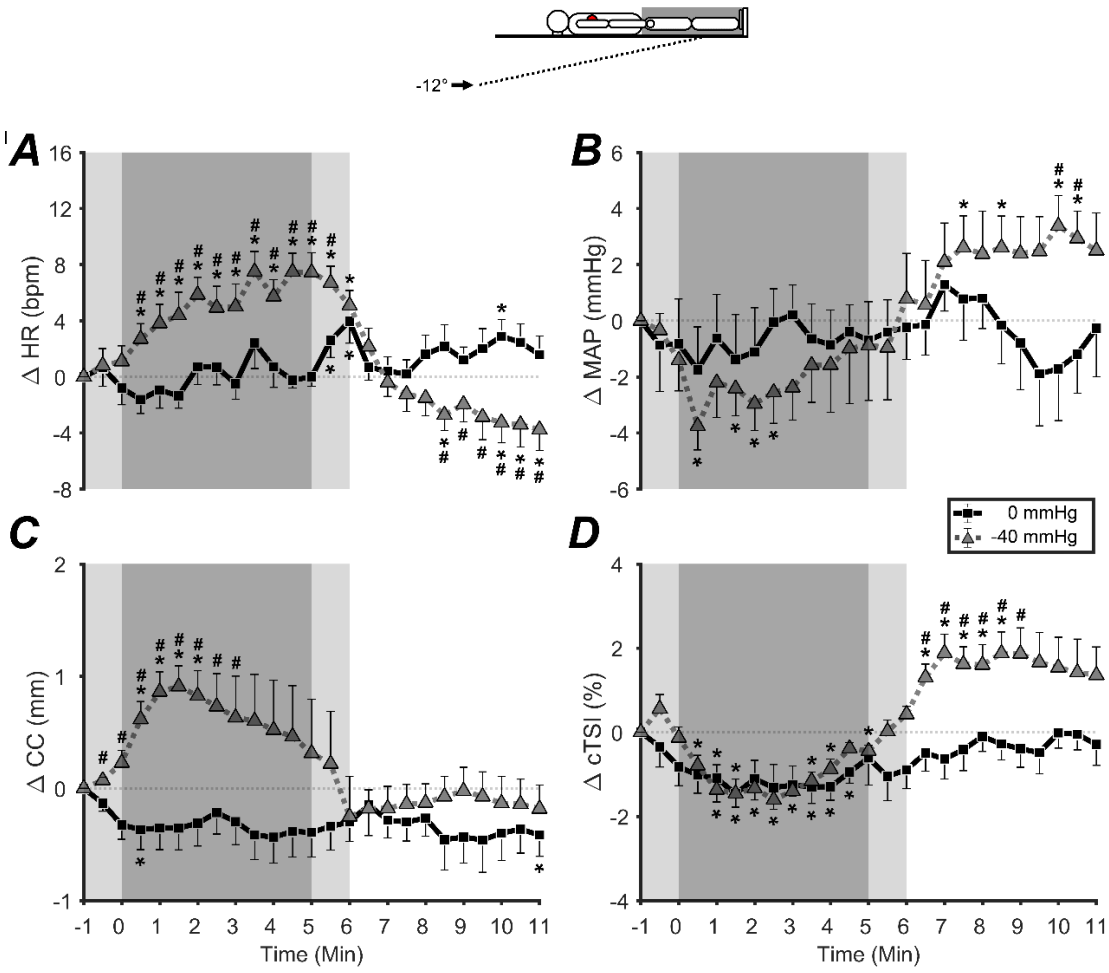

Figure 5.17 Mean changes from baseline (BL) for systemic, peripheral and cerebral hemodynamic measures during five minutes head-down tilt (HDT, -12°) with (-40 mmHg) and without (0 mmHg) lower-body negative pressure (LBNP), and recovery (0°, 0 mmHg).

A, mean heart rate (ΔHR) during -12° head-down tilt (HDT); **B**, averaged mean arterial pressure (ΔMAP) during -12° HDT; **C**, mean calf circumference (ΔCC) during -12° HDT; and **D**, mean pre-frontal cortex cerebral tissue saturation index (ΔcTSI) during -12° HDT.

Mean ± SEM is 30 s mean delta from final minute (min 5) mean of each baseline (BL) before tilt. **Black square**, without LBNP (0 mmHg); **grey triangle**, with LBNP (-40 mmHg). Shaded areas: **light grey**, one minute onset of tilt/pressure (min -1.0-0 and 5.0-6.0); **dark grey**, five minutes tilt (HDT: min 0.0-5.0); **white**, five minutes recovery (RR: min 6.0-11.0). *vs.* Baseline (*): * $p < 0.05$. *vs.* LBNP+/- (#): # $p < 0.05$; n = 16.

5.3.6 Individual responses and correlations

Significant positive changes from BL in mean middle cerebral artery (MCA) blood flow velocity (ΔcBFV) are corroborated by agreement of the interindividual trends for ΔcBFV to increase with -40 mmHg LBNP at -12° HDT (Figure 5.18B). Without LBNP (0 mmHg) about half of all participants exhibit a fall in ΔcBFV below the respective baseline (BL) immediately before (Figure 5.18A). In contrast, with the addition of -40 mmHg LBNP that trend is reversed and over half of participants show a tendency for increasing ΔcBFV above BL during the orthostatic challenge (min 0-5; Figure 5.18B).

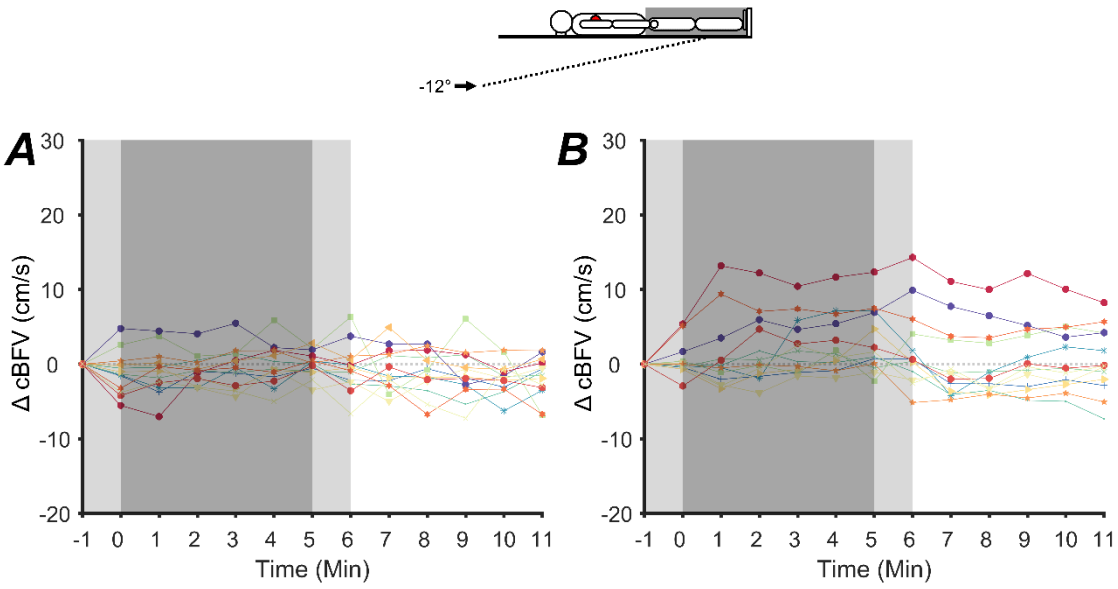

Figure 5.18 Individual participant changes from baseline (BL) for middle cerebral artery blood flow velocity (ΔcBFV) during five minutes head-down tilt (HDT, -12°) with (-40 mmHg) and without (0 mmHg) lower-body negative pressure (LBNP), and recovery (0°, 0 mmHg).

A, Individual changes from baseline (BL) in middle cerebral artery blood flow velocity (ΔcBFV) at -12° head-down tilt (HDT) without LBNP (0 mmHg); and **B**, Individual ΔcBFV at -12°HDT with LBNP (-40 mmHg).

Mean at each data point (± SEM) is calculated as a 60 s mean delta from the final minute (min 5) mean of the baseline (BL) immediately before each respective tilt/pressure. Shaded areas: **light grey**, one minute onset of tilt/pressure (min -1 to 0; and min 5 to 6); **dark grey**, five minutes tilt/pressure (HDT: min 0 to 5); **white**, five minutes recovery (RR: min 6 to 11).

Without LBNP there was no correlation between changes from BL in mean heart rate (ΔHR) and mean calf circumference (ΔCC; Figure 5.19A) or mean prefrontal cortex cerebral tissue saturation index (ΔcTSI) and ΔCC (Figure 5.19B) at all tilt angles tested (-24 to +12°). Similarly, there was no significant correlation between ΔHR and ΔCC during -40 mmHg (Figure 5.19C); however, a significant negative correlation between ΔcTSI and ΔCC was observed with LBNP (R^2=0.735, $F_{1,6}$=11.1, p=0.029; Figure 5.19D).

There was no relationship between changes from BL in ΔcBFV and ΔCC without LBNP (0 mmHg; Figure 5.20A). However, a significant peak Gaussian model fit was shown between ΔcBFV and ΔCC (R^2=0.970, $F_{1,6}$=48.1, p=0.005) during LBNP (-40 mmHg) in the final minute means (min 5) of each tilt/pressure profile; demonstrating ΔCC effect (at -40 mmHg) on positively changing ΔcBFV at a point with diminishing effect either side (Figure 5.20B).

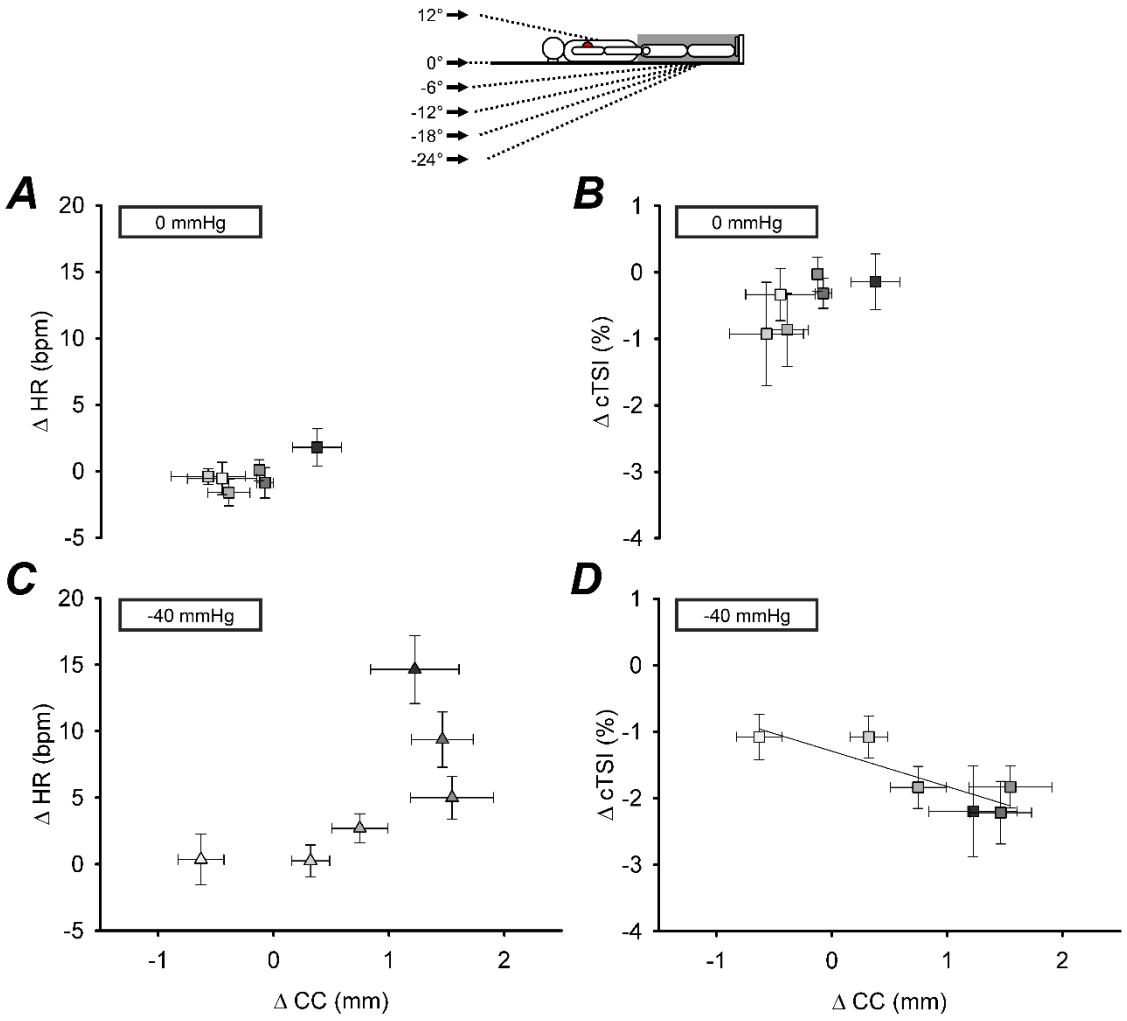

Figure 5.19 Relationship plots between mean changes from baseline (BL) for delta heart rate (ΔHR) and pre-frontal cortex cerebral tissue saturation index (ΔcTSI), against delta calf circumference (ΔCC) in the final minute (min 5) of head-down tilt (HDT, -6 to -24°) with (-40 mmHg) and without (0 mmHg) lower-body negative pressure (LBNP).

A, mean heart rate (ΔHR) *vs.* mean calf circumference (ΔCC) without LBNP (0 mmHg); **B**, mean pre-frontal cortex cerebral tissue saturation index (ΔcTSI) *vs.* ΔCC without; **C**, ΔHR *vs.* ΔCC with LBNP (-40 mmHg); and **D**, ΔcTSI) *vs.* ΔCC with LBNP.

Mean at each angle (± SEM) is calculated as a final minute (min 5) mean delta from the final minute (min 5) mean of the baseline (BL) immediately before each respective tilt/pressure. Marker shading: **white to dark grey**, +12, 0, -6, -12, -18 and -24° respectively. Linear regression polynomial (f = y0+a*x).

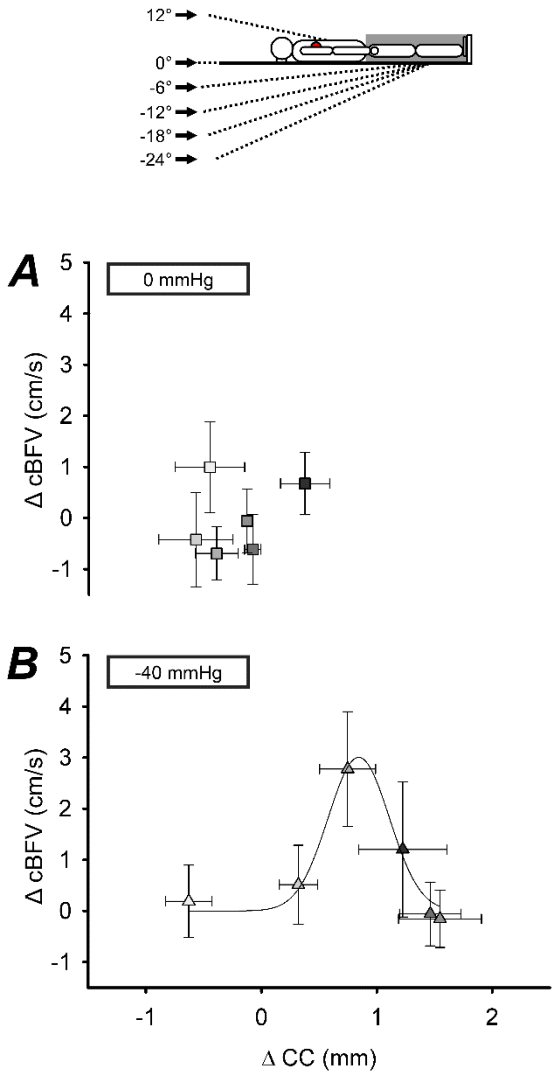

Figure 5.20 Relationship plots between mean changes from baseline (BL) for delta middle cerebral artery blood flow velocity (ΔcBFV) against mean delta calf circumference (ΔCC) in the final minute (min 5) of head-down tilt (HDT, -6 to -24°) with (-40 mmHg) and without (0 mmHg) lower-body negative pressure (LBNP).

A, mean delta middle cerebral artery blood flow velocity (ΔcBFV) *vs.* mean delta calf circumference (ΔCC) without LBNP (0 mmHg); and **B**, ΔcBFV *vs.* ΔCC with LBNP (-40 mmHg).

Mean at each angle (± SEM) is calculated as a final minute (min 5) mean delta from the final minute (min 5) mean of the baseline (BL) immediately before each respective tilt/pressure. Marker shading: **white to dark grey**, +12, 0, -6, -12, -18 and -24° respectively. Nonlinear regression peak Gaussian (f = a*exp(-.5*((x-x0)/b)^2)).

In summary, all 16 participants took part in every aspect of the study, exposed to six different tilt angles from head-up tilt (HUT, +12°), supine (0°) and head-down tilt (-6 to -24°) without (0 mmHg) and with lower-body negative pressure (-40 mmHg). No participant experienced syncope or exhibited presyncopal symptoms even at the +12° tilt angle in the presence of LBNP for five minutes. In general, HDT (without LBNP) had little effect on the central, systemic and cerebral hemodynamic measures; however, significant increases in cross-sectional area were measured in the jugular vein (on both sides). This 'venous engorgement' magnitude manifested as a function of decreasing angles of HDT (-6 to -24°) and a significant alleviation of these increases was measured with the addition of LBNP. In addition, ΔcBFV was significantly positive at -12° HDT with LBNP (-40 mmHg) compared to 0 mmHg, where a similar observation at +12°, 0°, -6°, -18° and -24° was not recorded.

5.4 Discussion

The purpose of this study was to investigate the effect of lower-body negative pressure (LBNP) on head-down tilt (HDT) induced venous congestion. Specifically, (i) to determine the HDT level at which venous congestion occurs; (ii) establish whether or not LBNP could abolish this congestion and to what benefit; and (iii) provide a better insight into mechanistic targets for future more effective spaceflight countermeasures; namely a greater focus on fluid shifts instead of the current simple emphasis on reintroduction of forces to the bones and muscles. Thus, providing a truly holistic spaceflight countermeasure with increased effectiveness.

The main findings of this study were that headward venous and arterial pressure increases, during HDT at -12° and below, was sufficient to elicit significant internal jugular vein (IJV) distension and thus venous congestion. Furthermore, tilt induced congestion was abolished when the quantity of fluid shifted to the periphery counteracted the magnitude of IJV distension; and surprisingly resulted in a marked increase in cerebral blood flow velocity (cBFV). Specifically at -12° HDT, lower-body negative pressure (LBNP) at -40 mmHg was sufficient to remove venous congestion but too low to induce central hypovolemia associated cerebral hemodynamic changes.

5.4.1 Emergence of venous congestion

In the present study, significant increases in IJV cross-sectional area (CSA) were measured only at -12° HDT and below. Previous research has reported maximal IJV distension occurs at around -25° and found to be significantly greater at -10° and below (Clenaghan *et al.*, 2005). Agreement with past research suggests HDT induced venous

congestion is likely to occur at a point between -10° and -12°. Additionally, further increases in the angle of HDT would intensify venous congestion up to -25°.

Head-down bed rest (HDBR) studies attempt to simulate unloading, and crucially the fluid shifted in space, with a standardised tilt angle of -6° (Sundblad & Orlov, 2015). However, justification for this angle of tilt is limited to theoretical calculations on the expected fluid shift (Clément, 2011) and an initial agreement in measurements made on Earth at -6° and in space (At'kov & Bednenko, 1992). An angle of -6° was decided upon as a suitable compromise taking into consideration participant comfort and magnitude of response (Pavy-Le Traon *et al.*, 2007). Crucially however, the stipulation for acceptable "magnitude of response" was pertaining to muscle atrophy and bone loss (At'kov & Bednenko, 1992); with no consideration of, the then undiscovered, visual impairment and intracranial pressure (VIIP) syndrome. It is postulated the inability of current HDBR models to elicit symptoms of VIPP is due to a lack of venous congestion affecting cerebral hemodynamics, intracranial, and intraocular pressure at -6°. Based on previous research and current data, it is suggested future HDBR research would need to reassess the magnitude of response and participant comfort dichotomy, especially if VIIP effects was the focus.

Wiener (2012) suggested HDT research was not useful, in exploring mechanisms associated with VIIP, as cerebral congestion could not be achieved where significant IJV engorgement occurs in spaceflight (Grigoriev *et al.*, 2011). However, in the present study, at HDT angle -12° and below, IJV-CSA was significantly increased. This finding further supports the idea at -6° (current HDBR standard) is insufficient to elicit venous congestion and therefore symptoms of VIIP.

Anatomical differences between both IJVs have been observed with mean CSA significantly higher on the right (Lichtenstein *et al.*, 2001), and also a higher incidence of VIIP in the right side (Marshall-Bowman *et al.*, 2013). In the present study, similar observations in IJV asymmetry were observed with a significantly greater mean CSA recorded in the right IJV, at -24° only, in all participants. Interestingly, with the addition of -40 mmHg LBNP the asymmetry was abolished providing confirmation of the potential beneficial effect fluid displacement has on ameliorating the effects of VIIP.

5.4.2 Beneficial fluid displacement

Removal of fluid from central compartment is usually associated with negative physiological responses that eventually lead to presyncopal symptoms and ultimately hemodynamic collapse. However, the addition of LBNP at -40 mmHg during -12° HDT actually increased cerebral blood flow velocity (cBFV) with jugular venous congestion removed. Specifically, an increased cBFV occurred as a result of LBNP induced peripheral fluid displacement and its beneficial effect on significant venous congestion at this point (-12° HDT). Supported by the observation that there was no significant difference in cBFV at all angles apart from -12°, which was significantly greater with the addition of LBNP. Additionally, there is evidence in the present study suggesting the cephalic fluid shift (HDT) is balanced by relocation of circulating volume to the lower periphery (LBNP). Measured HR, as an indicator of central hypovolemia, showed no difference between +/- LBNP conditions below -12° HDT as did the CC, as an indicator of fluid shifted to the lower periphery, at the greatest angle of tilt (-24°).

In the present study, significant fluid shifts measured by increases in calf circumference (ΔCC) were observed at tilt angles of -12° and above. Below -12° no change was

measured demonstrating a point in which the LBNP induced peripheral fluid shift was counteracted by a concurrent headward fluid shift induced by tilt. Therefore, the significance of -12° HDT, as a cross-over point with regard to hydrostatic pressure and venous congestion, is indicated. Similar findings were observed by Hinghofer-Szalkay *et al.* (2004) where the ability of LBNP to neutralize the cardiovascular effects of HDT were demonstrated. Specifically, LBNP levels of -15 to -35 mmHg were shown to correlate to HDT angles of -6 to -24° in heart rate (HR), specific volume regulating hormone aldosterone, and fluid displacement measured by thoracic impedance (Hinghofer-Szalkay *et al.*, 2004).

Current data showed a difference in ΔHR between -40 mmHg and angles of tilt above -12°, with no difference at -18° and -24°; indicative of agreement to past research. Similarly, fluid displacement measured by ΔCC during -18° and -24° HDT was counteracted by -40 mmHg; similar to thoracic impedance changes at -24° with -35 mmHg (Hinghofer-Szalkay *et al.*, 2004). The present research responses to HDT+LBNP were broadly similar to past research and, despite measuring ΔCC, demonstrated the ability of -40 mmHg LBNP to neutralize fluids shifts induced by -12° and greater HDT. Furthermore, a fluid balance was revealed during -12° HDT and provides explanatory substantiation for the unexpected increases in cerebral hemodynamics measurements made at this point.

5.4.3 Cerebral hemodynamics

Cerebral hemodynamics are tightly regulated by autoregulation and as such cBFV remains relatively resistant to small changes in systemic cardiovascular response to an orthostatic challenge. However, when mean arterial pressure (MAP) deviates from

between control levels (50-150 mmHg) a significant disruption can be observed. Similarly, a significant alteration to autoregulation may occur if the stimulus presents a unique challenge, such as altered hydrostatic pressures along the main column of blood within the body (Laing *et al.*, 2016). It is postulated venous congestion, induced by -12° HDT and above, leads to a significant disruption to normal autoregulatory response. Whilst this was not directly measured in the present study, Zhang (2013) demonstrated a marked deviation from the expected autoregulatory response when exposed to microgravity, in which the hydrostatic gradient is completely removed. Therefore, current short-term changes observed in cBFV may be explained by impaired cerebrovascular autoregulation brought about by venous congestion and rapid removal with LBNP. Further research is needed to explore other contributory mechanisms including the effect of blood gas concentrations on neuronal metabolisms affecting CBF and the role of the autonomic nervous system in regulation. Additionally, limitations of the NIRS methodology must be noted; measured changes in O_2Hb concentration do not differentiate between arterial inflow and venous outflow and there is an assumption of a steady-state in O_2 consumption of the cerebral tissue being measured (Pellicer & del Carmen Bravo, 2011).

The hypothesized space obstructive syndrome (SOS) proposed by Wiener (2012) facilitates the explanation of the significance of observed findings in the present study for spaceflight (Figure 5.21).

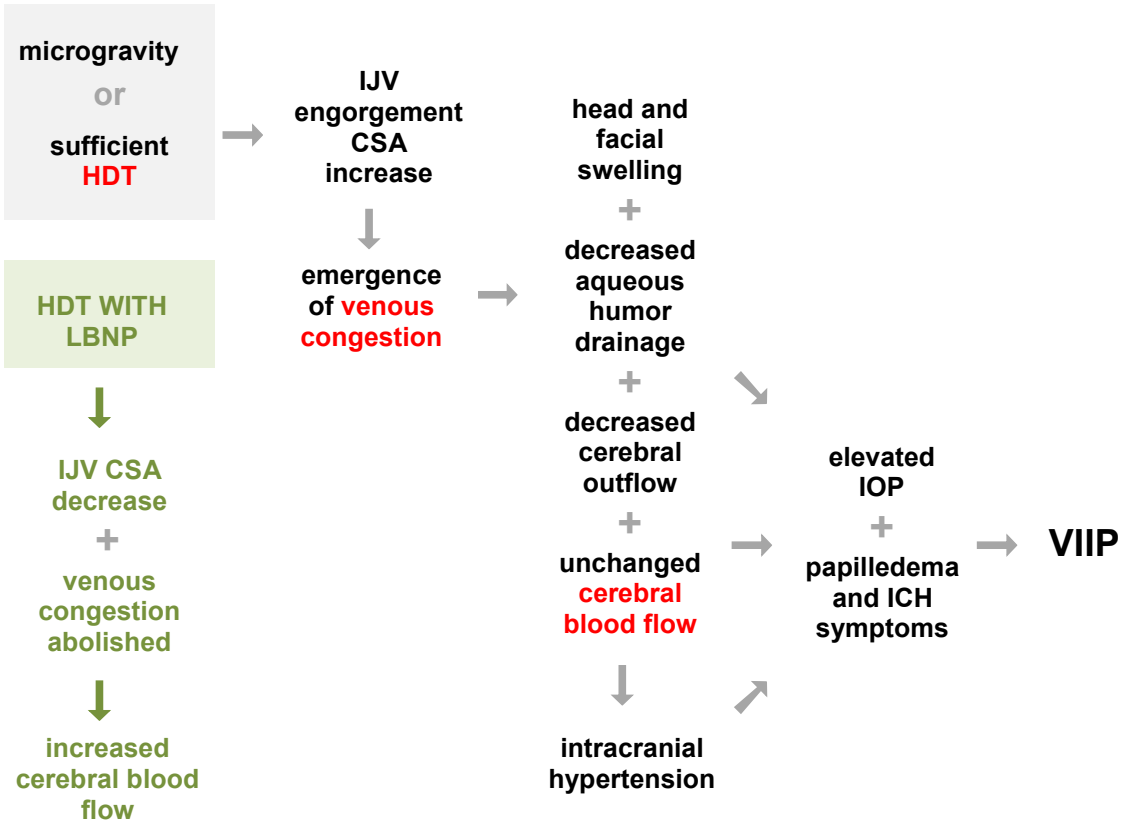

Figure 5.21 Hypothesised space obstructive syndrome (SOS) cascade phenomenon adapted from Wiener (2012).

HDT, head-down tilt, **IJV**, internal jugular vein; **CSA**, cross-sectional area; **IOP**, intraocular pressure; **ICH**, intracranial hypertension; and **VIIP**, vision impairment and intracranial pressure syndrome. **Green box/text**, adapted for present study.

An initial induced venous congestion, leading to the start of a detrimental cascade, may explain the emergence of VIIP in space and HDT below -6°. Confirmation in the validity of this process was supported by current data, where disruption to venous congestion elicited opposite responses to the hypothesised cascade. Specifically, published data from the present study revealed a significant decrease in intraocular pressure (IOP) when LBNP was applied to participants at the same angle of tilt. In addition, the divergence in IOP occurred at -12°, -18°, and -24° (Marshall-Goebel *et al.*,

2017) corroborating the existence and precise tilt/pressure combination for the abolition of venous congestion.

A significant negative correlation was observed between ΔCC and changes in prefrontal cortex cerebral tissue saturation index (ΔcTSI) as expected. LBNP as an orthostatic challenge was expected to reduce ΔcTSI and similar findings, of a reduction, have been observed during postural change from supine to standing (Kawai *et al.*, 1996). However, the relationship between ΔCC and changes in ΔcBFV were more complex. A peripheral fluid shift was expected to reduce ΔcBFV in a similar manner to ΔcTSI; however, when LBNP matched HDT it actually had a beneficial effect and an increase in ΔcBFV was recorded. Specifically, ΔcBFV was unchanged at angles above and below -12° HDT with LBNP at -40 mmHg; however, at precisely -12° an increase in ΔcBFV was measured. A non-linear peak Gaussian regression line of best fit was significant, demonstrating too little or too much fluid shifted to the periphery had no effect. However, LBNP pressure of -40 mmHg induced the ideal amount of fluid to remove venous congestion and significantly increase cBFV at -12°.

5.4.4 Future direction

The present research reinforces the important role venous congestion plays in cerebral hemodynamics on Earth with obvious implications for spaceflight induced VIIP. Furthermore, mechanisms that specifically target venous congestion may prove beneficial in ameliorating VIIP during long-duration missions.

Recommendations for future research focus include artificial gravity (AG) measures such as short-arm human centrifugation (SAHC) which, depending on the configuration, could diminish venous congestion whilst providing a gravitational stimulus to bones and

muscles. Additionally, results from NASA's 'Fluid Shifts' experiment (Stenger *et al.*, 2016) may deliver data confirming similar outcomes to those observed in the present study. Specifically, that blood shifted to the periphery has a benefit on venous congestion and VIIP; however, results are pending.

Finally, pharmacological/therapeutic interventions to reduce localised venous congestion may prove beneficial even if the reduction is small. Due to the long-term nature of VIIP pathology, minute changes in pressure may have a large impact on clinical outcome. We speculate administration of β-adrenergic antagonists could provide a therapeutic benefit on long-term localised venous congestion and therefore VIIP associated pathology; however, this has yet to be tested. Recent research has suggested the daily fluctuations (sleep/wake) in regional intracranial pressure may be exacerbating pathology associated with VIIP (Lawley *et al.*, 2017). The development of improved countermeasures would benefit from considering these findings, along with knowledge of venous congestion importance; ultimately leading to imaginative strategies, aimed at controlling ocular problems associated with microgravity.

5.4.5 Conclusions

Our results suggest that jugular venous congestion can be abolished with the addition of LBNP. Specifically, in the present study it was found venous congestion induced by HDT to -12° was abolished with the addition of -40 mmHg LBNP. However in order to benefit, from the relieving effect of fluid displacement, the LBNP level must be sufficiently matched against the severity of HDT induced venous congestion. It remains unclear what level of LBNP is required to remove microgravity induced venous congestion; with future research benefiting from a focus in this area. In summary:

- The inability of HDT to elicit VIIP on Earth is explained by insufficient venous congestion at the -6° tilt typically used.
- Significant increase in internal jugular vein (IJV) cross-sectional area (CSA) indicated venous congestion and coincided with a reduction in cerebral hemodynamics.
- Cerebral blood flow velocity (cBFV) increased during HDT+LBNP, demonstrating the successful abolition of venous congestion. However, significant cBFV increases were only measured when peripheral fluid shift matched congestion magnitude.
- LBNP behaves as a countermeasure, increasing cBFV, when significant IJV distension is present. However, prolonged LBNP would act as an orthostatic challenge, decreasing cBFV, when there is no congestion.

6 GENERAL DISCUSSION

6.1 Summary

The unifying hypothesis of this thesis is:

Orthostatic challenge induced peripheral fluid shifts offer protection to headward pressure increases and cerebral hemodynamics, by restoring hydrostatic gradients to Earth-like upright norms.

The data presented in this thesis are consistent with the hypothesis; and although the significance of jugular venous congestion was not initially stated, it was explored in detail in Chapter 5. The significance of venous congestion, taken together with the findings of the other experimental chapters, is addressed in the next section (section 6.2).

Chapter 3 was focused on venous cuff occlusion (VCO) and an investigation into this method as a simulated orthostatic challenge; with the aim:

(i) to investigate VCO induced fluid shift effects, on systemic cardiovascular response, and quantifying central blood relocation importance to orthostatic challenge.

The main findings of this study are as follows: (i) VCO pressures of 20-120 mmHg on both legs induced lower periphery vein distension; (ii) the magnitude of systemic response (heart rate, HR), mean arterial pressure (MAP), and total peripheral resistance (TPR) were not linked to increased leg volume; and (iii) cerebral tissue saturation index (cTSI) was unaffected by VCO and specifically the volume of fluid shifted to the periphery.

An established orthostatic challenge, such as lower-body negative pressure (LBNP), leads to an increased sympathetic outflow to the peripheral vasculature; despite an unchanged MAP (Frey *et al.*, 1994). However, in the present study whilst MAP was unchanged there was no evidence of sympathetic activation up to 100 mmHg. At VCO pressures of 120 mmHg an increase in TPR was measured but was present with participant discomfort suggesting pain activated sympathetic activity. Yamamoto *et al.* (1992) demonstrated the pain related response on TPR through the cold pressor test with an immediate systemic cardiovascular response measured in the absence of elevated TPR; with prolonged cold exposure causing a significant increase in TPR, playing an essential role to elevate MAP.

During a five minute sit-to-stand (STS) test ~157 mL of circulating volume is shifted to both lower limbs (Frey *et al.*, 1994); which is similar in magnitude to a head-up tilt (HUT) test to 53° for 30 minutes of ~192 mL (Laszlo *et al.*, 2001). In both STS and HUT, significant changes to the cardiovascular response (HR, MAP, and volume regulating hormones) were measured. However, in the present study a calculated ~135 mL volume of fluid was shifted to the periphery without any significant changes in HR, MAP, SV or TPR. In general, it was found VCO elicits significant fluid shifts, as measured by calf circumference, but is an inadequate orthostatic challenge; despite being used in the past as a spaceflight countermeasure (Arbeille *et al.*, 1995; Herault *et al.*, 2000).

Chapter 4 investigated the effect of a changing rotational axis position (RAP) during short-arm human centrifugation (SAHC) on hemodynamic response; with the aim:

(ii) to determine the effect of an altered gravitational gradient, due to a shift in rotational axis position (RAP) from head to heart-level during SAHC, on central, peripheral, and cerebral response.

The main findings of this study are as follows: (i) increasing the g-gradient, independent of g-level, elicits a comparable attenuation of central, peripheral, and cerebral response; in a similar manner to reducing g-level; (ii) cerebral oxygenation, during heart-level SAHC, was unsupported suggesting emergence of venous congestion; and (iii) overall increased tolerance to higher g-levels indicates suitability of this SAHC regime as part of a safe future spaceflight countermeasure.

It was hypothesised that SAHC with the centre of rotation at heart-level, whilst maintaining the same g-level at the feet, would have a beneficial effect on cerebral perfusion during the orthostatic challenge. Specifically, headward arterial pressure increases would act to maintain appropriate cerebral oxygenation despite significant central volume shifted to the periphery. However, this was not observed and it was thought concurrent headward venous pressure increases negated any arterial benefit and perhaps led to the emergence of jugular venous congestion, as described by Davis *et al.* (2008). Interestingly, venous congestion has also be implicated in visual impairment and intracranial pressure (VIIP) syndrome of astronauts (Wiener, 2012) and warranted further investigation.

Finally, chapter 5 explored jugular venous congestion induced by head-down tilt (HDT) and the effect lower-body negative pressure (LBNP); with the aim:

(iii) to evaluate the importance of venous congestion in microgravity and spaceflight analogues; and assess suitable amelioration methods.

It was hypothesised that venous congestion induced by HDT, and measurable by an increased internal jugular vein (IJV) cross-sectional area (CSA), would be abolished by the addition of LBNP. Secondly, the specific HDT angle, with the emergence of congestion, would be greater than the currently accepted spaceflight analogue of -6°. Thirdly, the LBNP level required for venous congestion removal would be tilt-dependant and consisting of a suitable pressure/tilt match. Specifically, an unmatched LBNP and tilt, either too great or too small, would be detrimental to appropriate cerebral blood flow.

The main findings of this study are as follows: (i) HDT induced jugular venous congestion occurred only at -12° and below; (ii) peripheral fluid shifts induced by -40 mmHg LBNP abolished venous congestion; and (iii) cerebral blood flow velocity (cBFV) increased when HDT-headward (-12°) and LBNP-peripheral (-40 mmHg) fluid shifts were balanced.

LBNP as an orthostatic challenge removed fluid from the central compartment and prolonged exposure would have led to a reduced venous return, cardiac pre-load, and eventual drop in cBFV (Hachiya *et al.*, 2012). In the present study, it was surprising to measure an increase in cBFV with the addition -40 mmHg LBNP. However, this observation was only made at a specific angle of tilt (-12°) for the LBNP used (-40 mmHg). Based on present data it is postulated, not only was venous congestion removed, but a favourable hydrostatic gradient was elicited; allowing for greater cerebral drainage and thus increased cBFV.

During weightlessness, the hydrostatic gradient of the central column of blood within the body is absent; and thought to be a contributory factor in venous congestion (Zhang

& Hargens, 2014) and, later on, the emergence of VIIP (Mader *et al.*, 2011). During -6° head-down bed rest (HDBR), visual acuity is unaffected (Nicogossian *et al.*, 1994) and also not able to elicit significant IJV dissention (Clenaghan *et al.*, 2005). Previous and present data, pertaining to venous congestion, suggest -6° HDT is insufficient to mimic spaceflight fluid shifts affecting mechanisms associated with VIIP pathology (Taibbi *et al.*, 2013). Based on the present study, HDBR research would benefit from an increase in the current standardized angle of -6° HDT. Specifically, -12° is suggested as a more suitable angle for HDT in order to elicit venous congestion and pressure changes across the body comparable to spaceflight (Figure 6.1B, C).

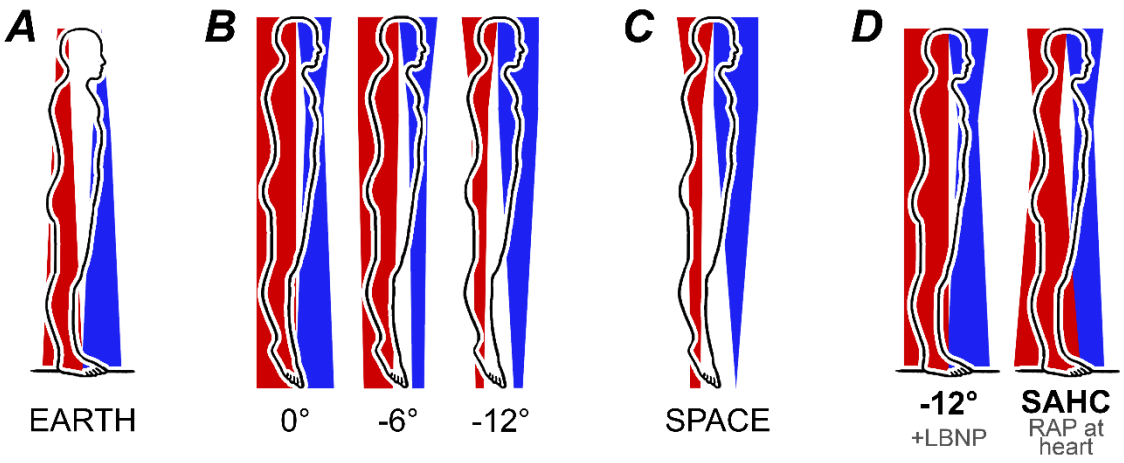

Figure 6.1 Schematic representation of expected hydrostatic gradients within the arterial and venous vasculature under different conditions.

A, standing on Earth; **B**, supine (0°) and head-down bed rest (HDBR); **C**, weightlessness; and **D**, countermeasures. **Red**, arterial; **blue**, venous.

6.2 Further studies

The importance of fluid shifts in relation to spaceflight-related hemodynamic changes has been outlined; and how this is related to hydrostatic gradient changes and venous congestion. Future research would benefit from directly measuring the expected hydrostatic gradients depicted in Figure 6.1; and provide supporting evidence of the significant role, fluid shifts, altered hydrostatic gradients and venous congestion have on spaceflight adaptation. Otto *et al.* (2015) outlined the possibly of irreversible degradation, related to visual acuity, with Nelson *et al.* (2014) suggesting poor cerebral drainage as a contributory factor. Further research into the potentially beneficial effect of shifting fluids to the periphery, and removing venous congestion, must be completed before future holistic countermeasures, focused on fluid redistribution, are finalised.

Fluid shift alone is unable to elicit significant hemodynamic changes (as shown in Chapter 3); however, when taken in the context of venous congestion, a correctly matched shift from the central to peripheral compartment can have beneficial effects. The findings of the present study are also importance to consider when simulating the effects of spaceflight on Earth and in particular to the first true “space sickness” of VIIP (Wiener, 2012).

However, implementation of HDBR at -12° HDT may be successful in simulating fluid shifts and venous congestion but, with the knowledge of irreversible visual acuity problems, would not be appropriate taken alone on ethical grounds. A more suitable approach would be to concurrently develop an improved and holistic SAHC countermeasure; specifically aimed at addressing cephalic fluid shifts, whilst maintaining suitable artificial gravity (AG), in order to minimise muscle and bone loss.

Furthermore, SAHC at heart-level could be used intermittently in space, exploring increased g-levels without reduced tolerance. Specifically, whether a greater intensity exercise and g-level could be successfully favoured over total duration of exposure; thus, potentially freeing up valuable crew time.

In conclusion, this thesis suggests that VCO is a poor model of gravitational fluid shifting but large g-gradient SAHC, via heart-level-RAP, is effective; and crucially, more tolerable at higher g-levels. Venous congestion may play an important role in microgravity fluid shift related OI and VIIP, which -6° bed rest studies fail to induce. Thus, AG with optimal RAP and venous congestion amelioration, may be a tolerable and more effective holistic spaceflight countermeasure.

"Zero-G and I feel fine!"

John Herschel Glenn, Jr. (1921-2016)
Former Astronaut and U.S. Senator

7 RESEARCH OUTPUTS

7.1 Published articles

1. **Laing C**, Green DA, Goswami N, Mulder E & Rittweger J. (2017). Lower-body negative pressure effects on peripheral and cerebral hemodynamics during head-down tilt induced jugular venous congestion. *Aerospace medicine and human performance* (in review).
2. **Laing C**, Green DA, Goswami N, Mulder E & Rittweger J. (2017). Effect of novel short-arm human centrifugation induced gravitational gradients upon cardiovascular responses and orthostatic tolerance. *Journal of Applied Physiology* (in review).
3. Stroetges J, **Laing C**, Johannes B, Mulder E, Rössler A, Trozic I, Rittweger J & Goswami N. (2017). Galanin and adrenomedullin plasma responses during artificial gravity on a human short-arm centrifuge. *Hypertension* (in review).
4. Marshall-Goebel K, Mulder E, Bershad E, **Laing C**, Eklund A, Malm J, Stern C & Rittweger J. (2017). Intracranial and Intraocular Pressure During Various Degrees of Head-Down Tilt. *Aerospace medicine and human performance* **88,** 10-16.
5. Patel K, Rössler A, Lackner HK, Trozic I, **Laing C**, Lorr D, Green DA, Hinghofer-Szalkay H & Goswami N. (2016). Effect of postural changes on cardiovascular parameters across gender. *Medicine* **95,** e4149.
6. **Laing C** & Russamono T. (2013). Short-term Exposure to Microgravity and the Associated Risk of Sudden Cardiac Arrest: Implications for Commercial Spaceflight. In *ESA Special Publication*, pp. 59.

7.2 Published abstracts

1. **Laing C**, Green DA, Mulder E, Goswami N & Rittweger J. (2015). Implementation of short-arm human centrifugation with an altered rotational axis position. *IEEE Aerospace Conference, 2016 Conference Proceedings.*
2. **Laing C**, Green DA, Mulder E, Goswami N & Rittweger J. (2015). Effect of a shift in rotational axis position on cardiovascular responses to centrifugation. *22nd European Low Gravity Research Association Symposium, 2015 Conference Proceedings.*

3. Stahn A, Maggioni MA, Villa F, Weller von Ahlefeld V, **Laing C**, Mulder E, Rittweger J, Petrat G, Merati G., Opatz O, Gunga HC & Castiglioni P. (2015). Erfassung von Flüssigkeitsverschiebungen bei künstlicher Gravitation mittels eines mobilen Systems der Bioimpedanzspekstroskopie: Erste Ergebnisse eines Prototypen. *Deutsche Gesellschaft für Luft- und Raumfahrtmedizin e.V. (DGLRM - German Society of Aerospace Medicine), 2015 Conference Proceedings.*
4. Stahn A, Maggioni MA, Villa F, **Laing C**, Mulder E, Rittweger J, Petrat G, Merati G, Opatz O, Gunga HC & Castiglioni P. (2015). Feasibility of a new mobile segmental bio-impedance spectroscopy device for tracking fluid shifts during different g-levels. *20th Humans in Space Symposium, 2015 Conference Proceedings.*
5. **Laing C**, Green DA, Mulder E, Goswami N & Rittweger J. (2015). Central hypovolemia induced by orthostatic challenge and the effect on cerebral hemodynamics. *KCL Tri-Divisional Postgraduate Symposium, 2015 Conference Proceedings.*

7.3 Congresses

6. **Laing C**. Can Human Centrifugation Make a Mission to Mars Possible? *Royal Aeronautical Society YPL*, Stevenage, UK, **Apr 7, 2016 (invited)**.
7. **Laing C**, Green DA, Mulder E, Goswami N & Rittweger J. Implementation of short-arm human centrifugation with an altered rotational axis position. *IEEE Aerospace Conference*, Montana, USA, **Mar 5-12, 2016**.
8. **Laing C,** Green DA, Mulder E, Goswami N & Rittweger J. Effect of a shift in rotational axis position on cardiovascular responses to centrifugation. *22nd European Low Gravity Research Association Symposium*, Corfu, Greece, **Sept 29-Oct 1, 2015**.
9. **Laing C**, Green DA, Mulder E, Goswami N & Rittweger J. Central hypovolemia induced by orthostatic challenge and the effect on cerebral hemodynamics. *King's College London PhD Symposium*, London, UK, **Jun 6-7, 2015**.
10. **Laing, C**. PhD and post-doc research at DLR - Projects and experiences. *UBM 2014 / 1st International Symposium on Space Life Sciences*, Marmara University, Istanbul, Turkey, **Nov 21-22, 2014 (invited)**.

7.4 Awards

National N E Rowe Award Royal Aeronautical Society, London, England	2016
LSBEB Ross McFarland Student Award Aerospace Medical Association, VA, USA	2016
Best Researcher Presentation King's College London, London, England	2015
Researcher Development Award King's College London, London, England	2015
International Space Life Science Symposium Travel grant Marmara University, Istanbul, Turkey	2014
ESA Sponsorship Award European Space Agency Education Office, Noordwijk, The Netherlands	2013
UK Space Agency Scholarship UKSA, Swindon, England	2013
The Health Axis Europe (HAE) Accelerator Participation Award German Federal Ministry of Education & Research, Bonn, Germany	2013
Rice University Business Plan Competition Finalist Rice Alliance for technology and Entrepreneurship, TX, USA	2013
TiE Travel Award The Indus Entrepreneurs (TiE), CA, USA	2013
ESA Travel Award European Space Agency Education Office, Noordwijk, The Netherlands	2012

8 REFERENCE LIST

Aaslid R, Lindegaard K-F, Sorteberg W & Nornes H. (1989). Cerebral autoregulation dynamics in humans. *Stroke* **20,** 45-52.

Ainslie PN. (2009). Have a safe night: intimate protection against cerebral hyperperfusion during REM sleep. *Journal of Applied Physiology* **106,** 1031-1033.

Ainslie PN & Duffin J. (2009). Integration of cerebrovascular CO2 reactivity and chemoreflex control of breathing: mechanisms of regulation, measurement, and interpretation. *American Journal of Physiology-Regulatory, Integrative and Comparative Physiology* **296,** R1473-R1495.

Akima H, Kubo K, Kanehisa H, Suzuki Y, Gunji A & Fukunaga T. (2000). Leg-press resistance training during 20 days of 6 head-down-tilt bed rest prevents muscle deconditioning. *European journal of applied physiology* **82,** 30-38.

Akima H, Kuno S, Suzuki Y, Gunji A & Fukunaga T. (1997). Effects of 20 days of bed rest on physiological cross-sectional area of human thigh and leg muscles evaluated by magnetic resonance imaging. *Journal of gravitational physiology: a journal of the International Society for Gravitational Physiology* **4,** S15-21.

Akima H, Ushiyama J, Kubo J, Tonosaki S-i, Itoh M, Kawakami Y, Fukuoka H, Kanehisa H & Fukunaga T. (2003). Resistance training during unweighting maintains muscle size and function in human calf. *Medicine and science in sports and exercise* **35,** 655-662.

Alfrey CP, Udden MM, Leach-Huntoon C, Driscoll T & Pickett MH. (1996). Control of red blood cell mass in spaceflight. *Journal of Applied Physiology* **81,** 98-104.

Altenkirch H, Fransson L & Koch G. (1988). Assessment of arterial and venous circulation in upper and lower extremities by venous occlusion strain gauge plethysmography. Normal values and reproducibility. *VASA Zeitschrift fur Gefasskrankheiten* **18,** 140-145.

Altenkirch H, Fransson L & Koch G. (1989a). Assessment of arterial and venous circulation in upper and lower extremities by venous occlusion strain gauge plethysmography. Normal values and reproducibility. *VASA Zeitschrift fur Gefasskrankheiten* **18,** 140-145.

Altenkirch H, Koch G & Koralewski H. (1989b). Variability and reproducibility of arterial and venous circulation parameters in the forearm and calf measured at one-week intervals. *VASA Zeitschrift fur Gefasskrankheiten* **19,** 21-25.

Arbeille P, Fomina G, Achaibou F, Pottier J & Kotovskaya A. (1995). Cardiac and vascular adaptation to 0g with and without thigh cuffs (Antares 14 and Altair 21 day Mir spaceflights). *Acta Astronautica* **36,** 753-762.

Arbeille P, Fomina G, Roumy J, Alferova I, Tobal N & Herault S. (2001). Adaptation of the left heart, cerebral and femoral arteries, and jugular and femoral veins during short-and long-term head-down tilt and spaceflights. *European journal of applied physiology* **86,** 157-168.

Arbeille P, Provost R, Zuj K & Vincent N. (2015). Measurements of jugular, portal, femoral, and calf vein cross-sectional area for the assessment of venous blood redistribution with long duration spaceflight (Vessel Imaging Experiment). *Eur J Appl Physiol* **115,** 2099-2106.

At'kov OIe & Bednenko VS. (1992). *Hypokinesia and weightlessness: clinical and physiologic aspects*. Intl Universities Pr Inc.

Aubert AE, Larina I, Momken I, Blanc S, White O, Kim Prisk G & Linnarsson D. (2016). Towards human exploration of space: the THESEUS review series on cardiovascular, respiratory, and renal research priorities. *npj Microgravity* **2,** 16031.

Bagian JP & Hackett P. (1991). Cerebral Blood Flow: Comparison of Ground-Based and Spaceflight Data and Correlation with Space Adaptation Syndrome. *The Journal of Clinical Pharmacology* **31,** 1036-1040.

Baisch F & Beck L. (1997). Post-Flight Orthostatic Intolerance. In *Anthrorack on the Spacelab D2 Mission*, pp. 45.

Baisch F & Petrat G. (1993). Body fluid distribution in man in space and effect of lower body negative pressure treatment. *The clinical investigator* **71,** 690-699.

Bates D, Maechler M & Bolker B. (2012). lme4: linear mixed-effects models using S4 classes. R package version 0.999375-42. 2011.

Battisti-Charbonney A, Fisher J & Duffin J. (2011). The cerebrovascular response to carbon dioxide in humans. *The Journal of physiology* **589,** 3039-3048.

Bellazzini MA, Rankin PM, Gangnon RE & Bjoernsen LP. (2009). Ultrasound validation of maneuvers to increase internal jugular vein cross-sectional area and decrease compressibility. *The American journal of emergency medicine* **27,** 454-459.

Blaber AP, Goswami N, Bondar RL & Kassam MS. (2011). Impairment of cerebral blood flow regulation in astronauts with orthostatic intolerance after flight. *Stroke* **42,** 1844-1850.

Blaber AP, Hinghofer-Szalkay H & Goswami N. (2013a). Blood volume redistribution during hypovolemia. *Aviation, space, and environmental medicine* **84,** 59-64.

Blaber AP, Zuj KA & Goswami N. (2013b). Cerebrovascular autoregulation: lessons learned from spaceflight research. *Eur J Appl Physiol* **113,** 1909-1917.

Bland JM & Altman D. (1986). Statistical methods for assessing agreement between two methods of clinical measurement. *The lancet* **327,** 307-310.

Bleeker MW, De Groot PC, Pawelczyk JA, Hopman MT & Levine BD. (2004). Effects of 18 days of bed rest on leg and arm venous properties. *Journal of applied physiology* **96,** 840-847.

Blomqvist CG & Stone HL. (1983). Cardiovascular adjustments to gravitational stress. *Comprehensive Physiology*.

Blumberg R. (1885). über den Einfluß der Schwere auf Kreislauf und Atmung. *Pflügers Arch ges Physiol* **37,** 467-478.

Bondar RL, Stein F, Vaitkus PJ, Johnston KW, Chadwick LC & Norris JW. (1990). Transcranial Doppler studies of flow velocity in middle cerebral artery in weightlessness. *The Journal of Clinical Pharmacology* **30,** 390-395.

Bootsma M, Swenne C & Bruschke A. (1996). Heart rate variability during repeated incremental head-up tilt discloses time dependence of individual autonomic dynamics. *Clinical cardiology* **19,** 62-68.

Bruce R, Blackmon J, Jones J & Strait G. (1963). Exercising testing in adult normal subjects and cardiac patients. *Pediatrics* **32,** 742-756.

Brunner MJ, Sussman MS, Greene AS, Kallman CH & Shoukas AA. (1982). Carotid sinus baroreceptor reflex control of respiration. *Circulation Research* **51,** 624-636.

Buckey J, Gaffney FA, Lane LD, Levine BD, Watenpaugh DE, Wright SJ, Yancy C, Meyer D & Blomqvist CG. (1996a). Central venous pressure in space. *Journal of Applied Physiology* **81,** 19-25.

Buckey J, Lane LD, Levine BD, Watenpaugh DE, Wright S, Moore W, Gaffney F & Blomqvist C. (1996b). Orthostatic intolerance after spaceflight. *Journal of Applied Physiology* **81,** 7-18.

Buckey JC, Peshock RM & Blomqvist CG. (1988). Deep venous contribution to hydrostatic blood volume change in the human leg. *The American journal of cardiology* **62,** 449-453.

Buckey Jr JC, Lane LD, Levine BD, Watenpaugh DE, Wright SJ, Moore WE, Gaffney FA & Blomqvist CG. (1996). Orthostatic intolerance after spaceflight. *J Appl Physiol* **81,** 7-18.

Bungo M, Charles J & Johnson Jr P. (1985). Cardiovascular deconditioning during space flight and the use of saline as a countermeasure to orthostatic intolerance. *Aviation, space, and environmental medicine* **56,** 985-990.

Caiozzo VJ, Rose-Gottron C, Baldwin KM, Cooper D, Adams G, Hicks J & Kreitenberg A. (2004). Hemodynamic and metabolic responses to hypergravity on a human-powered centrifuge. *Aviation, space, and environmental medicine* **75,** 101-108.

Carvil PA, Attias J, Evetts SN, Waldie JM & Green DA. (2017). The Effect of the Gravity Loading Countermeasure Skinsuit Upon Movement and Strength. *Journal of strength and conditioning research* **31,** 154-161.

Cassaglia PA, Griffiths RI & Walker AM. (2008a). Sympathetic nerve activity in the superior cervical ganglia increases in response to imposed increases in arterial pressure. *American Journal of Physiology-Regulatory, Integrative and Comparative Physiology* **294,** R1255-R1261.

Cassaglia PA, Griffiths RI & Walker AM. (2008b). Sympathetic withdrawal augments cerebral blood flow during acute hypercapnia in sleeping lambs. *Sleep* **31,** 1729-1734.

Chancellor JC, Scott GB & Sutton JP. (2014). Space Radiation: The Number One Risk to Astronaut Health beyond Low Earth Orbit. *Life* **4,** 491-510.

Charkoudian N, Joyner MJ, Johnson C, Eisenach J, Dietz N & Wallin B. (2005). Balance between cardiac output and sympathetic nerve activity in resting humans: role in arterial pressure regulation. *The Journal of physiology* **568,** 315-321.

Charles JB & Lathers CM. (1991). Cardiovascular adaptation to spaceflight. *The Journal of Clinical Pharmacology* **31,** 1010-1023.

Christensen NJ, Heer M, Ivanova K & Norsk P. (2005). Sympathetic nervous activity decreases during head-down bed rest but not during microgravity. *J Appl Physiol (1985)* **99,** 1552-1557.

Clauser CE, McConville JT & Young JW. (1969). Weight, volume, and center of mass of segments of the human body. DTIC Document.

Claydon VE & Hainsworth R. (2005). Increased postural sway in control subjects with poor orthostatic tolerance. *Journal of the American College of Cardiology* **46,** 1309-1313.

Claydon VE, Norcliffe LJ, Moore JP, Rivera M, Leon-Velarde F, Appenzeller O & Hainsworth R. (2005). Cardiovascular responses to orthostatic stress in healthy altitude dwellers, and altitude residents with chronic mountain sickness. *Experimental physiology* **90,** 103-110.

Clément G. (2011). *Fundamentals of space medicine*. Springer.

Clément G & Bukley A. (2007). *Artificial gravity*, vol. 20. Springer.

Clement G & Pavy-Le Traon A. (2004). Centrifugation as a countermeasure during actual and simulated microgravity: a review. *Eur J Appl Physiol* **92,** 235-248.

Clenaghan S, McLaughlin RE, Martyn C, McGovern S & Bowra J. (2005). Relationship between Trendelenburg tilt and internal jugular vein diameter. *Emergency medicine journal : EMJ* **22,** 867-868.

Convertino VA. (1998). Gender differences in autonomic functions associated with blood pressure regulation. *Am J Physiol Regul Integr Comp Physiol* **275,** R1909-R1920.

Convertino VA, Doerr DF & Stein SL. (1989). Changes in size and compliance of the calf after 30 days of simulated microgravity. *Journal of Applied Physiology* **66,** 1509-1512.

Convertino VA, Rickards CA & Ryan KL. (2012). Autonomic mechanisms associated with heart rate and vasoconstrictor reserves. *Clinical Autonomic Research* **22,** 123-130.

Convertino VA & Sandler H. (1995). Exercise countermeasures for spaceflight. *Acta Astronautica* **35,** 253-270.

Convertino VA, Tripp LD, Ludwig DA & Duff J. (1998). Female exposure to high G: chronic adaptations of cardiovascular functions. DTIC Document.

Cook SB, Clark BC & Ploutz-Snyder LL. (2007). Effects of exercise load and blood-flow restriction on skeletal muscle function. *Medicine and science in sports and exercise* **39,** 1708.

Cooke WH, Ryan KL & Convertino VA. (2004). Lower body negative pressure as a model to study progression to acute hemorrhagic shock in humans. *Journal of Applied Physiology* **96,** 1249-1261.

Cooper V & Hainsworth R. (2002). Effects of head-up tilting on baroreceptor control in subjects with different tolerances to orthostatic stress. *Clinical Science* **103,** 221-226.

Cooper VL & Hainsworth R. (2001). Carotid baroreceptor reflexes in humans during orthostatic stress. *Experimental Physiology* **86,** 677-681.

Dampney R, Coleman M, Fontes M, Hirooka Y, Horiuchi J, Li YW, Polson J, Potts P & Tagawa T. (2002). Central mechanisms underlying short-and long-term

regulation of the cardiovascular system. *Clinical and experimental pharmacology and physiology* **29,** 261-268.

Davis JR, Johnson R & Stepanek J. (2008). *Fundamentals of aerospace medicine*. Lippincott Williams & Wilkins.

Di Rienzo M, Castiglioni P, Iellamo F, Volterrani M, Pagani M, Mancia G, Karemaker JM & Parati G. (2008). Dynamic adaptation of cardiac baroreflex sensitivity to prolonged exposure to microgravity: data from a 16-day spaceflight. *Journal of Applied Physiology* **105,** 1569-1575.

Diaz A, Trigg C & Young LR. (2015). Combining ergometer exercise and artificial gravity in a compact-radius centrifuge. *Acta Astronautica* **113,** 80-88.

Diedrich A, Paranjape SY & Robertson D. (2007). Plasma and blood volume in space. *The American journal of the medical sciences* **334,** 80-85.

Donoviel D & Sutton J. (2013). Biomedical advances for spaceflight improve healthcare on Earth. *Current Biotechnology* **2,** 184-191.

Drummer C, Gerzer R, Baisch F & Heer M. (2000). Body fluid regulation in μ-gravity differs from that on Earth: an overview. *Pflügers Archiv* **441,** R66-R72.

Eckberg DL, Halliwill JR, Beightol LA, Brown TE, Taylor JA & Goble R. (2010). Human vagal baroreflex mechanisms in space. *J Physiol* **588,** 1129-1138.

Elwell C, Cope M, Edwards AD, Wyatt J, Reynolds E & Delpy D. (1992). Measurement of cerebral blood flow in adult humans using near infrared spectroscopy—methodology and possible errors. In *Oxygen Transport to Tissue XIV*, pp. 235-245. Springer.

Erdfelder E, Faul F & Buchner A. (1996). GPOWER: A general power analysis program. *Behavior research methods, instruments, & computers* **28,** 1-11.

ESA. (2011). Artificial Gravity with Ergometric Exercise (AGREE) - Accommodation Feasibility Study. *European Space Agency Technical Reports*.

Evans JM, Stenger MB, Moore FB, Hinghofer-Szalkay H, Rössler A, Patwardhan AR, Brown DR, Ziegler MG & Knapp CF. (2004). Centrifuge training increases presyncopal orthostatic tolerance in ambulatory men. *Aviation, space, and environmental medicine* **75,** 850-858.

Ferguson DW, Abboud FM & Mark AL. (1985). Relative contribution of aortic and carotid baroreflexes to heart rate control in man during steady state and dynamic increases in arterial pressure. *Journal of Clinical Investigation* **76,** 2265.

Fogarty J, Otto C, Kerstman E, Oubre C & Wu J. (2011). The visual impairment intracranial pressure summit report. *NASA Johnson Space Center, Houston, TX, Report No NASA/TP-2011-216160*.

Folino AF. (2007). Cerebral autoregulation and syncope. *Progress in cardiovascular diseases* **50,** 49-80.

Fong K, Arya M & Paloski W. (2007). Gender differences in cardiovascular tolerance to short radius centrifugation. *Journal of gravitational physiology: a journal of the International Society for Gravitational Physiology* **14,** P15-19.

Fortney SM. (1991). Development of lower body negative pressure as a countermeasure for orthostatic intolerance. *The Journal of Clinical Pharmacology* **31,** 888-892.

Frett T, Mayrhofer M, Schwandtner J, Anken R & Petrat G. (2014). An Innovative Short Arm Centrifuge for Future Studies on the Effects of Artificial Gravity on the Human Body. *Microgravity Science and Technology* **26,** 249-255.

Frey M & Hoffler GW. (1988). Association of sex and age with responses to lower-body negative pressure. *Journal of Applied Physiology* **65,** 1752-1756.

Frey M, Mader TH, Bagian JP, Charles JB & Meehan RT. (1993). Cerebral blood velocity and other cardiovascular responses to 2 days of head-down tilt. *Journal of applied physiology* **74,** 319-325.

Frey MAB, Tomaselli CM & Hoffler WG. (1994). Cardiovascular responses to postural changes: differences with age for women and men. *The Journal of Clinical Pharmacology* **34,** 394-402.

Fritsch-Yelle JM, Charles JB, Jones MM, Beightol LA & Eckberg DL. (1994). Spaceflight alters autonomic regulation of arterial pressure in humans. *Journal of Applied Physiology* **77,** 1776-1783.

Fritsch JM, Charles JB, Bennett BS, Jones MM & Eckberg DL. (1992). Short-duration spaceflight impairs human carotid baroreceptor-cardiac reflex responses. *Journal of Applied Physiology* **73,** 664-671.

Fu Q, Arbab-Zadeh A, Perhonen MA, Zhang R, Zuckerman JH & Levine BD. (2004). Hemodynamics of orthostatic intolerance: implications for gender differences. *Am J Physiol Heart Circ Physiol* **286,** H449-H457.

Fu Q, Witkowski S, Okazaki K & Levine BD. (2005). Effects of gender and hypovolemia on sympathetic neural responses to orthostatic stress. *American Journal of Physiology-Regulatory, Integrative and Comparative Physiology* **289,** R109-R116.

Gabrielsen A, Videbaek R, Johansen L, Warberg J, Christensen N & Norsk P. (1996). Immediate baroreflex-neuroendocrine interactions in humans during graded

water immersion. *Journal of gravitational physiology: a journal of the International Society for Gravitational Physiology* **3,** 22.

Gauer OH & Thron HL. (1965). Postural changes in the circulation. *Handbook of physiology Circulation* **2,** 2409-2439.

Giller CA, Levine BD, Meyer Y, Buckey JC, Lane LD & Borchers DJ. (1992). The cerebral hemodynamics of normotensive hypovolemia during lower-body negative pressure. *Journal of neurosurgery* **76,** 961-966.

Gisolf J, Gisolf A, van Lieshout JJ & Karemaker JM. (2005). The siphon controversy: an integration of concepts and the brain as baffle. *Am J Physiol Regul Integr Comp Physiol* **289,** R627-629.

Gopalakrishnan R, Genc KO, Rice AJ, Lee S, Evans HJ, Maender CC, Ilaslan H & Cavanagh PR. (2010). Muscle volume, strength, endurance, and exercise loads during 6-month missions in space. *Aviation, space, and environmental medicine* **81,** 91-104.

Gorgiladze GI & Bryanov II. (1989). Space motion sickness. *Kosm Biol Aviakosm Med* **23,** 4-14.

Goswami N, Bruner M, Xu D, Bareille M-P, Beck A, Hinghofer-Szalkay H & Blaber AP. (2015a). Short-arm human centrifugation with 0.4 g at eye and 0.75 g at heart level provides similar cerebrovascular and cardiovascular responses to standing. *European journal of applied physiology* **115,** 1569-1575.

Goswami N, Evans J, Schneider S, von der Wiesche M, Mulder E, Rössler A, Hinghofer-Szalkay H & Blaber AP. (2015b). Effects of Individualized Centrifugation Training on Orthostatic Tolerance in Men and Women. *PloS one* **10,** e0125780.

Goswami N, Grasser E, Roessler A, Schneditz D & Hinghofer-Szalkay H. (2009). The cardiovascular response to lower body negative pressure in humans depends on seal location. *Physiological Research* **58,** 311.

Gradwell D & Rainford DJ. (2016). *Ernsting's Aviation and Space Medicine 5E*. CRC Press.

Grasser EK, Goswami N, Rössler A, Vrecko K & Hinghofer-Szalkay H. (2009). Hemodynamic and neurohormonal responses to extreme orthostatic stress in physically fit young adults. *Acta Astronautica* **64,** 688-696.

Greenfield A, Whitney R & Mowbray J. (1963). Methods for the investigation of peripheral blood flow. *British Medical Bulletin* **19,** 101-109.

Greenleaf J, Bulbulian R, Bernauer E, Haskell W & Moore T. (1989). Exercise-training protocols for astronauts in microgravity. *Journal of Applied Physiology* **67,** 2191-2204.

Greenleaf JE. (1984). Physiology of fluid and electrolyte responses during inactivity: water immersion and bed rest.

Grigoriev AI, Kotovskaya AR & Fomina GA. (2011). The human cardiovascular system during space flight. *Acta Astronautica* **68,** 1495-1500.

Groothuis JT, van Vliet L, Kooijman M & Hopman MT. (2003). Venous cuff pressures from 30 mmHg to diastolic pressure are recommended to measure arterial inflow by plethysmography. *Journal of applied physiology* **95,** 342-347.

Gunga H-C, von Ahlefeld VW, Coriolano H-JA, Werner A & Hoffmann U. (2016). *Cardiovascular System, Red Blood Cells, and Oxygen Transport in Microgravity*. Springer.

Guyton AC. (1965). Interstitial fluid pressure: II. Pressure-volume curves of interstitial space. *Circulation research* **16,** 452-460.

Hachiya T, Hashimoto I, Saito M & Blaber AP. (2012). Peripheral vascular responses of men and women to LBNP. *Aviat Space Env Med* **83,** 118-124.

Hallgren E, Kornilova L, Fransen E, Glukhikh D, Moore ST, Clément G, Van Ombergen A, MacDougall H, Naumov I & Wuyts FL. (2016). Decreased otolith-mediated vestibular response in 25 astronauts induced by long-duration spaceflight. *Journal of neurophysiology* **115,** 3045-3051.

Hallgren E, Migeotte P-F, Kornilova L, Delière Q, Fransen E, Glukhikh D, Moore ST, Clément G, Diedrich A & MacDougall H. (2015). Dysfunctional vestibular system causes a blood pressure drop in astronauts returning from space. *Scientific reports* **5,** 17627.

Hargens AR, Bhattacharya R & Schneider SM. (2013). Space physiology VI: exercise, artificial gravity, and countermeasure development for prolonged space flight. *Eur J Appl Physiol* **113,** 2183-2192.

Hargens AR & Richardson S. (2009). Cardiovascular adaptations, fluid shifts, and countermeasures related to space flight. *Respiratory physiology & neurobiology* **169,** S30-S33.

Harms M, Colier W, Wieling W, Lenders J, Secher N & Van Lieshout J. (2000). Orthostatic tolerance, cerebral oxygenation, and blood velocity in humans with sympathetic failure. *Stroke* **31,** 1608-1614.

Herault S, Fomina G, Alferova I, Kotovskaya A, Poliakov V & Arbeille P. (2000). Cardiac, arterial and venous adaptation to weightlessness during 6-month MIR

spaceflights with and without thigh cuffs (bracelets). *European journal of applied physiology* **81,** 384-390.

Heymsfield SB, Martin-Nguyen A, Fong TM, Gallagher D & Pietrobelli A. (2008). Body circumferences: clinical implications emerging from a new geometric model. *Nutrition & Metabolism* **5,** 24.

Hiatt WR, Huang SY, Regensteiner JG, Micco AJ, Ishimoto G, Manco-Johnson M, Drose J & Reeves JT. (1989). Venous occlusion plethysmography reduces arterial diameter and flow velocity. *Journal of Applied Physiology* **66,** 2239-2244.

Hinghofer-Szalkay H. (2011). Gravity, the hydrostatic indifference concept and the cardiovascular system. *European journal of applied physiology* **111,** 163-174.

Hinghofer-Szalkay H, Haditsch B, Loder I, Pilz K, Rössler A & Jezova D. (2004). Head Down Tilt at− 6° to− 24° Can Neutralize the Cardiovascular Effects of LBNP at− 15 or− 35 mmHg. *Aviation, space, and environmental medicine* **75,** 947-951.

Hinghofer-Szalkay HG, Goswami N, Rössler A, Grasser E & Schneditz D. (2008). Reactive hyperemia in the human liver. *American Journal of Physiology-Gastrointestinal and Liver Physiology* **295,** G332-G337.

Hirayanagi K, Iwase S, Kamiya A, Watanabe Y, Shiozawa T, Yamaguchi N, Yajima K & Mano T. (2005). Alternations of static cerebral and systemic circulation in normal humans during14-day head-down bed rest. *Medical science monitor* **11,** CR570-CR575.

Hirofumi O, Otone E, Hiroshi I, Satosi I, Shigeo I, Yasuhiro N & Masato S. (2003). The effectiveness of regional cerebral oxygen saturation monitoring using near-infrared spectroscopy in carotid endarterectomy. *Journal of clinical neuroscience* **10,** 79-83.

Hughson RL, Yee NJ & Greaves DK. (2016). Elevated end-tidal PCO2 during long-duration spaceflight. *Aerospace medicine and human performance* **87,** 894-897.

Hull R, Van Aken WG, Hirsh J, Gallus AS, Hoicka G, Turpie AG, Walker I & Gent M. (1976). Impedance plethysmography using the occlusive cuff technique in the diagnosis of venous thrombosis. *Circulation* **53,** 696-700.

Hume KM & Ray CA. (1999). Sympathetic responses to head-down rotations in humans. *Journal of applied physiology* **86,** 1971-1976.

Ide K, Eliasziw M & Poulin MJ. (2003). Relationship between middle cerebral artery blood velocity and end-tidal PCO2 in the hypocapnic-hypercapnic range in humans. *Journal of Applied Physiology* **95,** 129-137.

Iwasaki K-i, Ogawa Y, Aoki K & Yanagida R. (2012). Cerebral circulation during mild+ Gz hypergravity by short-arm human centrifuge. *Journal of applied physiology* **112,** 266-271.

Iwasaki K, Hirayanagi K, Sasaki T, Kinoue T, Ito M, Miyamoto A, Igarashi M & Yajima K. (1998). Effects of repeated long duration +2Gz load on man's cardiovascular function. *Acta Astronaut* **42,** 175-183.

Iwasaki K, Levine BD, Zhang R, Zuckerman JH, Pawelczyk JA, Diedrich A, Ertl AC, Cox JF, Cooke WH, Giller CA, Ray CA, Lane LD, Buckey JC, Jr., Baisch FJ, Eckberg DL, Robertson D, Biaggioni I & Blomqvist CG. (2007). Human cerebral autoregulation before, during and after spaceflight. *J Physiol* **579,** 799-810.

Iwase S. (2005). Effectiveness of centrifuge-induced artificial gravity with ergometric exercise as a countermeasure during simulated microgravity exposure in humans. *Acta astronautica* **57,** 75-80.

Jeong S-M, Shibata S, Levine BD & Zhang R. (2012). Exercise plus volume loading prevents orthostatic intolerance but not reduction in cerebral blood flow velocity after bed rest. *American Journal of Physiology-Heart and Circulatory Physiology* **302,** H489-H497.

Jobsis FF. (1977). Noninvasive, infrared monitoring of cerebral and myocardial oxygen sufficiency and circulatory parameters. *Science* **198,** 1264-1267.

Johnston RS & Dietlein LF. (1977). Biomedical results from Skylab. NASA SP-377. In *Biomedical Results from Skylab*.

Joyner MJ, Dietz NM & Shepherd JT. (2001). From Belfast to Mayo and beyond: the use and future of plethysmography to study blood flow in human limbs. *Journal of Applied Physiology* **91,** 2431-2441.

Jünger EC, Newell DW, Grant GA, Avellino AM, Ghatan S, Douville CM, Lam AM, Aaslid R & Winn HR. (1997). Cerebral autoregulation following minor head injury. *Journal of neurosurgery* **86,** 425-432.

Kakurin L, Lobachik V, Mikhailov V & Senkevich YA. (1976). Antiorthostatic hypokinesia as a method of weightlessness simulation. *Aviation, space, and environmental medicine* **47,** 1083-1086.

Karpeles LM & Huff RL. (1955). Blood volume of representative portions of the musculoskeletal system in man. *Circulation research* **3,** 483-489.

Kawai Y, Murthy G, Watenpaugh D, Breit G, Deroshia C & Hargens A. (1993). Cerebral blood flow velocity in humans exposed to 24 h of head-down tilt. *Journal of Applied Physiology* **74,** 3046-3051.

Kawai Y, Okuda Y & Ogura K. (1996). Acute responses of brain oxygenation during postural change in humans. In *Proceedings of the Sixth World Congress for Microcirculation*, pp. 697-791.

Kawakami Y, Muraoka Y, Kubo K, Suzuki Y & Fukunaga T. (2000). Changes in muscle size and architecture following 20 days of bed rest. *Journal of gravitational physiology: a journal of the International Society for Gravitational Physiology* **7,** 53-59.

Keen J. (1961). A study of the arterial variations in the limbs, with special reference to symmetry of vascular patterns. *Developmental Dynamics* **108,** 245-261.

Kirkpatrick PJ, Lam J, Al-Rawi P, Smielewski P & Czosnyka M. (1998). Defining thresholds for critical ischemia by using near-infrared spectroscopy in the adult brain. *Journal of neurosurgery* **89,** 389-394.

Kooijman M, Poelkens F, Rongen GA, Smits P & Hopman MT. (2007). Leg blood flow measurements using venous occlusion plethysmography during head-up tilt. *Clinical Autonomic Research* **17,** 106.

Kozlovskaya I, Grigoriev AI & Stepantzov V. (1995). Countermeasure of the negative effects of weightlessness on physical systems in long-term space flights. *Acta astronautica* **36,** 661-668.

Krakow K, Ries S, Daffertshofer M & Hennerici M. (2000). Simultaneous assessment of brain tissue oxygenation and cerebral perfusion during orthostatic stress. *European neurology* **43,** 39-46.

Kramer LA, Sargsyan AE, Hasan KM, Polk JD & Hamilton DR. (2012). Orbital and intracranial effects of microgravity: findings at 3-T MR imaging. *Radiology* **263,** 819-827.

Kügler C, Strunk M & Rudofsky G. (2001). Venous pressure dynamics of the healthy human leg. *Journal of vascular research* **38,** 20-29.

Kurth DC, Steven JM & Nicolson SC. (1995). Cerebral oxygenation during pediatric cardiac surgery using deep hypothermic circulatory arrest. *The Journal of the American Society of Anesthesiologists* **82,** 74-82.

Laing C, Green DA, Mulder E, Goswami N & Rittweger J. (2016). Implementation of short-arm human centrifugation with an altered rotational axis position. In *Aerospace Conference, 2016 IEEE*, pp. 1-7. IEEE.

Laing C & Russamono T. (2013). Short-term Exposure to Microgravity and the Associated Risk of Sudden Cardiac Arrest: Implications for Commercial Spaceflight. In *ESA Special Publication*, pp. 59.

Lane HW, Bourland C, Barrett A, Heer M & Smith SM. (2013). The role of nutritional research in the success of human space flight. *Advances in Nutrition: An International Review Journal* **4,** 521-523.

Lassen NA. (1959). Cerebral blood flow and oxygen consumption in man. *Physiological reviews* **39,** 183-238.

Laszlo Z, Rossler A & Hinghofer-Szalkay H. (2001). Cardiovascular and hormonal changes with different angles of head-up tilt in men. *Physiological Research* **50,** 71-82.

Lawler LA, Halliwill JR, Summer JM, Joyner MJ & Mulvagh SL. (1998). Leg mass and lower body negative pressure tolerance in men and women. *J Appl Physiol* **85,** 1471-1475.

Lawley JS, Petersen LG, Howden EJ, Sarma S, Cornwell WK, Zhang R, Whitworth LA, Williams MA & Levine BD. (2017). Effect of gravity and microgravity on intracranial pressure. *J Physiol*.

LeBlanc A, Lin C, Shackelford L, Sinitsyn V, Evans H, Belichenko O, Schenkman B, Kozlovskaya I, Oganov V & Bakulin A. (2000). Muscle volume, MRI relaxation times (T2), and body composition after spaceflight. *Journal of Applied Physiology* **89,** 2158-2164.

Leblanc A, Matsumoto T, Jones J, Shapiro J, Lang T, Shackelford L, Smith SM, Evans H, Spector E, Ploutz-Snyder R, Sibonga J, Keyak J, Nakamura T, Kohri K & Ohshima H. (2013). Bisphosphonates as a supplement to exercise to protect bone during long-duration spaceflight. *Osteoporosis international : a journal established as result of cooperation between the European Foundation for Osteoporosis and the National Osteoporosis Foundation of the USA* **24,** 2105-2114.

LeBlanc A, Rowe R, Schneider V, Evans H & Hedrick T. (1995). Regional muscle loss after short duration spaceflight. *Aviat Space Environ Med* **66,** 1151-1154.

Lee S, Feiveson AH, Stein S, Stenger MB & Platts SH. (2015). Orthostatic intolerance after ISS and space shuttle missions. *Aerospace medicine and human performance* **86,** A54-A67.

Levine BD, Giller CA, Lane LD, Buckey JC & Blomqvist CG. (1994). Cerebral versus systemic hemodynamics during graded orthostatic stress in humans. *Circulation* **90,** 298-306.

Levine BD, Pawelczyk JA, Ertl AC, Cox JF, Zuckerman JH, Diedrich A, Biaggioni I, Ray CA, Smith ML & Iwase S. (2002). Human muscle sympathetic neural and haemodynamic responses to tilt following spaceflight. *The Journal of physiology* **538,** 331-340.

Levine BD, Zuckerman JH & Pawelczyk JA. (1997). Cardiac atrophy after bed-rest deconditioning. *Circulation* **96,** 517-525.

Lichtenstein D, Saifi R, Augarde R, Prin S, Schmitt J, Page B, Pipien I & Jardin F. (2001). The internal jugular veins are asymmetric. Usefulness of ultrasound before catheterization. *Intensive care medicine* **27,** 301-305.

Linden RJ & Mary D. (1982). Limitations and reliability of exercise electrocardiography tests in coronary heart disease. *Cardiovascular research* **16,** 675-710.

Litter J & Wood JE. (1954). The volume and distribution of blood in the human leg measured in vivo. I. The effects of graded external pressure. *Journal of Clinical Investigation* **33,** 798.

Loehr JA, Guilliams ME, Petersen N, Hirsch N, Kawashima S & Ohshima H. (2015). Physical Training for Long-Duration Spaceflight. *Aerosp Med Hum Perform* **86,** A14-23.

Loehr JA, Lee S, English KL, Sibonga J, Smith SM, Spiering BA & Hagan RD. (2011). Musculoskeletal adaptations to training with the advanced resistive exercise device. *Medicine and science in sports and exercise* **43,** 146-156.

Loenneke J, Wilson J, Wilson G, Pujol T & Bemben M. (2011). Potential safety issues with blood flow restriction training. *Scandinavian journal of medicine & science in sports* **21,** 510-518.

Loenneke JP, Fahs CA, Rossow LM, Sherk VD, Thiebaud RS, Abe T, Bemben DA & Bemben MG. (2012). Effects of cuff width on arterial occlusion: implications for blood flow restricted exercise. *European journal of applied physiology* **112,** 2903-2912.

Lundvall J, Bjerkhoel P, Edfeldt H, Ivarsson C & Länne T. (1993). Dynamics of transcapillary fluid transfer and plasma volume during lower body negative pressure. *Acta Physiologica* **147,** 163-172.

Lynnerup N, Astrup JG & Sejrsen B. (2005). Thickness of the human cranial diploe in relation to age, sex and general body build. *Head Face Med* **1,** 1-7.

Mack PB & LaChance PL. (1967). Effects of recumbency and space flight on bone density. *The American journal of clinical nutrition* **20,** 1194-1205.

Mader TH, Gibson CR, Pass AF, Kramer LA, Lee AG, Fogarty J, Tarver WJ, Dervay JP, Hamilton DR, Sargsyan A, Phillips JL, Tran D, Lipsky W, Choi J, Stern C, Kuyumjian R & Polk JD. (2011). Optic disc edema, globe flattening, choroidal folds, and hyperopic shifts observed in astronauts after long-duration space flight. *Ophthalmology* **118,** 2058-2069.

Madsen P, Lyck F, Pedersen M, Olesen H, Nielsen H & Secher N. (1995). Brain and muscle oxygen saturation during head-up-tilt-induced central hypovolemia in humans. *Clinical Physiology* **15,** 523-533.

Maillet A, Gauquelin G, Gunga H, Fortrat J, Kirsch K, Guell A, Bizollon CA & Gharib C. (1995). Blood volume regulating hormones response during two space related simulation protocols: four-week confinement and head-down bed-rest. *Acta Astronautica* **35,** 547-552.

Maillet A, Gunga HC, Gauquelin G, Fortrat JO, Hope A, Røcker L, Kirsch K & Gharib C. (1993). Effects of 28-day isolation (ESA-ISEMSI'90) on blood pressure and blood volume regulating hormones. *Aviation, space, and environmental medicine*.

Maratea E, Castillo-Pedraza C, Cooper L, Olivera H & Gologorsky E. (2013). Factors predictive of right internal jugular vein cross-sectional area change in response to Trendelenburg positioning.

Marshall-Bowman K, Barratt MR & Gibson CR. (2013). Ophthalmic changes and increased intracranial pressure associated with long duration spaceflight: An emerging understanding. *Acta Astronautica* **87,** 77-87.

Marshall-Goebel K, Mulder E, Bershad E, Laing C, Eklund A, Malm J, Stern C & Rittweger J. (2017). Intracranial and Intraocular Pressure During Various Degrees of Head-Down Tilt. *Aerosp Med Hum Perform* **88,** 10-16.

Matcher SJ, Kirkpatrick PJ, Nahid K, Cope M & Delpy DT. (1995). Absolute quantification methods in tissue near-infrared spectroscopy. In *Photonics West'95*, pp. 486-495. International Society for Optics and Photonics.

Matsnev E, Yakovleva IY, Tarasov I, Alekseev V, Kornilova L, Mateev A & Gorgiladze G. (1983). Space motion sickness: phenomenology, countermeasures, and mechanisms. *Aviation, space, and environmental medicine*.

Michael AP & Marshall-Bowman K. (2015). Spaceflight-Induced Intracranial Hypertension. *Aerosp Med Hum Perform* **86,** 557-562.

Miller JD, Pegelow DF, Jacques AJ & Dempsey JA. (2005). Skeletal muscle pump versus respiratory muscle pump: modulation of venous return from the locomotor limb in humans. *The Journal of physiology* **563,** 925-943.

Mohapatra S & Arenson HM. (1979). The measurement of peripheral blood flow by the electrical impedance technique. *Journal of medical engineering & technology* **3,** 132-137.

Montgomery LD, Kirk PJ, Payne PA, Gerber RL, Newton S & Williams B. (1977). Cardiovascular responses of men and women to lower body negative pressure. *Aviation, Space, and Environmental Medicine* **48,** 138-145.

Moore Jr AD, Center JS & McCleary MF. (2008). Evaluation of Maximal Oxygen Uptake and Submaximal Estimates of VO2max Before, During, and After Long Duration International Space Station Missions.

Moore Jr AD, Downs ME, Lee S, Feiveson AH, Knudsen P, Evetts SN & Ploutz-Snyder L. (2014). Peak Oxygen Uptake during and after Long-duration Space Flight.

Moore W, Gaffney F, Blomqvist C, Buckey Jr J, Lane L, Levine B, Watenpaugh D & Wright S. (1996). Orthostatic intolerance after spaceflight. *J Appl Physiol* **81,** 7-18.

Mulder ER, Stegeman DF, Gerrits KH, Paalman MI, Rittweger J, Felsenberg D & de Haan A. (2006). Strength, size and activation of knee extensors followed during 8 weeks of horizontal bed rest and the influence of a countermeasure. *Eur J Appl Physiol* **97,** 706-715.

Murkin J & Arango M. (2009). Near-infrared spectroscopy as an index of brain and tissue oxygenation. *British journal of anaesthesia* **103,** i3-i13.

NASA. (2015a). ISS One Year Crew. NASA, http://www.nasa.gov/content/one-year-crew.

NASA. (2015b). NASA's Journey to Mars: Pioneering Next Steps in Space Exploration. *NASA, NP-2015-08-2018-HQ, Washington, DC*.

Naulaers G, Meyns B, Miserez M, Leunens V, Van Huffel S, Casaer P, Weindling M & Devlieger H. (2007). Use of tissue oxygenation index and fractional tissue oxygen extraction as non-invasive parameters for cerebral oxygenation. *Neonatology* **92,** 120-126.

Nelson ES, Mulugeta L & Myers JG. (2014). Microgravity-induced fluid shift and ophthalmic changes. *Life* **4,** 621-665.

Nicogossian A, Huntoon CL & Pool S. (1994). Space Physiology and Medicine Lea and Febiger. *Malvern, PA*.

Norsk P. (1992). Gravitational stress and volume regulation. *Clinical Physiology* **12,** 505-526.

Norsk P, Asmar A, Damgaard M & Christensen NJ. (2015). Fluid shifts, vasodilatation and ambulatory blood pressure reduction during long duration spaceflight. *The Journal of Physiology* **593,** 573-584.

Norsk P & Christensen NJ. (2009). The paradox of systemic vasodilatation and sympathetic nervous stimulation in space. *Respir Physiol Neurobiol* **169, Supplement,** S26-S29.

Norsk P, Damgaard M, Petersen L, Gybel M, Pump B, Gabrielsen A & Christensen NJ. (2006). Vasorelaxation in space. *Hypertension* **47,** 69-73.

Nylin G & Celander H. (1950). Determination of blood volume in the heart and lungs and the cardiac output through the injection of radiophosphorus. *Circulation* **1,** 76-83.

Ogoh S, Volianitis S, Nissen P, Wray DW, Secher NH & Raven PB. (2003). Carotid baroreflex responsiveness to head-up tilt-induced central hypovolaemia: effect of aerobic fitness. *The Journal of physiology* **551,** 601-608.

Orwoll ES, Adler RA, Amin S, Binkley N, Lewiecki EM, Petak SM, Shapses SA, Sinaki M, Watts NB & Sibonga JD. (2013). Skeletal health in long-duration astronauts: nature, assessment, and management recommendations from the NASA Bone Summit. *Journal of bone and mineral research* **28,** 1243-1255.

Otto C, Norsk P, Shelhamer M & Davis J. (2015). The Visual Impairment Intracranial Pressure Syndrome in Long Duration NASA Astronauts: An Integrated Approach.

Panerai RB. (1998). Assessment of cerebral pressure autoregulation in humans-a review of measurement methods. *Physiological measurement* **19,** 305.

Partsch B & Partsch H. (2005). Calf compression pressure required to achieve venous closure from supine to standing positions. *Journal of Vascular Surgery* **42,** 734-738.

Patel K, Rössler A, Lackner HK, Trozic I, Laing C, Lorr D, Green DA, Hinghofer-Szalkay H & Goswami N. (2016). Effect of postural changes on cardiovascular parameters across gender. *Medicine* **95**.

Paulson O, Strandgaard S & Edvinsson L. (1989). Cerebral autoregulation. *Cerebrovascular and brain metabolism reviews* **2,** 161-192.

Pavy-Le Traon A, Heer M, Narici MV, Rittweger J & Vernikos J. (2007). From space to Earth: advances in human physiology from 20 years of bed rest studies (1986-2006). *Eur J Appl Physiol* **101,** 143-194.

Pellicer A & del Carmen Bravo M. (2011). Near-infrared spectroscopy: a methodology-focused review. In *Seminars in fetal and neonatal medicine*, pp. 42-49. Elsevier.

Petersen LG, Damgaard M, Petersen JC & Norsk P. (2011). Mechanisms of increase in cardiac output during acute weightlessness in humans. *Journal of applied physiology* **111,** 407-411.

Phillips C. (2010). Changes in venomotor tone during sympathoexcitation: influence of gender and female cycle phase. In *School of Sport and Exercise Sciences*, pp. 206. University of Birmingham, Birmingham.

Pigula FA, Nemoto EM, Griffith BP & Siewers RD. (2000). Regional low-flow perfusion provides cerebral circulatory support during neonatal aortic arch reconstruction. *The Journal of Thoracic and Cardiovascular Surgery* **119,** 331-339.

Pointel J, Gin H, Drouin P, Vernhes G & Debry G. (1981). Venous plethysmography: measuring techniques and normal values. *Angiology* **32,** 145-154.

Polk J. (2009). Flight Surgeon Perspective: Gaps in human health, performance, and safety. *Committee of the decadal survey on biological and physical sciences in space National Research Council, Washington, DC*.

Pump B, Kamo T, Gabrielsen A & Norsk P. (2001). Mechanisms of hypotensive effects of a posture change from seated to supine in humans. *Acta physiologica scandinavica* **171,** 405-412.

Purkayastha S & Sorond F. (2012). Transcranial Doppler ultrasound: technique and application. In *Seminars in neurology*, pp. 411. NIH Public Access.

Ray CA. (2000). Interaction of the vestibular system and baroreflexes on sympathetic nerve activity in humans. *American Journal of Physiology-Heart and Circulatory Physiology* **279,** H2399-H2404.

Ray CA & Monahan KD. (2002). Aging attenuates the vestibulosympathetic reflex in humans. *Circulation* **105,** 956-961.

Rickards CA, Johnson BD, Harvey RE, Convertino VA, Joyner MJ & Barnes JN. (2015). Cerebral blood velocity regulation during progressive blood loss compared with lower body negative pressure in humans. *Journal of Applied Physiology* **119,** 677-685.

Rittweger J, Frost HM, Schiessl H, Ohshima H, Alkner B, Tesch P & Felsenberg D. (2005). Muscle atrophy and bone loss after 90 days' bed rest and the effects of flywheel resistive exercise and pamidronate: results from the LTBR study. *Bone* **36,** 1019-1029.

Roberts D, Tsao Y & Breckenridge A. (1986). The reproducibility of limb blood flow measurements in human volunteers at rest and after exercise by using mercury-in-Silastic strain gauge plethysmography under standardized conditions. *Clinical Science* **70,** 635-638.

Rowell LB. (1993). *Human cardiovascular control*. Oxford University Press.

Rowell LB, O'Leary DS & Kellogg DL. (1996). *Integration of cardiovascular control systems in dynamic exercise*. Wiley Online Library.

Russomano T, May F, Dalmarco G, Baptista RR, Gauger P, Petrat G & Beck L. (2015). A Gender comparison of Cardiovascular Responses to Lower Body Negative Pressure Exposure. *American Journal of Medical and Biological Research* **3,** 95-101.

Sarin S, Scurr J & Smith P. (1992). Mechanism of action of external compression on venous function. *British journal of surgery* **79,** 499-502.

Scott JM, Esch BT, Goodman LS, Bredin SS, Haykowsky MJ & Warburton DE. (2007). Cardiovascular consequences of high-performance aircraft maneuvers: implications for effective countermeasures and laboratory-based simulations. *Applied physiology, nutrition, and metabolism* **32,** 332-339.

Scott JP, Jungius J, Connolly D & Stevenson AT. (2013). Subjective and objective measures of relaxed+ Gz tolerance following repeated+ Gz exposure. *Aviation, space, and environmental medicine* **84,** 684-691.

Shackelford LC, LeBlanc AD, Driscoll TB, Evans HJ, Rianon NJ, Smith SM, Spector E, Feeback DL & Lai D. (2004). Resistance exercise as a countermeasure to disuse-induced bone loss. *Journal of Applied Physiology* **97,** 119-129.

Shaw JA & Murray DG. (1982). The relationship between tourniquet pressure and underlying soft-tissue pressure in the thigh. *J Bone Joint Surg Am* **64,** 1148-1152.

Shi S-J, South DA & Meck JV. (2004). Fludrocortisone does not prevent orthostatic hypotension in astronauts after spaceflight. *Aviation, space, and environmental medicine* **75,** 235-239.

Shoemaker JK, Hogeman CS, Khan M, Kimmerly DS & Sinoway LI. (2001). Gender affects sympathetic and hemodynamic response to postural stress. *Am J Physiol Heart Circ Physiol* **281,** H2028-H2035.

Shortt TL & Ray CA. (1997). Sympathetic and vascular responses to head-down neck flexion in humans. *American Journal of Physiology-Heart and Circulatory Physiology* **272,** H1780-H1784.

Sibonga JD. (2013). Spaceflight-induced bone loss: is there an osteoporosis risk? *Current osteoporosis reports* **11,** 92-98.

Smith C, Goswami N, Robinson R, von der Wiesche M & Schneider S. (2013). The relationship between brain cortical activity and brain oxygenation in the prefrontal cortex during hypergravity exposure. *Journal of Applied Physiology* **114,** 905-910.

Sokal RR & Rohlf FJ. (1969). *The principles and practice of statistics in biological research*. WH Freeman and company San Francisco.

Stenger M, Dulchavsky S & Hargens AR. (2016). Fluid Shifts Before, During, and After Prolonged Space Flight and their Association with Intracranial Pressure and Visual Impairment (Fluid Shifts). NASA, http://www.nasa.gov.

Stenger MB, Evans JM, Patwardhan AR, Moore FB, Hinghofer-Szalkay H, Rössler A, Ziegler MG & Knapp CF. (2007). Artificial gravity training improves orthostatic tolerance in ambulatory men and women. *Acta Astronautica* **60,** 267-272.

Stewart JM. (2013). Common syndromes of orthostatic intolerance. *Pediatrics* **131,** 968-980.

Stewart JM, Rivera E, Clarke DA, Baugham IL, Ocon AJ, Taneja I, Terilli C & Medow MS. (2011). Ventilatory baroreflex sensitivity in humans is not modulated by chemoreflex activation. *American Journal of Physiology-Heart and Circulatory Physiology* **300,** H1492-H1500.

Strandgaard S & Paulson OB. (1984). Cerebral autoregulation. *Stroke* **15,** 413-416.

Sun X-Q, Yao Y-J, Yang C-B, Jiang S-Z, Jiang C-L & Liang W-B. (2005). Effect of lower-body negative pressure on cerebral blood fl ow velocity during 21 days head-down tilt bed rest. *Medical science monitor* **11,** CR1-CR5.

Sundblad P & Orlov O. (2015). Guidelines for Standardization of Bed Rest Studies in the Spaceflight Context.

Suzuki H, Takanashi J-i, Kobayashi K, Nagasawa K, Tashima K & Kohno Y. (2001). MR imaging of idiopathic intracranial hypertension. *American journal of neuroradiology* **22,** 196-199.

Taibbi G, Kaplowitz K, Cromwell RL, Godley BF, Zanello SB & Vizzeri G. (2013). Effects of 30-day head-down bed rest on ocular structures and visual function in a healthy subject. *Aviation, space, and environmental medicine* **84,** 148-154.

Taneja I, Moran C, Medow MS, Glover JL, Montgomery LD & Stewart JM. (2007). Differential effects of lower body negative pressure and upright tilt on splanchnic blood volume. *American Journal of Physiology-Heart and Circulatory Physiology* **292,** H1420-H1426.

Tank J, Baevsky RM, Funtova, II, Diedrich A, Slepchenkova IN & Jordan J. (2011). Orthostatic heart rate responses after prolonged space flights. *Clin Auton Res* **21,** 121-124.

Thornton W, Hoffler G & Rummel J. (1977). Anthropometric changes and fluid shifts. *Biomedical Results from Skylab*.

Thornton WE & Hoffler G. (1974). Hemodynamic studies of the legs under weightlessness.

Tiecks FP, Lam AM, Aaslid R & Newell DW. (1995). Comparison of static and dynamic cerebral autoregulation measurements. *Stroke* **26,** 1014-1019.

Tito DA, Anderson G, Carrico JP, Clark J, Finger B, Lantz GA, Loucks ME, MacCallum T, Poynter J & Squire TH. (2013). Feasibility analysis for a manned mars free-return mission in 2018. In *Aerospace Conference, 2013 IEEE*, pp. 1-18. IEEE.

Tonino RP & Driscoll PA. (1988). Reliability of maximal and submaximal parameters of treadmill testing for the measurement of physical training in older persons. *Journal of gerontology* **43,** M101-M104.

Traon APL, Costes-Salon MC, Vasseur-Clausen P, Bareille MP, Maillet A & Parant M. (2002). Changes in kinetics of cerebral auto-regulation with head-down bed rest. *Clinical physiology and functional imaging* **22,** 108-114.

Trappe S, Costill D, Gallagher P, Creer A, Peters JR, Evans H, Riley DA & Fitts RH. (2009). Exercise in space: human skeletal muscle after 6 months aboard the International Space Station. *Journal of Applied Physiology* **106,** 1159.

Trappe T, Trappe S, Lee G, Widrick J, Fitts R & Costill D. (2006). Cardiorespiratory responses to physical work during and following 17 days of bed rest and spaceflight. *Journal of applied physiology* **100,** 951-957.

Tschakovsky M, Shoemaker JK & Hughson R. (1995). Beat-by-beat forearm blood flow with Doppler ultrasound and strain-gauge plethysmography. *Journal of Applied Physiology* **79,** 713-719.

Tzeng Y-C, Willie CK, Atkinson G, Lucas SJ, Wong A & Ainslie PN. (2010). Cerebrovascular regulation during transient hypotension and hypertension in humans. *Hypertension* **56,** 268-273.

Ursino M & Lodi CA. (1997). A simple mathematical model of the interaction between intracranial pressure and cerebral hemodynamics. *Journal of Applied Physiology* **82,** 1256-1269.

Van Lieshout JJ, Wieling W, Karemaker JM & Secher NH. (2003). Syncope, cerebral perfusion, and oxygenation. *Journal of Applied Physiology* **94,** 833-848.

Videbaek R & Norsk P. (1997). Atrial distension in humans during microgravity induced by parabolic flights. *Journal of Applied Physiology* **83,** 1862-1866.

Wagner E. (1886). Fortgesetzte Untersuchungen über den Einfluss der Schwere auf den Kreislauf. *Pflügers Archiv European Journal of Physiology* **39,** 371-386.

Watanabe Y, Ohshima H, Mizuno K, Sekiguchi C, Fukunaga M, Kohri K, Rittweger J, Felsenberg D, Matsumoto T & Nakamura T. (2004). Intravenous pamidronate prevents femoral bone loss and renal stone formation during 90-day bed rest. *Journal of Bone and Mineral Research* **19,** 1771-1778.

Watenpaugh DE. (2016). Analogs of microgravity: head-down tilt and water immersion. *J Appl Physiol (1985)* **120,** 904-914.

Watenpaugh DE, Breit GA, Buckley TM, Ballard RE, Murthy G & Hargens AR. (2004). Human cutaneous vascular responses to whole-body tilting, Gz centrifugation, and LBNP. *Journal of Applied Physiology* **96,** 2153-2160.

Watenpaugh DE, Buckey JC, Lane LD, Gaffney FA, Levine BD, Moore WE, Wright SJ & Blomqvist CG. (2001). Effects of spaceflight on human calf hemodynamics. *Journal of Applied Physiology* **90,** 1552-1558.

Watenpaugh DE & Hargens AR. (1996). The cardiovascular system in microgravity. *Comprehensive Physiology*.

Waters WW, Ziegler MG & Meck JV. (2002). Postspaceflight orthostatic hypotension occurs mostly in women and is predicted by low vascular resistance. *J Appl Physiol* **92,** 586-594.

Weiss M, Dullenkopf A, Kolarova A, Schulz G, Frey B & Baenziger O. (2005). Near-infrared spectroscopic cerebral oxygenation reading in neonates and infants is associated with central venous oxygen saturation. *Pediatric Anesthesia* **15,** 102-109.

Wesseling K, Jansen J, Settels J & Schreuder J. (1993). Computation of aortic flow from pressure in humans using a nonlinear, three-element model. *Journal of applied physiology* **74,** 2566-2573.

Whinnery JE & Whinnery AM. (1990). Acceleration-induced loss of consciousness: a review of 500 episodes. *Archives of Neurology* **47,** 764-776.

Whinnery T & Forster EM. (2013). The+ Gz-induced loss of consciousness curve. *Extreme Physiology & Medicine* **2,** 1.

White DD, Gotshall RW & Tucker A. (1996). Women have lower tolerance to lower body negative pressure than men. *Journal of Applied Physiology* **80,** 1138-1143.

White RP & Markus HS. (1997). Impaired dynamic cerebral autoregulation in carotid artery stenosis. *Stroke* **28,** 1340-1344.

Wiener TC. (2012). Space Obstructive Syndrome: Intracranial Hypertension, Intraocular Pressure, and Papilledema in Space. *Aviation, Space, and Environmental Medicine* **83,** 64-66.

Wilkinson IB & Webb DJ. (2001). Venous occlusion plethysmography in cardiovascular research: methodology and clinical applications. *British journal of clinical pharmacology* **52,** 631-646.

Willie CK, Tzeng YC, Fisher JA & Ainslie PN. (2014). Integrative regulation of human brain blood flow. *The Journal of physiology* **592,** 841-859.

Wilson MH, Imray CH & Hargens AR. (2011). The headache of high altitude and microgravity—similarities with clinical syndromes of cerebral venous hypertension. *High altitude medicine & biology* **12,** 379-386.

Yamamoto K, Iwase S & Mano T. (1992). Responses of muscle sympathetic nerve activity and cardiac output to the cold pressor test. *The Japanese journal of physiology* **42,** 239-252.

Yang Y, Baker M, Graf S, Larson J & Caiozzo VJ. (2007). Hypergravity resistance exercise: the use of artificial gravity as potential countermeasure to microgravity. *J Appl Physiol* **103,** 1879-1887.

Yates B, Siniaia M & Miller A. (1995). Descending pathways necessary for vestibular influences on sympathetic and inspiratory outflow. *American Journal of Physiology-Regulatory, Integrative and Comparative Physiology* **268,** R1381-R1385.

Yates B, Yamagata Y & Bolton P. (1991). The ventrolateral medulla of the cat mediates vestibulosympathetic reflexes. *Brain research* **552,** 265-272.

Yates BJ & Bronstein AM. (2005). The effects of vestibular system lesions on autonomic regulation: observations, mechanisms, and clinical implications. *Journal of Vestibular Research* **15,** 119-129.

Yoshitani K, Kawaguchi M, Miura N, Okuno T, Kanoda T, Ohnishi Y & Kuro M. (2007). Effects of hemoglobin concentration, skull thickness, and the area of the cerebrospinal fluid layer on near-infrared spectroscopy measurements. *The Journal of the American Society of Anesthesiologists* **106,** 458-462.

Zhang L-F. (2013). Region-specific vascular remodeling and its prevention by artificial gravity in weightless environment. *European journal of applied physiology* **113,** 2873-2895.

Zhang L-F & Hargens AR. (2014). Intraocular/Intracranial Pressure Mismatch Hypothesis for Visual Impairment Syndrome in Space. *Aviation, Space, and Environmental Medicine* **85,** 78-80.

Zhang R, Zuckerman JH, Pawelczyk JA & Levine BD. (1997). Effects of head-down-tilt bed rest on cerebral hemodynamics during orthostatic stress. *Journal of Applied Physiology* **83,** 2139-2145.

Zuj KA, Arbeille P, Shoemaker JK, Blaber AP, Greaves DK, Xu D & Hughson RL. (2012). Impaired cerebrovascular autoregulation and reduced CO(2) reactivity after long duration spaceflight. *Am J Physiol Heart Circ Physiol* **302,** H2592-2598.